AD-A039 968 BOEING COMMERCIAL AIRPLANE CO SEATTLE WASH F/G 1/2
TIRE RUNWAY INTERFACE FRICTION PREDICTION SUBSYSTEM.(U)
MAR 77 M K WAHI, H H STRAUB F33657-74-C-0129
UNCLASSIFIED ASD-TR-77-7 NL

1 OF 3
AD
A039968

ASD-TR-77-7

TIRE RUNWAY INTERFACE FRICTION PREDICTION SUBSYSTEM

Boeing Commercial Airplane Company
P. O. Box 3707
Seattle, Washington 98124

March 1977

Technical Report ASD-TR-77-7
Combat Traction II, Phase II (Extended)
Final Report Task I
May 1975 – December 1975

DEPUTY FOR ENGINEERING
AERONAUTICAL SYSTEMS DIVISION
AIR FORCE SYSTEMS COMMAND
Wright-Patterson Air Force Base, Ohio 45433

NOTICE

When Government drawings, specifications, or other data are used for any purpose other than in connection with a definitely related Government procurement operation, the United States Government thereby incurs no responsibility nor any obligation whatsoever; and the fact that the Government may have formulated, furnished, or in any way supplied the said drawings, specifications, or other data, is not to be regarded by implication or otherwise as in any manner licensing the holder or any other person or corporation, or conveying any rights or permission to manufacture, use, or sell any patented invention that may in any way be related thereto.

This report has been prepared by the Boeing Commercial Aircraft Company, Renton, Washington, under USAF Contract F33657-74-C-0129 for the Deputy for Engineering, Aeronautical Systems Division, Wright-Patterson AFB, Ohio.

This report has been reviewed and cleared for open publication and/or public release by the appropriate Office of Public Information (OI) in accordance with AFR 190-13 and DOD 5230.9. There is no objection to unlimited distribution to the public at large or by the Defense Documentation Center (DDC) to the National Technical Information Service (NTIS).

This report has been reviewed and approved for publication.

David B Tremblay

DAVID B. TREMBLAY
Technical Expert

FOR THE COMMANDER

John F. Andrews

JOHN F. ANDREWS, Lt Col, USAF
Chief, Flight Equipment Division
Directorate of Flight Systems Engineering
Deputy for Engineering

Copies of this report should not be returned unless return is required by security considerations, contractual obligations, or notice on a specific document.

SECURITY CLASSIFICATION OF THIS PAGE (When Data Entered)

REPORT DOCUMENTATION PAGE

READ INSTRUCTIONS BEFORE COMPLETING FORM

1. REPORT NUMBER: ASD-TR-77-7	2. GOVT ACCESSION NO.
3. RECIPIENT'S CATALOG NUMBER	
4. TITLE (and Subtitle): TIRE RUNWAY INTERFACE FRICTION PREDICTION SUBSYSTEM	5. TYPE OF REPORT & PERIOD COVERED: Final May [illegible] - Dec [illegible] 1975
	6. PERFORMING ORG. REPORT NUMBER
7. AUTHOR(s): M. K. Wahi[illegible] H. H. Straub	8. CONTRACT OR GRANT NUMBER(s): F33657-74-C-0129 (Extended)
9. PERFORMING ORGANIZATION NAME AND ADDRESS: Boeing Commercial Airplane Company, P. O. Box 3707, Seattle, Washington 98124	10. PROGRAM ELEMENT, PROJECT, TASK AREA & WORK UNIT NUMBERS: 021A9363
11. CONTROLLING OFFICE NAME AND ADDRESS: Air Force Systems Command, Andrews AFB, Maryland	12. REPORT DATE: Mar[illegible] 1977 13. NUMBER OF PAGES: 188 (202 p.)
14. MONITORING AGENCY NAME & ADDRESS (if different from Controlling Office): Deputy for Subsystems, Aeronautical Systems Division, Wright-Patterson AFB, Ohio	15. SECURITY CLASS. (of this report): Unclassified 15a. DECLASSIFICATION/DOWNGRADING SCHEDULE

16. DISTRIBUTION STATEMENT (of this Report)

DISTRIBUTION STATEMENT A
Approved for public release; Distribution Unlimited

17. DISTRIBUTION STATEMENT (of the abstract entered in Block 20, if different from Report)

402 120

18. SUPPLEMENTARY NOTES

390 145

19. KEY WORDS (Continue on reverse side if necessary and identify by block number)

Combat Traction
Tire-Runway Friction
Friction Measuring Devices
Tire Correlation Model

20. ABSTRACT (Continue on reverse side if necessary and identify by block number)

An analytical tire model ~~has been~~ was developed that correlates with existing tire test data to within ±5%. The model consists of a prediction equation expressing the relationships between seven dimensionless groups (pi terms) needed to define the aircraft tire-runway interface friction. A tire test program ~~has been~~ was recommended to validate the said model. A specification criteria has been established for the interface Friction Prediction Subsystem and various ground vehicles in use to date ~~have been~~ were evaluated. None of the vehicles meets the specification criteria.

DD FORM 1 JAN 73 1473 EDITION OF 1 NOV 65 IS OBSOLETE

SECURITY CLASSIFICATION OF THIS PAGE (When Data Entered)

PREFACE

This report was prepared by M. K. Wahi and H. H. Straub of the Boeing Commercial Airplane Company under a USAF Contract F33657-74-C-0129 (extended). The program was divided into three tasks. Task I involved the formulation of a tire correlation model, a test outline to validate the model; establishment of a friction prediction subsystem specification criteria and evaluation of existing ground vehicles. This report describes all aspects of the work performed in completing Task I of this contract. The work described herein was performed from May 1975 to December 1975.

Task II involved a sensitivity analysis of airplane braking distance on the Boeing Brake Control Simulator for the USAF B-52, KC-135 and F-111 airplanes to validate the general prediction model developed in the previous contracted effort. Task III required establishing compatibility between Task II and Task I subsystems and recommend a test program to verify the effectiveness and reliability of this Total Braking Prediction System (TBPS). The work conducted under Tasks II and III of this contract was performed from August 1975 to December 1976 and is reported in ASD-TR-77-6, volumes I and II.

The authors are indebted to Messers N. S. Attri, W. G. Nelson and A. J. P. Lloyd for their guidance and technical contribution as respective program managers at various stages of the contract.

The authors are also indebted to Messers. W. V. Tracy, ASD/ENFEM, D. B. Tremblay, ASD/ENFE, Lt. Col. R. Kennah, ASD/AEAA and Capt. R. Cauley, AFCEC/EMR of the USAF for their program support.

TABLE OF CONTENTS

TABLE OF CONTENTS (Concluded)

LIST OF ILLUSTRATIONS

LIST OF ILLUSTRATIONS (Continued)

LIST OF ILLUSTRATIONS (Concluded)

LIST OF TABLES

LIST OF ABBREVIATIONS AND SYMBOLS

A	tire aspect ratio, H/w or $D-d/_{2w}$
C_L	airplane coefficient of lift
C_D	airplane coefficient of drag
D	diameter of undeflected, inflated tire
d	wheel or rim diameter
d_{tr}	tire tread depth
d_{tx}	runway macro texture depth
F_e	engine idle thrust
G	resultant force on tire acting parallel with runway surface
g	acceleration due to gravity
G_B	tangential force on tire due to braking alone
G_F	fluid drag force on tire
G_R	rolling resistance of tire and wheel
G_x	retarding component of G, acting parallel to direction of forward motion
H	height of undeflected, inflated tire section
h	fluid depth on runway
p	tire inflation pressure
S	stopping distance for braking segment
s	braking slip ratio, $1-\omega/_{\omega R}$
t	time
V	aircraft ground speed
w	width of undeflected, inflated tire section
Z	normal (to runway) load on tire

LIST OF ABBREVIATIONS AND SYMBOLS (Concluded)

δ	tire vertical deflection
μ, μ_{max}	medium or peak available tire-runway coefficient of friction
μ_{skid}	locked wheel or full skid coefficient of friction
π	Pi, dimensionless group
ρ	fluid density
ψ	angle of yaw
ω	wheel angular velocity

SUMMARY

This report describes the effort completed to:

- Determine parameters that most significantly influence tire-runway wet friction.
- Formulate a model that could be used to predict tire-runway wet friction.
- Recommend a tire test program to validate the prediction model.
- Develop a specification for a Friction Prediction Subsystem and evaluate existing ground vehicles.

During Task Ia, a thorough literature survey was conducted to establish the range of Type VII tires in use, types of runway surfaces in use and a list of numerous factors effecting tire-runway interface phenomenon. Both commercial and military aircraft tires and runways were studied.

The initial list of parameters was reviewed and reduced by eliminating those involving directional control, those relevant to fluid drag and spray patterns (take-off problems) rather than to braking force and by grouping interdependent terms. The resultant list is:

- Peak available ground friction (μ)
- Tire aspect ratio $\left(\frac{D-d}{2w}\right)$, groove depth ($d_{tr}$), inflation pressure (p), vertical load (Z)
- Fluid depth (h) and density (ρ)
- Runway micro and macro texture (d_{tx})
- Forward ground speed (V)

Subsequently a prediction model was developed that correlates with existing tire test data to within ± 5%. The model consists of a prediction equation expressing the relationships between seven dimensionless groups (pi terms) needed to define the tire-runway interface friction. The equation is of the form:

$$(\pi_1) = C_1 (\pi_2)^{C_2} (\pi_3)^{C_3} (\pi_4)^{C_4} (\pi_5)^{C_5} (\pi_6)^{C_6} (\pi_7)^{C_7}$$

where $(\pi_1) = (\mu), (\pi_2) = (\frac{d_{tx}}{D}), (\pi_3) = (\frac{d_{tr}}{D}), (\pi_4) = (\frac{h}{D}), (\pi_5) = (\frac{D-d}{2w}),$

$(\pi_6) = (Z/_{pD\sqrt{wD}}), (\pi_7) = (\rho V^2 D^2/_Z)$

and C_1 through C_7 are experimental constants to be determined from tire test results.

During Task Ib. a test program was outlined to substantiate the conclusions of Task Ia. The recommended test plan is compatible with the two existing tire test facilities at NASA Langley and Naval Air Test Facility, Lakehurst, N. J.

Assuming that the recommended test data will be collected and that the prediction model will be validated in its present form or improved upon as necessary, a specification criteria was established for a Friction Prediction Subsystem (FPSS), under Task Ic. The principal requirement remains to dynamically simulate the tire-runway interface by using a ground vehicle equipped with an aircraft type of tire and a skid control system.

Under Task Id, various ground vehicles in use today were evaluated using the specification criteria just described. All of the vehicles can provide various types of information on runway slipperiness but fail to meet the established criteria. The inability of any vehicle to generate reproducible results makes them incompatible with the desired prediction accuracy in wet runway operations.

SECTION I

INTRODUCTION

Under previous efforts of this contract (ref. 1) a prediction model was formulated using dimensional analysis. The prediction equation (p. 101, ref. 1) had a general format:

$$(Sg/_{V^2}) = C(\mu)^{\alpha}(CL/_{CD})^{\beta}(\rho V^6/_{Fe^g}2)^{\delta}$$

The equation permits the calculation of the airplane stopping (braking) distance, provided information on airplane and weather parameters and *an accurate and meaningful measurement or prediction of the tire-runway friction coefficient was available.* It was realized that a Friction Prediction Subsystem (FPSS) was needed to generate the italicized information. The present effort is one such step in that direction. Figures 1 and 2 depict the basic program plan.

A large number of tire sizes are used under a broad range of loads, and inflation pressures on modern aircraft (Tables A-1 to A-3, Appendix A.). A summary of the range of tire parameters is shown in Table 1. The runways used by these aircraft, have a variety of texture and roughnesses, (Tables B-1 to B-4, Appendix B) that significantly contribute to the level of friction generated at the tire runway interface especially under wet conditions. A summary of the range of runway parameters is shown in Table 2.

An appreciation of the factors that may influence road hold* may be gained from Fig. 3. This model representing tire road hold has been derived from the variables listed by a number of authors as being important in the road hold phenomenon (ref. 2-7). There are four main factors influencing road hold: tire, pavement, lubricant, and operating condition. These have been sub-divided into forty-seven variables which are listed in Table 3. Certain of these variables within each of the groups inter-relate with others in the group and even with variables outside the group. For example, tire tread surface degradation (15) is directly related to the compound antidegradent system (12) and hence to the tread surface condition (14), which is a function of the mode of operation of the tire at any instant in time. The interdependency of variables within different groups is illustrated by the way the pavement macro-texture (28) governs the lubricant film depth (22) together with the water dispersal efficiency of the tire tread pattern design (5).

This model although appearing complex is essentially simplified. There is a whole technology based industry concerned with improving the reinforcing properties of carbon black (9) represented in the model by one sphere, yet carbon black could have been subdivided into structure, particle size, surface activation, etc. Many of the individual variables illustrated could be subdivided in a similar manner.

The phenomenology of friction and factors affecting the available tire-ground coefficient of friction are detailed in Appendix C.

*(Here the term *road hold* implies tire-runway interaction under various operating conditions.)

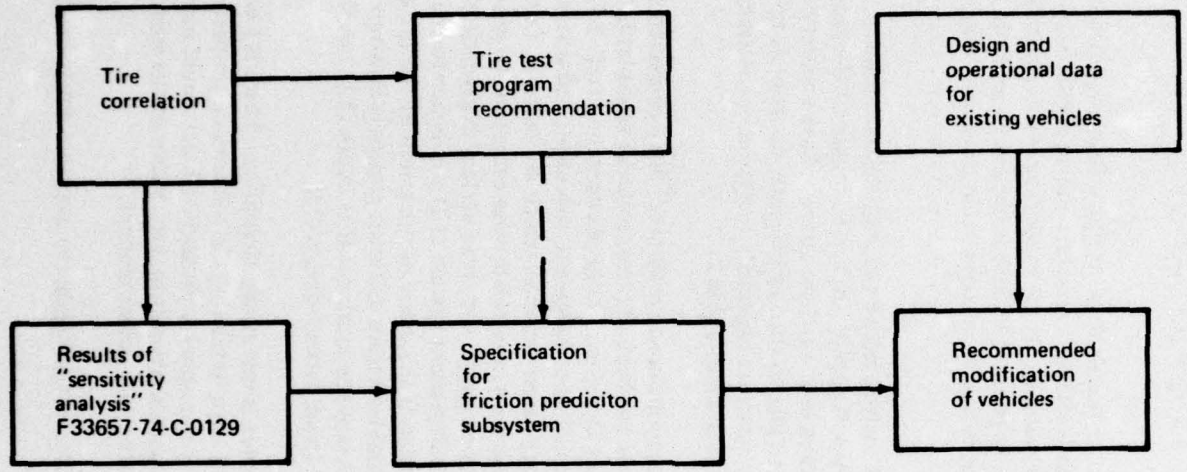

Figure 1.—Program Plan

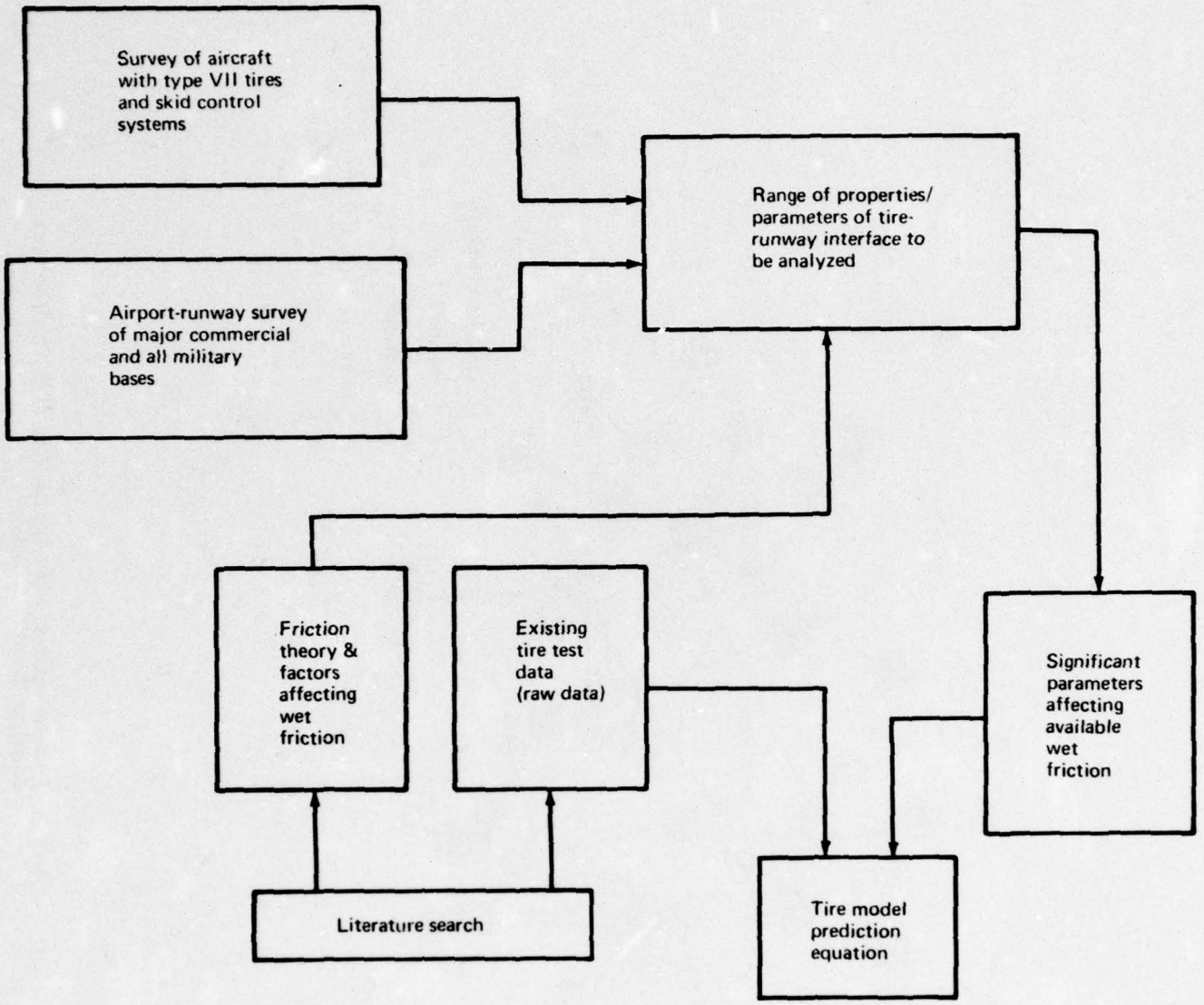

Figure 2.—Tire Correlation Concept

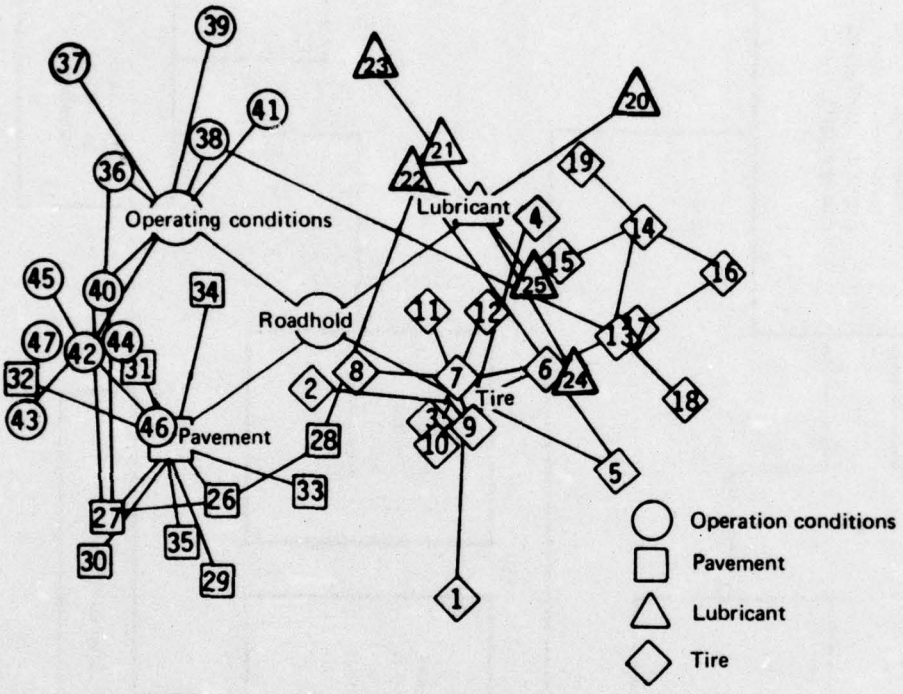

Figure 3.—Model of Factors Effecting the Roadhold Phenomenon. (Adapted from Reference 7)

Table 1.—Range of Type VII Aircraft Tire Parameters

Parameter	Range		Airplane	
	From	To	From	To
Tire size, in.	18 x 5.5	56 x 16	Lear jet	B-52
Aspect ratio	.66	.91	F4	F-14
Speed, mph	175	275	A7A	F104
Inflation pressure, psi	100	360	Lear jet	F4B
Loads, lbs	4000	76000	Lear jet	B-52

Common parameters

- Cross ply design
- Reinforced rib (RR)
- 4 or 5 circumferential grooves
- Tubeless
- Natural rubber base
- Used on main gears

Table 2.—Range of Runway Parameters

Surface:	Asphalt	or	concrete
Treatment:*	Plant mix Conventional Grooved Slurry seal		Marshal asphalt German antiskid coat Porous friction course Crushed rock
Texture depth	.004 in. (.10 mm)	to	.09 in. (2.25 mm)

*Treatment applicable to asphalt and/or concrete. (See tables B-1 to B-4.)

Table 3.—Inter-Relating Factors that Contribute to the Roadhold Phenomenon (key to Fig. 3)

Tire	1. Tire load	Pavement	26. Surface texture
	2. Tire inflation pressure		27. Micro-texture
	3. Tire size		28. Macro-texture
	4. Tire construction & design		29. Resistance to polishing by traffic
	5. Tire tread pattern design		30. Resistance to abrasion & crushing strength
	6. Tire tread compound subdivided as:		31. Weathering characteristics
	7. Chemical formulation		32. Temperature
	8. Polymer type		33. Thermal properties
	9. Carbon black type		34. Matrix properties
	10. Curing system		35. Contamination
	11. Other ingredients	Operating Conditions	36. Traffic density
	12. Anti-degradent system		37. Velocity
	13. Physical properties		38. Tire slip, peak or locked wheel conditions
	14. Tread surface conditions		39. Site design
	15. Surface degradation		40. Prevailing climatic conditions
	16. Chemical/physical absorption		41. Testing vehicle design
	17. Thermal properties		42. Method of measurement
	18. Dynamic properties		43. Stopping distance
	19. Surface temperature		44. Decelerometer
Lubricant	20. Viscosity		45. Cornering force coefficient
	21. Surface tension		46. Braking force coefficient
	22. Film depth		47. Towed vehicle (impending slide)
	23. Film strength		
	24. Temperature		
	25. Impurities		

Due to the apparent complexity of the problem, it was decided to limit the scope of the present analysis by considering only:

a) Wet Runways (only water, no rubber, dirt, salt, oil deposits etc.)

b) Braked Rolling (no yawed rolling/directional control)

c) Peak μ or μ_{max} (no locked wheel situations)

d) Texture depth (no individual asperities, shape, roundness, arrangement etc.)

This helped reduce the number of variables to be considered for model formulation. The list of parameters was further trimmed down by grouping interrelated variables and excluding those having more relevance to fluid drag and spray patterns rather than friction force. Some parameters, although important, could not be included in the final model due to non existence of any relevant test data e.g. viscosity and density variation of contaminant mixtures. Using conventional dimentional analysis techniques the number and form of the dimensionless groups, or pi terms were obtained.

Statistical curve fitting techniques were used to develop a relationship (or equation) between dependent and any other independent variable while all other parameters are held constant. This process was repeated for each variable. These component equations were then combined to form a prediction equation, provided the necessary and sufficient conditions generated during the analysis were met (Appendix G).

The above correlation concept will only be meaningful if sufficient test data are developed, under controlled conditions, to prove the feasibility. Accordingly a test program has been outlined. Recommendations have been made with regard to test conditions, variables to be measured and modes of tire operation to be explored to prove the feasibility of utilizing the prediction model to calculate aircraft stopping distance. The two existing tire test facilities, NASA Langley Loads Track, Hampton, Virginia and Naval Air Test Facilities, Lakehurst, New Jersey have been evaluated for their capabilities and compatibility with the desired test conditions.

The prediction model and the resulting test program recommendations have been used along with reference 1 results to establish a general specification for a Friction Prediction Subsystem. All existing ground vehicles used for assessment of runway friction have been evaluated against this specification and recommendations have been made for possible modifications.

SECTION II
SELECTION OF PERTINENT PARAMETERS

Figure 4 is a flow chart where each block represents a major step of analysis in the formulation of the prediction equation.

Table 4 lists significant parameters after excluding those that are outside the scope of the present work. The list is based on parameters discussed in Appendix C and for reasons spelled out in introduction. The following paragraphs present reasons for further refinement of the list.

1. TIRE TREAD COMPOUND

Pneumatic tires usually contain a variety of rubber compositions, each designed to contribute some particular factor to overall performance. Rubber compounds designed for a specific function will usually be similar but not identical in composition and properties, although in some cases there can be significant differences between compounds in tires of various types. The guiding principle in development of rubber compositions for tires is to achieve the best balance of properties for a particular type of tire service (ref. 8).

Tire manufacturers over the years have each developed their own tread compounding mixes and formulas and consider this as proprietary information. However, it is recognized that all aircraft tires are manufactured from natural rubber based polymers and their compounding from one manufacturer to the next one does not vary extensively. It will therefore not be considered as an independent variable for model formulation.

2. FLUID VISCOSITY AND DENSITY

As stated under the 3-zone concept (see Appendix C) the retarding forces developed in zones 1 and 2 are respectively dependent upon the density and viscosity of the fluid. However, their contribution to the available tire ground coefficient of friction is much smaller than that of zone 3 where the bulk of effective retarding force is generated. The variation of these two parameters should be that of the viscosity and density of the contaminated mixture of rain water, sleet, grit, mud, salt, detritus, grease, tire rubber, fuel and so on. No meaningful test data is available even for individual contaminants. As a result, they cannot presently be considered as independent variables for the model. However, during dimensional analysis, density is retained for dimensional homogeneity and not as an independent variable.

3. PAVEMENT TEXTURE (See also Appendix C)

A number of researchers (ref. 9-16) have generally agreed that large-scale (macro-) texture largely affects the rate at which friction decreases with increased speed. On the other hand the level of friction at a given speed, particularly at low speeds, is mainly a function of the fine-scale (micro-) texture. Micro-texture has been generally considered an inherent characteristic of individual aggregate particles, whereas macro-texture is taken as the roughness of the aggregate - matrix combination.

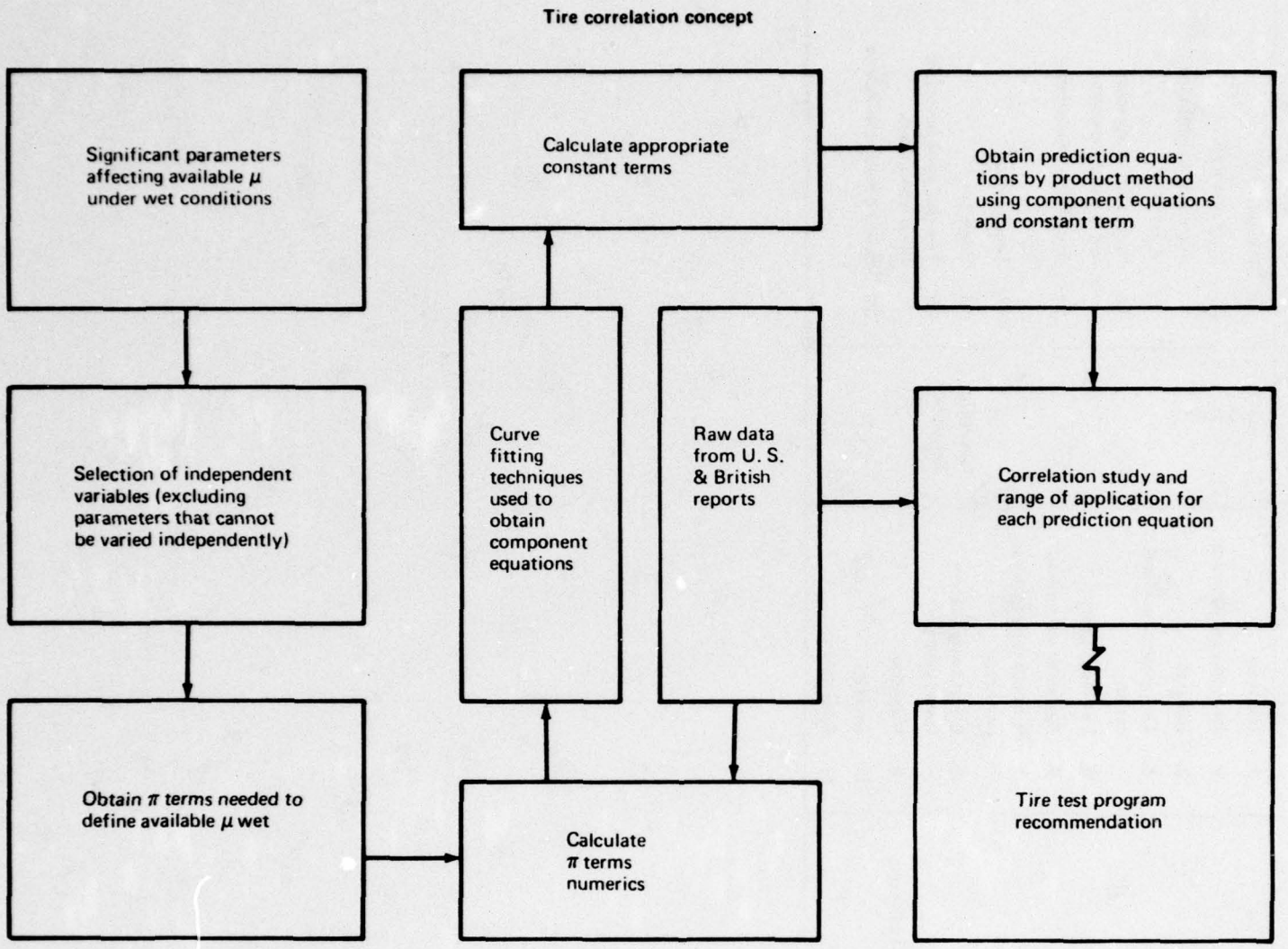

Figure 4.—Block Diagram for Task I Analysis

Table 4.—Significant Parameters

Tire	1. Tire load	Pavement	12. Micro-texture
	2. Tire inflation pressure		13. Macro-texture
	3. Tire size		14. Resistance to polishing by traffic
	4. Tire construction and design		15. Resistance to abrasion and crushing strength
	5. Tire tread pattern		16. Weathering Characteristics
	6. Tire tread compound		17. Temperature
	7. Polymer type (natural, synthetic)	Operating Conditions	18. Velocity
	8. Surface degradation (tread wear)		19. Tire slip, peak or locked wheel conditions
Lubricant	9. Viscosity		20. Braking force coefficient
	10. Density		
	11. Film depth		

Surface texture effects on μ are treated in references 17 and 18. Figure 5 gives an indication of the variation of μ with velocity for various surface types which are defined in Figure 6. The surface types (A, B, C, D and E) represent classes of runway having different surface macro-texture depths but all with essentially harsh micro-textures. Figure 6 lists macro-texture depths for a large number of runways and divides these into five classes; the average texture depth of each class is approximately that represented by the corresponding typical surface (ref. 19-25).

An illustration of the effect of a smooth micro-texture is given in Figure C6, (Appendix C). Such situations can arise if,

1) A runway is constructed using a rounded or polished gravel aggregate - a comparatively rare event,

2) A roadway is used as a runway, since the higher traffic density on roads makes polishing of the surface material a severe problem.

3) A runway has large areas of smooth polished surface.

In the light of the above discussion it was decided to use the runway macro-texture depth as the independent surface parameter.

4. OTHER PARAMETERS

Loss of friction is usually most severe during the first 2 years after construction (ref. 26). Thereafter, the rate of polishing decreases and eventually reaches a stable level of smoothness. Most runways in use today are at least two years old.

The only form of rubber abrasion under wet conditions, called scoring (ref.7), is related to the content of carbon black in the tread. In the absence of any meaningful quantitative data, its inclusion is not justified. Finally, weathering and pavement temperature effects on friction have been shown to be related to the surface texture, already included in the list.

The parameters not discussed in the preceding paragraphs are independent variables and are included in the final list of the pertinent variables, Table 5.

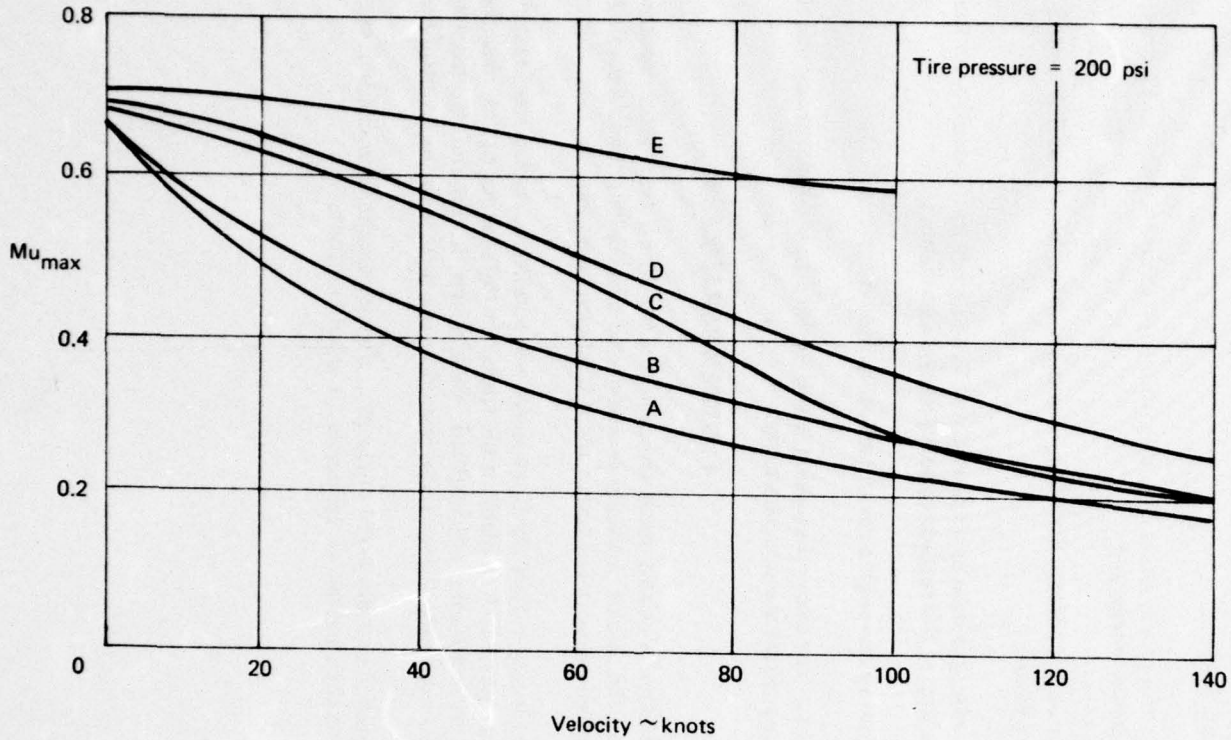

Figure 5.—Mu_{max} - Velocity Curves for Various Surfaces

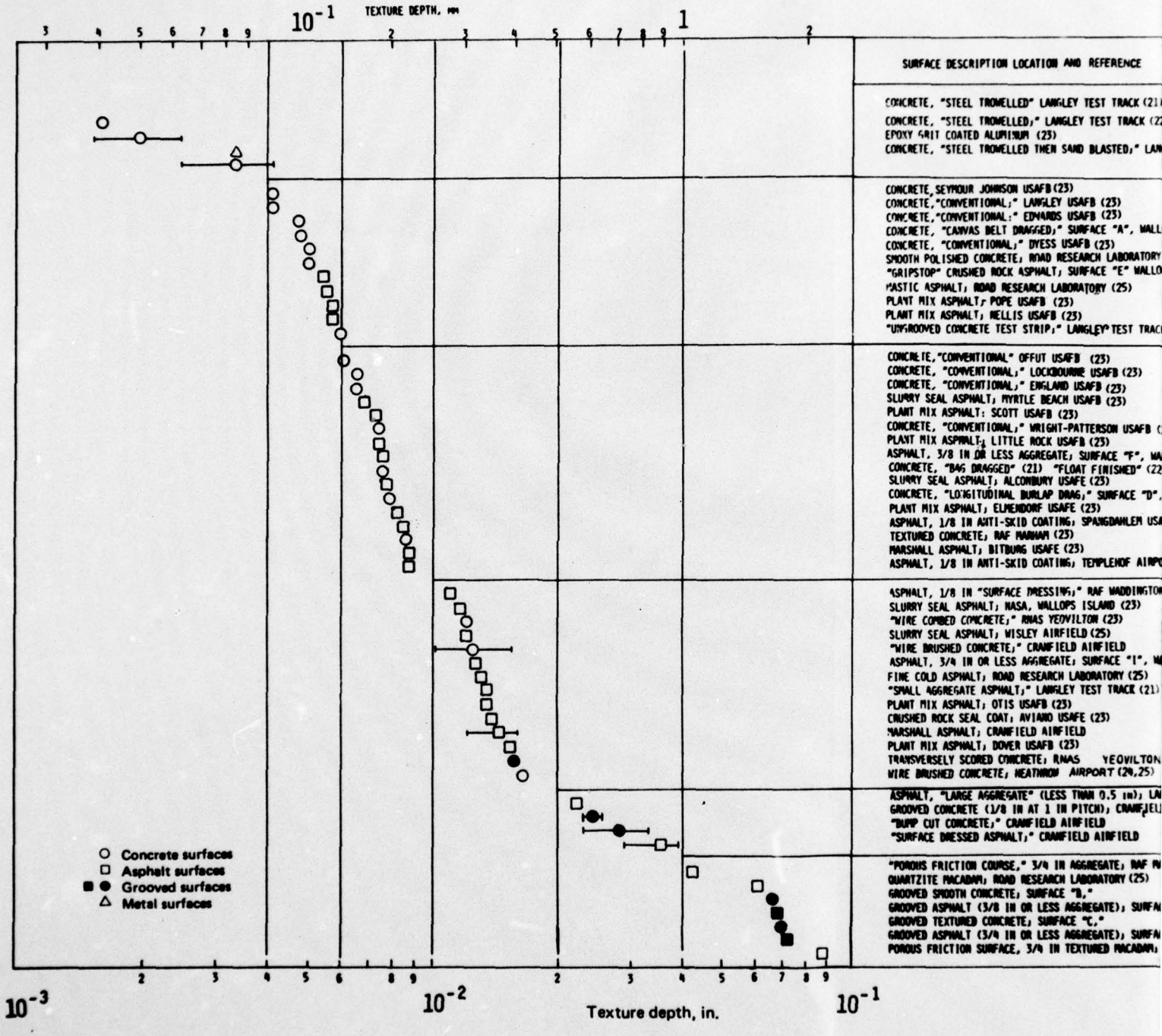

Figure 6.—Classification of Runway Surfaces: Texture Depths Measured by Grease or Sand Pat
(Adapted from Ref. 18)

SURFACE DESCRIPTION LOCATION AND REFERENCE	SURFACE TYPE
CONCRETE, "STEEL TROWELLED" LANGLEY TEST TRACK (21) CONCRETE, "STEEL TROWELLED," LANGLEY TEST TRACK (22) EPOXY GRIT COATED ALUMINUM (23) CONCRETE, "STEEL TROWELLED THEN SAND BLASTED," LANGLEY TEST TRACK (22)	NOT TYPICAL OF CONVENTIONAL RUNWAYS
CONCRETE, SEYMOUR JOHNSON USAFB (23) CONCRETE, "CONVENTIONAL," LANGLEY USAFB (23) CONCRETE, "CONVENTIONAL," EDWARDS USAFB (23) CONCRETE, "CANVAS BELT DRAGGED," SURFACE "A", WALLOPS ISLAND TEST RUNWAY (19,20) CONCRETE, "CONVENTIONAL," DYESS USAFB (23) SMOOTH POLISHED CONCRETE; ROAD RESEARCH LABORATORY (25) "GRIPSTOP" CRUSHED ROCK ASPHALT; SURFACE "E" WALLOPS ISLAND TEST RUNWAY (19,20) PLASTIC ASPHALT; ROAD RESEARCH LABORATORY (25) PLANT MIX ASPHALT; POPE USAFB (23) PLANT MIX ASPHALT; NELLIS USAFB (25) "UNGROOVED CONCRETE TEST STRIP," LANGLEY TEST TRACK (19,20)	TYPE "A" MAINLY VERY SMOOTH CONCRETE RUNWAYS, SOME SMOOTH ASPHALT RUNWAYS
CONCRETE, "CONVENTIONAL" OFFUT USAFB (23) CONCRETE, "CONVENTIONAL," LOCKBOURNE USAFB (23) CONCRETE, "CONVENTIONAL," ENGLAND USAFB (23) SLURRY SEAL ASPHALT; MYRTLE BEACH USAFB (23) PLANT MIX ASPHALT: SCOTT USAFB (23) CONCRETE, "CONVENTIONAL," WRIGHT-PATTERSON USAFB (23) PLANT MIX ASPHALT; LITTLE ROCK USAFB (23) ASPHALT, 3/8 IN OR LESS AGGREGATE; SURFACE "F", WALLOPS ISLAND TEST RUNWAY (19,20) CONCRETE, "BAG DRAGGED" (21) "FLOAT FINISHED" (22); LANGLEY TEST TRACK SLURRY SEAL ASPHALT; ALCORBURY USAFB (23) CONCRETE, "LONGITUDINAL BURLAP DRAG," SURFACE "D", WALLOPS ISLAND TEST RUNWAY (19,20) PLANT MIX ASPHALT; ELMENDORF USAFB (23) ASPHALT, 1/8 IN ANTI-SKID COATING; SPANGDAHLEM USAFB (23) TEXTURED CONCRETE; RAF MARHAM (25) MARSHALL ASPHALT; BITBURG USAFB (23) ASPHALT, 1/8 IN ANTI-SKID COATING; TEMPLEHOF AIRPORT (23)	TYPE "B" TYPICAL OF MOST LIGHTLY TEXTURED CONCRETE AND MOST SMALL AGGREGATE ASPHALT
ASPHALT, 1/8 IN "SURFACE DRESSING," RAF WADDINGTON (23) SLURRY SEAL ASPHALT; NASA, WALLOPS ISLAND (23) "WIRE COMBED CONCRETE," RNAS YEOVILTON (23) SLURRY SEAL ASPHALT; WISLEY AIRFIELD (25) "WIRE BRUSHED CONCRETE," CRANFIELD AIRFIELD ASPHALT, 3/4 IN OR LESS AGGREGATE; SURFACE "I", WALLOPS ISLAND TEST RUNWAY (19,20) FINE COLD ASPHALT; ROAD RESEARCH LABORATORY (25) "SMALL AGGREGATE ASPHALT;" LANGLEY TEST TRACK (21) PLANT MIX ASPHALT; OTIS USAFB (23) CRUSHED ROCK SEAL COAT; AVIANO USAFE (23) MARSHALL ASPHALT; CRANFIELD AIRFIELD PLANT MIX ASPHALT; DOVER USAFB (23) TRANSVERSELY SCORED CONCRETE; RNAS YEOVILTON (23) WIRE BRUSHED CONCRETE; HEATHROW AIRPORT (24,25)	TYPE "C" HEAVILY TEXTURED CONCRETES AND THE MAJORITY OF HARSHER TYPES OF ASPHALT
ASPHALT, "LARGE AGGREGATE" (LESS THAN 0.5 in); LANGLEY TEST TRACK (21) GROOVED CONCRETE (1/8 IN AT 1 IN PITCH); CRANFIELD AIRFIELD "BURP CUT CONCRETE," CRANFIELD AIRFIELD "SURFACE DRESSED ASPHALT;" CRANFIELD AIRFIELD	TYPE "D" SHALLOW GROOVING AND SCORING, SOME LARGE AGGREGATE ASPHALT
"POROUS FRICTION COURSE," 3/4 IN AGGREGATE; RAF MARHAM (23) QUARTZITE MACADAM; ROAD RESEARCH LABORATORY (25) GROOVED SMOOTH CONCRETE; SURFACE "B," GROOVED ASPHALT (3/8 IN OR LESS AGGREGATE); SURFACE "G," GROOVED TEXTURED CONCRETE; SURFACE "C," GROOVED ASPHALT (3/4 IN OR LESS AGGREGATE); SURFACE "H," POROUS FRICTION SURFACE, 3/4 IN TEXTURED MACADAM; RAE, FARNBOROUGH (25)	GROOVES 1/4 IN x 1/4 IN AT 1 IN PITCH, WALLOPS ISLAND TEST RUNWAY (19,20) TYPE "E" DEEP GROOVED SURFACES, "OPEN TEXTURED" AND "POROUS FRICTION COURSE" SURFACES

10^{-1}

es: Texture Depths Measured by Grease or Sand Patch Methods

Table 5.—Pertinent Parameters

Variables	Notation
Peak available mu	μ
Forward ground speed	V
Tire inflation pressure	p
Tire tread depth	d_{tr}
Tire outside deameter	D
Tire width	w
Tire vertical load	Z
Runway macro-texture depth	d_{tx}
Fluid depth	h

SECTION III
DEVELOPMENT OF PREDICTION MODEL

1. DIMENSIONAL EQUATION

Having identified the pertinent and independent variables, Table 5, the first and most important step in forming a prediction model has been completed. The second step is to express the dependent variable as a function of the independent variables so that:

$$\mu = F(V, p, d_{tr}, D, w, Z, d_{tx}, h, \rho) \tag{1}$$

where ρ = fluid density, and has been included only for dimensional homogeneity, not as an independent variable.

The dimensional matrix that can be formed for the fundamental units (mass, length, and time) of the ten parameters in Eq. 1 is of rank 3, so that, according to Buckingham's π theorem (ref. 27), these would yield seven independent π terms. By inspection and analysis, they can be written

$$(\mu), (d_{tx}/D), (d_{tr}/D), (h/D), \frac{(D-d)^*}{2w}, (Z/\rho D\sqrt{wD}), \text{and } (\rho V^2D^2/Z),$$

Thus:

$$(\mu) = F\left(\frac{d_{tx}}{D}, \frac{d_{tr}}{D}, \frac{h}{D}, \frac{D-d}{2w}, \frac{Z}{pD\sqrt{wD}}, \frac{\rho V^2D^2}{Z}\right) \tag{2}$$

or $$(\pi_1) = F(\pi_2, \pi_3, \pi_4, \pi_5, \pi_6, \pi_7) \tag{2a}$$

where: $(\pi_1) = (\mu)$

$(\pi_2) = (d_{tx}/D)$

$(\pi_3) = (d_{tr}/D)$

$(\pi_4) = (h/D)$

$(\pi_5) = (D\text{-}d/2w)$

$(\pi_6) = (Z/pD\sqrt{wD})$

$(\pi_7) = (\rho V^2D^2/Z)$

*d is the wheel or rim diameter and $\left(\frac{D-d}{2w}\right)$ is defined as the tire aspect ratio.

Appendix D shows the detailed analysis of arriving at Eq 2 and Eq 2a. The application of dimensional analysis, including the pi theorem, leads to a type of equation involving an unknown function, of which Eq 2 is an example. Before a prediction equation can be formulated, the nature of the function must be determined.

The general nature of the function (ref. 27) can be shown to be

$$a = C_\alpha a_1^{C_1} a_2^{C_2} a_3^{C_3} \cdots\cdots\cdots a_n^{C_n} \qquad (3)$$

in which the dependent variable, a, is expressed as a dimensionless coefficient (C_α) multiplied by the product of the pertinent independent variables, each raised to the appropriate power. The nature of coefficient C_α must be determined experimentally. Also, the exponents C_1, C_2 etc. are to be determined from test data.

2. LITERATURE SEARCH FOR EXISTING TIRE-TEST DATA

The complexity of friction phenomenon is evident from the number of variables involved. To date it has not been possible to express many of these quantities in rigorous form. It is therefore the practice of authors to simply describe all materials and geometry of test devices together with test results (ref. 28). The nature of the present study necessitated the sorting of the wide range of conditions that influence available friction and then an attempt to express the magnitude of each effect. Unfortunately, the influence of runway surface variables is usually measured by one type of test, tire variables are measured by another type of test and other variables may be measured by a third. To make matters worse, many authors repeat parts of their work over several papers presented to conferences, symposia, annual meetings of societies etc. Key concepts may appear as the closing sentence in a lengthy paper.

With this in mind a thorough literature survey in the general area of tire-road interaction was undertaken with an intention to extract as much usable data (for model use) as possible. A summary of the resulting tire test data used for this survey is shown in Appendix E as Figures E1 through E9 and Table E-1. (See refs. 18, 21, 50, 52, 53, and 54 for additional details). Numerous other test data are available but cannot be used for the model under consideration. Even though attempts were made to use only aircraft tire test data, some automotive tire data had to be included e.g. Fig. E-4, as no such data is available for aircraft tires. Also the automotive tire data used is for μ_{skid} (locked-wheel) conditions while all other data is μ_{peak} type. Virtually no aircraft tire test data and very little on automotive tires is available on the aspect ratio effects. Data for model use was therefore generated from two test points available at each speed (refs. 53 and 54).

Many other prudent engineering judgements had to be made as to the quantitative nature of basic test data required for model verification but missing from the test reports containing the subject data. Caution must therefore be practiced such that the material presented in this report is used only in its technical context (i.e. as a working concept) and not in its numerical content until model verification has been conducted e.g. through Task Ib recommendations.

Appendix E also shows the calculations of π terms using raw data read from Figures E1 through E9, along with other basic data, in tabulated form.

3. COMPONENT EQUATIONS

The best procedure for evaluating a function is to arrange the observations so that all but one of the pi terms containing the independent variables in the function remain constant. Then the remaining independent pi term is varied to establish a relationship between it and the dependent variable (π_1 term). This procedure is repeated for each of the pi terms in the function; the resulting relationships between π_1 and the other individual pi terms are called component equations. Statistical curve fitting computer programs were used to generate the component equations (see Appendix F). A summary of the equations is listed in Table 6.

4. GENERALIZED FUNCTIONS

When the component equations have been determined, they are combined in a certain manner to give a general relationship. It is possible for some of the component equations to be combined by multiplication, while others require addition in the formation of the resultant prediction equation. In general, these two methods are adequate for the majority of engineering problems. For the problem on hand, the nature of available data (multiple sources, variety of test conditions, both automotive and aircraft tires, laboratory and actual runway tests etc.) prevented a rigorous analysis as to which of the two methods should be used. Based on past experience it was decided to use the multiplication method and revise it if necessary when more data becomes available to validate the model. Table G-1, Appendix G shows a list of possible combinations of sets of component equations to form prediction equations, each set having six equations. The necessary and sufficient conditions to be met for the function to be a product were developed and translated into tests of validity. Again, these tests of validity cannot be tried until a systematic set of data under controlled test conditions (i.e. data obtained for all pi terms on one tire, one surface etc.) is made available. All aspects of the development of prediction equations discussed in this paragraph are detailed in Appendix G. The major equations of interest are repeated in succeeding paragraphs.

$$(\pi_1) = (C)(\pi_1)\,\bar{3}\rightarrow\bar{7}\,(\pi_1)\,\bar{2},\bar{4}\rightarrow\bar{7}\,(\pi_1)\,\bar{2},\bar{3},\bar{5}\rightarrow\bar{7}\,(\pi_1)\bar{2}\rightarrow\bar{4},\bar{6},\bar{7}$$

$$(\pi_1)\,\bar{2}\rightarrow\bar{5},\bar{7}\,(\pi_1)\,\bar{2}\rightarrow\bar{6} \qquad (52)$$

where the bar denotes a constant (held) value.

Table 6.—Summary of Component Equations

V-Knots	Equation	Eq. No.	Type of Surface
25	$(\pi_1) = 1.3757\ (\pi_2)^{.7046}$	(4)	All
50	$(\pi_1) = 1.0633\ (\pi_2)^{.7887}$	(5)	"
75	$(\pi_1) = .5994\ (\pi_2)^{.7265}$	(6)	"
100	$(\pi_1) = .1337\ (\pi_2)^{.3361}$	(7)	"
25	$(\pi_1) = .4659\ (\pi_3)^{.1200}$	(8)	All
50	$(\pi_1) = .4181\ (\pi_3)^{.2501}$	(9)	"
75	$(\pi_1) = .2281\ (\pi_3)^{.2234}$	(10)	"
100	$(\pi_1) = .1032\ (\pi_3)^{.1192}$	(11)	"
25	$(\pi_1) = .3650\ (\pi_4)^{-.0714}$	(12)	A
50	$(\pi_1) = .1005\ (\pi_4)^{-.3347}$	(13)	"
75	$(\pi_1) = .0532\ (\pi_4)^{-.4113}$	(14)	"
100	$(\pi_1) = .0290\ (\pi_4)^{-.5376}$	(15)	"
25	$(\pi_1) = .4246\ (\pi_4)^{-.0742}$	(16)	C
50	$(\pi_1) = .2159\ (\pi_4)^{-.1864}$	(17)	"
75	$(\pi_1) = .0910\ (\pi_4)^{-.3820}$	(18)	"
100	$(\pi_1) = .0509\ (\pi_4)^{-.4645}$	(19)	"
25	$(\pi_1) = .3990\ (\pi_4)^{-.1518}$	(20)	E
50	$(\pi_1) = .2472\ (\pi_4)^{-.1773}$	(21)	"
75	$(\pi_1) = .1001\ (\pi_4)^{-.4004}$	(22)	"
100	$(\pi_1) = .0716\ (\pi_4)^{-.4254}$	(23)	"
25	$(\pi_1) = .4098\ (\pi_5)^{.3089}$	(24)	All
50	$(\pi_1) = .4096\ (\pi_5)^{.6450}$	(25)	"
75	$(\pi_1) = .4303\ (\pi_5)^{1.3555}$	(26)	"
100	$(\pi_1) = .4979\ (\pi_5)^{3.0071}$	(27)	"

Table 6.—Summary of Component Equations (Concluded)

V-Knots	Equation	Eq. No.	Type of Surface
25	$(\pi_1) = .5536\ (\pi_6)^{.1117}$	(28)	A
50	$(\pi_1) = .4502\ (\pi_6)^{.2002}$	(29)	"
75	$(\pi_1) = .3609\ (\pi_6)^{.2204}$	(30)	"
100	$(\pi_1) = .2825\ (\pi_6)^{.1942}$	(31)	"
25	$(\pi_1) = .7633\ (\pi_6)^{.1665}$	(32)	C
50	$(\pi_1) = .6312\ (\pi_6)^{.1602}$	(33)	"
75	$(\pi_1) = .4583\ (\pi_6)^{.1257}$	(34)	"
100	$(\pi_1) = .3332\ (\pi_6)^{.0992}$	(35)	"
25	$(\pi_1) = .8890\ (\pi_6)^{.1855}$	(36)	E
50	$(\pi_1) = .7956\ (\pi_6)^{.1482}$	(37)	"
75	$(\pi_1) = .7241\ (\pi_6)^{.1254}$	(38)	"
100	$(\pi_1) = .6699\ (\pi_6)^{.1110}$	(39)	"
50 psi	$(\pi_1) = .3473\ (\pi_7)^{-.3129}$	(40)	A
100	$(\pi_1) = .3170\ (\pi_7)^{-.2455}$	(41)	"
200	$(\pi_1) = .2899\ (\pi_7)^{-.2308}$	(42)	"
300	$(\pi_1) = .2394\ (\pi_7)^{-.2546}$	(43)	"
50	$(\pi_1) = .4466\ (\pi_7)^{-.2443}$	(44)	C
100	$(\pi_1) = .4118\ (\pi_7)^{-.2515}$	(45)	"
200	$(\pi_1) = .3793\ (\pi_7)^{-.2469}$	(46)	"
300	$(\pi_1) = .3399\ (\pi_7)^{-.2214}$	(47)	"
50	$(\pi_1) = .7150\ (\pi_7)^{-.06403}$	(48)	E
100	$(\pi_1) = .6889\ (\pi_7)^{-.05716}$	(48)	"
200	$(\pi_1) = .6265\ (\pi_7)^{-.0418}$	(50)	"
300	$(\pi_1) = .5548\ (\pi_7)^{-.0345}$	(51)	"

The analysis shows that the value of the constant term C is of the form:

$$C = \frac{1}{\left[F\left(\bar{\pi}_2 \rightarrow \bar{\pi}_7\right)\right]^5} \tag{53}$$

Thus the prediction equation is of the form:

$$F\left(\pi_2 \rightarrow \pi_7\right) =$$

$$\frac{F\left(\pi_2, \bar{\pi}_3 \rightarrow \bar{\pi}_7\right) F\left(\pi_3, \bar{\pi}_2 \rightarrow \bar{\pi}_7\right) F\left(\pi_4, \bar{\pi}_2 \rightarrow \bar{\pi}_7\right) F\left(\pi_5, \bar{\pi}_2 \rightarrow \bar{\pi}_7\right) F\left(\pi_6, \bar{\pi}_2 \rightarrow \bar{\pi}_7\right) F\left(\pi_7, \bar{\pi}_2 \rightarrow \bar{\pi}_6\right)}{\left[F\left(\bar{\pi}_2 \rightarrow \bar{\pi}_7\right)\right]^5} \tag{54}$$

The equations constituting a test for the validity of Eq 54 are shown to be (see Appendix G):

$$\left\{ \frac{F\left(\pi_2, \bar{\pi}_3 \rightarrow \bar{\pi}_7\right) F\left(\pi_3, \bar{\pi}_2 \rightarrow \bar{\pi}_7\right) F\left(\pi_4, \bar{\pi}_2 \rightarrow \bar{\pi}_7\right) F\left(\pi_5, \bar{\pi}_2 \rightarrow \bar{\pi}_7\right) F\left(\pi_6, \bar{\pi}_2 \rightarrow \bar{\pi}_7\right)}{\left[F\left(\bar{\pi}_2 \rightarrow \bar{\pi}_7\right)\right]^5} \equiv \right.$$

$$\left. \text{or:} \quad \frac{F\left(\pi_2, \bar{\pi}_3 \rightarrow \bar{\bar{\pi}}_7\right) F\left(\pi_3, \bar{\pi}_2 \rightarrow \bar{\bar{\pi}}_7\right) F\left(\pi_4, \bar{\pi}_2 \rightarrow \bar{\bar{\pi}}_7\right) F\left(\pi_5, \bar{\pi}_2 \rightarrow \bar{\bar{\pi}}_7\right) F\left(\pi_6, \bar{\pi}_2 \rightarrow \bar{\bar{\pi}}_7\right)}{\left[F\left(\bar{\pi}_2 \rightarrow \bar{\bar{\pi}}_7\right)\right]^5} \right\} \tag{55}$$

$$\left\{ \frac{F\left(\pi_3, \bar{\pi}_2 \rightarrow \bar{\pi}_7\right) F\left(\pi_4, \bar{\pi}_2 \rightarrow \bar{\pi}_7\right) F\left(\pi_5, \bar{\pi}_2 \rightarrow \bar{\pi}_7\right) F\left(\pi_6, \bar{\pi}_2 \rightarrow \bar{\pi}_7\right) F\left(\pi_7, \pi_2 \rightarrow \pi_6\right)}{\left[F\left(\bar{\pi}_2 \rightarrow \bar{\pi}_7\right)\right]^5} \equiv \right.$$

$$\left. \frac{F\left(\pi_3, \bar{\bar{\pi}}_2 \rightarrow \bar{\pi}_7\right) F\left(\pi_4, \bar{\bar{\pi}}_2 \rightarrow \bar{\pi}_7\right) F\left(\pi_5, \bar{\bar{\pi}}_2 \rightarrow \bar{\pi}_7\right) F\left(\pi_6, \bar{\bar{\pi}}_2 \rightarrow \bar{\pi}_7\right) F\left(\pi_7, \bar{\bar{\pi}}_2 \rightarrow \bar{\pi}_6\right)}{\left[F\left(\bar{\bar{\pi}}_2 \rightarrow \bar{\pi}_7\right)\right]^5} \right\} \tag{55a}$$

The values $\bar{\bar{\pi}}_2$ and $\bar{\bar{\pi}}_7$ are values of π_2 and π_7 held constant at some value other than $\bar{\pi}_2$ and $\bar{\pi}_7$. Thus from the observed data:

$\bar{\pi}_7 = \frac{\rho V^2 D^2}{Z}$ @ V = 25 knots — the primary set of data, for example

$\bar{\bar{\pi}}_7 = \frac{\rho V^2 D^2}{Z}$ @ V = 50 knots

$\bar{\bar{\bar{\pi}}}_7 = \frac{\rho V^2 D^2}{Z}$ @ V = 75 knots — Supplementary sets of data

$\bar{\bar{\bar{\bar{\pi}}}}_7 = \frac{\rho V^2 D^2}{Z}$ @ V = 100 knots

If the supplementary sets of data satisfy either Eq. 55 or 55a, the general equation can be formed by multiplying the component equations together and dividing by the constant, as indicated in Eq. 54.

Another test of validity is to calculate the value of the constant C of Eq. 52. The test requires that any of the six component equations (see Table G-1) should yield an identical value for C. For reasons given in earlier paragraphs the two validity tests were assumed to be applicable. The value of constant C for each prediction equation was calculated from a product function of the values generated by six component equations of each set, see Appendix G. It should be emphasized here that these values of constants are theoretical and that the true values can only be generated from a complete set of controlled test conditions. Table G-2, Appendix G shows the calculated values of "C" for the 48 possible prediction equations and Table G-3, Appendix G shows the corresponding prediction equations. The four prediction equations in each set e.g. Eq. G-9, G-10, G-11 and G-12; Eq. G-13 - G-16 and so on (see the combination Table G-4) generated solutions that were within ± 1% of each other. It was therefore possible to average these 48 equations into 12 (prediciton) equations as shown in Table G-5. Each of these 12 equations is applicable to a type of surface i.e. A, C or E and a given velocity i.e. 25, 50, 75 or 100 knots. The next logical step was to determine if these equations were interchangeable for a given type of surface i.e. each equation being applicable for the full velocity range. The analysis showed that this could be achieved with full success in some equations and with partial success in others by modifying the velocity pi term. Accordingly, applicable equations were modified and are shown in Table 7.

Table 7.—Summary of Prediction Equations

Surface Type	V* Kn	EQUATION	Equation Number
A	25	$(\pi 1) = 1.1619\ (\pi_2)^{.7046}\ (\pi_3)^{.1200}\ (\pi_4)^{-.0714}\ (\pi_5)^{.3089}\ (\pi_6)^{.1117}\ (\pi_7)^{-(.2609 + .00946\ \Delta V)}$	(52)
C	25	$(\pi_1) = 1.3039\ (\pi_2)^{.7046}\ (\pi_3)^{.1200}\ (\pi_4)^{-.0742}\ (\pi_5)^{.0389}\ (\pi_6)^{.1665}\ (\pi_7)^{-(.2410 - .00076\ \Delta V + .00023\ \Delta V^2)}$	(53)
E	25	$(\pi_1) = 1.4157\ (\pi_2)^{.7046}\ (\pi_3)^{.1200}\ (\pi_4)^{-.1518}\ (\pi_5)^{.3089}\ (\pi_6)^{.1855}\ (\pi_7)^{-(.0493 + .00916\ \Delta V + .00024\ \Delta V^2)}$	(54)
A	50	$(\pi_1) = .9470\ (\pi_2)^{.7887}\ (\pi_3)^{.2501}\ (\pi_4)^{-.3347}\ (\pi_5)^{.6450}\ (\pi_6)^{.2002}\ (\pi_7)^{-(.2619 + .00988\ \Delta V)}$	(55)
C	50	$(\pi_1) = 1.1566\ (\pi_2)^{.7887}\ (\pi_3)^{.2501}\ (\pi_4)^{-.1864}\ (\pi_5)^{.6450}\ (\pi_6)^{.1602}\ (\pi_7)^{-(.2345 + .0007\ \Delta V + .0004\ \Delta V^2)}$	(56)
E	50	$(\pi_1) = 1.0724\ (\pi_2)^{.7887}\ (\pi_3)^{.2501}\ (\pi_4)^{-.1773}\ (\pi_5)^{.6450}\ (\pi_6)^{.1482}\ (\pi_7)^{-(.0468 + .01184\ \Delta V + .0004\ \Delta V^2)}$	(57)
A	75	$(\pi_1) = .6731\ (\pi_2)^{.7265}\ (\pi_3)^{.2234}\ (\pi_4)^{-.4113}\ (\pi_5)^{1.3555}\ (\pi_6)^{.2204}\ (\pi_7)^{-(.2612 + .0194\ \Delta V - .000193\ \Delta V^2)}$	(58)
C	75	$(\pi_1) = .5840\ (\pi_2)^{.7265}\ (\pi_3)^{.2234}\ (\pi_4)^{-.3820}\ (\pi_5)^{1.3555}\ (\pi_6)^{.1257}\ (\pi_7)^{-(.2411 + .05315\ \Delta V - .000834\ \Delta V^2)}$	(59)
E	75	$(\pi_1) = .4494\ (\pi_2)^{.7265}\ (\pi_3)^{.2234}\ (\pi_4)^{-.4004}\ (\pi_5)^{1.3555}\ (\pi_6)^{.1254}\ (\pi_7)^{-(.0493 + .0726\ \Delta V - .001\ \Delta V^2)}$	(60)

* Value used to derive the equation and $\Delta V = 0$ at V*

SECTION IV
MODEL TO RAW DATA CORRELATION

The prediction equations were next used to correlate back with the raw data used in the model formulation. A summary of errors in correlation is listed in Table 8.

For a given surface (type), the three prediction equations are interchangeable, alternate solutions for π_1, the dependent variable in the prediction equation. Thus Eq. 52, 55 and 58 are interchangeable although their prediction accuracies are different at different velocities (see Table 8). Similarly Eq. 53, 56 and 59 are interchangeable and so are Eq. 54, 57 and 60. Eq. 55, 56 and 57 yield the best results for the three surfaces at all velocities and are therefore the best solutions for use.

The formulation of the prediction equation has been accomplished with the use of dimensional analysis. A complex dynamic process has been defined by means of dimensional terms and the resulting equation appears with the general format

$$(\pi_1) = C_\alpha(\pi_2)^\beta\ (\pi_3)^\gamma\ (\pi_4)^\delta\ (\pi_5)^\epsilon\ (\pi_6)^\zeta\ (\pi_7)^\eta$$

where exponents $\beta, \gamma, \delta, \epsilon, \zeta, \eta$ and constant C_α are to be determined from experimental data and additionally C_α is a function of $\pi_2, \pi_3, \pi_4, \pi_5, \pi_6, \pi_7$. Thus, information about variables held constant (while varying one at a time) is mandatory to be able to calculate C_α and engineering judgement (reasonable assumptions) was made in the present analysis about missing numerical information. Therefore tests of validity cannot be performed unless test data is collected under fully controlled conditions for all parameters on a given tire.

Having established the prediction equation and assuming its validity, it can then be used along with the brake control simulator for airplane sensitivity studies to arrive at the effective μ_{wet} for a given set of conditions as shown in Figure 7. This information could then be transmitted to the pilot or the flight engineer or used in a fashion as deemed necessary.

Table 8.—Summary of Percentage Errors

Surface Type	Velocity Knots	Predicted (π_1) Using			Actual (π_1)	Percent Deviation From Actual Value		
		Eq. (52)	Eq. (55)	Eq. (58)				
A	25	.2496	.2483	.2495	.2496	0	-.5	0
	50	.2008	.1654	.1364	.1654	-	0	-
	75	.1101	.1088	.1114	.1114	-1.2	-2.3	0
	100	.0736	.0754	.0720	.0720	2.2	4.7	0
		Eq. (53)	Eq. (56)	Eq. (59)				
C	25	.5510	.5512	.5509	.5511	0	0	0
	50	.4518	.3644	.2831	.3644	-	0	-
	75	.2379	.2374	.2377	.2377	0	0	0
	100	.0971	.0970	.0970	.0970	0	0	0
		Eq. (54)	Eq. (57)	Eq. (60)				
E	25	.9730	.9340	.9755	.9730	0	-4.0	.3
	50	.9258	.5856	.3743	.5856	-	0	-
	75	.3707	.3571	.3708	.3708	0	-3.7	0
	100	.1053	.1054	.1056	.1054	0	0	0

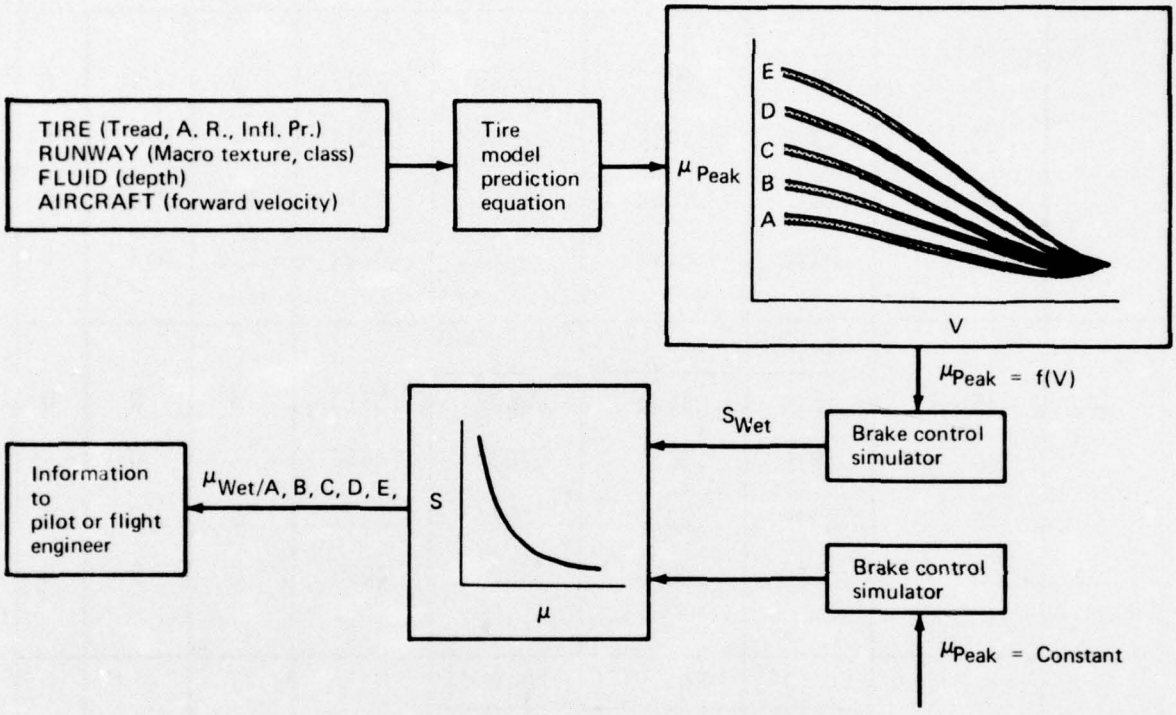

Figure 7.—Use of Tire Model

SECTION V
TEST PROGRAM RECOMMENDATIONS

As explained in Sections III and IV, the available tire test data is non-uniform. Data on aircraft tire, automotive tire, peak mu, locked wheel mu, yawed tire, braked rolling and many other conditions had to be mixed together to create data sets. Data gathering techniques are only partially defined or completely missing from most reports. Numerical values for parameters that were invariable during the experiments are quite often missing or defined qualitatively e.g. damp; smooth concrete etc. It is therefore imperative that a uniform set of data be generated under fully controlled conditions to validate the prediction model. With this in mind a test program has been outlined as follows.

1. PURPOSE OF TEST:

- To conduct tire testing under fully controlled conditions i.e. being able to vary one parameter at a time while holding all other parameters at fixed values.
- Investiage Type VII aircraft tires under various loads, inflation pressures, water depths, runway textures, tread depths, aspect ratios, forward speeds and at peak conditions of operation.
- Use this experimental data to validate and improve the tire correlation model.

2. TEST SPECIMEN AND RELATED EQUIPMENT:

The recommended list of tire sizes, design, and needed equipment has been prepared to be compatible with the need to cover most applicable ranges of aircraft operations. Restrictions on maximum tire size have been imposed by the capabilities of existing facilities as explained later. However, all but two aircraft tire sizes (B-52, and DC-10-30) in use today are covered by this range. The need for various equipment is obviously related to the test procedure dictated by dimensional analysis and desired accuracy for the model validation.

A list of Recommended Test Specimen and Related Equipment follows.

- 4 sizes of tires: 20, 30, 40 and 50 in. O.D. (for example)
- Tires to have 4 or 5 circumferential grooves
- Means of maintaining small water depths from .01" to .10"
- Means of preparing and maintaining different textures
- Means of monitoring tread groove depths
- Means of hunting for peak friction
- Means of inducing brake cycling e.g. @ 10 to 20% slip-ratio
- Tires of identical O.D. but different aspect ratio

3. TEST CONDITIONS

Table 9 shows the number of conditions needed to be run for each tire specimen and each type of surface for a meaningful validation of the tire model. Some other aspects of recommended testing are as follows:

- Range of loads: may be extracted from applicable aircraft (using that particular tire) operations manual.
- No. of runs: Ideally all possible combinations of interrelated variables (π terms) should be run. This would amount to several thousand test runs. The test program has been outlined such that it would satisfy the absolutely necessary data requirements for verification of the model with minimum cost.
- It is realized that tires have maximum inflation pressure ratings and maximum load ratings. Thus not all tires can be inflated to 300 psi. Two alternatives are available. The tire manufacturers recommended range could be divided into five equal segments thus keeping the number of runs constant, or the number of runs could be reduced by just running the tire in 50 psi increments up to its maximum limit.
- Depending on the available length of test strips, more than one surface could be tested in the same run e.g. ref. NASA TN D-4323. Thus if 3 surfaces were tested in each run, the number of runs could be reduced by 50%.
- Aspect Ratio Variation: This aspect of the program might be somewhat tricky or even difficult to achieve i.e., to vary the AR on a constant diameter tire. One precedent is the Type VII and LXX tires tested for the B737 program. (See refs. 53 and 54.) One solution might be to run these two tires again (for the A. R. testing at least) and have another pair of tires of identical diameter but of different size than 737 tires. This would at least give trends if not a conclusive result about the effect of the A. R. on μ wet.

Table 9.—Test Conditions

Tire size	d_{tx}	d_{tr}	in.	A.R.	Infl. PR. psi	Velocity ~ knots	No. of runs
20" O.D. (TIRE I)	A	NEW 80% 60% 40% 20% 60%	.02 .04 .06 .08 .10 .06	.65 .75 .80 .85 .95 .80	300 250 200 150 100	125 100 75 50 25	5

- 85 conditions to be repeated for tires II, III, IV each
- 85 x 4 conditions to be repeated for surfaces B, C, D, E each
- Total no. of conditions to be run = 85 x 4 x 5 = 1700
- Total no. of runs needed if 3 surfaces in one run = 680

4. DATA ANALYSIS:

The data collected from the test program should be analyzed in a manner identical to that used in handling the existing tire test data. The data is to be used to conduct the two validity tests for model formulation with 7π terms. Effort should be made to eliminate or combine some of the π terms to reduce the complexity of the model. This will depend upon the degree of influence of each term on the dependent variable "π_1". More precise curve fitting techniques should be used to arrive at component equations. This will assure better accuracy in the calculation of exponents and constants which in turn would yield a more accurate prediction equation. Efforts should also be made to convert the prediction equation solution into a graphical solution form; a nomograph or a carpet plot, e.g., figure 8, to give a better understanding of in practice use of the model. If this multifaceted analysis indicates need for additional tire testing, that would simplify the model for instance, or help better understand the interface phenomena, recommendations should accordingly be made.

5. TEST FACILITY EVALUATION

As part of the contract requirements, the recommended tire test program was to be considered for existing test facilities and still be in line with the philosophy emerging for tire correlation. The tire test facilities at NASA Langley Loads Track, Hampton, Virginia and the Naval Air Test Facility, Lakehurst, New Jersey were visited for this purpose. The two facilities were evaluated for their test capabilities and compatibility with the desired test conditions. The facilities are described in some detail in Appendix H. A comparative evaluation is depicted in Table 10. Basically both facilities can be used with minor modifications for the intended testing. In addition, the following observations are thought to be relevant:

NASA LANGLEY LOADS TRACK

The test surface preparation work has to be subcontracted as in the past. The test personnel are experienced in conducting the recommended testing and fully understand Project "Combat Traction". It takes about 30 to 40 minutes to pump the water out after each run. Instrumentation will have to be installed for induced cyclic braking. The test carriage doesn't carry any extra dead weight and thus its inertia cannot be manipulated. Masking effects have proven to be a major concern in past testing and some corrective measures would be needed to obtain meaningful data.

NATF, LAKEHURST

An acceleration test track has recently been modified for the purpose of tire testing. The test surface is presently only 200 feet long, but sufficient space is available to expand it to a 1000 feet. A series of 30" wide slabs constitute the test bed and can be turned around or upside down. This can help reduce the masking effect problem if a transverse travel mechanism for tires could be designed. Slabs are poured (and prepared) at the test site and any desired texture can be obtained but no surface wetting system has yet been installed. Speeds of up to 200 knots can be achieved and a typical velocity decay of 2 knots has been measured on the test site. Up to 18 runs per day have been made in the past. The facility requires about twice as many people for operation as the NASA Langley Loads Track. Tires up to 50" O.D. can be accomodated. The facility is available for governmental agencies and industry use.

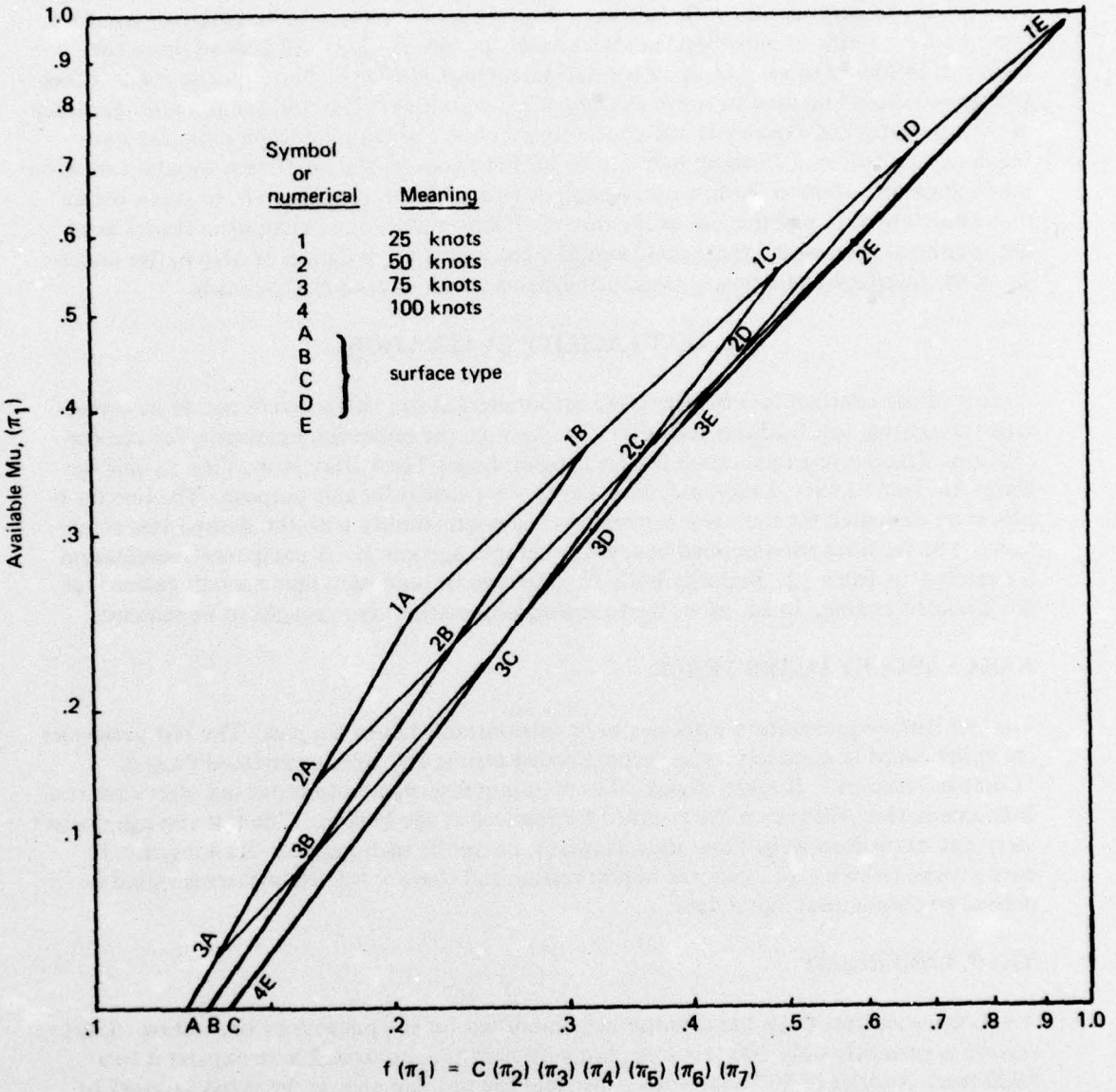

Figure 8.—Nomograph Solution of Prediction Equation

Table 10.—Existing Tire Testing Facilities Comparison

Evaluation criteria	NASA Langley, VA	NATF, Lakehurst, N.J.
Test strip	1100' x 15"	200' x 30"
Possible extension	No	Yes, 1000'
Texture	200 to 300' strips	Slabs 10' x 30"
Max speed	105 knots	200 knots
Velocity decay/run	8 knots	2.5 knots
Estimated no. of runs/day	8	16
Tire O.D. (max)	50"	50"
Masking effect	Yes	Yes
Instrumentation	Self contained	Telemetry

SECTION VI
SPECIFICATION OF FRICTION PREDICTION SUBSYSTEM

An overall picture of a Friction Prediction Subsystem (FPSS) concept is shown in Figure 9. The tire correlation concept was presented in Figure 2 while the ground vehicle development criteria are depicted in Figure 10. As details of the tire model development have been covered in Section III, the scope and requirements for a ground vehicle as a part of the FPSS are discussed in this section.

1. SCOPE:

This specification covers the general requirements for a Friction Prediction Subsystem (FPSS). The specification lists the basic ingredients of the design and the mode of operation of the subsystem. The specification has been developed based on reference 1 results (the airplane sensitivity analysis) and the tire correlation concept developed under Task Ia. of the persent contract.

The system covered by this specification is intended only for use in evaluation of tire-runway friction forces and to provide guidelines in determination and correlation of coefficients of friction on various airport surfaces.

The method utilizes a measurement representing the steady state friction force on a rolling test wheel as it is braked over a wetted pavement surface under constant load and at a constant/variable speed while its major plane is parallel to its direction of motion and perpendicular to the pavement.

2. GROUND RULES

1. Development must be consistent with the approach used in Combat Traction II, Sensitivity Analysis.

2. Only a measurement of the peak Mu is meaningful as it will be used in the prediction equation.

3. Sufficient difference exists in the construction of automotive and aircraft tires, that only an aircraft tire should be used on the ground vehicle.

4. The selected tire should be exposed to the static load it is designed to carry at the recommended inflation pressure and deflection.

5. Tire operation on the ground vehicle must duplicate dynamic conditions of aircraft tires. This dictates the use of an antiskid system or similar device for operation near peak friction.

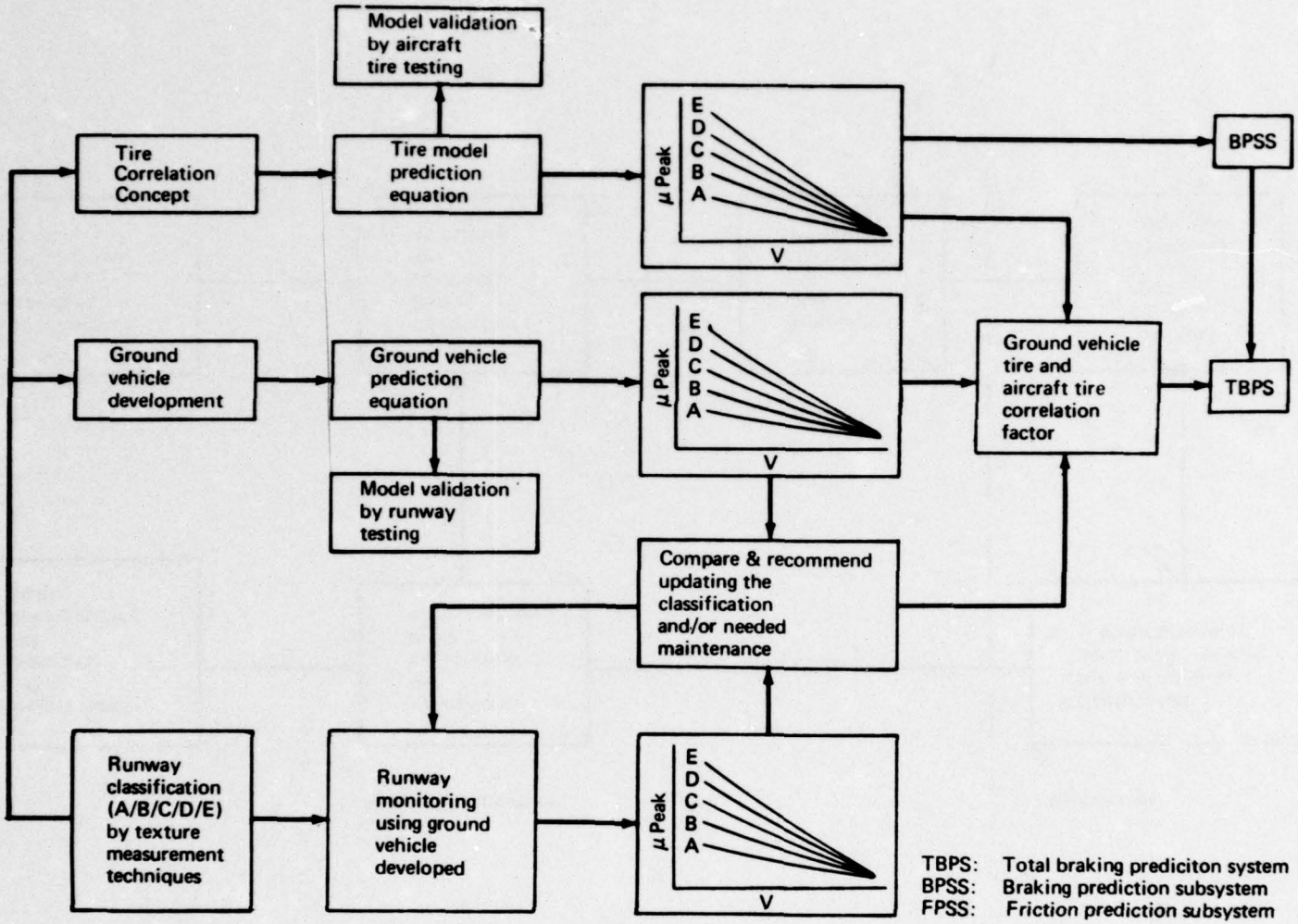

Figure 9.—FPSS Concept

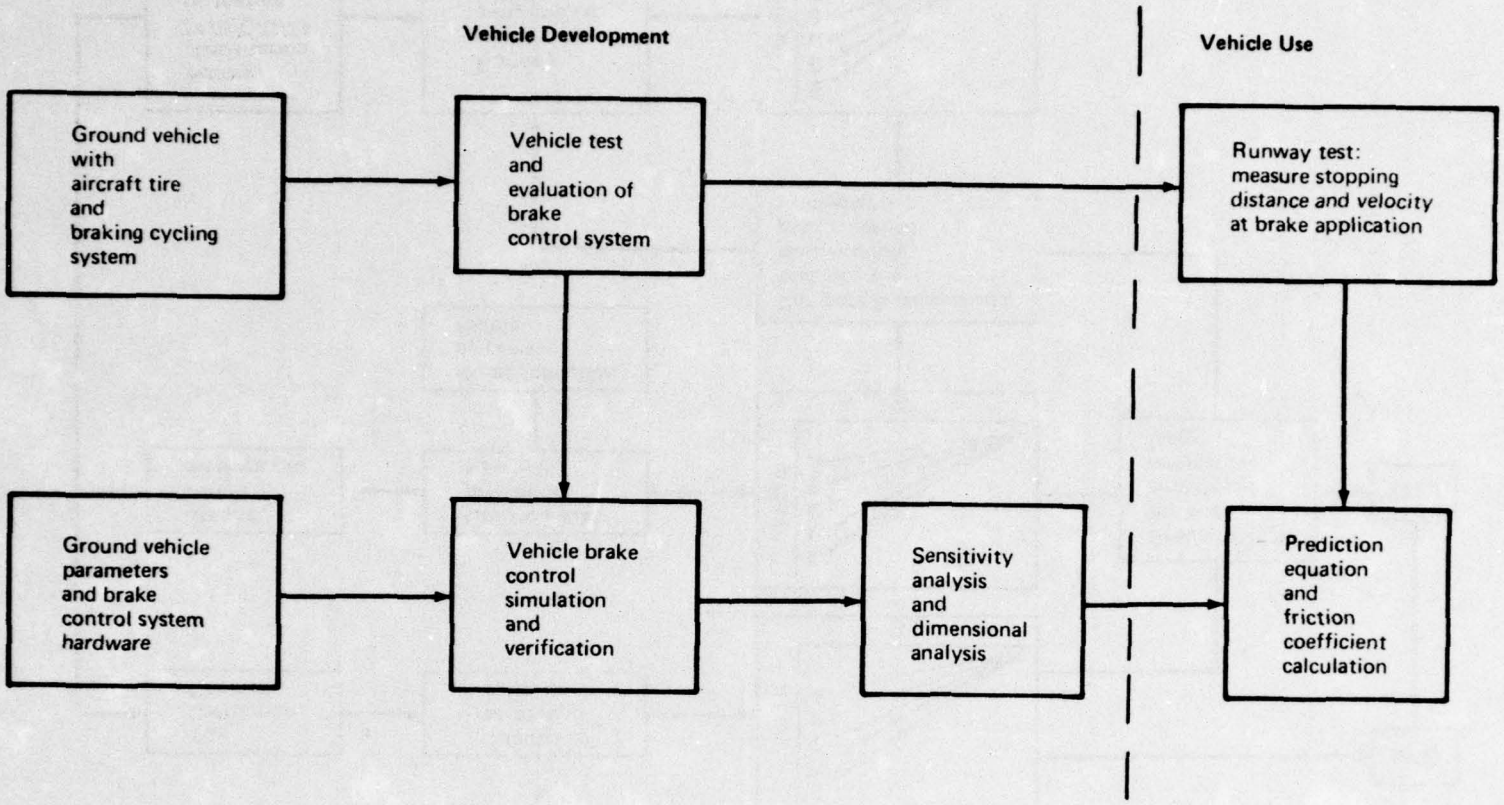

Figure 10.—Ground Vehicle Criteria for FPSS

3. TIRE

The manufacturers recommended loading condition of the tire will dictate the weight and size of the vehicle. A large tire will demand a prohibitivly large weight in simulating the proper loading condition. Therefore, small aircraft tires are recommended. With the development of a tire correlation model the evaluation results of a small tire can be scaled to any tire size. A suitable candidate appears to be for example the 16 x 4.4 - 4PR type VII tire used on the Aero Commander rated at 1100 lbs and 55 psi inflation pressure.

4. FRICTION PREDICTION SUBSYSTEM REQUIREMENTS

The Friction Prediction Subsystem (FPSS) consists of a runway evaluation trailer and a towing vehicle.

1. The trailer shall be supported by one aircraft tire and two automotive tires.

2. The aircraft tire shall be used for friction evaluation of the runway and carry a nominal load of no less than 1000 lbs.

3. The aircraft tire shall be fitted with a suitable wheel and brake.

4. The brake on the aircraft tire shall be capable of generating a locked wheel condition under all anticipated operational conditions.

5. The brake shall be actuated by hydraulic power and shall be controlled by an antiskid system.

6. The antiskid system shall be capable of maintaining a stopping efficiency of 85% or better over all operating conditions.

7. The suspension system of the evaluation tire shall maintain normal tire ground contact when operating on a prepared runway at all FPSS operating speeds.

8. The trailer shall be equipped with an instrumentation and recording system capable of measuring the following:

   a. True vehicle velocity

   b. Distance traveled during trailer braking

   c. Towing force between trailer and tow vehicle

9. The instrumentation and recording system shall have an accuracy of at least ±2%. Internal calibration shall be provided.

10. All systems on the trailer shall be self-contained and shall be powered by the tow vehicle's electrical supply.

11. The towing vehicle shall be capable of attaining a speed of 70 MPH when pulling the unbraked trailer on a level runway.

12. The towing vehicle shall be capable of accelerating the unbraked trailed to 70 MPH in a distance of less than 1000 ft.

13. The towing vehicle shall be a conventional automobile or truck equipped with a control panel to permit the start and stop of the recording equipment, and the initiation of the trailer braking. A display panel shall indicate the brake application speed and the braking distance. A display of towing force as a function of vehicle speed shall also be recorded and used later for monitoring of runway friction condition.

14. In operation the vehicle and trailer shall be accelerated to 70 MPH as quickly as possible on the test runway. Then the clutch of the towing vehicle shall be used to disengage the engine. Once this is accomplished, full braking with the evaluation trailer shall commence and continue until a full stop is reached. The vehicle speed and towing force shall be recorded continuously during braking. The vehicle shall maintain a straight path down the runway during the braking run.

15. A braking prediction equation shall be developed by computer simulation, vehicle tests, and dimensional analysis for the calculation of stopping distance. This equation shall be based on the measured brake application speed, friction coefficient, and other parameters unique to the vehicle. In order to prove the validity of the ground vehicle, similarity to the airplane prediction equations must exist.

5. FRICTION PREDICTION SUBSYSTEM APPLICATION

The FPSS will be used to measure and monitor runway friction. In applying the friction coefficient to the airplane prediciton equation a tire correlation factor must be used to modify the friction value. This is necessitated by the difference in tire size and speed range between the ground vehicle and airplane. The concept for correlating tire friction data has been developed but must still be proven by extensive testing. The application of the FPSS and the tire correlation factor to the total braking prediction system is shown in Figure 11. The Mu value used in the airplane brake distance prediction equation must be developed with the brake control simulator for a wet runway. This value is developed by using a velocity-dependent Mu (wet) and comparing the resulting braking distance to that computed with a constant Mu. Each velocity dependent Mu curve will represent a particular runway under particular environmental conditions and state of wear and tear and will have an "equivalent" velocity independent Mu for each airplane. Such data can be developed on a matrix basis for a series of airplanes and measured runway conditions.

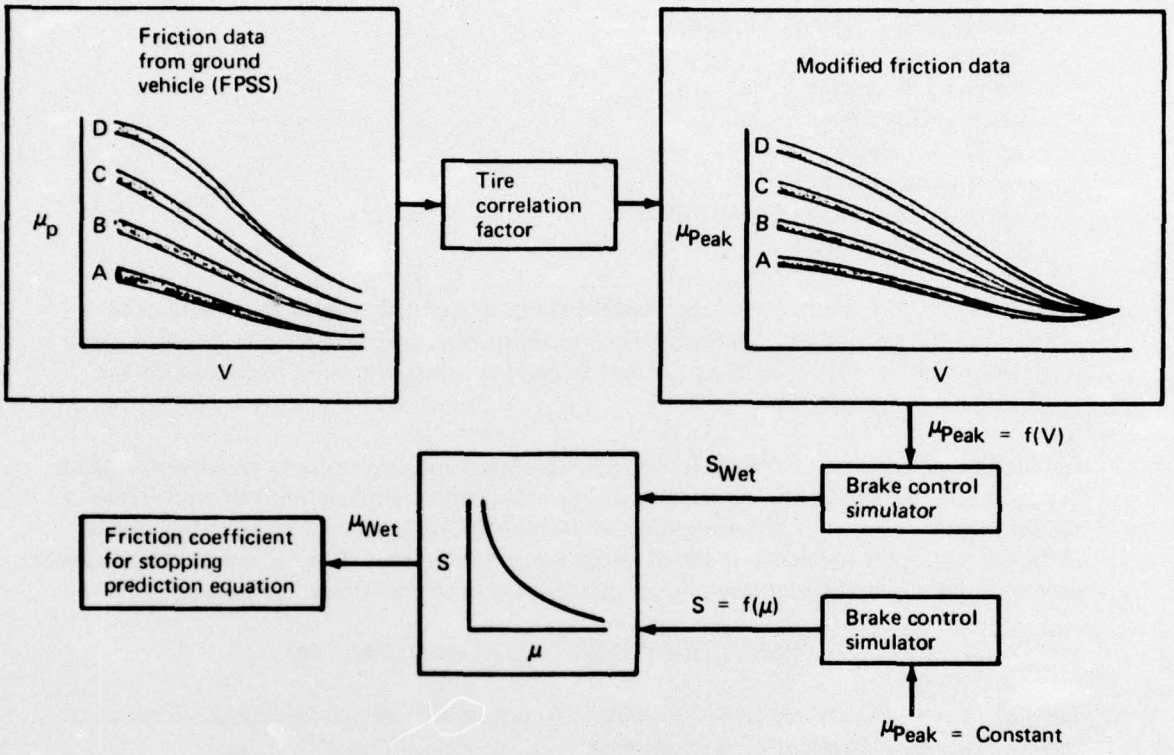

Figure 11.—Total Braking Prediction System

SECTION VII
REVIEW OF VEHICLES AND MODIFICATIONS

The requirements for the Friction Prediction Subsystem (FPSS) developed in Section VI are compared to the operational conditions and designs of several existing ground vehicles such as:

Diagonally Braked Vehicle (DBV)
ASTM Skid Trailer (Test Method)
French Stradographe
French LPC Trailer
British Miles Trailer
British Mu-Meter
Swedish Skiddometer
James Brake Decelerometer (JBD)
British Tapley Meter

Evaluation of the vehilces includes a consideration of the basic design, the operational aspects and the type of data presently developed during a typical test run. Possible modifications to the existing measuring systems to meet the recommended requirements for the FPSS are also discussed.

Detailed description of each vehicle's design, operation and type of data developed is given in Appendix I. A comparison summary of important differences among various vehicles is shown in Table 11. A general evaluation of all vehicles has been made and various points of view of different segments of the industry are presented first. This is followed by another evaluation of the vehicles by the criteria established under this study, Section VI.

1. RESULTS OF THE ICAO STUDY (REF. 56)

The objective of the program was "to define the degree of correlation that exists between various types of equipment used in the measuring of runway braking action."

The speed/friction curves show some variation between equipment when the results are compared between types of surfaces. The high reading of the skiddometer may be due to the use of patterned tires. In general the LPC - trailer gave the lowest values and different by a considerable amount from the Miles-trailer which is of similar construction. The Mu-Meter and Stradographe tended to be fairly close in their readings at 40 mph. The Miles-trailer tended to be insensitive to water depth. For example, the reading changed from .44 to .38 at 40 mph on polished concrete for a water depth increase from .011 inches to .067 inches respectively (the latter coming in the flooded range). On fine textured asphalt the Miles-trailer at 40 mph gave hardly any change of reading when the water depth increased from .015 inches to .032 inches.

The DBV ratios showed very little change for variation in water depth on the Crowthorne surfaces or on the French surfaces e.g. (a) on fine textured asphalt the SDR "wet-to-dry" Stopping Distance Ratio increased from 1.44 to 1.62 for an increase in water depth from .013 inches to .067 inches, respectively (b) on polished concrete the SDR became *smaller*

Table 11.—Differences in Ground Vehicle Friction Measuring Devices

Vehicle	Tire size	Tread pattern	Tire pressure	Type of friction measured	Operational mode of measurements
DBV	7.5 x 14	Smooth	24 psi	Skid	Continuous skid 60 mph to stop.
A STM (std.)	7.50 x 14	Smooth	24	Skid	Continuous skid 40 mph to stop.
Stradographe	6.10 x 15.75	Smooth	Not available	Skid or variable slip	Intermittent—skid out—selected speeds from 105 mph to zero.
LPC trailer	6.5 x 15	Smooth	N.A.	Skid	Intermittent skid @ selected speeds from 85 mph to zero.
Miles trailer	4 x 16	Patterned	20	Skid	Intermittent skid at selected speeds from 100 mph to zero.
Mu-meter	4 x 16	Smooth	10	Side force toeout angle 7½%	Continuous measurement at 40 mph fixed speed.
Skiddometer	4 x 16	Treaded	17	Fixed slip (17%)	Continuous measurements at 40 mph fixed speed.
JBD	–	–	–	Skid	Maximum deceleration measured @ 25 mph.
Tapleymeter	–	–	–	Skid	Maximum deceleration measured @ 25 mph.

when the water depth increased from .011 inches to .067 inches, (c) on Chateauroux brushed concrete the SDR increased from 1.56 to 1.72 when the water depth increased from .013 inches to .056 inches, respectively.

The report concluded that a great lack of precision is evident among the measuring devices tested. Even greater lack of precision is evident at the lower test speeds (under 40 mph) and on the lower friction surfaces.

2. FAA EVALUATION TEST (REF. 57)

Figure 12 shows FAA's reported water depth data and NASA-DBV measured SDR values. The measured data as reported in FAA concorde special condition test report (ref. 57), clearly points out to the inability of DBV to correlate with measured water depth data.

3. VARIOUS POINTS OF VIEW:

ALPA's POINT OF VIEW: (REF. 62)

Strenuous efforts over many years have gone into the development of specialized vehicles which would provide accurate indications of runway slipperiness. Vehicles which have been developed for this purpose include the Tapley Meter, the James Brake Decelerometer used by the United States Air Force in determining runway condition readings (RCR), the Swedish Skiddometer, and the Miles Single-Wheel Braking Trailer. Most of these vehicles attempt, by means of one clever technique or another, to measure values of pure μ. However, some measure at only one speed whereas others measure over a range of speeds; some measure values of sliding μ; others measure peak μ; some measure a combination of rolling resistance and side force; and many provide dramatic differences in their readings even on the same surface. The task has proved to be enormous and very complex, but most discouraging of all, results almost always have poor correlation with airplane performance.

FAA'S POINT OF VIEW (REF. 63) GROUND VEHICLE FRICTION MEASURING DEVICES.

What progress has been made to resolve the controversy over an acceptable method for measuring runway surface friction, and to derive a meaningful relationship of this measurement to aircraft stopping performance? A great deal of research and investigation has been conducted over the past ten years to establish a technology base that considers all aspects of runway surface friction characteristics and associated measuring devices. The two most frequently mentioned ground measuring vehicles in this country are the DBV, and the British developed Mu-Meter. Several other devices have been developed; however, these two appear to have the best potential for acceptance in the United States. Their operational mode of measurement and physical profiles are different, which has been the dominant factor in the current controversy over this subject.

Unfortunately, test results on all friction measuring devices have shown minimal relationship for the purpose of predicting aircraft stopping distances. Notwithstanding the Mu-Meter's limitations, it does provide an effective engineering and maintenance tool for the airport owner's use in determining the condition of his runways. The marginal surface areas can then be treated so as to improve their antiskid properties to an acceptable level.

Ref: Rep. # FAA-FS-160-74-2

TABLE VII Ground Vehicle Correlation Test
Roswell, N. M.
Runway 03, Oct. 22, 1973

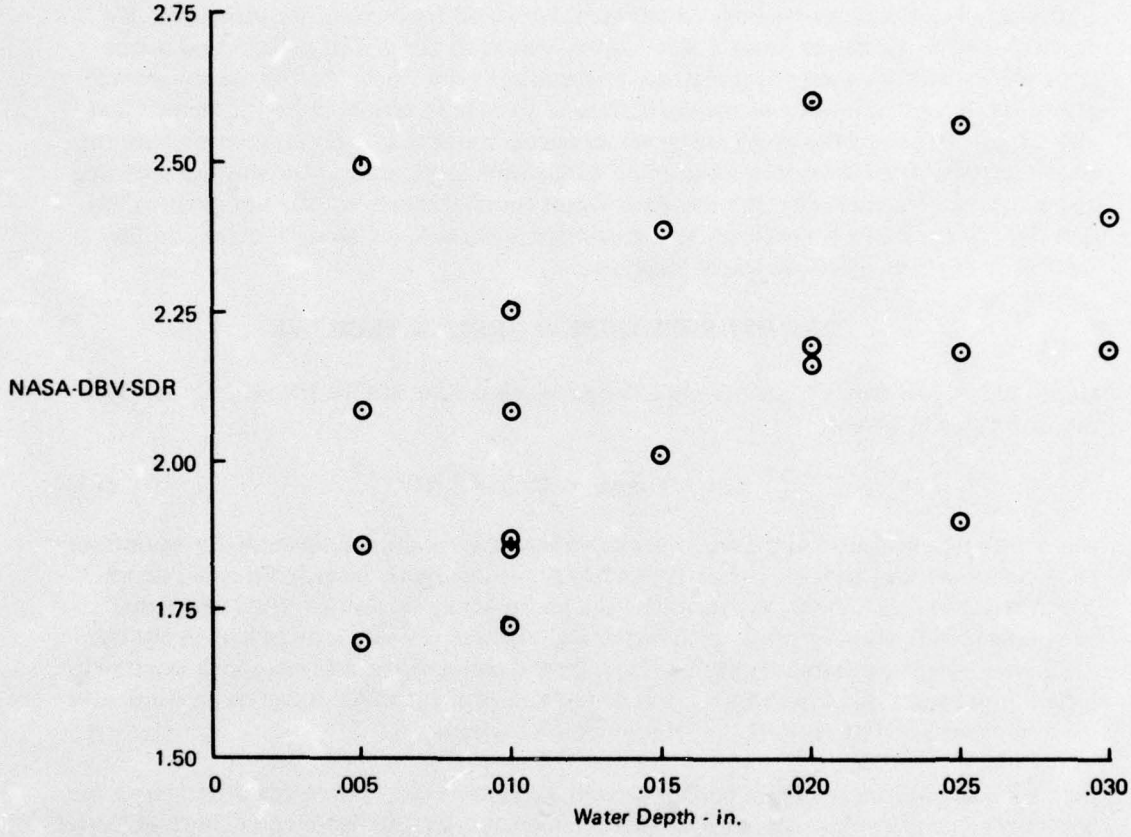

Figure 12.—DBV Correlation with Water Depth

U. K. CAA'S POINT OF VIEW (Reference 62)

The United Kingdom Civil Aviation Authority (CAA) observers were present at the B-727 and DC-9 tests (joint NASA, USAF, FAA tests, Combat Traction II, Phase I), and have examined a new method of analysis of the tests results relating to the test aircraft and the DBV/Mu-Meter. Their report provides details of a method for predicting aircraft stopping distance based on the calculated friction coefficient (aircraft mu), calculated aircraft deceleration and the Mu-Meter reading. In addition, a method is proposed for using the DBV deceleration related to the aircraft deceleration instead of the wet/dry stopping distance ratio and the aircraft energy/dry distance relationship. The British (CAA) theory promulgates that the determination of the coefficient of friction experienced by the aircraft and also the calculation of the deceleration values appear to show a better correlation with the Mu-Meter/DBV than the direct comparison with stopping distance or the wet/dry stopping distance ratio. Furthermore, in using these terms (mu/deceleration), the test results show that the types of runway surfaces, type of contaminant, and the use of new tires on the aircraft can have an effect on the correlation.

4. TIRE HYDROPLANING & GROUND VEHICLES

Horne and Joyner (ref. 64) give the following empirical equation for the velocity at which the hydroplaning begins:

$$V \text{ mph} = 10.35\sqrt{p_i}\,(\text{psi}) \qquad (62)$$

(p_i = inflation pressure) but the authors stress that this equation holds only for smooth or close-patterned tires, and for ribbed tires when the water depth exceeds the grove depth. Allbert (ref. 41) has shown, however, that the minimum hydroplaning speed of a radial tire on an indoor drum increases with increasing inflation pressure only as long as the tire deflection is kept constant; at constant load, hydroplaning speed decreases with increasing inflation pressure. Allbert also cites (ref. 41) instances of hydroplaning of worn truck tires on certain road surfaces at half the velocity predicted by eq. 62.

Figure 13 taken from reference 65 compares the results obtained for a smooth or worn tire with Horne's equation. It can be seen that even when total spin-down was compared to the equation, the hydroplaning inception speeds were far below those predicted. The study concluded that it is extremely difficult, if not impossible, to derive an equation for hydroplaning velocity that would fit all tires under varying conditions. Incidently, the data shown in Figure 13 is for a tire size 7.75 x 14 (smooth) whereas the tire size used on the DBV is 7.50 x 14 (smooth).

Thus the claims made by proponents of the DBV and the Mu-Meter that the tires used on these vehicles are capable of indicating hydroplaning (see description, Appendix I) situations on the runway are questionable.

5. ASTM SKID TRAILERS

Application of complex empirical test methods usually results in problems of test data reproductibility; application of ASTM E274 has proven to be no exception. Meyer et al

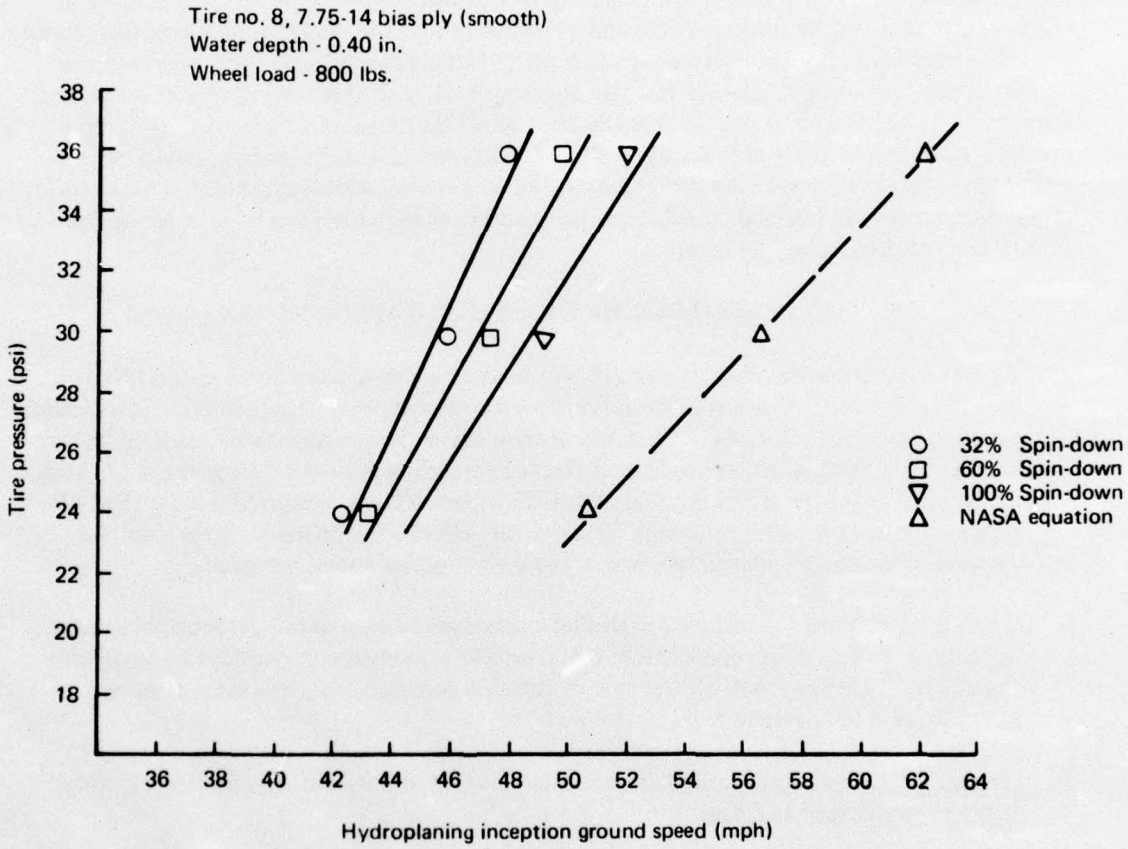

Figure 13.—Comparison of Experimental Results to NASA Equation

(ref. 66) made a comprehensive study to determine how reproducibility under ASTM E274 might be improved. Among other things they concluded that "Because skid testers operate at relatively high speeds, the ultimate calibration should be a dynamic one using surfaces of known and invariable friction properties."

The skid number of a particular pavement is not a constant but varies with a number of factors. The major factors are vehicle speed, surface moisture conditions, and polishing of the pavement under traffic conditions. The locked-wheel skid number at a speed of 40 mph determined by ASTM trailers has been widely used as indicative of available friction. For most pavements it is actually indicative of available friction in the locked-wheel mode at that particular time at a trailer speed of 40 mph. For many pavements the skid number is highly dependent on the testing speed, and at higher speeds the ASTM trailer skid tester may actually give misleading results because the trailer's internal watering system does not adequately wet the surface before the test tire encounters it. For this reason, much of the skid number data determined at high speeds (more than 40 mph) may be biased. That is, skid numbers determined at 60 mph by using the ASTM trailer internal watering system may be higher than the skid number determined by using an external watering system. One example of an external system is a tank truck depositing water on the pavement in advance of the skid tester. Another example is rain.

6. ACCELEROMETER METHODS (JBD/TAPLEY METER)

a. The braking qualities of a runway can be obtained by measuring the deceleration force resulting from the application of brakes to a moving vehicle. One technique is to install an accelerometer in a truck. The truck is then driven at a certain speed, full brakes are applied, and the maximum reading of the accelerometer is noted during the skid. If the instrument is set to record the maximum value, the value so recorded will be that which occurs just as the brakes are applied before the wheels start to skid. If the damping characteristics of the instrument are suitable this will be a measure of μ_{max}.

b. Tests have also been conducted with the accelerometer free to indicate instantaneous values, i.e. not set to record the maximum deceleration force; however, this procedure requires considerable skill on the part of the test personnel to get correct readings. (See Figure I-19, Appendix I).

c. The accelerometer test method gives usable results but has some disadvantages, which can be summarized as follows:

   a) The actual operations test has to be carried out at a sufficient number of points on the runway to give an overall picture of the braking qualities of the runway as a whole. The time required for the complete test using the accelerometer mounted in a truck is some 3-4 times that required using the trailer method. A mean value for a runway has to be numerically computed, which requires some time.

   b) Training of the test personnel is necessary. Tests of type (b) are difficult to do correctly and therefore only (a) can be considered practical.

c) The truck will be exposed to high wear by the repeated locking of the wheels followed by acceleration to test braking speed.

d. The main advantage of the test method is that the equipment cost, other than that of a truck which will usually be available for other purposes, will be small, being of the order of $100.

7. FRENCH VEHICLES (STRADOGRAPHE/LPC TRAILER)

Not enough data or a documented description of either vehicle is available. Efforts to translate available pamphlets from French to English did not help much as it mostly turned out to be sales oriented material. However, the limited description indicates that the Stradographe might have more merit than other vehicles in that it is better instrumented, test wheel is isolated from the wagon and has variable slip mechanism. More detailed study as well as comparison with some aircraft test data is necessary before any conclusions can be reached.

8. DBV & MU-METER EVALUATION

Certain specification criteria were developed for friction measuring vehicles as a result of reference 1 study. Using these criteria both the DBV and Mu-Meter were evaluated. It was found that both performed their respective functions for which they were designed but failed to meet the vehicle criteria and thus data generated by these vehicles were of qualitative value only. In addition, model laws (based on pi terms developed for BPSS) were also applied to both vehicles and showed that one is a distorted model while the other a dissimilar one, both needing additional analytical and experimental work before they could be made suitable friction measuring devices.

9. MILES TRAILER

The Miles-trailer is used by the British and the American manufacturers for wet runway certification of aircraft to comply with British CAA regulations. It is not used at airports to obtain day to day measurements of runway braking action. The vehicle has been included here as it was used during an FAA evaluation of Proposed Landing Certification Rules, reference 57 study, and might be considered for further development.

10. SKIDDOMETER

The ICAO Study (ref. 56) data shows that the skiddometer and the Mu-meter have a strong correlation but the skiddometer indicates slightly higher values of friction probably because it uses a treaded tire. Thus the Skiddometer behaves much the same way as the Mu-meter.

11. EVALUATION OF VEHICLES BY THE FPSS SPECIFICATION

The FPSS specification developed in Section VI showed that the principal requirement remains to dynamically simulate the tire-runway interface by using a ground vehicle equipped with an aircraft type VII tire and use of an antiskid system (or similar device to induce brake cycling) to insure peak mu operation. When this criteria is applied to the vehicles under consideration it is clear that none of the vehicles meets this criteria and both principal requirements remain to be met.

12. POSSIBLE MODIFICATIONS

As pointed out in reference 1 study, proper distortion and prediction factors need to be applied when using distorted or dissimilar models. In addition, various ground rules laid out in Section VI for the vehicle development must be met to generate meaningful data. One simple approach to this effect is shown in Figure 14.

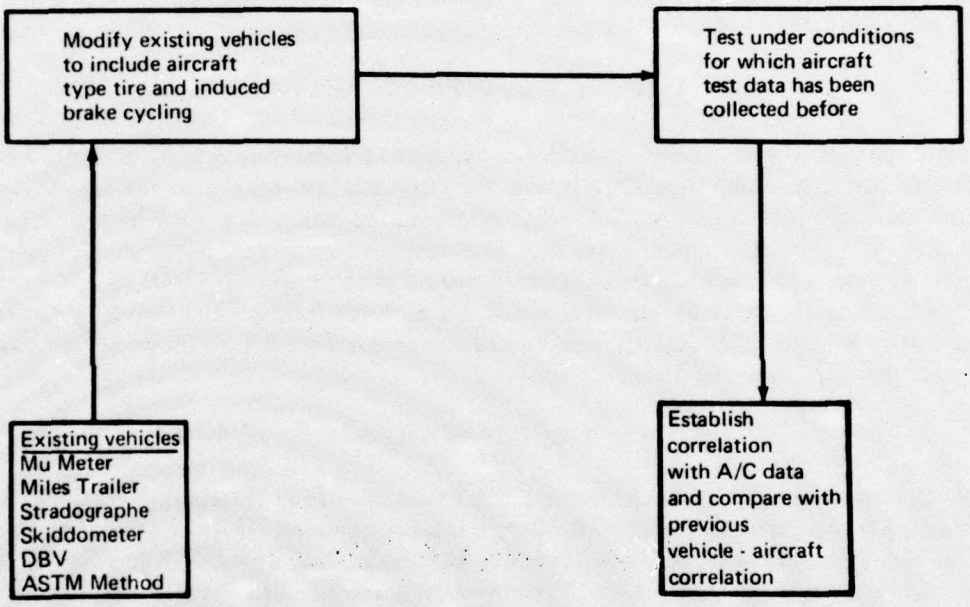

Figure 14.—Minimum Risk Validity Test For FPSS Concept

SECTION VIII
CONCLUSIONS AND RECOMMENDATIONS

It is to be noted that despite considerable progress in recent years, the tire traction literature still lacks a common focus or conclusion. Thus, at present there seem to be no generally applicable formulas that can be used reliably to design tires to obtain satisfactory operation under all conditions. Further, at best, the basic understanding of friction and wear and their control seems to be empirical.

For many years the tire-pavement interface studies have been undertaken by the tire engineer, tire chemist and pavement engineer mainly in isolation. The tire maker for example wants to know how to build a tire to last long, ride smoothly and above all not blow out. More cooperation between tire and pavement designers is a must.

The vast amount of data available in the literature has aided in the better understanding of the complex problem of tire-pavement interactions; however, the data have been primarily derived from different sources employing different methods. There is no comprehensible means of analyzing and comparing all the available data due to incompatibility of test conditions, measuring techniques, and the presence of numerous unspecified variables influencing the relative values of data obtained from different test programs.

Available tire test data is non-uniform. Data on aircraft tire, automotive tire, locked wheel μ, peak μ, yawed tire, braked rolling and many other conditions had to be mixed together for want of better data. Data gathering techniques are only partially defined or completely missing from most reports. Numerical values for parameters that were invariable during the experiments are quite often missing or defined qualitatively as wet, damp, flooded, smooth concrete etc.

- There exists need for more effort towards standarized calibration and watering techniques, and a need for studying the effect of suspension geometry and the dynamics of the vehicle involved.

- A good number of small and portable test devices have been developed. Some have been developed to aid in the studies of the resistance of road materials to polishing. Other devices were developed out of the conviction that adequate simulation of real tire-road behavior must be possible if a tester is designed from first principles.

- Skid trailers show a reasonably good agreement in their ability to measure pavement slipperiness. Differences are observed between the vehicles in their relative surface rating ability under wet conditions. More divergence is observed among the trailer results at higher speeds.

- Variation in results also occurs or is observed due to different test rubber/tire used, its size, amount of wetting etc.

- A much greater confidence in the skid results from different test techniques is needed, however, if these are to be used for routine testing and for maintaining a prescribed antiskid level for improved runway safety.

- The principal of dimensional analysis can be used to define the runway-tire interface problem and to predict available friction.

- The prediction equation approach seems to be workable within reasonable tolerances but more conclusive statements can only be made when more data becomes available and the model is tested for validity.

- Tire test data must be collected under fully controlled conditions. Therefore, the recommended test program under Section V must be carried out.

- In order for the FPSS concept to be operationally meaningful, the following areas of work have to be resolved in addition to carrying out the tire test work:

    - Classification of Runways

    - Runway Monitoring System Standarization

    - Ground Vehicle Development and Test

    - Enacting and Enforcing Regulations Regarding Proper Maintenance of Runway Friction Levels

    - Method of Measuring/Indicating Rainfall Intensity/Water Depth

APPENDIX A
SURVEY OF TYPE VII AIRCRAFT TIRES

The tire survey applies to the following:

1) Type VII or equivalent (new design, type VIII etc.) tires.

2) Airplanes with skid control systems only.

3) Main gear tire characteristics only.

4) Rated values for load, inflation pr. and speed are listed. The operational values are different (data not readily available)

5) All major airplanes in military and commercial use have been listed.

The information contained in Tables A1 through A3 was compiled from references 29 through 34.

Table A-1.—U.S. Military Aircraft with Type VII Tires Listed by Function Group

S NO.	AIRPLANE				TIRE CHARACTERISTICS (MAIN GEAR ONLY)								SKID CONTROL SYSTEM	
	MANUFACTURER	MODEL	POPULAR NAME	UTILIZED AS	TIRE SIZE	PLY RATING	ASPECT RATIO	SPEED MPH	RATED PRESSURE PSI	LOAD-LBS	TREAD DESIGN	TIRE TYPE	TYPE	SUPPLIER
1	Lockheed	F104, A,B C,D,J, DJ G (early)	Starfighter	Fighter	25 x 6.75	18TL	.84	275	300	10500	RR G	VIII	-	G
2	Lockheed	F104G	Starfighter	Fighter	26 x 8.0 - 14	16TL	.75	275	235	12700	RR	VIII	-	G
3	LTV	A7D	Corsair II	Fighter	28 x 9.0 - 14	22TL	.75	200	235	18100	Rib	VIII	MKIII	H
4	McDonnell-Douglas	F4B	Phantom II	Fighter	30 x 8.0	26TL	.86	248	360	24100	RR CP	VII	MKII	H
5	North American	F-100	Super Sabre	Fighter	30 x 8.8	22TL	.87	250	295	21000	RR	VII	-	H
6	McDonnell-Douglas	F4C,J	Phantom II	Fighter	30 x 11.50 - 14.5	24TL	.66	240	243	25000	RR CP	VIII	MKII	H
7	McDonnell-Douglas	F-15	-	Fighter	34.5 x 9.75 - 18	22TL	.85	-	-	-	-	-	MKIII	H
8	Fairchild Hiller	F105	Thunder-chief	Fighter	36 x 11	24TL	.83	160/250	235	26000	R/RR	VII	-	G
9	Grumman	F-14A	TomCat	Fighter	37 x 11.50 - 16	28TL	.91	180	245	31200	RR	ND	-	Bendix
10	General Dynamics	F-111A	-	Fighter	47 x 18 - 18	30TL	.81	225	175	43700	RR	VII	-	G
11	General Dynamics	B-58A	Hustler	Bomber	22 x 7.7 - 12	16TL	.67	275	280	10500	RR G	VIII	-	G
12	North American	XB70A	Valkyrie	Bomber	40 x 17.50 - 18	40TL	.63	-	-	-	-	VIII	-	SPAD
13	North American	B-1		Bomber	C44.5 x 16-21	-	.73	225	200	42500	RR	ND	MKIII	H
14	General Dynamics	FB111A	-	Bomber	47 x 18 - 18	36TL	.31	250	215	54600	RR	VII	-	G
15	Boeing	B47E	Stratojet	Bomber	56 x 16	36TL	.88	-	-	-	-	VII	MKI	H
16	Boeing	B52, F,G,H	Stratofor-tress	Bomber	56 x 16	38TL	.88	250	315	76000	RR	VII	MKI	H
17	Lockheed	C140A	Jetstar	Transport	26 x 6.6	14TL	.88	200	225	10000	R	VII	MKII	H
18	McDonnell-Douglas	C9A	-	Transport	40 x 14	24TL	.86	225	170	27700	RR	VII	MKII	H
19	Lockheed	C141	Starlifter	Transport	44 x 16	28TL	.80	200/225	185/200	38400	RR	VII		Bendix
20	Boeing	VC137C	-	Transport	46 x 16	28TL	.80	200/225	210	41800	RR	VII	MKII	H
21	Boeing	KC-135	Strato-tanker	Transport	49 x 17	26TL	.84	200/225	170	39600	R	VII	MKI,MKII	H
22	Lockheed	C5A	Galaxy	Transport	49 x 17	26TL	.84	200/225	170	39600	R	VII	MKII	H
23	LTV	A7A, B	Corsair II	Attack	28 x 9.0	22TL	.89	173	235	16650	R	VII	MKIII	H
24	Hawker Siddeley	AV-8A	Harrier	Attack	26.00 x 7.75-13	-	.84	-	-	-	-	British	Adaptive	Dunlop/ H[illegible]
25	North American	RA5C	Vigilante	RCCE	36 x 11	28TL	.83	200	290	31500	R	VII	MKII	H
26	Boeing	T-43A	737-200	Trainer	40 x 14	24TL	.86	200/225	170	27700	RR	VII	MKIII	H
27	Boeing	E-3A	707-300	AWACS	46 x 16	28TL	.80	200/225	210	41800	RR	VII	MKII	H
28	Boeing	E-4A/B	747-200	Command Post	49 x 17	30TL	.84	200/225	190	46400	RR	VII	MKIII	H

Table A-2.—U.S. Military Aircraft with Type VII Tires Listed in Ascending Tire Sizes

S. NO.	AIRPLANE				TIRE CHARACTERISTICS (MAIN GEAR ONLY)								SKID CONTROL SYSTEM	
	MANUFACTURER	MODEL	POPULAR NAME	UTILIZED AS	TIRE SIZE	PLY RATING	ASPECT RATIO	SPEED MPH	RATED PRESSURE PSI	LOAD-LBS	TREAD DESIGN	TIRE TYPE	TYPE	SUPPLIER
1	General Dynamics	B-58A	Hustler	Bomber	22 x 7.7 - 12	16TL	.67	275	280	10500	RR G	VIII	-	G
2	Lockheed	F104, A,B C,D,J, DJ, G (early)	Starfighter	Fighter	25 x 6.75	10TL	.84	275	300	13000	RR	VII	-	G
3	Lockheed	C140A	Jetstar	Transport	26 x 6.6	14TL	.88	200	225	10000	R	VII	MKII	H
4	Hawker Siddeley	AV-8A	Harrier	Attack	26.00 x 7.75-13	-	.84	-	-	-	-	British	Adaptive	Dunlop/Hytrol
5	Lockheed	F104G	Starfighter	Fighter	26 x 8.0 - 14	16TL	.75	275	235	12700	RR	VIII	-	G
6	LTV	A7A, B	Corsair II	Fighter	28 x 9.0	22TL	.89	173	235	16650	R	VII	MKIII	H
7	LTV	A7D	Corsair II	Fighter	28 x 9.0 - 14	22TL	.75	200	285	18100	Rib	VIII	MKIII	H
8	McDonnell-Douglas	F4B	Phantom II	Fighter	30 x 8.0	26TL	.86	248	360	24100	RR CP	VII	MKII	H
9	North American	F-100	Super Sabre	Fighter	30 x 8.8	22TL	.87	250	295	21000	RR	VII	-	H
10	McDonnell-Douglas	F4C,J	Phantom II	Fighter	30 x 11.50 -14.5	24TL	.66	240	243	25000	RR CP	VIII	MKII	H
11	McDonnell-Douglas	F-15	-	Fighter	34.5 x 9.75 - 18	22TL	.85	-	-	-	-	-	MKIII	H
12	North American	RA5C	Vigilante	RCCE	36 x 11	28TL	.83	200	290	31500	R	VII	MKII	H
13	Fairchild Hiller	F105	Thunderchief	Fighter	36 x 11	24TL	.83	160/250	235	26000	R/RR	VII	-	G
14	Grumman	F-14A	TomCat	Fighter	37 x 11.50 - 16	28TL	.91	180	245	31200	RR	ND	-	Bendix
15	McDonnell-Douglas	C9A	-	Transport	40 x 14	24TL	.86	225	170	27700	RR	VII	MKII	H
16	Boeing	T-43A	737-200	Trainer	40 x 14	24TL	.86	200/225	170	27700	RR	VII	MKIII	H
17	North American	XB70A	Valkyrie	Bomber	40 x 17.50 - 18	40TL	.63	-	-	-	-	VIII	-	SPAD
18	Lockheed	C141	Starlifter	Transport	44 x 16	28TL	.80	200/225	185/200	38400	RR	VII	-	Bendix
19	North American	B-1	-	Bomber	C44.5 x 16-21	-	.73	225	200	42500	RR	ND	MKIII	H
20	Boeing	VC137C	-	Transport	46 x 16	28TL	.80	200/225	210	41800	RR	VII	MKII	H
21	Boeing	E-3A	707-300	AWACS	46 x 16	28TL	.80	200/225	210	41800	RR	VII	MKII	H
22	General Dynamics	F-111A	-	Fighter	47 x 18 - 18	30TL	.81	225	175	43700	RR	VII	-	G
23	General Dynamics	FB111A	-	Bomber	47 x 18 - 18	36TL	.81	250	215	54600	RR	VII	-	G
24	Lockheed	C5A	Galaxy	Transport	49 x 17	26TL	.84	200/225	170	39600	R	VII	MKII	H
25	Boeing	KC-135	Strato-tanker	Transport	49 x 17	26TL	.84	200/225	170	39600	R	VII	MKI,MKII	H
26	Boeing	E-4A/B	747-200	Command Post	49 x 17	30TL	.34	200/225	190	46400	RR	VII	MKIII	H
27	Boeing	B47E	Stratojet	Bomber	56 x 16	36TL	.88	-	-	-	-	VII	MKI	H
28	Boeing	B52, F,G,H	Stratofor-tress	Bomber	56 x 16	38TL	.88	250	315	76000	RR	VII	MKI	H

Table A-3.—World's Major Aircraft (Commercial and Military) with Type VII Tires Listed Alphabetically by Manufacturer.

	AIRPLANE				TIRE CHARACTERISTICS (MAIN GEAR ONLY)								SKID CONTROL SYSTEM	
S. NO.	MANUFACTURER	MODEL	POPULAR NAME	UTILIZED AS	TIRE SIZE	PLY RATING	ASPECT RATIO	SPEED MPH	RATED PRESSURE-PSI	LOAD LBS	TREAD DESIGN	TIRE TYPE	TYPE	SUPPLIER
1	Aero Commander	AE1121	Jet Commander	Business	24 X 7.7	14TL	.92	200	135	8200	-	-	-	G (Goodyear)
2	Grumman Aircraft	-	Gulfstream II	Business	34 X 9.25 - 16	16TL	.98	200	155	15,500	Rib Reinf.	ND (New Design)	-	GY
3	Lear	23,24, 25	Learjet	Business	18 X 5.5	8TL/10TL	.87	180/200	105/140	3050/4000	RR CP	VII	MKII	GY, H (Hydroaire)
4	Lockheed	-6, -8	JetStar	Business	26 X 6.6	14TL	.88	200	225	10000	R (Rib)	VII	-	GY
5	North American Rockwell	40, 60	Sabreliner	Business	26 X 6.6	12TL/14TL	.88	200	185/225	8600/10000	R	"	-	GY
		70	"	"	22 X 5.75 - 12	10TL	.87	180	180	5700	RR	ND	-	GY
6	British Aircraft	-200, -400	BAC-111	Civil (Transport)	40 X 12	16TL/18TL	.87	180/200	130/150	18500/21000	RR	VII	MKI	GY, H
7	Boeing	707-120	707	"	46 X 16	24TL	.80	200	170	35700	RR	"	MKI	H
		707-320,B		"	"	26TL	.80	200/225	185	38300	RR	"	MKII	H
		707-320C		"	"	28TL	.80	200/225	210	41800	RR	"	MKII	H
		720/720B		"	40 X 14	24TL	.86	225	170	27700	RR	"	MKI	H
		727/100	727	"	49 X 17	26TL	.84	200/225	170	39600	R	"	MKII	H
		727 200C/QC		"	49 X 17	28TL	.84	200/225	180	43200	RR	"	MKIII	H
		727-200		"	50 X 20.0 -20	24TL	.75	200	135	38200	RR	ND	MKIII	H
		737-100	737	"	40 X 14	22TL	.86	200/225	155	25000	RR	VII	MKIII	H, GY
		737-200		"	40 X 14	24TL	.86	200/225	170	27700	RR	VII	MKIII	H
					C40 X 14.0 -21	22TL	.68	225	155	25400	RR	ND	MKIII	H
		747-100	747	"	46 X 16	28TL	.80	200/225	210	41800	RR	VII	MKIII	H
		747B	"	"	46 X 16	30 TL	.80	225	225	44800	RR	"	MKIII	H
		747-200/747B		"	49 X 17	30 TL	.84	200/225	190	46,400	RR	VII	MKIII	H
8	Canadair	CL144	-	"	40 X 12	22TL	.87	180	190	26700	RR	VII	-	Bendix
9	Convair	CV600		"	39 X 13	14TT	.86	LS	75	12800	R	"	MKIE	H
		880M		"	39 X 13	22TL	.86	200/225	165	24600	RR	"	MKI	H
		990		"	41 X 15.0 - 18	22TL	.77	200	170	28600	RR	ND	MKII	H
		990HW		"	41 X 15.0 - 18	24TL	.77	225	190	31,400	RR	"	MKII	H
9'	De Havilland (Canada)	DMC-6	Twin Otter	"	11.00 - 12	8	.903	120	45	6300	Rib	III	MK III	H
					15.00 - 12	10	.83	120	43	9500	AW	III	MK III	H
		DMC-7	QL 1185	"	30 x 9 - 15	18	.83	250	295	21000	RR	VII	MK III	H

Table A-3.—World's Major Aircraft (Commercial and Military) with Type VII Tires Listed Alphabetically by Manufacturer (Continued)

	AIRPLANE				TIRE CHARACTERISTICS (MAIN GEAR ONLY)								SKID CONTROL SYSTEM	
S NO.	MANUFACTURER	MODEL	POPULAR NAME	UTILIZED AS	TIRE SIZE	PLY RATING	ASPECT RATIO	SPEED MPS	RATED PRESSURE PSI	LOAD LBS	TREAD DESIGN	TIRE TYPE	TYPE	SUPPLIER
10	Dassault	Mystere 20	Falcon Myst.	Civil	26 X 6.6D	10TL	.88	200/225	150	6900	-	-	-	G
		1-70	Falcon	"	26 X 6.6D	10TL	.88	"	150	6900	-		-	G
		1-68	Falcon	"	26 X 6.6D	10TL	.88	"	150	6900	-		-	G
		10	Falcon	"	22 X 5.75 - 12	8TL	.87	-	130	4255	-		-	G
		Fan Jet -	Falcon Mercure	Civil "	29.5 X 9.15 46 X 16	- -	- -	- -	133 141	- -	- -	- -	- -	G SPAD
11	European Consortium	A300B	Airbus	"	46 X 16 -20		.81	-	-	-	-		-	SPAD
12	Fokker	F-28	-	"	39 X 13	14	.86	200	100	15000	RR	VII	-	G
		F-28(Flo)	-	"	40 X 14	14 1	.86	200	91	14900	-	"	-	G
13	Handley Page	-	Herald	"	34 X 11.75 - 14	12	.85	120	80	12000	-	-	-	G
14	Hawker-Siddeley	748	AVRO	"	34 X 11.75 - 14	12	.85	120	80	12000	-	-	-	Maxaret
		1C	Trident	"	34 X 9.50 - 18	16	.84	200	175	14900	-	-	-	Maxaret
		1E,2E,3B	"	"	36 X 10.00 - 18	14	.90	200	155	18000	-	-	-	Maxaret
15	Lockheed	382B		"	56 X 20.0 - 20	22TL	.90	-	-	-	RR	ND	MKII	H
		382E	-	"	56 X 20.0 - 20	24TL	.90	200	110	38500	RR	"	MKII	H
		L-1011-1		"	50 X 20.0 -20	32TL	.75	225	190	53800	RR	"	-	G
16	MBB (Germany)	HFB-320	HANSA	Civil	30.92 X 8.77 - 16	-	.85	-	-	-	-	-	-	G
17	McDonnell-Douglas	DC-8	DC-8	"	44 X 16	26TL	.80	200	185	35500	RR	VII	MKI	H
		DC-8HV		"	44 X 16	28TL	.80	200/225	185/200	38400	RR	"	MKII	H
		DC-8-50F		"	44 X 16	28TL	.80	"	"	"	RR	"	MKII	H
		DC-8-61-62		"	44 X 16	30TL	.80	200/225	210	41700	RR	"	MKII	H
		DC-8-63/62		"	44 X 16	32TL	.80	225	225	45000	RR	"	MKIII	H
		DC-8 62H/ DC863		"	44.5 X 16.5 - 16	30TL	.86	200/225	195	42500	RR	ND VII	MKII	H

Table A-3.—World's Major Aircraft (Commercial and Military) with Type VII Tires Listed Alphabetically by Manufacturer (Continued)

	AIRPLANE				TIRE CHARACTERISTICS (MAIN GEAR ONLY)								SKID CONTROL SYSTEM	
S NO.	MANUFACTURER	MODEL	POPULAR NAME	UTILIZED AS	TIRE SIZE	PLY RATING	ASPECT RATIO	SPEED MPH	RATED PRESSURE-PSI	LOAD-LBS	TREAD DESIGN	TIRE TYPE	TYPE	SUPPLIER
17	McDonnell-Douglas (Cont)	DC-9-10	DC-9	Civil (Transport)	40 X 14	18TL	.86					VII	MK II	H
		DC-9 10 (11-12-14-15)		"	40 X 14	20TL	.86	225	135	22300	RR	"	MKII	H
		DC-9 30 (31)		"	40 X 14	22TL	.86	200/225	155	25000	RR	"	MKIII	H
		DC-9 30 (32)		"	40 X 14	24TL	.86	225	170	27700	RR	"	MKIII	H
		DC-9 30 (33)(41)		"	41 X 15.0 - 18	22TL	.77	200	170	28600	RR	ND	MKIII	H
					42 X 15.0 - 16	20TL	.87	-	-	-	-	ND	MKIII	H
		DC-9 (Flotation)		"	42 X 15.0 - 16	22TL	.87	-	-	-	-	"	MKIII	H
		DC-10-10	DC-10	"	50 X 20.0 - 20	32TL	.75	225	190	53800	RR	"	-	G
		DC-10 20/30		"	52 X 20.5 - 23	26TL	.71	235	165	55000	RR	"	-	G
18	Snias (Aerospatiale)	MK VIA	Caravelle	Civil	35 X 9.00 - 17	16TL	.95	200	170	16300	RR	British	-	G
		MK X	"	"	35 X 9.00 - 17	16TL	.95	200	170	16300	RR	"	-	G
		-	Concorde	"	47 X 15.75 - 22	26 TL	.79	250	190	46700		Aquagrip	-	SPAD
19	Vickers	742/745	Viscount	"	36 X 10.75 - 16½	12TT	.91	-	-	-	-	-	-	G
		812	"	"	36 X 10.75 - 16½	16TL	.91	160	140	16700	Dimple	British	-	G
		952	Vanguard	"	49 X 17	24TL	.84	-	-	-	-	-	-	G
		-	VC-10	"	50 X 18	24	.84	200	140	36400	-	-	-	Maxaret
		-	Super VC-10	"	50 X 18	26	.84	225	160	40500	-	-		Maxaret
20	Boeing	B47E	Stratojet	AF	56 X 16	36TL	.88	-	-	-	-	VII	MKI	H
		B52,F,G,H	Stratofort-ress	AF	56 X 16	38TL	.88	250	315	76000	RR	"	MKI	H
		KC-135	Stratotanker	AF	49 X 17	26TL	.84	200/225	170	39600	R	"	MKI, MK..	-
		VC137C	-	AF	46 X 16	28TL	.80	200/225	210	41800	RR	"	MKI	-
		T-43A	737-200	Trainer	40 x 14	24TL	.86	200/225	170	27700	RR	"	MK III	H
		E-3A	707-300	AWACS	46 x 16	28TL	.80	200/225	210	41800	RR	"	MK II	H
		E-4A/B	747-200	Command Post	49 x 17	30TL	.84	200/225	190	46400	RR	"	MK III	H

Table A-3.—World's Major Aircraft (Commercial and Military) with Type VII Tires Listed Alphabetically by Manufacturer (Concluded)

S NO.	AIRPLANE				TIRE CHARACTERISTCS (MAIN GEAR ONLY)								SKID CONTROL SYSTEM	
	MANUFACTURER	MODEL	POPULAR NAME	UTILIZED AS	TIRE SIZE	PLY RATING	ASPECT RATIO	SPEED MPH	RATED PRESSURE-PSI	LOAD-LBS	TREAD DESIGN	TIRE TYPE	TYPE	SUPPLIER
21	Fairchild Hiller	F105	Thunder-	Military	36 X 11	24TL	.83	160/250	235	26000	R/RR	VII	-	G
22	General Dynamics	B-58A	Hustler	"	22 X 7.7 - 12	16TL	.67	275	280	10500	RR G	VIII	-	G
		F-111A	-	"	47 X 18 - 18	30TL	.81	225	175	43700	RR	VII	-	G
		FB111A	-	"	47 X 18 - 18	36TL	.81	250	215	54600	RR	VII	-	G
23	Grumman	F-14A	TomCat	"	37 X 11.50 - 16	28TL	.91	180	245	31200	RR	ND	-	Bendix
24	Kawasaki	P-2J	-	Military	34 X 9.9	14TL	.86	160	150	14000	R	VII	-	G
25	LTV	A7A, B	Corsaie 11	Navy	28 X 9.0	22TL	.89	173	235	16650	R	VII	MKIII	H
		A7D	"	"	28 X 9.0 - 14	22TL	.75	200	285	18100	Rib	VIII	MKIII	H
26	Lockheed	F104, A, B	Starfighter	Military	25 X 6.75	18TL	.94	275	300	13000	RR	VII	-	G
		F104 C,D,J, DJ	"	"	25 X 6.75	18TL	.94	275	300	13000	RR	"	-	G
		F104G (early)	"	AF	25 X 6.75	18TL	.94	275	300	13000	RR	"	-	G
		F104G	"	"	26 X 8.0 - 14	16TL	.75	275	235	12700	RR	VIII	-	G
		C140A	Jetstar	"	26 X 6.6	14TL	.88	200	225	10000	R	VII	MKII	H
		C141	Starlifter	"	44 X 16	28TL	.80	200/225	185/200	38400	RR	"	-	Bendix
		C5A	Galaxy	"	49 X 17	26TL	.94	200/225	170	39600	R	"	MKII	H
27	McDonnell-Douglas	C9A	-	"	40 X 14	24TL	.86	225	170	27700	RR	"	MKII	H
		F4B	Phantom 11	Navy	30 X 8.0	26TL	.86	248	360	24100	RR CP	"	MKII	H
		F4C	"	Military	30 X 11.50 - 14.5	24TL	.66	240	243	25000	RR CP	VIII	MKII	H
		F4J	"	"	30 X 11.50 - 14.5	24TL	.66	240	243	25000	RR CP	"	MKII	H
		F-15	-	"	34.5 X 9.75 - 18	22TL	.85	-	-	-	-	-	MKIII	H
28	North American	RA5C	Vigilante	"	36 X 11	28TL	.83	200	290	31500	R	VII	MK II	H
		XB70A	Valkyrie	"	40 X 17.50 - 18	40TL	.63	-	-	-	-	VIII	-	SPAD
		F-100	Super Sabre	AF	30 X 8.8	22TL	.87	250	295	21000	RR	VII	-	H
29	VFW Fokker (Germany)	191B	VAK	Military	22 X 8.5 - 11	16TL	.64	250	210	10000	RR CP	VIII	-	G

APPENDIX B
SURVEY OF MILITARY AND COMMERCIAL RUNWAYS

Runway/Airport Survey Applies as Follows:

1) Top 100 U. S. Commercial Airports Only.

2) All USAF Active AFB's Listed (including Europe and Pacific)

3) All Naval Facilities Included.

4) All AAF's Facilities Included.

5) Only the Longest Runway for Each Airport Listed.

6) Texture Depth (When Included) Measured by Grease/Sand Patch Method.

7) LCN Values for Commercial Airports Only. Others not Available.

The information contained in Tables B1 through B4 was compiled from references 23 and 35 through 40.

AIRPORTS AND RUNWAYS-NOMENCLATURE

ABBREVIATION	STANDS FOR	ABBREVIATION	STANDS FOR
AL	Alabama	MO	Missouri
AK	Alaska	MT	Montana
AZ	Arizona	NE	Nebraska
AR	Arkansas	NV	Nevada
CA	California	NH	New Hampshire
CZ	Canal Zone	NJ	New Jersey
CO	Colorado	NM	New Mexico
CT	Connecticut	NY	New York
DE	Delaware	NC	North Carolina
DC	District of Columbia	ND	North Dakota
		OH	Ohio
FL	Florida	OK	Oklahoma
GA	Georgia	OR	Oregon
GU	Guam	PA	Pennsylvania
HI	Hawaii	RI	Rhode Island
ID	Idaho	SC	South Carolina
IL	Illinois	SD	South Dakota
IN	Indiana	TN	Tennessee
IA	Iowa	TX	Texas
KS	Kansas	UT	Utah
KY	Kentucky	VT	Vermont
LA	Louisiana	VA	Virginia
ME	Maine	WA	Washington
MD	Maryland	WV	West Virginia
MA	Massachusetts	WI	Wisconsin
MI	Michigan	WY	Wyoming
MN	Minnesota		
MS	Mississippi		

ABBREVIATION	STANDS FOR
AAF	Army Air Field
AFB	Air Force Base
ANGB	Air National Guard Base
ASP	Asphalt, bitumen or tar macadam (black top surface)
CON	Concrete or Cement (white surface)
MCAS	Marine Corps Air Station
NAF	Naval Air Facility
NAS	Naval Air Station
S	Single Wheel
T	Twin Wheel
TT	Twin Tandem
TDT	Twin Dual Tandem
LCN	Load Classification Number

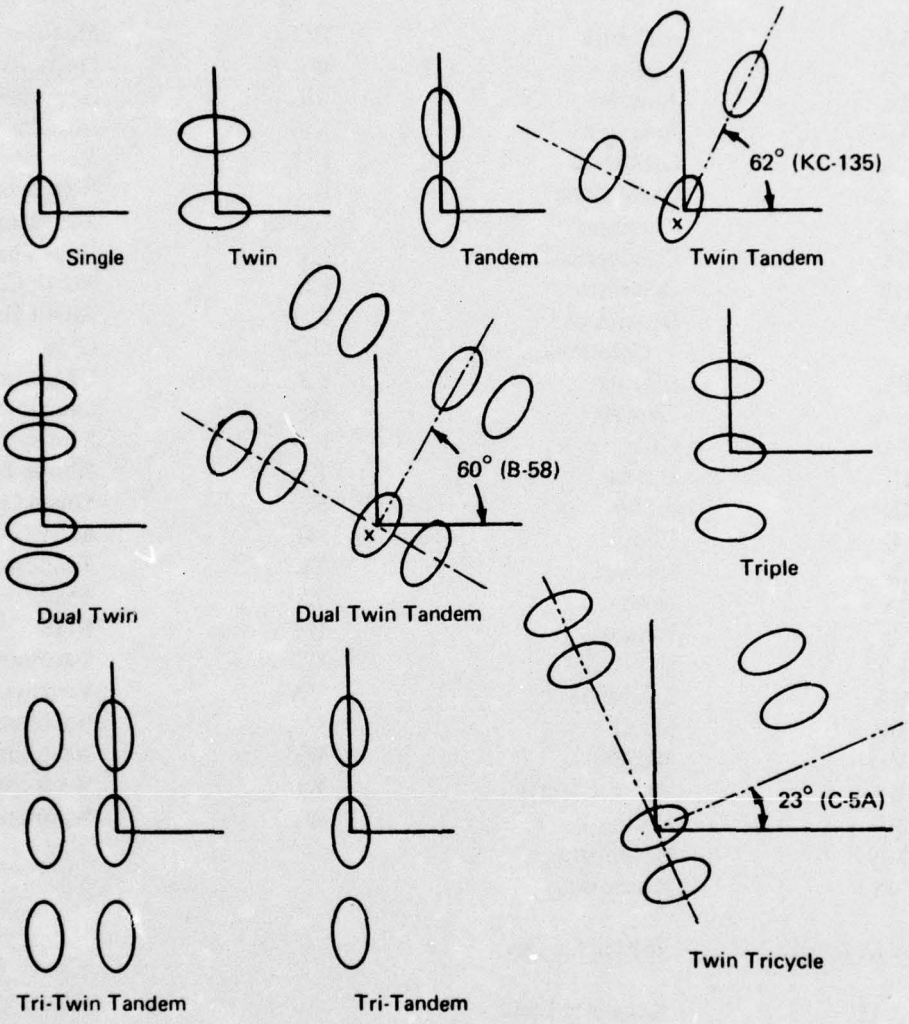

1. The X marked on a wheel indicates the critical wheel used in the summation of principal movements.

2. The angular orientation is that required for maximum block count and can be used for positioning similar gear types.

Figure B-1.—Landing Gear Configurations

Table B-1.—Major Commercial U.S. Airports

AIRPORT				RUNWAY					RUNWAY					
NAME	LOCATION: CITY/STATE	ICAO/FAA IDENT. CODE	ELEVATION FEET	DESIGNATION	DIMENSIONS - LENGTH x WIDTH, FEET	SURFACE	TREATMENT	TEXTURE DEPTH mm	Weight Bearing Capacity (1000 lbs) S	T	TT	TDT	LCN	
Albany County	Albany, N.Y.	ALB	288	1/19	6000 x	Asphalt			72	104	184			72
Albuquerque Int'l	Albuquerque, NM	ABQ	5352	8/26	13400 x 300	Asphalt			80	130	280			87
Anchorage Int'l	Anchorage, AK	ANC	124	6R/24L	10900 x 150	Asphalt			100	200	400			87
The William B. Hartsfield Atlanta International	Atlanta, GA	ATL	1026	15/33	10000 x	Asphalt			150	200	360			87
Robert Mueller Muni.	Austin, TX	AUS	632	12/30	7300 x	Asphalt			75	90	140			20
Birmingham Muni.	Birmingham, AL	BHM	643	5/23	10000 x	Concrete			175	205	350			80
Boise Air Terminal (Gowen Field)	Boise, ID	BOI	2858	10R/28L	9700 x 200	Asphalt			60	145	230			50
Gen. Edward L. Logan Intl	Boston, MA	BOS	19	15R/33L	10100 x 150	Asphalt/ Concrete			100	200	400			95
Greater Buffalo Int'l	Buffalo, NY	BUF	723	5/23	8100 x	Concrete			70	90	149			72
Charleston AFB/Muni	Charleston, SC	CHS	45	15/33	9000 x	Asphalt/ Concrete			125	275	350	775		27
Kanawha	Charleston, WV	CRW	982	5/23	6300 x	Asphalt/ Concrete			120	160	260			50
Douglas Muni.	Charlotte, NC	CLT	749	5/23	7800 x	Asphalt/ Concrete			75	95	150			36
Lovell Field	Chattanooga, TN	CHA	682	14/32	7400 x	Asphalt			120	160	265			73
Chicago Midway	Chicago, IL	MDW	619	31L/13R	6500 x	Asphalt	Grooved, 1" x ¼" x ¼"		100	175	265			73
Chicago O'hare Int'l	Chicago, IL	ORD	667	14R/32L	11600 x 200	Concrete			100	185	350			95
Greater Cincinnati	Cincinnati, OH	CVG	890	9R/27L	9500 x 150	Asphalt/Con			100	150	262			50
Cleveland-Hopkins Int'l	Cleveland, OH	CLE	792	5R/23L	9000 x 150	Concrete			100	170	287			80
Peterson Field	Colorado Springs, CO	COS	6172	17/35	11000 x	Asphalt			115	175	345			176
Columbia Metropolitan	Columbia, SC	CAE	236	11/29	7500 x	Asp/Con			72	128	235			59
Port Columbus Intl.	Columbus, OH	CMH	816	10/28	10700 x	Asphalt			100	150	300			48
Dallas Love Field	Dallas/Ft.Worth,TX	DAL	487	13/31	8800 x 150	Concrete			100	200	350			73
James M. Cox - Dayton Muni.	Dayton, OH	DAY	1008		9500 x	Concrete			100	200	350			44
Stapleton Intl.	Denver, CO	DEN	5331	8/26	11500 x 150	Asp/Con			125	175	285			95
Des Moines Muni.	Des Moines, IA	DSM	957	12L/30R	9000 x	Concrete			100	128	218			44
Detroit Metropolitan Wayne Co.	Detroit, MI	DTW	639	3L/21R	10500 x 200	Concrete			100	185	350			80
El Paso Int'l	El Paso, TX	ELP	3956	4/22	12100 x 150	Asphalt			100	180	350			73
Fresno Air Terminal	Fresno, CA	FAT	332	11L/29R	9200 x 150	Concrete			100	150	255			80
Kent Co.	Grand Rapids, MI	GRR	794	18/36	7600 x	Asp/Con			100	185	350			36
Austin Straubel	Green Bay, WI	GRB	695	6R/24L	7700 x	Concrete			140	175	300			28

Table B-1.—Major Commercial U.S. Airports (Continued)

AIRPORT				RUNWAY					RUNWAY					
NAME	LOCATION: CITY/STATE	ICAO/FAA IDENT. CODE	ELEVATION FEET	DESIGNATION	DIMENSIONS LENGTH x WIDTH, FEET	SURFACE	TREATMENT	TEXTURE DEPTH mm	Weight Bearing Capacity (1000 lbs)				LCN	
									S	T	TT	TDT		
Greensboro/High Point/ Winston Salem Regional	Winston Salem, NC	GSO	926	5/23	8200 x 150	Asphalt			124	170	240			37
Harrisburg Int'l - Olmsted Field	Harrisburg, PA	MDT	308	13/31	9500 x	Concrete			155	330	550			177
Bradley Int'l	Hartford/Spfld.,CT	BDL	173	15/33	9500 x	Asp/Con			200	200	350			44
General Lyman Field	Hilo, HI	ITO	37	8/26	9800 x 150	Asphaltic			115	185	350			80
Honolulu Int'l	Honolulu, HI	HNL	13	8/26	12371 x 150	Asphaltic/ Con			100	200	400			177
Houston International	Houston, TX	IAH	98	8426R	9400 x 150	Concrete			120	155	265			59
Huntsville-Madison Co. Jetport/Carl T. Jones Field	Huntsville, AL	HSV	629	18/36	8000 x	Asphalt			130	160	250			72
Indianapolis (weir-cood) Muni.	Indianapolis, IN	IND	797	4L/22R	10000 x 150	Concrete			85	120	210			38
Allen C. Thompson Field	Jackson, MS	JAN	345	15/33	8500 x	Concrete			130	165	300			80
Jacksonville Int'l	Jacksonville, FL	JAX	29	7/25	8000 x	Concrete			100	160	265			37
Kuhului	Kuhului, HI	OGG	57	17/35	5077 x 200	Asphalt			-	-	-			50
Kansas City Muni.	Kansas City, MO	MKC	758	18/36	7000 x	Asp/Con	1" x 1/8" x 1/4"		75	150	300			80
McGhee Tyson	Knoxville, TN	TYS	981		4000 x 9000 x	Concrete			84	-	-			40
McCarran Intl.	Las Vegas, NV	LAS	2171	7/25	12500 x 150	Asphalt			60	100	172			36
Lihue	Kauai, HI	LIH	149	3/21	6000 x	Asphalt			23	38	-			44
Adams Field	Little Rock, AR	LIT	257	4/22	7000 x	Asphalt			70	95	150			33
Hollywood, Burbank	Los Angeles, CA	BUR	775	15/33	6900 x 300	Asphalt			100	200	400			53
Los Angeles Int'l	Los Angeles, CA	LAX	126	7L/25R	12100 x 150	Asphalt			80	120	210			100
Ontario Int'l	Los Angeles, CA	ONT	952	7/25	10000 x 150	Asp/Con			70	80	140			55
Orange Co.	Los Angeles, CA	SNA	54	1L/9R	5700 x 150	Asphalt			25	-	-			28
Standiford Field	Louisville, KY	SDF	497	1/19	7800 x	Concrete			82	105	190			50
Dane County Regional Traux Field	Madison, WI	MSN	862	18/36	7600 x	Concrete			100	200	350			38
Memphis Int'l	Memphis, TN	MEM	331	17/35	9300 x	Concrete			100	173	338			21
Fort Lauderdale - Hollywood Int'l	Miami/Ft. Lauderdale, FL	FLL	10	13/31	8000 x 150	Asphalt			115	200	400			73
Miami Intl	Miami/ Ft. Lau. FL	MIA	9	9L/27R	10500 x 150	Asphalt			130	170	350			80
General Mitchell Field	Milwaukee, WI	MKE	722	1L/19R	9900 x 200	Concrete			100	150	255			38
Minneapolis - St.Paul Int'l	Minneapolis/St. Paul MN	MSP	840	11R/29L	10000 x 200	Concrete			65	85	145			30
Bates Field	Mobile, AL	MLI	218	14/32	6800 x	Asphalt			50	70	110			72

Table B-1.—Major Commercial U.S. Airports (Continued)

AIRPORT				RUNWAY					RUNWAY					
NAME	LOCATION: CITY/STATE	ICAO/FAA IDENT. CODE	ELEVATION FEET	DESIGNATION	DIMENSIONS LENGTH X WIDTH, FEET	SURFACE	TREATMENT	TEXTURE DEPTH mm	Weight Bearing Capacity (1000 lbs) S	T	TT	TDT	LCN	
Quad City	Moline, IL	MLI	589	12/30	6500 x	Asp/Con			75	90	145		53	
Monterey Penninsula	Monterey, CA	MRY	244	6/24	6600 x	Asphalt			100	160	300		36	
Nashville, Metropolitan	Nashville, TN	BNA	597	2L/20R	8000 x	Asphalt	Grooved		90	130	208		95	
New Orleans Int'l (Moisant Field)	New Orleans, LA	MSY	4	10/28	9200 x 150	Asp/Con			137	185	350		68	
Newark Int'l	Newark, NJ	EWR	18	4R/22L	9800 x 150	Asphalt			-	350	650		160	
John F. Kennedy Intl.	New York, NY	JFK	12	13R/31L	14600 x 150	Concrete								
				4R/22L	8400 x 150	Concrete	Grooved, 1" x 3/8" x 1"		100	185	340		95	
La Guardia	New York, NY	LGA	21	13/31,4/22	7000 x 150	Asphalt			80	105	280		72	
Patrich Henry Intl	Newport News, VA	PHF	41	6/24	8000 x	Concrete			100	200	350		-	
Norfolk Regional	Norfolk, VA	ORF	27	5/23	7500 x	Asphalt			95	143	270		50	
Will Rogers World	Oklahoma City, OK	OKC	1294	17/35	9800 x	Asp/Con			200	200	350		87	
Eppley Airfield	Omaha, NE	OMA	983	14R/32L	8500 x	Asp/Con	Grooved		100	184	346		95	
Orlando Jetport (McCoy)	Orlando, FL	MCO	96	18L/36R	12000 x	Concrete			155	330	540		177	
Philadelphia Int'l	Philadelphia, PA	PHL	23	9R/27L	10500 x 200	Concrete			-	-	350		97	
Phoenix-Sky Harbor Intl	Phoenix, AZ	PHX	1128	8R/26L	10300 x 150	Asphalt			100	200	350		80	
Greater Pittsburgh Intl	Pittsburg, PA	PIT	1203	10L/28R	10500 X 150	Concrete			100	225	400		87	
Portland Intl.	Portland, OR	PDX	26	10R/28L	11000 x 150	Asphalt			170	200	360		74	
Theodore Francis Green State	Providence, RI	PVD	56	5R/23L	6400 x 200	Concrete			70	85	145		37	
Raleigh Durham	Raleigh Durham,NC	RDU	436	5/23	7500 x	Asphalt			135	175	285		48	
Reno Intl.	Reno, NV	RNO	4411	16/34	9000 x 150	Concrete			100	170	350		62	
Richard Evelyn Byrd. Intl.	Richmond, VA	RIC	168	15/33	9000 x 150	Asphalt			125	160	240		42	
Roanoke Muni.	Roanoke, VA	ROA	1175	15/33	5900 X	Asphalt			70	100	175		59	
Rochester Monroe Co.	Rochester, N.Y.	ROC	560	4/22	8000 x 150	Asp/Con			100	130	218		72	
Sacramento Metropolitan	Sacramento, CA	SMF	23	16/34	8600 x 150	Asp/Con			126	175	290		80	
Salt Lake City Intl	Salt Lake City, UT	SLC	4226	16R/34L	9900 x 150	Asphalt			60	200	330		80	
San Antonio Intl.	San Antonio, TX	SAT	809	12R/30L	8500 x 150	Asp/Con			100	128	200		53	
San Diego Intl - Lindbergh Field	San Diego, CA	SAN	15	9/27	9400 x 200	Concrete			100	150	250		125	
Metropolitan Oakland Intl.	Oakland, CA	OAK	6	11/29	10000 x 150	Asphalt			200	200	400		186	

Table B-1.—Major Commercial U.S. Airports (Concluded)

AIRPORT				RUNWAY					RUNWAY					
NAME	LOCATION: CITY/STATE	ICAO/FAA IDENT. CODE	ELEVATION FEET	DESIGNATION	DIMENSIONS - LENGTH x WIDTH, FEET	SURFACE	TREATMENT	TEXTURE DEPTH mm	Weight Bearing Capacity (1000 lbs)				LCN	
									S	T	TT	TDT		
San Jose Muni.	San Jose, CA	SJC	56	12R/30L	8900 x 150	Asphalt			200	200	300			73
San Francisco Intl.	San Francisco, CA	SFO	10	10L/28R	11900 x 200	Asphalt			60	190	350			125
Seattle Tacoma Intl.	Seattle/Tacoma, WA	SEA	428	16L/34R	11900 x 150	Concrete			160	200	320			95
Shreveport Regional	Shreveport, LA	SHV	257		7300 x	Concrete			55	70	169			28
Spokane Intl.	Spokane, WA	GEG	2372	3/21	9000 x 150	Concrete			100	200	350			62
Lambert-St.Louis Intl.	St. Louis, MO	STL	589	12R/30L	10000 x 200	Asp/Con?			100	184	346			80
Syracuse-Hancock Intl	Syracuse, NY	SYR	421	10/28	9000 x 150	Asphalt			72	102	140			95
Tampa Int'l	Tampa, FL	TPA	27	18R/36L	8700 x 150	Asp/Con			75	140	220			37
Toledo Express	Toledo, OH	TOL	684	7/25	8700 x	Asp/Con			100	125	223			72
Tucson Int'l	Tucson, AZ	TUS	2630	11L/29R	12000 x 150	Asp/Con			160	205	305			87
Tulsa Intl	Tulsa, OK	TUL	676	17L/35R	10000 x	Concrete			50	200	400			100
Baltimore-Wash. Intl.	Baltimore, MD	BAL	146	15R/33L	9500 x 150	Asp/Con			100	220	500			200
Washington Nat'l	Washington, DC	DCA	15	18/36	6900 x	Asphalt	Grooved, 1" x 1/8" x1/8"		110	200	360			62
Dulles Intl.	Washington, DC	IAD	313	R/19L	11500 x 150	Concrete			200	250	450			177
Palm Beach Int'l	Palm Beach, FL	PBI	19	9L/27R	8000 x 150	Asphalt			85	200	400			73
Wichita Mid Continent	Wichita, KS	ICT	1332	1/19	7300 x	Concrete			100	175	300			62

Table B-2.—Active U.S. Air Force Bases (Including Europe and Pacific)

AIRPORT				RUNWAY					RUNWAY						
NAME	LOCATION CITY/STATE	ICAO/FAA IDENT. CODE	ELEVATION FEET	DESIGNATION	DIMENSIONS LENGTH X WIDTH FEET	SURFACE	TREATMENT	TEXTURE DEPTH mm	Weight Bearing Capacity (1000 lbs)						
									S	T	TT	TDT			
Altus AFB	Altus, OK	LTS	1378	17/35	13400 x	Concrete			145	245	330	450			
Andrews AFB	Camp Springs, MD	ADW	279	1L/19R	9700 x	Concrete			75	130	210				
Barksdale AFB	Shreveport, LA	BAD	167	14/32	11700 x	Asphalt			155	260	300				
Beale AFB	Marysville, CA	BAB	113	14/32	12000 x 300	Concrete	Grooved,1" x ¼" x ½"		160	300	490	(SWL 65/	psi	560)	
Bergstrom AFB	Austin, TX	BSM	541	17R/35L	12200 x	Asp/Con			155	330	550				
Blytheville AFB	Blytheville, AR	BYH	255	17/35	11600 x	Concrete			155	235	455				
Cannon AFB	Clovis, NM	CVS	4295	3/21	10000 x	Concrete			75	150	240	745			
Carswell AFB	Fort Worth, TX	FWH	650	17/35	12000 x	Concrete			150	215	550				
Castle AFB	Merced, CA	MER	188	12/30	11800 x	Asphalt			155	200	415				
Charleston AFB/Muni	Charleston, SC	CHS	45	15/33	9000 x	Asp/Con			125	275	350	775			
Columbus AFB	Columbus, MS	CBM	219	13/31	12000 x	Asp/Con			155	230	450				
Craig AFB	Selma, AL	SEM	166	14/32	8000 x	Asphalt			33	54	-				
Davis-Monthan AFB	Tucson, AZ	DMA	2705	12/30	13600 x	Asp/Con			155	210	345				
Dillingham AFB	Oahu, HI	HDH	15		9000 x	Asphalt			40	120	180				
Dobbins AFB	Marietta, GA	MGE	1068	11/29	10000 x	Concrete			200	300	560				
Dover AFB	Dover, DE	DOV	28	1/19	9600 x	Asphalt	Plant Mix	.387	155	205	350	TDT			
Duluth Intl	Duluth, MN	DLH	1429	9/27	10100 x	Concrete			100	125	210				
Dyess AFB	Abilene, TX	DYS	1789	16/34	13500 x 300	Asp/Con	Conventional	.127	155	250	500				
Edwards AFB	Edwards, CA	EDW	2302	4/22	16800 x 300	Concrete	Conventional	.119	160	200	560	(SWL 65)	AUW	800)	
Eglin AFB	Valparaiso, FL	VPS	85	18/36	12000 x	Asphalt			135	205	500				
Eielson AFB	Fairbanks, AK	AEI	545	13/31	14500 x 150	Asphalt			155	180	290	AUW	620)		
Ellington AFB	Houston, TX	EFD	40	4/22	9000 x 150	Concrete	Conventional	-	80	160	259				
Elmendorf AFB	Anchorage, AK	AED	212	5/23	10000 x 200	Asphalt	Plant Mix	.208	156	200	340	(AUW	769)		
Ellsworth, AFB	Rapid City, SD	RCA	3276	12/30	13500 x	Asp/ Con			160	280	500				
England AFB	Alexandria, LA	AEX	89	14/32	9300 x	Concrete	Conventional	.166	160	200	460				
Fairchild AFB	Spokane, WA	SPA	2462	5/23	13900 x	Asp/Con			155	220	550				
Francis E. Warren AFB Cheyenne Muni	Cheyenne, WY	CYS	6156		9200 x	Concrete			100	125	210				
George AFB	Victorville, CA	VCV	2875	16/34	10000 x	Asphalt			60	200	440	TDT			
Glasgow AFB	Glasgow, MT	GGW	2760		13500 x	Concrete			100	200	500				
Goodfellow AFB	San Angelo, TX	GOF	1877	4/22	5500 x	Asphalt			30	50	-				
Grand Forks AFB	Grand Forks, ND	RDR	911	17/35	12300 x	Concrete			155	280	470	(SWL 65/	psi	650)	
Griffiss AFB	Rome, NY	RME	504	4/22	11800 x	Concrete			100	240	500				
Grissom AFB	Peru, IN	GUS	813	4/22	12500 x	Concrete	Plant Mix (Asp.Taxiway)		100	200	450				
Hamilton AFB	San Rafael, CA	SRF	3	12/30	8000 x	Asp/Con			55	127	150				

Table B-2.—Active U.S. Air Force Bases (Including Europe and Pacific) (Continued)

AIRPORT				RUNWAY					RUNWAY					
NAME	LOCATION: CITY/STATE	ICAO/FAA IDENT. CODE	ELEVATION FEET	DESIGNATION	DIMENSIONS - LENGTH x WIDTH, FEET	SURFACE	TREATMENT	TEXTURE DEPTH (in)	Weight Bearing Capacity (1000 lbs)					
									S	T	TT	TDT		
Hickam AFB/Honolulu Intl. Airport	Oahu, HI	HNL	13	8/26	12400 x 150	Asphalt			100	200	400			
Hill AFB	Ogden, UT	HIF	4785	14/32	13500 x	Asphalt			155	330	560			
Holloman AFB	Alamogordo, NM	HMN	4093	15/33	12200 x	Asphalt			100	155	380			
Homestead AFB	Homestead FL	HST	7	5/23	11200 x	Asp/Con			155	280	545	775		
Keesler AFB	Biloxi, MS	BIX	26	3/21	2900 x	Asphalt			65	175	203			
Kelly AFB	San Antonio, TX	SKF	690	15/33	11500 x	Concrete			144	200	380			
Kincheloe AFB	Sault Ste.Marie,MI	INR	799	15/33	12000 x	Concrete			155	330	600			
Kirtland AFB	Albuquerque, NM	ABQ	5352	8/26	13400 x	Asphalt			80	180	280			
K. I. Sawyer AFB	Gwinn, MI	SAW	1220	1/19	12300 x	Asp/Con	Slurry Seal		155	175	310			
Langley AFB	Hampton, VA	LFI	10	7/25	10000 x 150	Concrete	Conventional	.103	55	90	190			
Laughlin AFB	Del Rio, TX	DLF	1081	13R/31L	8800 x	Asphalt			30	60	60			
Little Rock AFB	Jacksonville, AR	LRF	311	24/06	12000 x 200	Asphalt	Plant Mix	.187	125	200	330			
Lockbourne AFB	Lockbourne, OH			23L/05R	12100 x 200	Concrete	Conventional	.165						
Loring AFB	Lime Stone, ME	LIZ	746	1/19	12100 x	Asphalt	Slurry Seal		155	265	445			
Luke AFB	Glendale, AZ	LUF	1101	3/21	10000 x	Asphalt			55	155	210			
MacDill AFB	Tampa, FL	MCF	13	4/22	11400 x	Asphalt			65	210	380	700		
Malstrom AFB	Great Fall, MT	GFA	3525	2/20	11500 x	Asp/Con	Conventional(conc. ramp)		65	200	280			
March AFB	Riverside, CA	RIV	1533	13/31	13300 x	Concrete			65	260	530			
Mather AFB	Sacramento, CA	MHR	96	4R/22L	11300 x	Concrete			160	280	500			
Maxwell AFB	Montgomery, AL	MXF	169	18/36	7000 x	Asphalt			65	150	180			
McChord AFB	Tacoma, WA	TCM	322	16/34	10100 x 150	Asphalt	Plant Mix		155	220	390	800		
McClellan AFB	Sacramento, CA	MCC	76	16/34	10600 x	Concrete			155	300	500			
McConnell AFB	Wichita, KS	IAB	1371	18/36	12000 x	Concrete			60	190	340	-		
McGuire AFB	Wrightstown, NJ	WRI	133	18/36	10000 x	Asphalt	Plant Mix		100	200	400			
Minneapolis-St.Paul Intl.	Minneapolis, MN	MSP	840	11/29	10000 x	Concrete			65	85	145			
Minot AFB	Minot, ND	MIB	1668	11/29	13200 x	Concrete			65	270	500			
Moody AFB	Valdosta, GA	VAD	233	18/36	8000 x	Asphalt			160	200	300			
Mountain Home AFB	Mountain Home, ID	MUO	2996	12/30	13500 x	Asp/Con			155	200	330	(SWL 65/psi 500)		
Myrtle Beach AFB	Myrtle Beach, SC	MYR	25	17/35	9500 x	Asp/Con	Slurry Seal	.173	50	110	220	650		
Nellis AFB	Las Vegas, NV	LSV	1868	03L/21R	10100 x 150	Asphalt	Plant Mix	.144	60	160	265	650		

Table B-2.—Active U.S. Air Force Bases (Including Europe and Pacific) (Continued)

AIRPORT				RUNWAY					RUNWAY					
NAME	LOCATION: CITY/STATE	ICAO/FAA IDENT. CODE	ELEVATION FEET	DESIGNATION	DIMENSIONS LENGTH x WIDTH, FEET	SURFACE	TREATMENT	TEXTURE DEPTH mm	Weight Bearing Capacity (1000 lbs) S	I	II	TDT	LCN	
Norton AFB	San Bernardino, CA	SBD	1156	5/23	10000 x	Concrete			120	185	390			
Offutt AFB	Omaha, NE	OFF	1047	12/30	11700 x 300	Concrete	Conventional + Grooved, 1¼" x ¼" x ¼"	.154	155	245	375			
Otis AFB	Falmouth, MA	FMH	132	14/32	9500 x	Asphalt	Plant Mix	.338	65	160	330			
Patrick AFB	Cocoa Beach, FL	COF	9	2/20	9000 x	Asphalt			70	175	-	720		
Pease AFB	Portsmouth, NH	PSH	101	16/34	11300 x	Asp/Con			120	200	450			
Plattsburgh AFB	Plattsburgh, NY	PBG	235	17/35	11700 x	Concrete			155	320	510			
Pope AFB	Fayetteville, NC	POB	218	4/22	7500 x	Concrete	Asphalt, Plant Mix	.144	66	155	344	680		
Randolph AFB	San Antonio, TX	RND	761	14L/32R	8300 x	Concrete			30	60	60			
Reese AFB	Lubbock, TX	REE	3338	17L/35R	10500 x	Asp/Con			50	100	215	SWL 25		
Richards-Gebaur AFB	Grandview, MO	GVW	1090	18/36	9000 x	Asp/Con			75	180	200			
Rickenbacker AFB	Columbus, OH	LCK	744	5/23	12100 x	Asp/Con			155	265	510			
Robins AFB	Macon, GA	WRB	294	14/32	12000 x	Asp/Con			65	300	600	300		
Scott AFB	Belleville, IL	BLV	453	13/31	7000 x 150	Asp/Con	Plant Mix	.184	85	120	250	-		
Seymour-Johnson AFB	Goldsboro, NC	GSB	109	08/26	11700 x 300	Concrete	Grooved, 2" x ¼" x ¼"	.102	130	235	440	800		
Shaw AFB	Sumter, SC	SSC	252	4L/22R	10000 x	Concrete			85	165	355			
Shemya AFB	Shemya, AK	ASY	97	10/28	10000 x 150	Asphalt	Plant Mix, Grooved 1¼" x ¼" x ¼"							
Sheppard AFB/ Wichita Falls Muni	Wichita Falls, TX	SPS	1015	15/33	13100 x	Concrete			155	220	540			
Tinker AFB	Oklahoma City, OK	TIK	1291	17/35	11100 x	Asp/Con			85	230	330	732		
Travis AFB	Fairfield, CA	SUU	62	3/21	11000 x	Asp/Con			155	260	470	720	SW 65/	psi 650
Tyndall AFB	Panama City, FL	PAM	18	13/31	10000 x	Concrete			55	110	245			
Vance AFB	Enid, OK	END	1307	17/35	9200 x	Asp/Con			50	95	140			
Vandenberg AFB	Lompac, CA	VBG	368	12/30	8000 x	Asp/Con			65	200	370			
Webb AFB	Big Spring, TX	BGS	2561	17R/35L	9100 x	Asphalt			85	165	215			
Westover AFB	Chicopee, MA	CEF	245	5/23	11600 x	Asp/Con			155	280	570	778		

Table B-2.—Active U.S. Air Force Bases (Including Europe and Pacific) (Continued)

AIRPORT				RUNWAY					RUNWAY						
NAME	LOCATION: CITY/STATE	ICAO/FAA IDENT. CODE	ELEVATION FEET	DESIGNATION	DIMENSIONS LENGTH x WIDTH, FEET	SURFACE	TREATMENT	TEXTURE DEPTH mm	Weight Bearing Capacity (1000 lbs)				LCN	
									S	T	TT	TDT		
Whiteman AFB	Knob Noster, MO	SZL	869	18/36	12400 x	Concrete			150	220	440			
Wheeler AFB	Oahu, HI	HHI	840	9/24	5600 x 300	Asphalt			60	120	140			
Williams AFB	Chandler, AZ	CHD	1385	12/30	10400 x	Concrete			55	100	120			
Wright Patterson AFB	Dayton, OH	FFO	324	05L/23R	12600 x 300	Asp/Con	Conventional	.185	155	220	550			
Wurtsmith AFB	Oscoda, MI	OSC	634	6/24	11800 x	Concrete	Conventional		155	330	550			
Brooks AFB	, TX		594		5200 x	Concrete							20	
Chanute AFB	, IL.		624		6301 x	Concrete							27	
L.G. Hanscom AFB	Befford, MA	BED	133		7000 x	Concrete								
Northwest Guam AFB	Guam		624		8500 x	Asphalt								
Wake Is. AFB	Wake Island	WAK			9800 x	Asphalt								

Table B-2.—Active U.S. Air Force Bases (Including Europe and Pacific) (Concluded)

AIRPORT				RUNWAY				RUNWAY	RUNWAY					
NAME	LOCATION CITY/STATE	ICAO/FAA IDENT. CODE	ELEVATION FEET	DESIGNATION	DIMENSIONS LENGTH X WIDTH,FEET	SURFACE	TREATMENT	TEXTURE DEPTH mm	Weight Bearing Capacity (1000 lbs)				LCN	
									S	T	TT	TDT		
U.S. Air Forces in Europe:														
Alconbury RAF	Alconbury, England	EGWZ	160	12/30	9000 x 200	Asphalt	Porous Friction Course		95	155	310	680		
Athenai APT	Ellinkon, Greece	LGAT	90	15L/33R	11000 x 197	Asphalt			-	-	-	800		
Aviano AB	Pagliano E Gori, Italy	LIPA	413	5/23	8600 x 148	Asphalt	Crushed Rock Seal Coat		80	220	315	660		
Bentwaters RAF	Bentwaters, England	EGVJ	86	7/25	8900 x 150	Asphalt			90	160	240	-		
Bitburg AB	Bitburg, Germany	EDAB	1228	6/24	8200 x 148	Asphalt	Marshal Asphalt		70	200	300	-		
Goose AB	Goose, Labrador	CYYR	156	9/27	11000 x 300	Concrete			-	-	600	-		
Hahn AB	Hahn, Germany	EDAH	1649	4/22	8000 x 148	Asphalt			35	180	265	-		
Incirlik AB	Adana, Turkey	LTAG	239	5/23	10000 x 200	Asphalt			155	220	350	-		
Lajes AB	Azores, Portugal	LPLA	180	16/34	10800 x 300	Asphalt			174	-	265	-		
Lakenheath RAF	Lakenheath, England	EGUL	32	6/24	9000 x 150	Asphalt			65	220	440	-		
Mildenhall RAF	Mildenhall, England	EGUN	33	11/29	9200 x 200	Asphalt	Slurry Seal		54	220	470	-		
Ramstein AB	Landstuhl, Germany	EDAR	780	9/27	8000 x 150	Asphalt			71	187	325	-		
Rhein Main AB	Frankfurt, Germany	EDAF	368	7L/25R	12800 x 150	Concrete			-	-	-	800		
Sembach AB	Sembach, Germany	EDAS	1052	7/25	7900 x 150	Asphalt	1/8 in. German Anti-skid coat		60	155	195	-		
Spangdahlem AB	Binsfeld, Germany	EDAD	1197	5/23	10000 x 150	Asphalt	" " " " "		70	165	270	-		
Torrejon AB	Madrid, Spain	LETO	1994	5/23	13400 x 200	Asphalt			120	230	420	760		
Upper Heyford RAF	Bicester, England	EGUA	437	9/27	9600 x 200	Asphalt			90	180	320	-		
Wiesbaden AB	Wiesbaden, Germany	EDAW	460	8/26	7000 x 120	Asphalt			50	120	170	-		
Zweibrucken AB	Zweibrucken, Germany	EDAM	1133	3/21	7900 x 150	Asphalt			85	125	210	610		
Pacific Air Forces:														
Anderson AFB	Guam, Guam	PGUA	624	6L/24R	11200 x 200	Concrete			70	230	480	(SWL/200/F.P. 100 psi)	177	
Ching Chuan Kang AB	Kung Kuan, Taiwan	RCMQ	665	18/36	12000 x 200	Concrete			145	283	470			
Clark AFB	Luzon, Philippines	RPMK	478	2/20	10500 x 150	Concrete			60	200	410			
Kadena AFB	Okinawa, Japan	RODN	142	5L/23R	12100 x 300	Asp/Con			155	245	364			
Korat AB	Nakhon, Thailand	VTUN	729	6/24	9800 x 148	Concrete			(SWL 75)					
Kunsan AB	Kunsan, Korea	RKJK	32	17/35	900 x 150	Concrete			100	145	330			
Misawa AB	Misawa, Japan	RJSM	119	10/28	10000 x 150	Asp/Con			65	170	230			
NKP AB	Nakhon West, Thailand	VTUW	579	15/33	8000 x 150	Asphalt			100	140	177			
Osan AB	K-55, Korea	RKSO	35	9/27	9000 x 150	Concrete			75	168	268			
U-Tapao AB	Ban U-Tapao, Thailand	VTBU	59	18/36	11500 x 200	Concrete			100	200	400			
Udorn AB	Udon Thani, Thailand	VTUD	584	12/30	10000 x 125	Concrete			(SWL-25/200 psi)					
Yokota AB	Honshu, Japan	RJTY	457	18/36	11000 x 200	Concrete			150	300	478			

Table B-3.—Active U.S. Naval Air Stations

AIRPORT				RUNWAY					RUNWAY					
NAME	LOCATION: CITY/STATE	ICAO/FAA IDENT. CODE	ELEVATION FEET	DESIGNATION	DIMENSIONS LENGTH x WIDTH, FEET	SURFACE	TREATMENT	TEXTURE DEPTH mm	Weight Bearing Capacity (1000 lbs)				LCN	
									S	T	TT	TDT		
Alameda NAS (Nimitz Field)	Alameda, CA	NGZ	15	13/31	8000 X	Asphalt/ Concrete			105	165	308	SWL 50		
Cecil Field NAS	Jacksonville, FL	NZC	80	18L/36R	12500 X	Asphalt/ Concrete			105	165	315			
Chase Field NAS	Beeville, TX	NIR	190	13R/31L	8000 X	Asphalt/ Concrete			95	123	185			
Corpus Christi NAS	Corpus Christi, TX	NGP	19	13R/31L	8000 X	Asphalt/ Concrete			154	264	417			
Dallas NAS (Hansley Field)	Dallas, TX	NBE	495	17/35	8000 X	Asphalt/ Concrete			85	140	275			
Atlanta NAS/Dobbins AFB	Marietta, GA	NCQ	1068	11/29	10000 X	Concrete			200	300	560			
Fallon NAS (Van Voorhis Field)	Fallon, NV	NFL	3934	13/31	14000 X	Asphalt/ Concrete			90	116	177	SWL 42		
Glenview NAS	Glenview, IL	NBU	653	17/35	8000 X	Asphalt/ Concrete			72	115	250			
Jacksonville NAS (Towers Field)	Jacksonville, FL	NIP	22	13/31	8000 X	Asphalt/ Concrete			115	192	300			
Key West NAS (Boca Chica Field)	Key West, FL	NQX	6	7/25	10000 X	Asphalt/ Concrete			95	173	339			
Kingsville NAS	Kingsville, TX	NQI	50	13R/31L	8000 X	Concrete/ Asphalt			105	137	205			
Lakehurst NAS	Lakehurst, NJ	NEL	103	6/24	5000 X	Asphalt			105	137	205			
Lemoore NAS (Reeves Field)	LeMorre, CA	NLC	237	14/32	1350 X	Asphalt/ Concrete			156	225	385	SWL 74		
Los Alamitos NAS	Los Alamitos, CA	NTB	35	4/22	8000 X	Asphalt/ Concrete			34	82	123			
Memphis NAS	Memphis, TN	NQA	322	3/21	8000 X	Asphalt/ Concrete			86	112	168	SWL 41		
Meridian NAS (McCain Field)	Meridian, MS	NMM	317	18/36	8000 X	Concrete			173	300	525			
Miramar NAS (Mitscher Field)	Miramar, CA	NKX	477	6L/24R	12000 X	Concrete			116	181	308	SWL 55		
Moffett Field NAS	Mountain View, CA	NUQ	34	14R/32L	9200 X	Asphalt/ Concrete			63	112	257	SWL 30		
Norfolk NAS (Chambers Field)	Norfolk, VA	NGU	15	10/28	7300 X	Asphalt/ Concrete			121	214	412			
North Island NAS (Halsey Field)	San Diego, CA	NZY	24	11/29	8100 X	Concrete			112	194	358			
Ocean NAS (Sourcek Field)	Oceana, VA	NTU	22	5/23	12000 X	Asphalt/ Concrete			115	170	260			

Table B-3.—Active U.S. Naval Air Stations (Concluded)

AIRPORT				RUNWAY					RUNWAY					
									Weight Bearing Capacity (1000 lbs)				LCN	
NAME	LOCATION: CITY/STATE	ICAO/FAA IDENT. CODE	ELEVATION FEET	DESIGNATION	DIMENSIONS LENGTH x WIDTH, FEET	SURFACE	TREATMENT	TEXTURE DEPTH mm	S	T	TT	TDT		
Patuxent River NAS	Patuxent, MD	NHK	38	6/24	11800 X	Concrete			126	188	340			
Pensacola NAS (Forrest Sherman Field	Pensacola, FL	NPA	30	6R/24L	8000 X	Asphalt/ Concrete			114	206	382			
Point MUGU NAS	Point Mugu, CA	NTD	13	3/21	11100 X	Asphalt/ Concrete			195	243	364	SWL 88		
Saufley Field NAS	Pensalcola, FL	NUN	85	9/27	6000 X	Asphalt			63	82	123			
South Weymouth NAS (Shea Field)	South Weymouth, MA	NZW	161	17/35	7000 X	Asphalt/ Concrete			95	124	186			
Whidbey Island NAS (Ault Field)	Whidbey IS., WA	NUW	47	6/24	8000 X	Concrete			142	257	455			
Whiting Field NAS - No	Mieton, FL	NSE	200	13/31	6000 X	Asphalt			36	47	70			
Willow Groove NAS	Willow Groove, PA	NXX	361	15/33	8000 X	Asphalt/ Concrete			95	161	318			

Table B-4.—Active U.S. Army Air Fields

AIRPORT				RUNWAY					RUNWAY					
NAME	LOCATION: CITY/STATE	ICAO/FAA IDENT. CODE	ELEVATION FEET	DESIGNATION	DIMENSIONAL LENGTH x WIDTH,FEET	SURFACE	TREATMENT	TEXTURE DEPTH mm	Weight Bearing Capacity (1000 lbs)				LCN	
									S	T	TT	TDT		
Biggs AAF (Fort Bliss)	Biggs, TX	BIF	3947	3/21	13600 X	Asphalt/ Concrete			220	330	440			
Blackstone AAF - Allen C. Perkinson Muni. (Fort Pickett)	Blackstone, VA	BKT	428	18/36	5200 X	Asphalt/ Concrete								
Butts AAF (Fort Carson)	Butts, CO	FCS	5838	12/30	4500 X	Asphalt			17	27	(AUW 90)			
Cairns AAF (Fort Rucker)	Ozark, AL	OZR	305	18/36	5000 X	Asphalt			36	64				
Campbell AAF (Fort Campbell)	Campbell, KY	HOP	571	4/22	11800 X	Concrete			100	190	310			
Davison AAF (Fort Belvoir)	Davison, VA	DAA	69	14/32	4000 X	Asphalt			18	30				
Devens AAF (Fort Devens)	Ayer, MA	AYE	268	2/20	3700 X	Asphalt			(AUW 130)					
Felker AAF (Fort Eustis)	Felker, VA	FAF	12	14/32	3000 X	Asphalt								
Forney AAF (Fort Leonard Wood)	Forney, MO	TBN	1158	14/32	5000 X	Asphalt			100	140	225			
Fritzsche AAF (Fort Ord)	Monterey, CA	OAR	134	11/29	3000 X	Asphalt			(SWL 20)	(AUW 50)				
Godman AAF (Fort Knox)	Godman, KY	FTK	753	17/35	5200 X	Concrete			14	20				
Gray AAF (Fort Lewis)	Tacoma, WA	GRF	301	15/33	6100 X	Asphalt			65	200	330			
Grayling AAF	Camp Graying, MI	55D	1152		5000 X	Asphalt			35	45	80			
Haley AAF (Fort Sheridan)	Haley, IL	FSN	690		3100 X	Asphalt			10	-	-			
Henry Post AAF (Fort Sill)	Lawton, OK	FSI	1187	17/35	5000 X	Concrete			100	135	195			
Hood AAF (Fort Hood)	Killeen TX	HLR	923	15/33	4700 X	Asphalt			33	82	-			
Hunter AAF	Savannah, GA	SVN	42	9/27	11400 X	Asphalt			93	142	235			
Lawson AAF (Fort (Benning)	Columbus, GA	LSF	232	14/32	8200 X	Asphalt/ Concrete			65	220	320	(SWL 100/psi 200)		
Marshall AAF (Fort Riley)	Junction City, KS	FRI	1065	4/22	4500 X	Concrete			12	21	-			
Phillips AAF (Aberdeen Proving Ground)	Aberdeen, MD	ARG	57	4/22	8000 X	Asphalt			90	200	500			

Table B-4.—Active U.S. Army Air Fields (Concluded)

AIRPORT				RUNWAY					RUNWAY					
NAME	LOCATION: CITY/STATE	ICAO/FAA IDENT. CODE	ELEVATION FEET	DESIGNATION	DIMENSIONS LENGTH x WIDTH, FEET	SURFACE	TREATMENT	TEXTURE DEPTH mm	Weight Bearing Capacity 1000 lbs.				LCN	
									S	T	TT	TDT		
Polk AAF (Fort Polk)	Leesville, LA	POE	330	15/33	4100 X	Asphalt			65	85				
Redstone AAF (Red Stone Arsenal)	Redstone, AL	HUA	685	17/35	7000 X	Asphalt			(MAW 600)					
Robert Gray AAF (Fort Hood)	Killeen, TX	GRK	1015	15/33	10000 X	Asphalt/ Concrete			65	180	280	720		
Seneca AAF	Romulus, NY	SSN	646	16/34	4000 X	Asphalt								
Sherman AAF (Fort Leavenworth)	Sherman, KS	FLV	770	15/33	5900 X	Asphalt			32	97	-			
Simmons AAF (Fort Bragg)	Fayetteville, NC	FBG	242	9/27	3000 X	Asphalt			21	36				
Tipton AAF (Fort Meade)	Odenton, MD	FME	150	10/28	3000 X	Asphalt								
Wheeler-Sack AAF (Fort Drum)	Wheeler-Sack, NY	GTB	680		5000 X	Concrete			93	142	235			
Wright AAF (Fort Stewart)	Hinesville, GA	LHW	46	5L/32R	5000 X	Asphalt/ Concrete			60	104	125			

APPENDIX C
PHENOMENOLOGY OF FRICTION

This section deals with the frictional and retarding forces that can be developed when aircraft tires are operated on prepared, hard runway surfaces. The mechanisms whereby such forces are generated at the tire-ground contact area are briefly described. Particular consideration is then given to the effects on braking force of changes in tire, runway surface and aircraft design and operational factors. Reference 17 material has been freely used in this section and frequently quoted as such.

FRICTIONAL AND RETARDING FORCES ACTING ON A TIRE

The forces which can act on a tire and decelerate its forwarding motion are rolling resistance, braking friction, yawed rolling and braking forces (if considered), and fluid drag force (see Figures C1 and C2). For unyawed tires, the resultant tangential force, G, on the tire is the component G_x, acting, parallel to the direction of forward motion, i.e.

$$G_x = G = G_R + G_B + G_F = Z\mu \qquad \text{(C-1)}$$

COEFFICIENT OF FRICTION DURING BRAKING

The frictional force developed in the tire-ground contact area and the coefficient of friction vary greatly with changes in braking slip ratio, as is shown schematically in Figure C3.

BRAKING ON DRY SURFACES

The development of braking force on dry surfaces may be illustrated by reference to Figure C4 which shows the passage of a single tread element through the tire-ground contact area. In Figure C4, when the tread element first makes contact with the ground, it is practically undeflected and stationary relative to the surface. As it progresses toward the rear of the contact area the longitudinal deflecton of, and the tangential force on, the element increases and at some point sliding commences (initially the sliding speed relative to the surface is very low).

FRICTIONAL FORCE ON A TREAD ELEMENT

In the tire-ground contact area, the frictional force on each tread element is the product of:

(i) the normal load on the element (which is itself governed by the distribution of bearing pressure in the contact area), and

(ii) the local coefficient of friction between the tread material in the element and the runway surface.

RESULTANT BRAKING FORCE ON TIRE

The braking force developed by a tire is the sum of the components of the frictional forces on all tread elements in the ground contact area acting parallel to the direction of forward motion.

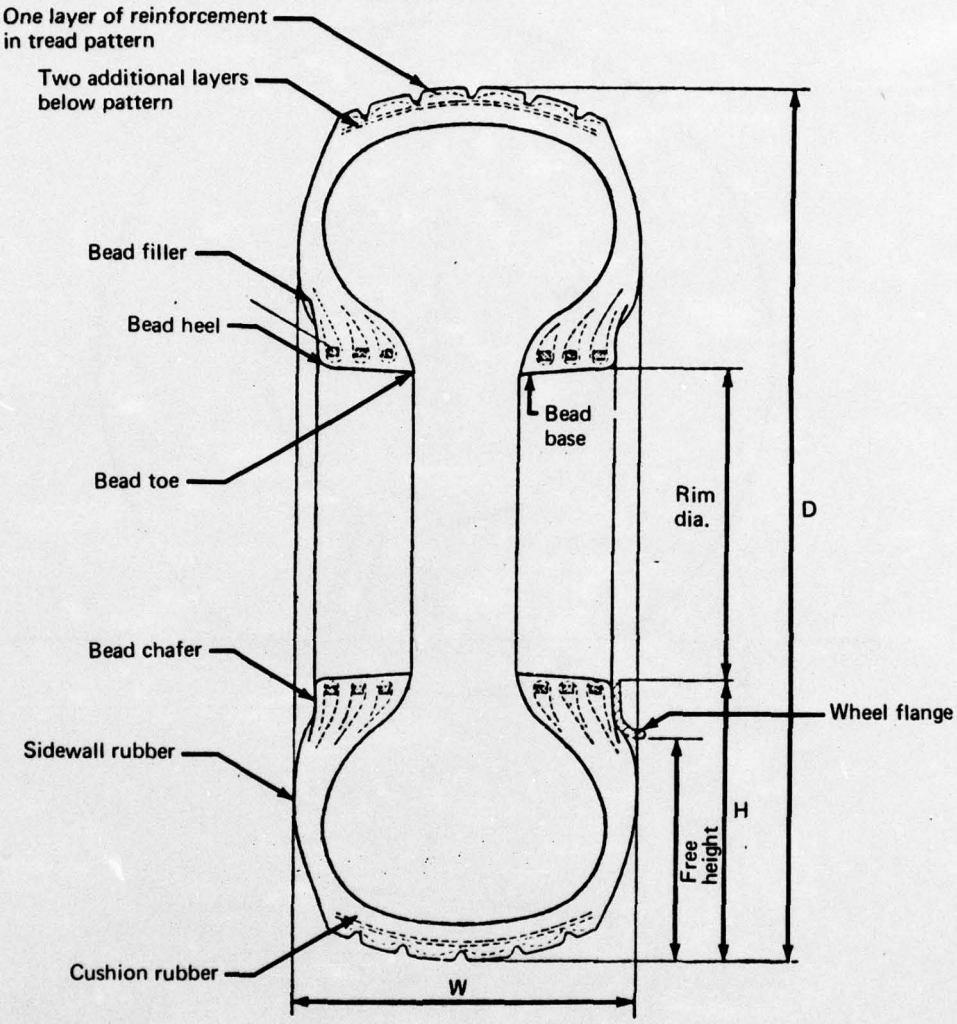

Figure C1.—Cross Section of a Typical Aircraft Tire

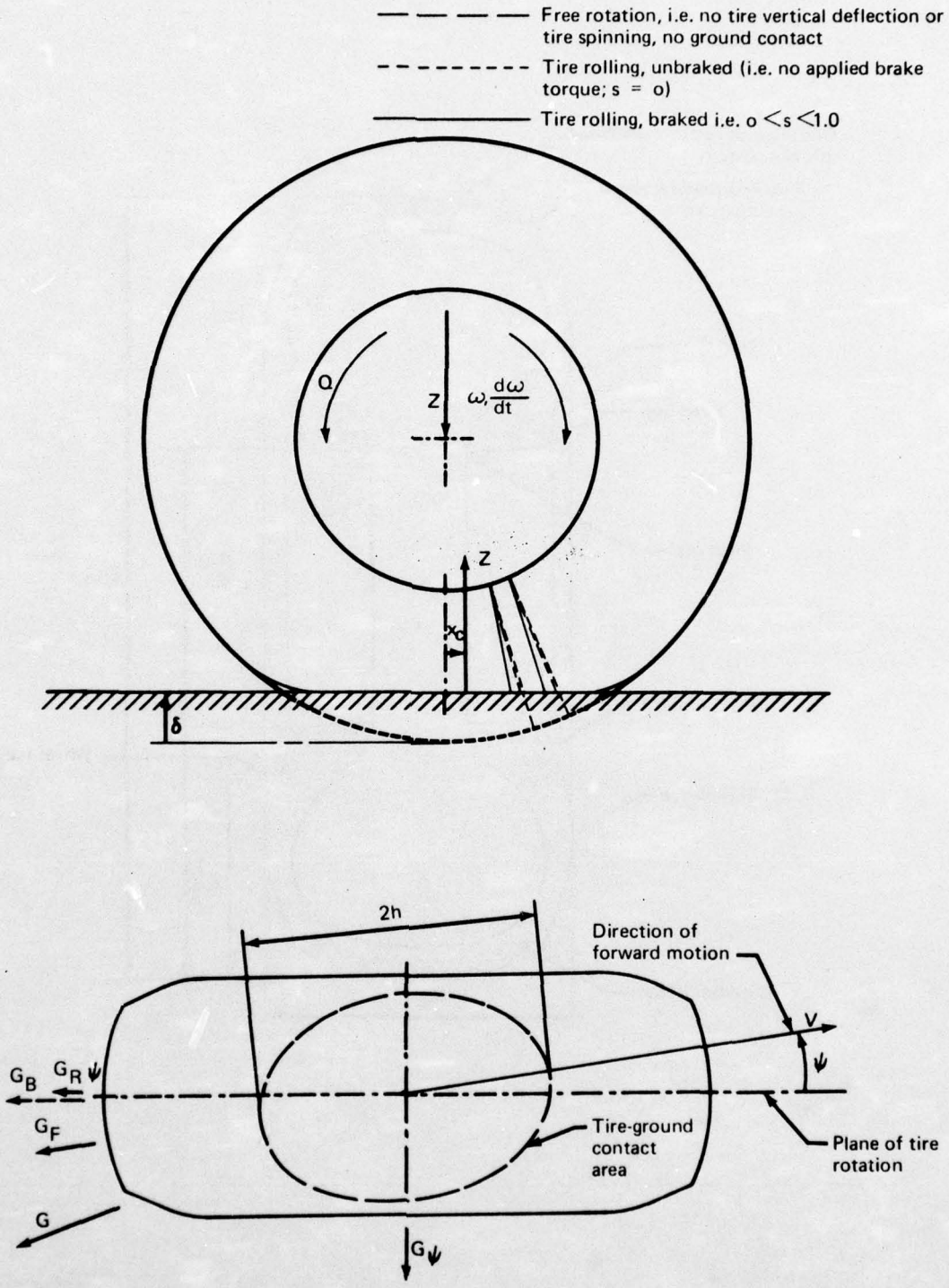

Figure C2.—Tire Forces and Moments

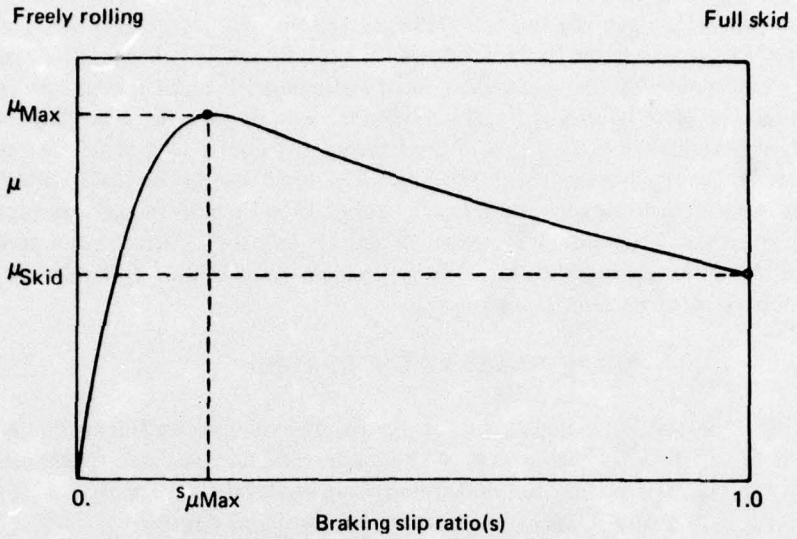

Figure C3.—Typical Variation of Tire-Ground Coefficient of Friction with Braking Slip Ratio

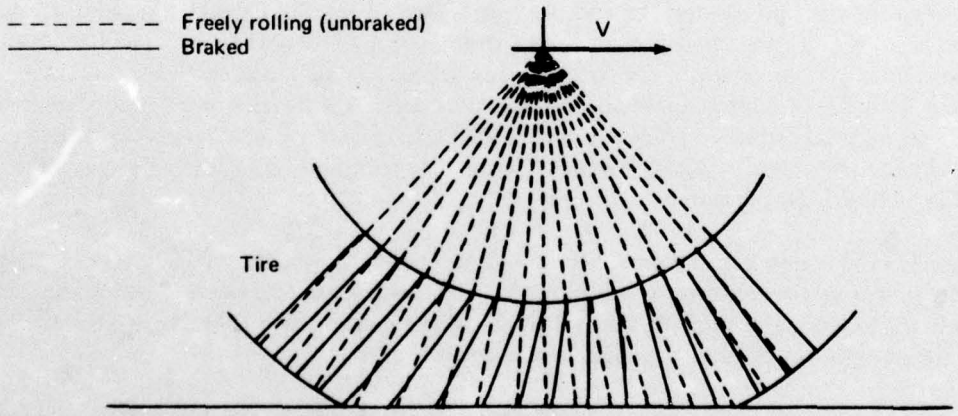

Figure C4.—Schematic Illustration of Deformation of Cross-Ply Tire Elements Due to Braking

At low braking slip ratios, sliding is detectable only at the rear of the tire-ground contact area. If the brake torque, and hence slip ratio, is increased, sliding occurs at higher values of V and may be observed at points nearer to the front of the contact area. It is hypothesized that this process can continue until further changes in local sliding speeds and temperatures produce no net increase in the total frictional force on the tire. The braking force is then the maximum possible in that situation, G_{max}, and the tire-runway coefficient of friction is μ_{max}. Further increase in "s, braking slip ratio" produces a net decrease in the total frictional force. Tire longitudinal deflections in the contact area cannot then be maintained and rapid increases in local sliding speeds and tire slip ratio occur. When s = 1.0, the entire contact area is sliding at speed V and the braking force developed is the locked-wheel or full-skid value, G_{skid}. The tire-runway coefficient of friction is then μ_{skid}.

BRAKING ON WET SURFACES

The presence of a fluid, which is usually water, on a runway decreases the available tire-ground coefficient of friction. The effects of fluid such as slush, oil, fuel, foam, etc. are basically similar to those of water. Some differences in the available coefficient of friction are to be expected as a result of variations in fluid viscosity and density.

The tire-ground contact area in wet conditions can be divided into three zones as illustrated in Figure C5.

Zone 1 is the region where impact of the tire with the surface fluid generates sufficient pressure to overcome the inertia of the fluid. Much of the fluid is either ejected as spray or forced beneath the tire into the tread grooves (if present) or into the drainage paths provided by the surface texture. Throughout Zone 1 a continuous, relatively thick fluid layer exists between the tire and the runway surface and the only retarding force developed is that due to fluid drag.

Zone 2 is a transition region. After the bulk of the fluid is displaced, a thin film remains between the tire and the surface. At the rear of Zone 1, and in Zone 2, a rapid outflow of fluid is prevented, and fluid pressures are maintained, by viscous effects. The thin film first breaks down at points where the local bearing pressure is high, e.g. at sharp surfaces asperities. In the presence of a lubricant such as water, the coefficient of friction of rubber on hard surfaces is greatly reduced from the dry surface value and varies little with changes in sliding speed and temperature. Thus, in general, very little frictional force is generated wherever a thin film of fluid persists.

Zone 3 is the region of predominantly dry contact and, although obviously smaller than the contact area in dry conditions, it is here that most of the braking force is generated. The tendency for tread elements towards the rear of the contact area to slide may be increased by the presence of fluid at the edges of the contact area.

In wet conditions, the tire-ground coefficient of friction depends on the relative sizes of Zones 1, 2 and 3. These are determined by the surface texture, the depth, density and viscosity of the fluid, the tread pattern and inflation pressure of the tire and the time, t, for a tread element to pass through the contact area, given by

$$t = \frac{\text{length of contact area}}{\text{tire peripheral speed}} = \frac{2h}{\omega \times \text{rolling radius of tire}}$$

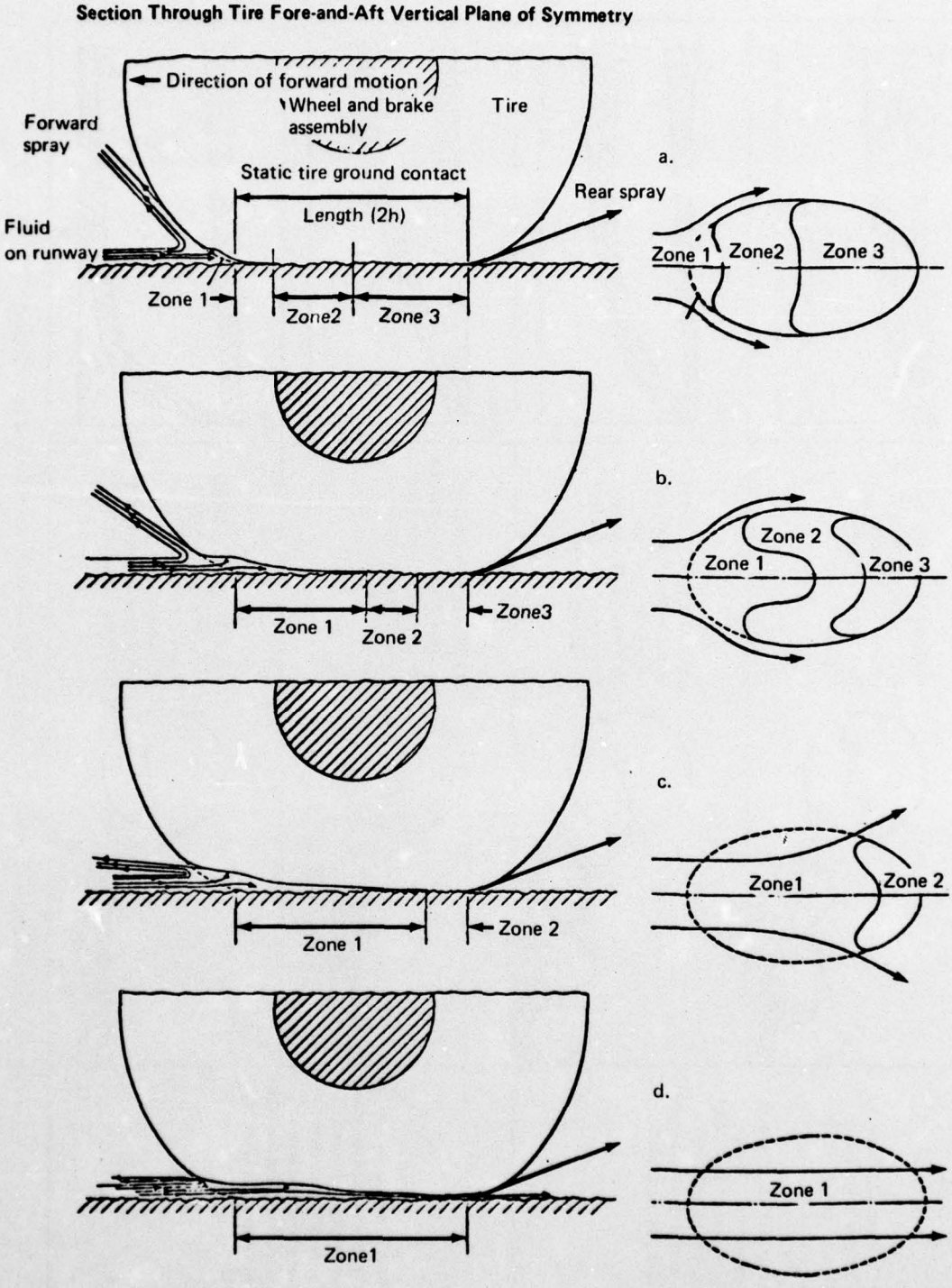

Figure C5.—Effect of Forward Speed on the Tire-Ground Contact Area in Wet Condition

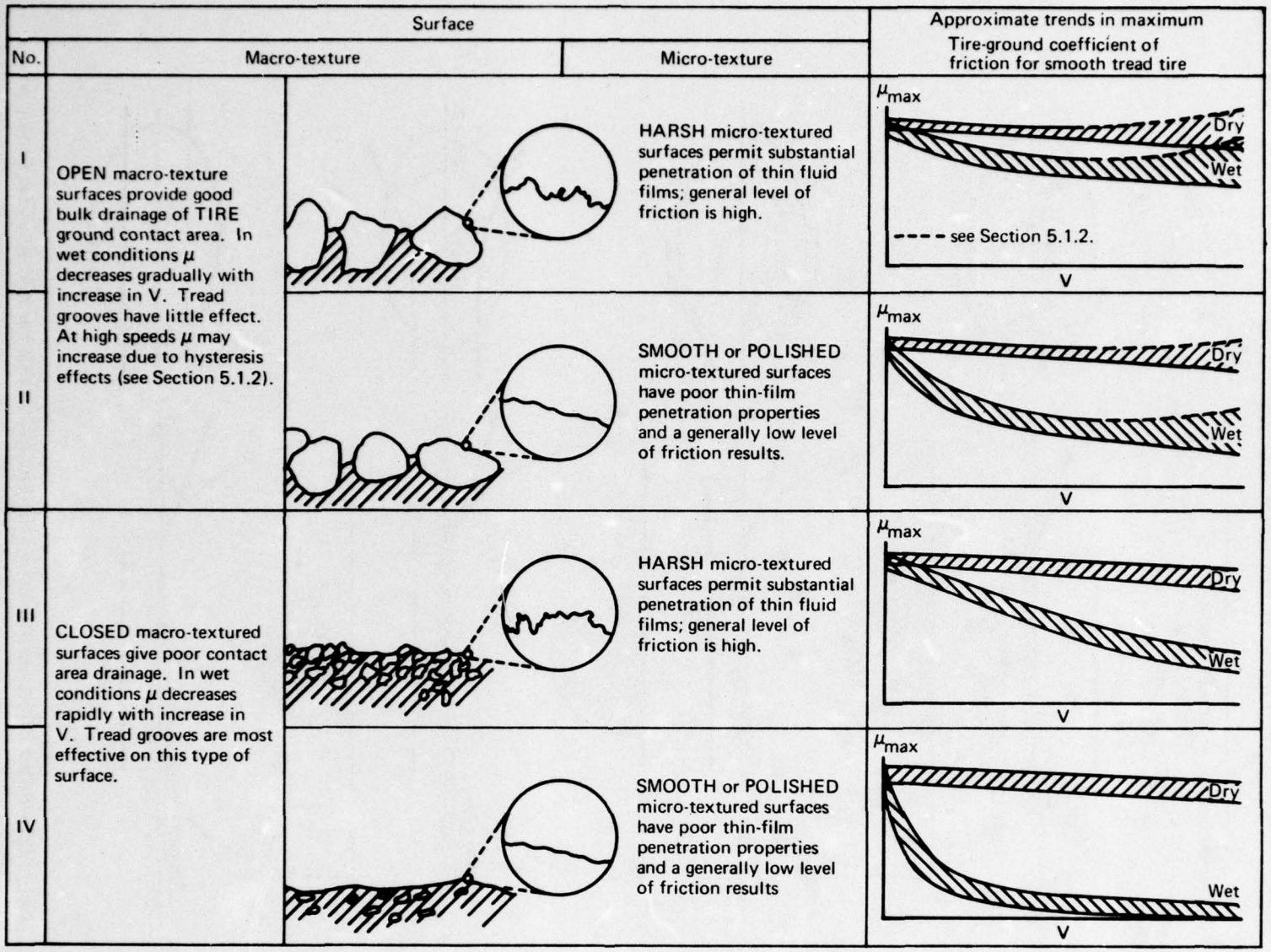

Figure C6.—Effect of Surface Texture on Tire-Ground Coefficient of Friction

where rolling radius of tire is the ratio $\left(\frac{\text{horizontal rolling velocity}}{\text{wheel angular velocity}}\right)$.

Figure C5 also shows the effect of increased forward speed on the relative sizes of Zones 1, 2 and 3. In Figure C5b the tire forward speed is higher than in Figure C5a so that Zone 1 extends farther back into the contact area and Zones 2 and 3 occupy a horsehoe-shaped region at the rear. In Figure C5c, at a still higher speed, contact with the ground is all but lost. In this condition the tire develops very little braking force. Finally, in Figure C5d, the tire is moving at a speed such that Zone 1 extends throughout the contact area. (When dry contact with the ground ceases, the tire is said to be "planing".)

FACTORS AFFECTING THE AVAILABLE TIRE-GROUND COEFFICIENT OF FRICTION DURING BRAKING

TIRE DESIGN AND CONSTRUCTION

Tire design factors, e.g. size, aspect ratio, strength (ply rating), type of construction, materials and tread pattern, influence the coefficient of friction in so far as they determine the distribution and average value of bearing pressure in the tire-ground contact area. The direct effects of these design factors on the available coefficient of friction are discussed below.

There is no evidence that tire diameter directly affects the coefficient of friction available on wet or dry surfaces.

On wet surfaces, at a given forward speed, the time available for the removal of fluid is determined by the length of the contact area. Conventional tires, of low aspect ratio, have proportionately shorter contact lengths under given loading conditions than tires of high aspect ratio. Thus, on wet surfaces at high speed, tires of relatively low aspect ratio (also known as "low profile tires") may give reduced values of braking coefficient of friction. See figures C7 and C8.

Tire size and section shape are not independent parameters; they are related to the design loads and construction of the tire. At present, all aircraft tires in general usage are of cross-ply construction. Tests with car tires suggest that the use of radial-ply construction may provide a small increase in braking force on wet surfaces. See figure C9.

TIRE TREAD MATERIAL

The treads of most aircraft tires are made with compounds based on natural rubber polymers. The frictional properties of rubber compounds depend on the particular polymer and upon the quantities of filler and extender oil used to produce a practical tread material.

Car (ref. 44) and trailer (ref. 46) tests show that some tread compounds (usually, but not necessarily, based on synthetic rubber polymers) can give significantly higher coefficients of friction on surfaces of large macro-texture depth. This effect when present, usually increases with increase in forward speed and is particularly beneficial in wet conditions. See figure C10. However, such compounds are at present considered unsuited to most aircraft applications, since their physical characteristics do not provide an optimum solution to the many demands placed on a tread material.

Cornering force machine test

Load: 800 lb.
Inflation pressure: 300 p.s.i.
Automobile tires of equivalent
Overall diameter
Same groove and rib dimensions
for both tires
(Ref. 41)

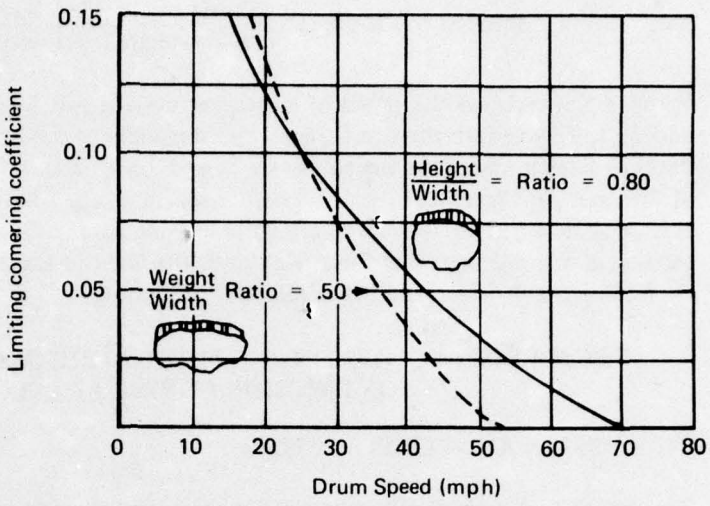

Figure C7.—Comparison of Tires Having Different Sectional Shape

Road surface:

Wet asphaltic concrete with fine slag screenings .04 inch water cover depth
(Ref. 42)

Tire no.
5. .6

○ □ 20 mph
△ ▲ 40 mph
● ■ 60 mph

Tire-size

(5) 7.75-14
(6) D70-14
Both tires were belted and diagonal cross-ply highway type pattern with 7 ribs.

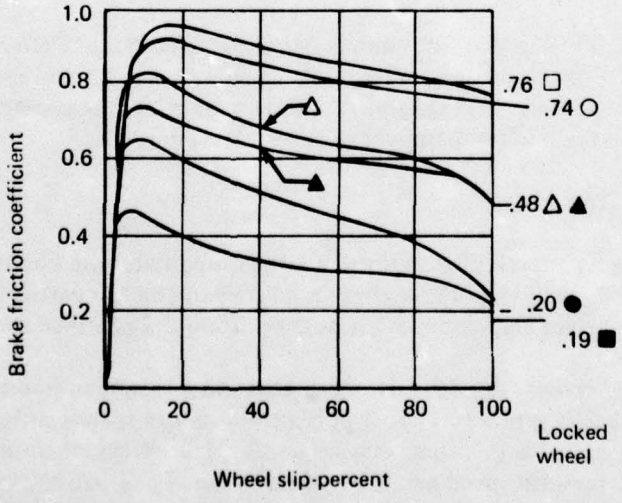

Figure C8.—Aspect Ratio Effect on Tire Brake Force Characteristics

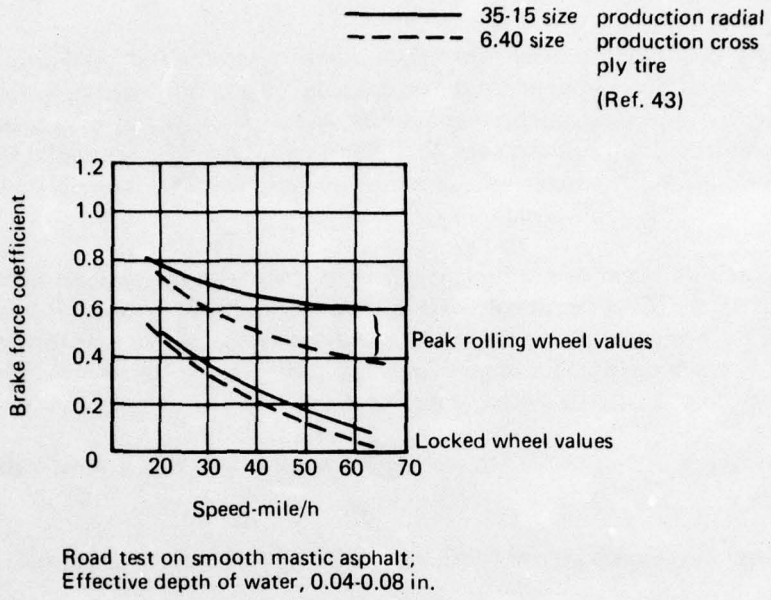

Figure C9.—Comparison of Production Radial and Conventional Tires.

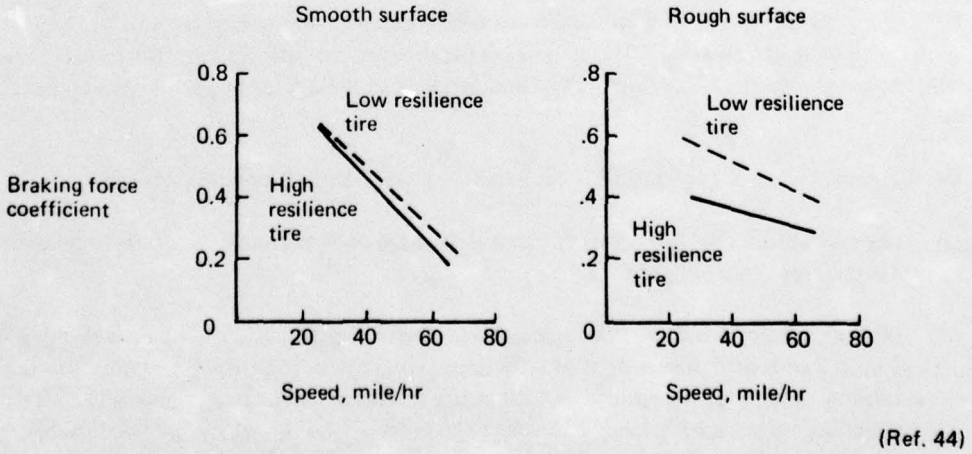

Figure C10.—Skidding Resistance of Tires of Different Resilience on Surfaces of Different Textures.

TIRE TREAD PATTERN

The primary function of a tread pattern is to improve the tire frictional properties on wet surfaces. Two distinct types of tread design features are widely used to achieve this. Firstly, circumferential grooves in the tire remove bulk quantities of fluid from the contact area. This is of greatest benefit on surfaces such as III and IV in figure C6. Secondly, the wiping action at sharp edges of, for example, cuts, slots and grooves, assists in breaking down the thin fluid film in Zone 2 of the contact area.

The available coefficient of friction appears to increase with increasing number of circumferential grooves. However, detailed experimental work (refs. 43 and 45) involving closer control of the geometrical properties of the test tire treads, shows that further increase in μ is unlikely when the number of grooves is increased beyond four or five. See figures C11 and C12. Such tests also show that μ increases with:

(i) Increase in tread groove width (within the range of practical groove widths), See figure C13.

(ii) Increase in the ratio groove width/rib width (up to a limit of about 0.4),

(iii) Decrease in the "mean flow distance", i.e. the mean distance that a fluid must travel laterally in the contact area before reaching a groove, slot etc.; See figure C14.

The tread patterns on most current aircraft-type tires consist solely of circumferential ribs and grooves. Grove depth has a considerable effect on the ability of the tread pattern to remove rapidly large quantities of fluid from the tire-ground contact area. References 41, 49 and 25 show that in wet conditions the available coefficient of friction decreases with decrease in tread groove depth, the effect being particularly severe on smooth surfaces such as III and IV in Figure C6.

INFLATION PRESSURE

Inflation pressure is an adequate approximation to the average tire-ground bearing pressure, although carcass stiffness and tread effects produce some differences. Since it is a more convenient parameter to work with, inflation pressure is used here in preference to bearing pressure.

On wet surfaces, a change in inflation pressure results in two primary effects.

(i) In general, the coefficient of friction decreases with increase in inflation pressure (refs. 22 and 46). See Figure C15.

(ii) In deep water, Zone 1 of the tire-ground contact area can be large compared with Zones 2 and 3 and at high speeds it may become so great that contact between the tire and the runway is lost. It is found that increasing inflation pressure (provided the static tire-ground contact area is kept constant) tends to offset this effect. Consequently, under these conditions, the higher inflation pressure at which the tire is designed to operate, the greater the speed can be before this loss of contact occurs.

AD-A039 968 BOEING COMMERCIAL AIRPLANE CO SEATTLE WASH F/G 1/2
TIRE RUNWAY INTERFACE FRICTION PREDICTION SUBSYSTEM.(U)
MAR 77 M K WAHI, H H STRAUB F33657-74-C-0129
UNCLASSIFIED ASD-TR-77-7 NL

2 OF 3
AD
A039968

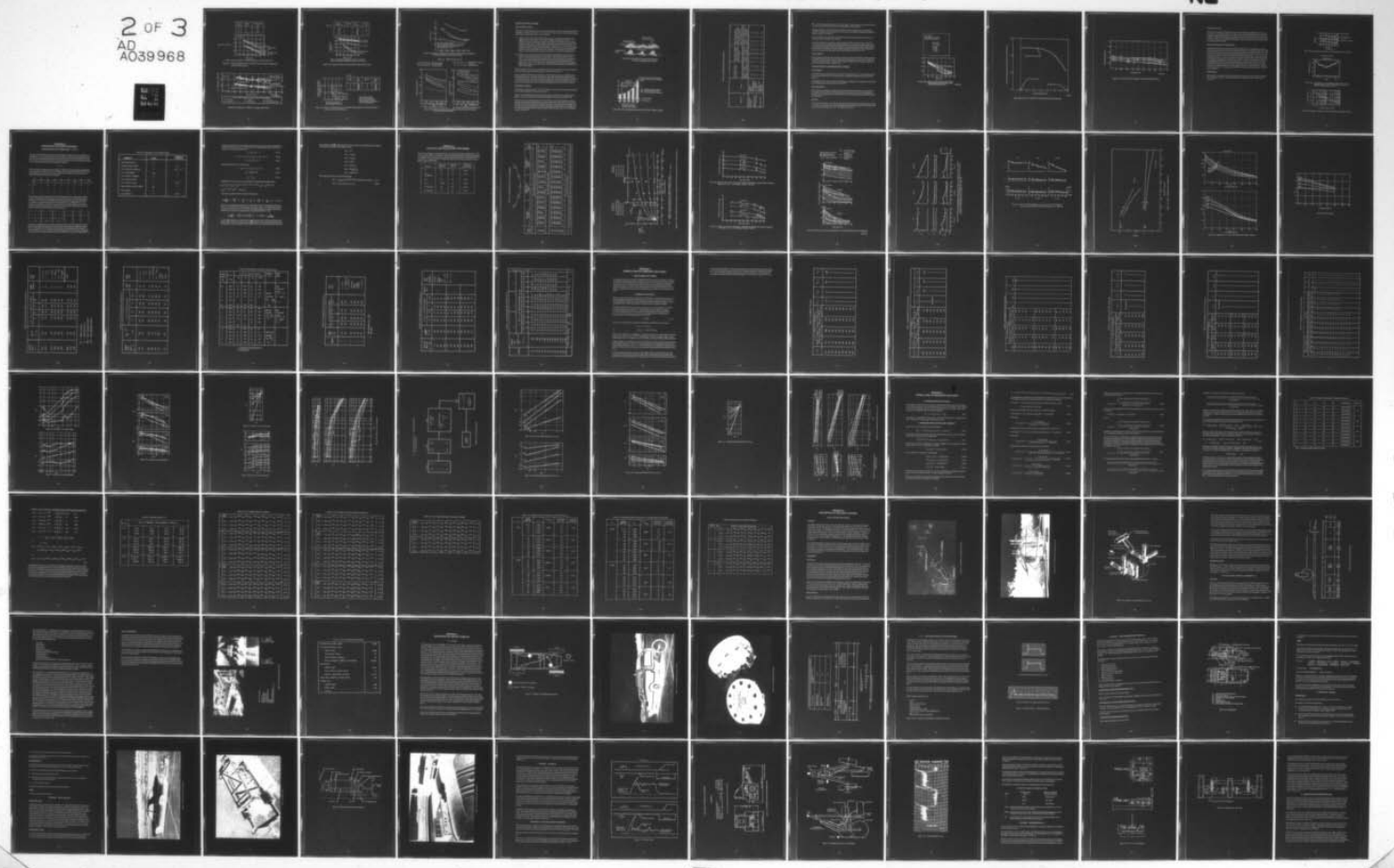

Rib (No.)	Grooves (No.)	Grooves width (in.)
5	4	0.2
6	5	0.2
7	6	0.2

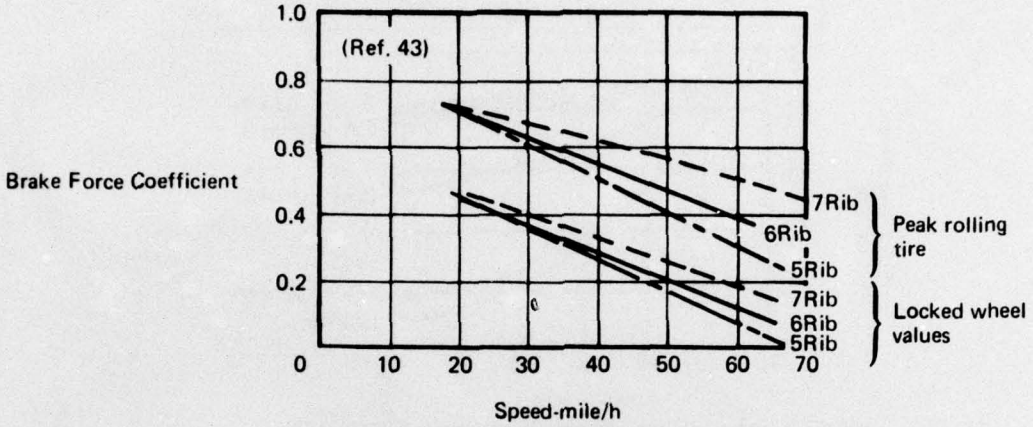

Surface–smooth mastic asphalt, tires–185X15 radial ply, water depth–0.05–0.10 in.

Figure C11.—Results of Braking Tests on Tires with Four, Five and Six Equal Width Circumferential Grooves

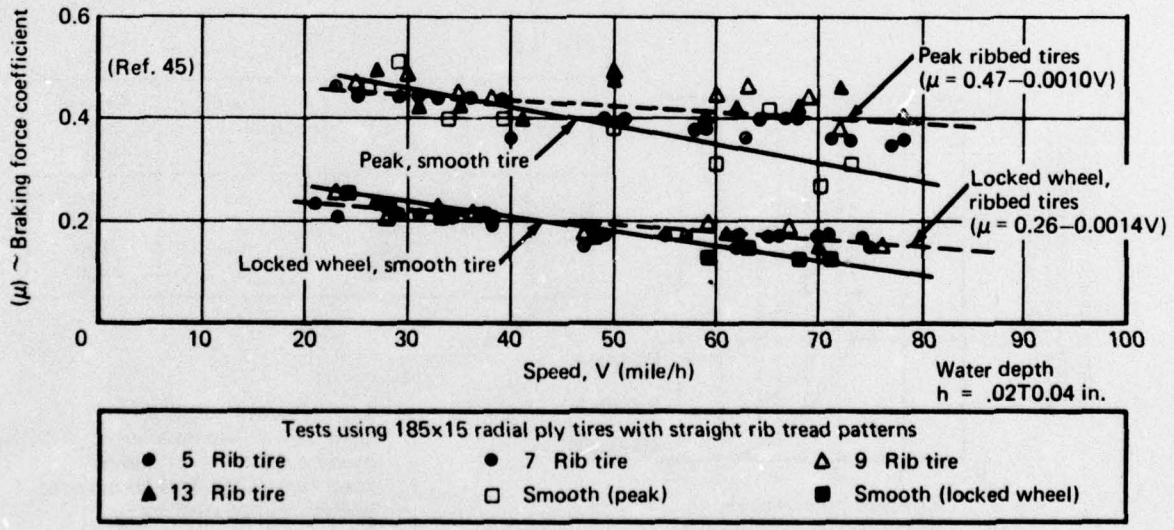

Figure C12.—Experiment 1 Results on Rounded Gravel Carpet

(Ref. 43)

Grove Width (in)	Grooves (in)	Rib width (in)	Ribs (no.)
0.02		0.5	5
0.1		0.5	5
0.2		0.5	5
0.3		0.5	5
0.4		0.5	5

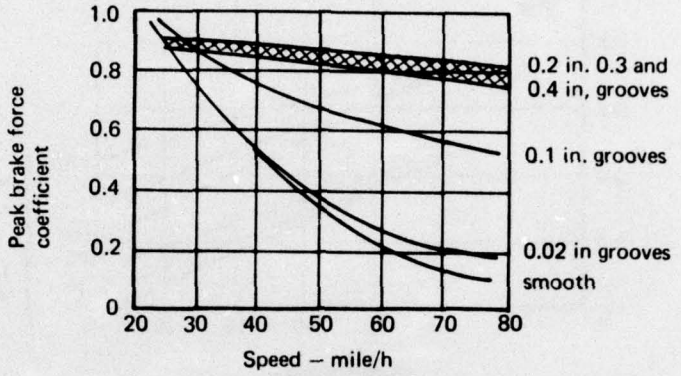

Test on experimentally produced five-rib patter tire, 185x15 radial ply; water depth, 0.03-0.08 in; surface, smooth concrete.

Figure C13.—Effects of Change in Groove Width on Peak Braking Force

(Ref. 43)

Ribs (no.)	Rib width (in)	Grooves (no)	Groove width (in)
3	0.36	12	0.10
9	0.50	8	0.15
7	0.66	6	0.20
5	0.92	4	0.30

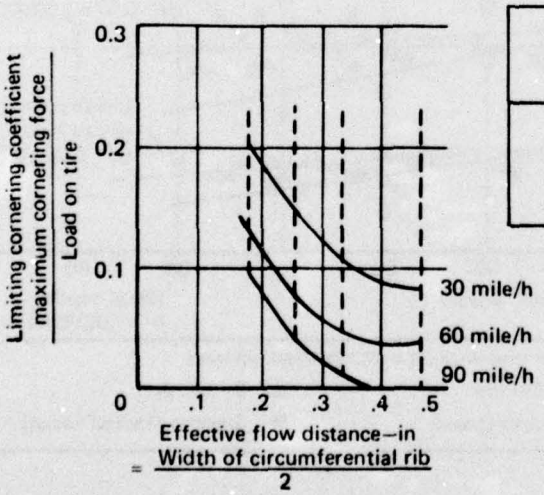

Test on indoor machine: Load, 870 lb. tire inflation pressure, 26 lb/in^2; effective water film, 0.008 in at 60 miles /h; surface, murled steel drum.

Figure C14.—Effective Cornering Grip for Tires Having Tread Patterns with Various Number of Smooth Circumferential Grooves

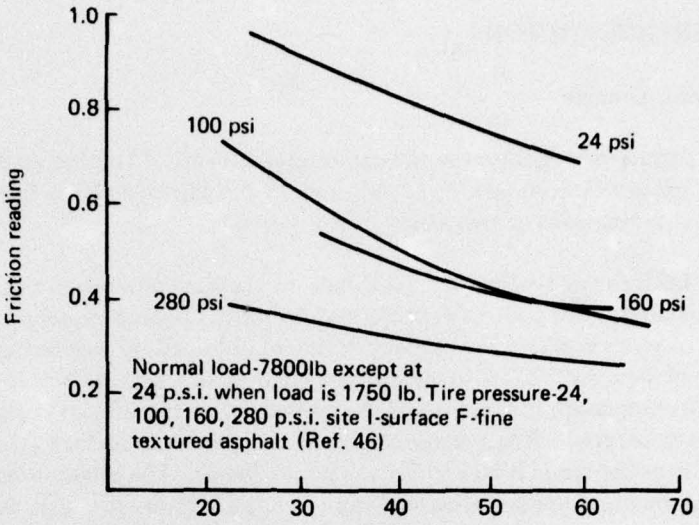

Figure C15.—Relationship Between Impending-Skid Braking-Force Coefficient and Speed with Heavy Load Friction Vehicle.

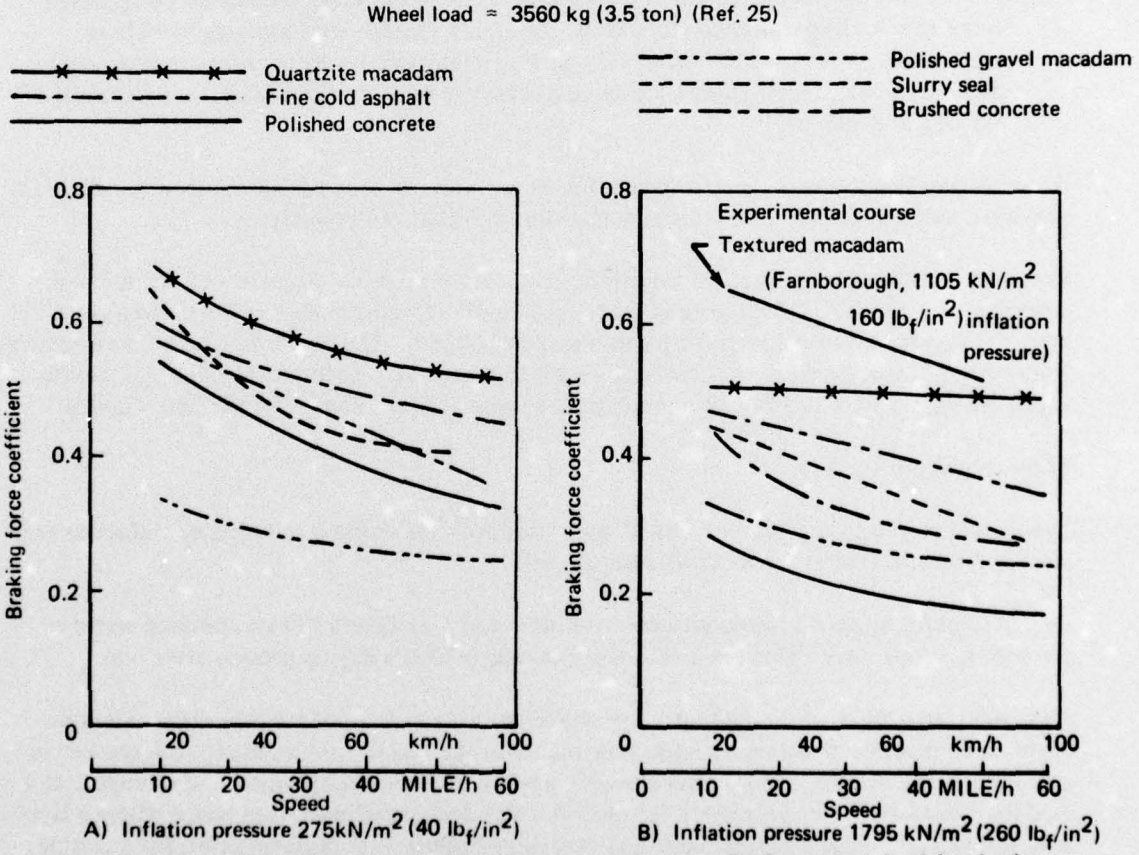

Figure C16.—Effect of Surface Texture on Braking Performance-Anti-Locked Wheel Braking-All Surfaces Wet

RUNWAY SURFACE FACTORS

Surface Material, Texture

The effect of surface material on the tire-ground coefficient of friction arises principally from differences in surface texture (ref. 7, 21, 41, and 43). Figure C6 shows four idealized surfaces that illustrate combinations of two scales of texture.

(i) Large or macro-scale texture - this depends on the sizes and relative quantities of the aggregates used. This scale of texture may be judged approximately by the eye. A measure of surface macro-texture depth can be obtained by working a known volume of grease or sand (ref. 25) into the surface voids until a smooth finish is obtained. The average texture depth is the ratio of the volume of grease (ref. 21) or sand used to the surface area covered. When measured in this way, runway surface macro-texture depths usually lie in the range 0.004 to 0.1 in (0.1 to 3mm). The dimensions of individual stones can be much greater than this (up to about 0.75 in, 20 mm). See figure C16.

(ii) Small or micro scale texture - this is the texture of the individual stones of which the runway is constructed and depends on the shape of the stones and how they wear (ref. 7). It may not, in general, be judged by the eye but differences may be apparent to the touch. Experimental work (refs. 7 and 47) suggests that asperity heights as small as 40×10^{-6} in. (10^{-3} mm) play an important role in the friction process, particularly on wet surfaces where they serve to break down thin fluid films. See Figures C17 and C18 and Table C1.

While, in practice, runways vary considerably in texture, the four surfaces shown in Figure C6 provide a useful means of characterizing the extremes that can be met.

For wet conditions, the effects of variations in surface texture on μ_{max} are illustrated and described in figure C6. This figure indicates the close relationship that exists between the effect of surface texture, tire tread pattern and fluid depth. The curves in figure C6 are drawn for a smooth tread tire; the effect of using a rib tread tire is to reduce the fall of μ_{max} with speed for surfaces III and IV but not to affect appreciably the curves for surfaces I and II.

Fluid Depth on Runway

In this report, the terms "damp", "wet" and "flooded" are defined in terms of surface appearance and the circumstances in which each occurs.

Damp: surface appears discolored compared to the dry condition but no standing water is present, e.g. dew, very light rain and in the final stages of the drying process after rain.

Flooded: large areas with standing water above the tops of the surface asperities. The rain required to produce flooding depends very much on the macro-texture depth, the camber or cross-fall of the runway surface, the available paths and the wind direction and strength. It is rare for a runway to be completely flooded, but flooded conditions often occur where a runway follows the original ground contours through a hollow or depression or at, for example, runway intersections.

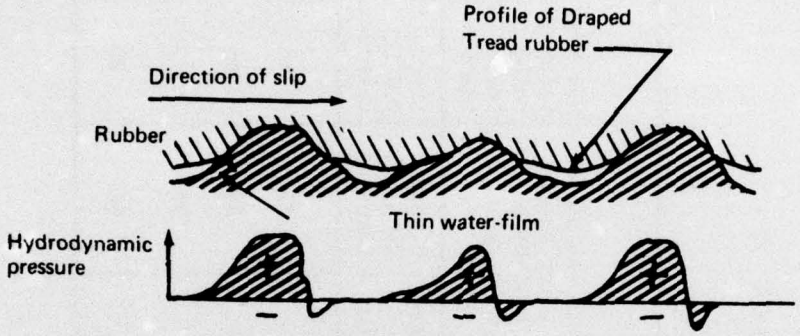

Figure C17.—Generation of Hydrodynamic Pressures on Individual Asperities of Wet Road

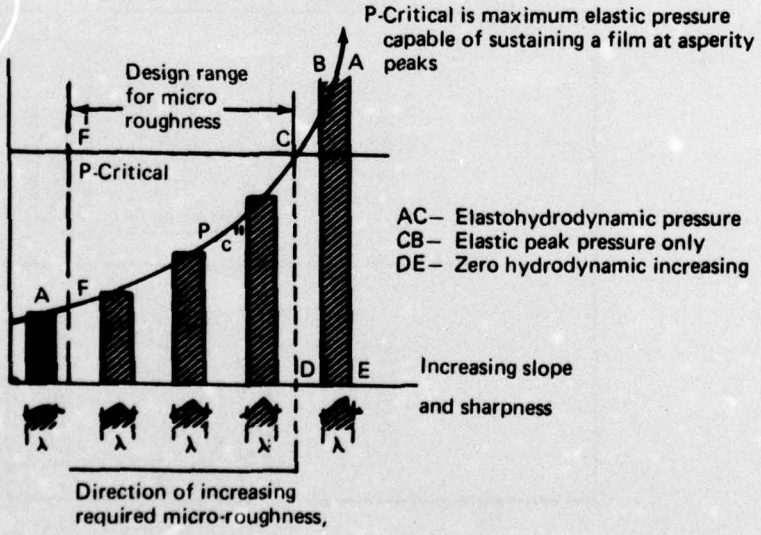

Figure C18.—Micro-Roughness Requirements for Different Asperity Shapes

Table CI.—Polished Stone Value Tests (Ref. 7)

Material	Source	Initial wet skid resistance values		Wet skid resistance value after three hours polishing with 36 corn emery		Wet skid resistance value (Polished Stone Value) after polishing for a further three hours with emery flour	
		Standard R.R.L. Compound	High Wet Grip Compound	Standard R.R.L. Compound	High Wet Grip Compound	Standard R.R.L. Compound	High Wet Skid Resistance Compound
Carboniferous Limestone	Chipping Sodbury Gloucestershire	65	70	55	65	45	55
Augite Diorite	Leicestershire	82	89	72	80	65	80
Calcined Bauxite	C.E. Ramsden Co. Ltd. Stoke-on-Trent	97	105	94	96	79	84
Millstone Grit	Ambergate, Derbyshire	95	97	91	92	85	90

Wet: an average condition between flooded and damp. Overall, water may be present up to the the tops of the surface asperities with scattered puddles of greater depth.

In damp conditions, with the exception of surfaces such as I in figure C6, the coefficient of friction is noticeably reduced from the dry surface value, the effect becoming most marked on surfaces such as IV in figure C6.

In wet conditions, the effect on μ of changes in tire tread pattern and surface texture are as described earlier. See figure C19 (ref. 48).

In flooded conditions, the removal of bulk quantities of fluid from the tire-ground contact area by means of, for example, large aggregate surfaces, grooved surfaces, porous surfaces and tread grooves is essential if satisfactory braking is to be obtained at high speed. When surfaces such as III and IV in figure C6 become flooded, a significant proportion of the retarding force that can be generated at high speeds results from fluid drag on the tire (ref. 50).

Surface Deposits

Surface deposits commonly met on runways (sand, grit, dust, rubber deposits, hardened smears of asphalt binder and paint) reduce the macro-texture depth and, in some cases, can affect the surface micro-texture depth. However, due to lack of available data and involved complexity these are outside the scope of present work.

AIRCRAFT DESIGN AND OPERATIONAL FACTORS

Forward Speed

In general, μ_{max} and μ_{skid} decrease with increase in forward speed. The only significant exception to this pertains to the use of synthetic rubber compounds on large macro-texture depth surfaces.

The additional effects that arise when forward speed is increased in wet conditions are described under braking on wet surfaces (three zone concept).

Wheel Arrangement

Where wheels are arranged in multiple units, interference effects may occur on wet srufaces if the passage of one tire either removes fluid from, or places it in the path of, a following tire. However, wheel arrangement has a greater relevance to fluid drag forces and spray patterns than to braking force.

Tire Wear:

For a typical aircraft-type, rib-tread tire, when groove depths have been reduced to about 20 per cent or less of the unworn value, the remaining tread may be "flattened out" under load and the tire may behave as if smooth (ref. 21). See figures C20 and C21.

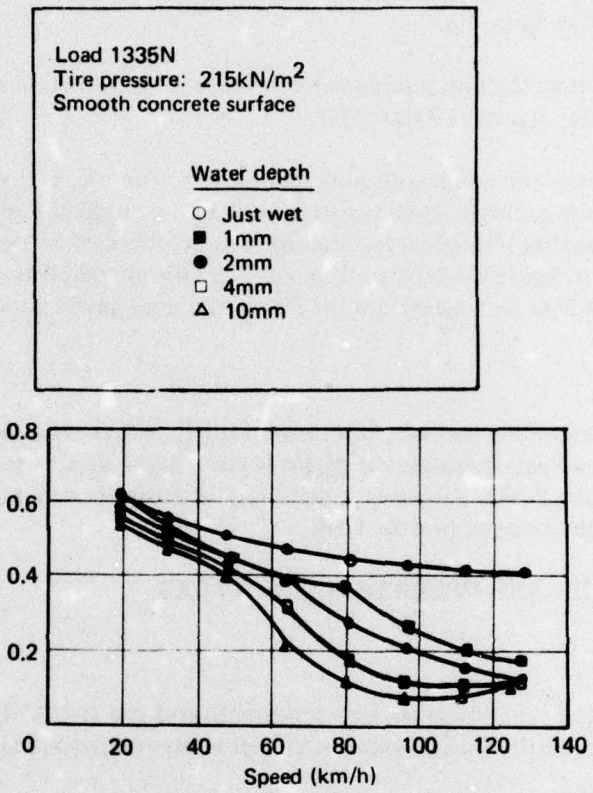

Figure C19.—Effect of Water Depth on the Locked Wheel Braking Force Coefficient with A Radial Ply Patterned Tire *(Ref. 48)*

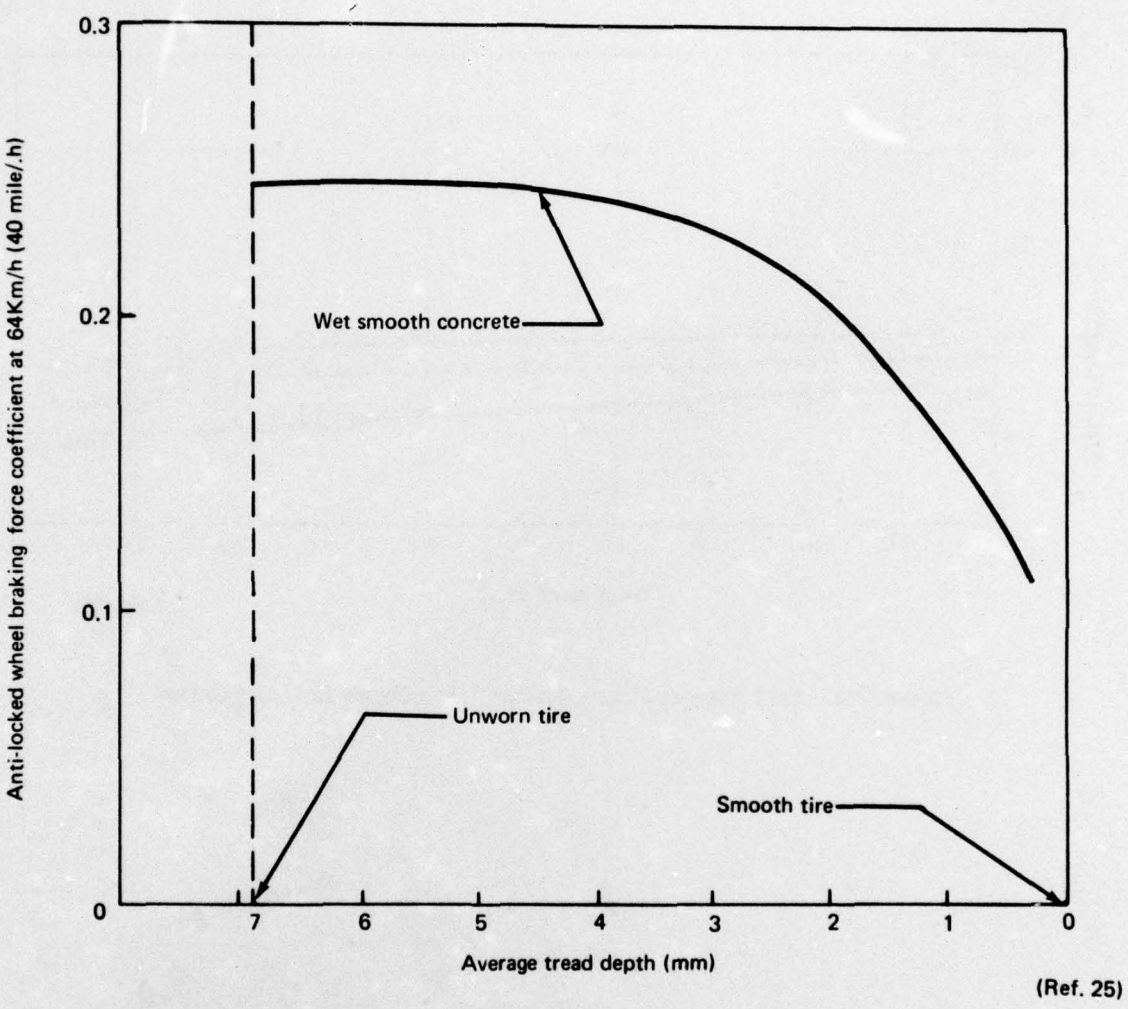

Figure C20.—Effect of Tread Wear on Braking Performance-Surface Wet

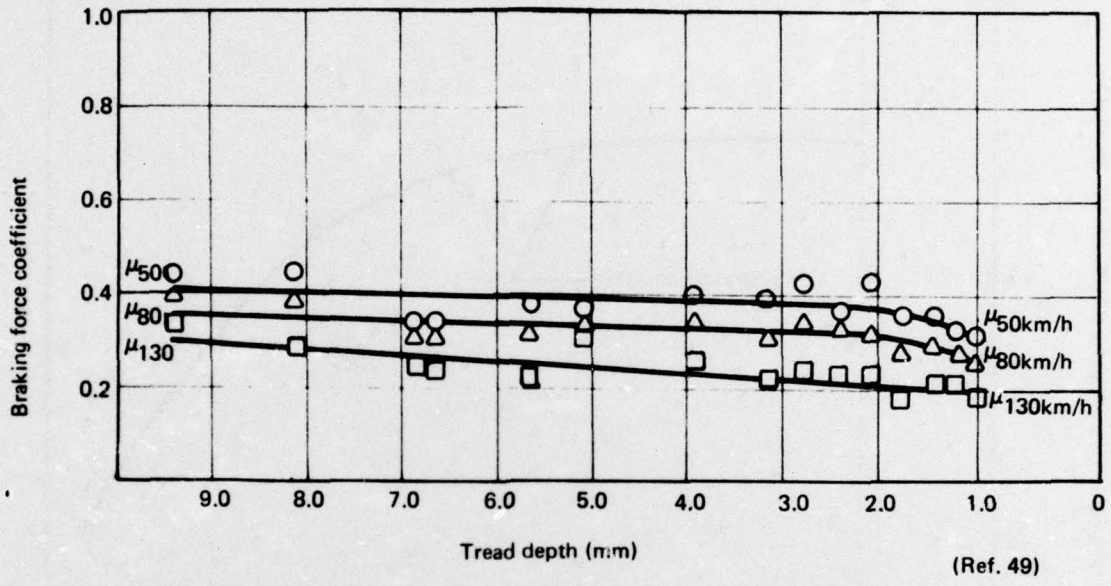

Figure C21.—Peak Braking Force Against Tread Depth-Bridport Gravel

Normal Load on Tire

The effect of normal load changes on μ for dry or wet surfaces is negligible (ref. 22), since the tire acts as an elastic body and the contact area increases uniformly with load with little change in average bearing pressure. The effect of the rise in inflation pressure, which occurs as the tire deflects under increasing normal load, is small. For example, the pressure rise due to loading a tire from zero to its rated deflection, i.e. at rated load (ref. 34), is 3 to 4 percent of the rated inflation pressure.

Pavement Temperature and Climate Effect

Skid resistance tends to decrease with increase in temperature. The magnitude of the loss depends on the texture of the surface as well as the viscosity of the surface material, see figure C22. Freezing of pavement occurs at ambient temperatures several degrees below 32°F. The presence of ice has an important effect in modifying the surface texture. The friction coefficient ranges from 0.15 on hard ice to almost zero on wet frozen surface. The change in skid resistance with time of year is a function of the climatic conditions affecting the weathering of the aggregate topography, coupled with the action of traffic accelerating the break-up of the topography weakened by the weathering action. A study has been made on a by-pass (7,000 vehicles per day) using a vehicle and a Skid Resistance Tester to measure wet skid resistance, and taking samples from the pavement surfaces for examination in the scanning electron microscope. The change in skid resistance throughout the year is shown in Fig. C23 for a braking area.

Traffic Density

Loss of friction is usually most severe during the first 2 years after construction, see Figure C24. Thereafter, the rate of polishing decreases and eventually reaches a stable level of smoothness.

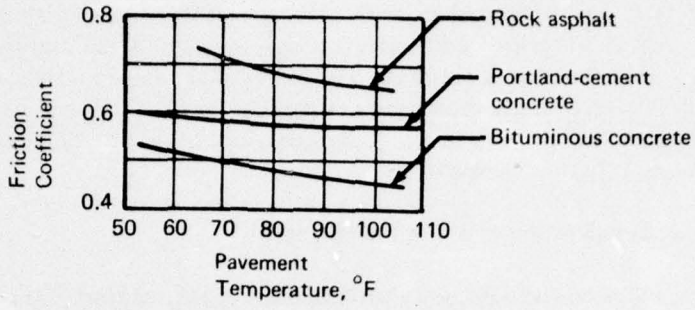

Figure C22.—Temperature Influence on Frictional Resistance, (Ref. 26)

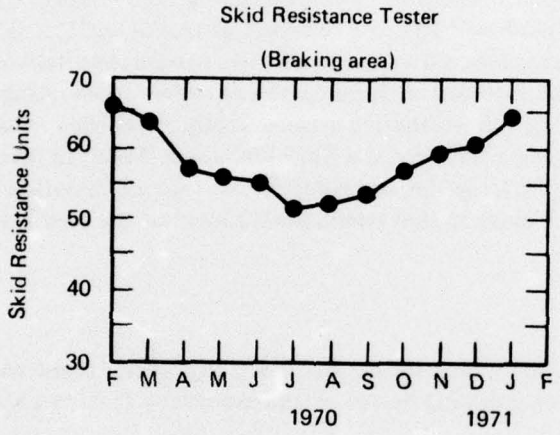

Figure C23.—The Variation in Skid Resistance with Time of Year, All Measurements Taken Within A Braking Area on A Medium Trafficked Road. (Ref. 7)

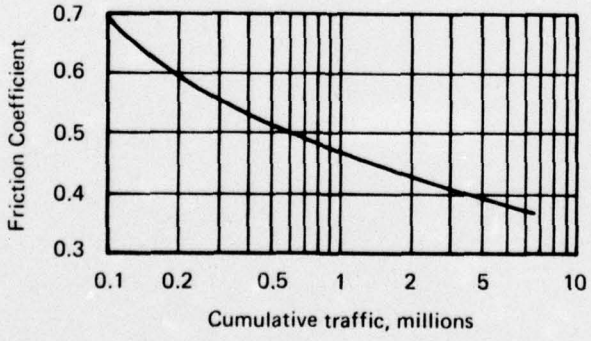

Figure C24.—Effect of Traffic on Friction Coefficient of Pavement Surface.

APPENDIX D
DIMENSIONAL ANALYSIS TECHNIQUE

DETERMINATION OF Pi TERMS (REFS. 1, 27 & 51)

The easiest and most orderly procedure for developing pi terms from a list of variables is as follows (ref. 51). The ten parameters needed to define the problem are summarized in Table D-1, where their fundamental dimensions are also presented in the mass (M), length (L), and time (T) system. The list of parameters can be reduced from ten to nine by writing, by inspection, one pi term that is already a nondimensional quantity.

$$\pi_1 = \mu$$

Next we arrange the remaining nine quantities in a matrix with their fundamental dimensions. Across the top of the array we write the variables, and down the left side we write the fundamental dimensions, in this case M, L, and T. Under each variable, we write the powers to which each dimension is raised in each variable.

	C_1	C_2	C_3	C_4	C_5	C_6	C_7	C_8	C_9
	V	P	d_{tr}	D	w	Z	d_{tr}	h	ρ
M	0	1	0	0	0	1	0	0	1
L	1	-1	1	1	1	1	1	1	-3
T	-1	-2	0	0	0	-2	0	0	0

We now apply the matrix algebra theorem, which states that "from a matrix there will be a number of independent equations equal to the rank of the matrix"; the rank of the matrix is defined to be the order of the highest-order determinant of the matrix that differs from zero. Because in dimensional analysis there always exists more columns than rows, and because a determinant is a matrix with equal number of rows and columns, we can select numerous combinations of different columns from the matrix and combine them into determinants. Some of the determinants from our matrix are:

$$\begin{vmatrix} 1 & 0 & 1 \\ -1 & 1 & 1 \\ -2 & 0 & -2 \end{vmatrix} \quad \text{(a)} \qquad \begin{vmatrix} 0 & 1 & 0 \\ 1 & -1 & 1 \\ -1 & -2 & 0 \end{vmatrix} \quad \text{(b)} \qquad \begin{vmatrix} 0 & 1 & 1 \\ 1 & 1 & -3 \\ 0 & -2 & 0 \end{vmatrix} \quad \text{(c)} \qquad \begin{vmatrix} 1 & 1 \\ -1 & 0 \end{vmatrix} \quad \begin{vmatrix} 0 & 1 \\ 1 & -3 \end{vmatrix} \quad \begin{vmatrix} 1 & 1 \\ -1 & -3 \end{vmatrix}$$

The order of a determinant is the number of columns or rows in the determinant. The first three determinants are third-order determinants, and the last three are second-order determinants. Although the determinants of (a) equals zero, the determinant of (b) equals - 1.0 and is, therefore, not zero. This observation means that the rank of our matrix is 3 and that the total number of dimensionless products in a complete set is equal to the total number of

Table D-1.—Parameters for Tire Correlation Model

PARAMETER	SYMBOL	FUNDAMENTAL DIMENSION
Peak Available Mu	μ	-
Forward ground speed	V	LT^{-1}
Tire inflation pressure	p	$ML^{-1}T^{-2}$
Tire tread depth	d_{tr}	L
Tire nominal diameter	D	L
Tire section width	w	L
Tire vertical load	Z	MLT^{-2}
Runway macro-texture depth	d_{tx}	L
Fluid depth	h	L
Fluid density	ρ	ML^{-3}

variables minus the rank of their dimensional product or minus the number of independent equations. Thus we have 9-3, or 6 more π terms. Our three equations can be written by inspection from the preceding matrix as:

$$C_2 + C_6 + C_9 = 0 \qquad \text{(D-1a)}$$

$$C_1 - C_2 + C_3 + C_4 + C_5 + C_6 + C_7 + C_8 - 3C_9 = 0 \qquad \text{(D-1b)}$$

$$C_1 + 2C_2 + 2C_6 = 0 \qquad \text{(D-1c)}$$

Solving in terms of C_4, C_6, and C_9 we get

$$C_4 = C_1 + 2C_2 - C_3 - C_5 - C_7 - C_8 \qquad \text{(D-2a)}$$

$$C_6 = -\left(\frac{C1}{2} + C_2\right) \qquad \text{(D-2b)}$$

$$C_9 = \tfrac{1}{2} C_1 \qquad \text{(D-2c)}$$

Substitution for C_4, C_6, and C_9 in a statement of dimensional homogeneity gives:

$$\left\{(V)^{C1}\,(p)^{C2}\,(d_{tr})^{C3}\,(D)^{[C1 + 2C2 - C3 - C5 - C7 - C8]}\,(w)^{C5}\,(Z)^{[-\frac{1}{2}C1 - C2]}\right.$$
$$\left.(d_{tx})^{C7}\,(h)^{C8}\,(\rho)^{\frac{1}{2}C1} = M^\circ L^\circ T^\circ\right\}$$

Collection of exponents with the same coefficient gives:

$$\left(VD\frac{\sqrt{\rho}}{\sqrt{Z}}\right)^{C_1}\left(\frac{pD^2}{Z}\right)^{C_2}\left(\frac{d_{tr}}{D}\right)^{C_3}\left(\frac{w}{D}\right)^{C_5}\left(\frac{d_{tx}}{D}\right)^{C_7}\left(\frac{h}{D}\right)^{C_8} = M^\circ L^\circ T^\circ$$

These six nondimensional quantities are the additional pi terms. In dimensional analysis, pi terms can be multiplied to form new groups of pi terms. They can be inverted; they can be squared, or their square roots can be taken. Such manipulations are proper and are usually performed to create a more convenient ratio of physical phenomena. Thus:

$$\left(VD\frac{\sqrt{\rho}}{\sqrt{Z}}\right)^2 = \left(\frac{\rho V^2 D^2}{Z}\right) \text{ and } \left[\left(\frac{pD^2}{Z}\right)\right]^{-1} \times \left(1/\sqrt{w/D}\right) = \left(\frac{Z}{pD\sqrt{wD}}\right)$$

The term $\left(\frac{w}{D}\right)$ is defined, by some authors, as the tire aspect ratio. However, the aircraft tire manufacturers define the tire aspect ratio as $\left(\frac{D-d}{2w}\right)$ where d is the rim or wheel diameter. Since this parameter is readily available (in the numeric form) in tire data tables, (w/D) pi term was

also modified to be $(\frac{D-d}{2w})$. Rearrangement of the six pi terms obtained algebraically, together with the one pi term written by inspection, gives:

$$(\pi_1) = (\mu)$$

$$(\pi_2) = (d_{tx/D})$$

$$(\pi_3) = (d_{tr/D})$$

$$(\pi_4) = (h/D)$$

$$(\pi_5) = (D\text{-}d/_{2w})$$

$$(\pi_6) = (Z/_{pD\sqrt{wD}})$$

$$(\pi_7) = (\rho V^2 D^2/Z)$$

This result yields the functional relationship that:

$$(\mu) = F\,(d_{tx/D},\ d_{tr/D},\ h/D,\ D\text{-}d/_{2w},\ Z/_{pD\sqrt{wD}},\ \rho V^2 D^2/Z) \qquad \text{(D-3)}$$

or

$$(\pi_1) = F\,(\pi_2, \pi_3, \pi_4, \pi_5, \pi_6, \pi_7) \qquad \text{(D-3a)}$$

APPENDIX E
RAW DATA AND CALCULATION OF PI TERMS

Table E-1 and Figures E-1 through E-8C show the raw data taken from references 18, 21, 50, 52, 53, and 54. Tables E-2 through E-7 show the actual data points transcribed from Figures E-1 through E-8C as well as their conversion to nondimensional terms. The calculation for π_1 through π_7 are straightforward. The following array shows the interrelationship of various figures, references and tables.

Figure No.	Taken from reference No.	Converted to table no.	Shows data variation between
E-1	21	E-2	π_1, π_2
E-2, -3 plus Table E-1	50	E-3	π_1, π_3
E-4	52	E-4	π_1, π_4
E-5, -6	53, 54	E-5	π_1, π_5
E-7, 8a, 8b, 8c	18	E-6	π_1, π_6
E-7, 8a, 8b, 8c	18	E-7	π_1, π_7

Table E-1.—Groove Dimensions for Tires Investigated

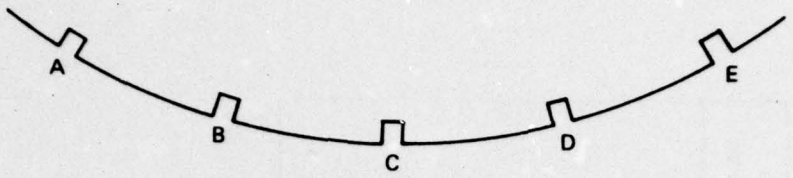

Tread wear, percent	Desired depth, in., for groove—					Average depth, in., before tests for groove—					Average depth, in., after tests for groove—					Av. groove width, in.
	A	B	C	D	E	A	B	C	D	E	A	B	C	D	E	
(a) Tire I (dimple tread, nonuniform wear)																
0	0.250	0.250	0.250	0.250	0.250	0.199	0.227	0.212	0.202	0.195	0.189	0.216	0.198	0.190	0.184	0.290
50	.216	.155	.125	.155	.216	.206	.150	.120	.137	.203	.195	.136	.104	.126	.192	↓
80	.194	.098	.050	.098	.194	.185	.098	.047	.103	.183	.177	.093	.057	.094	.172	
90	.175	.094	.037	.094	.175	.177	.093	.037	.094	.172	.170	.088	.032	.087	.168	
100	.073	.059	0	.059	.073	.071	.052	0	.051	.072	.058	.043	0	.041	.053	↓
(b) Tire II (smooth tire, uniform wear)																
20	0.192	0.192	0.192	0.192	0.192	0.188	0.193	0.192	0.193	0.187	0.180	0.186	0.186	0.186	0.179	0.220
60	.144	.144	.144	.144	.144	.142	.150	.145	.136	.135	.138	.147	.142	.130	.130	↓
75	.060	.060	.060	.060	.060	.064	.066	.064	.073	.061	.059	.060	.060	.068	.060	
80	.048	.048	.048	.048	.048	.049	.045	.049	.047	.046	.044	.040	.044	.040	.040	
85	.036	.036	.036	.036	.036	.036	.039	.039	.043	.036	.029	.035	.035	.038	.033	
90	.024	.024	.024	.024	.024	.024	.023	.024	.024	.023	.021	.018	.022	.020	.020	
95	.012	.012	.012	.012	.012	.015	.015	.016	.015	.016	.010	.010	.010	.010	.010	
100	0	0	0	0	0	0	0	0	0	0	0	0	0	0	0	----
(c) Tire III (new tire, uniform wear)																
0	0.240	0.240	0.240	0.240	0.240	0.242	0.242	0.238	0.235	0.241	0.230	0.230	0.225	0.223	0.230	0.375

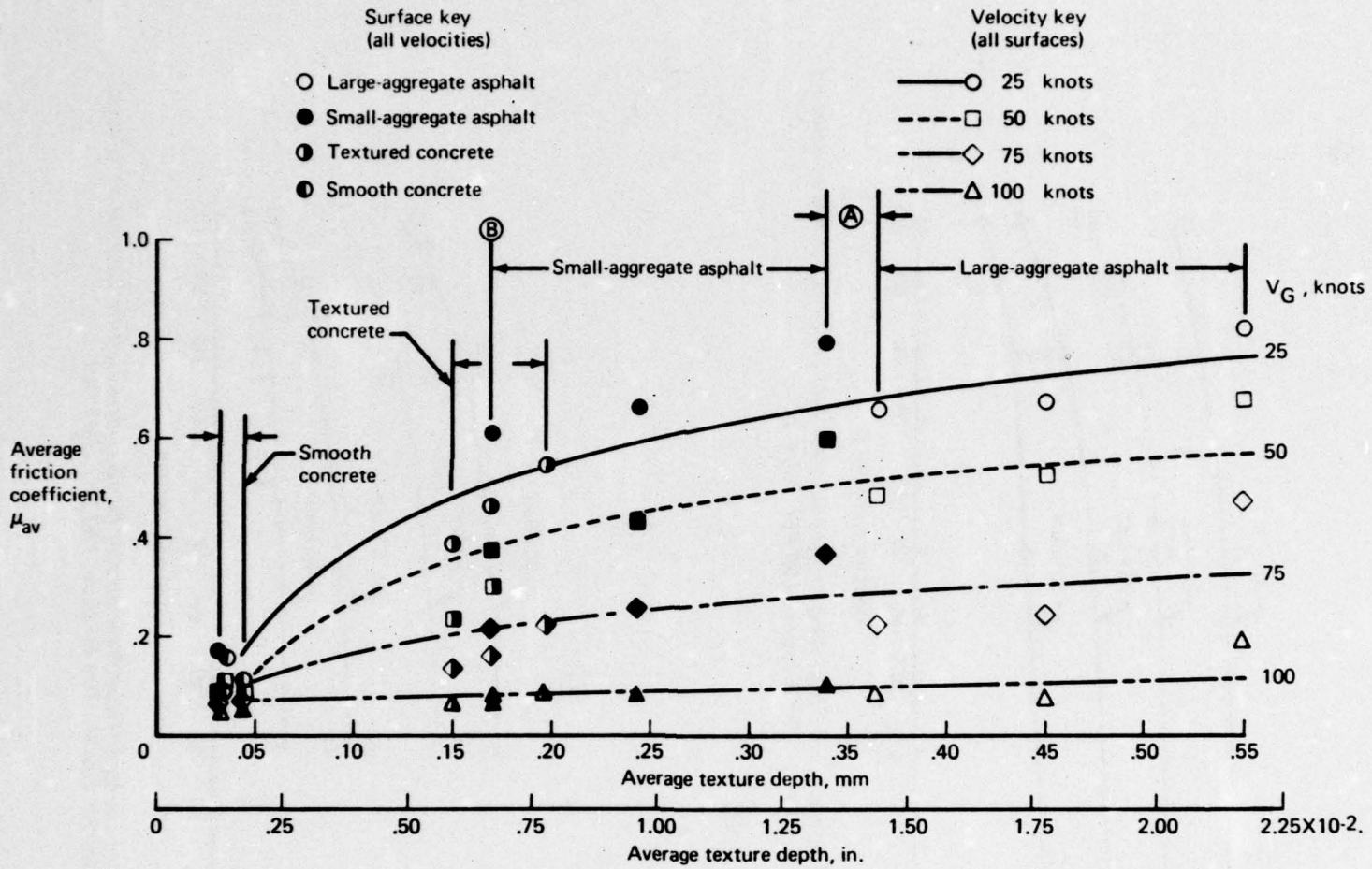

Note: Smooth tire (tire 1); vertical load, F_V = 12,000 lb. (53,400 N); tire inflation pressure, p = 140 lb/in^2 (97 N/cm^2); water depth = 0.1 to 0.2 inch (0.25 to 0.51 cm). (Ref. 21)

Figure E-1.—Effect of Measured Surface Roughness on Average Friction Coefficient Developed on A Flooded Runway.

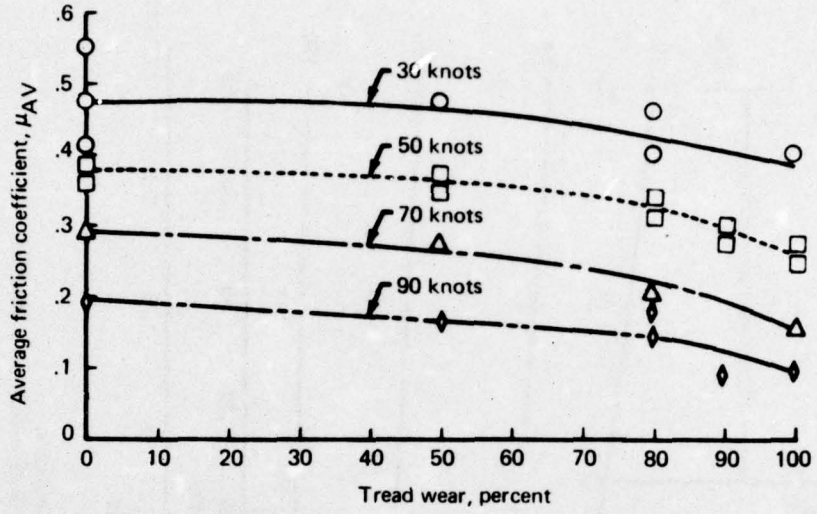

Figure E-2—Effects of Nonuniform Tread Wear on Wet-Runway Braking Effectiveness at Selected Velocities for Tire I. Tire Pressure, 150 PSI. (Ref. 50)

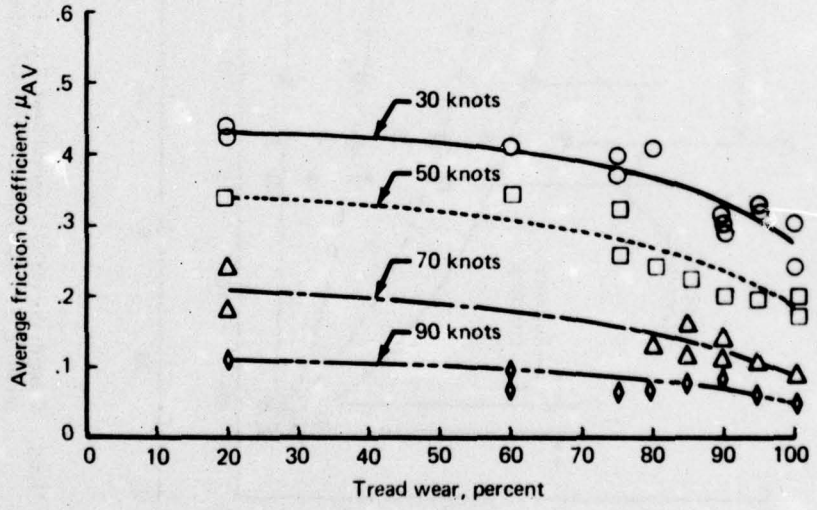

Figure E-3.—Effects of Uniform Tread Wear on Wet-Runway Braking Effectiveness at Selected Velocities for Tire II. Tire Pressure, 150 psi. (Ref. 50)

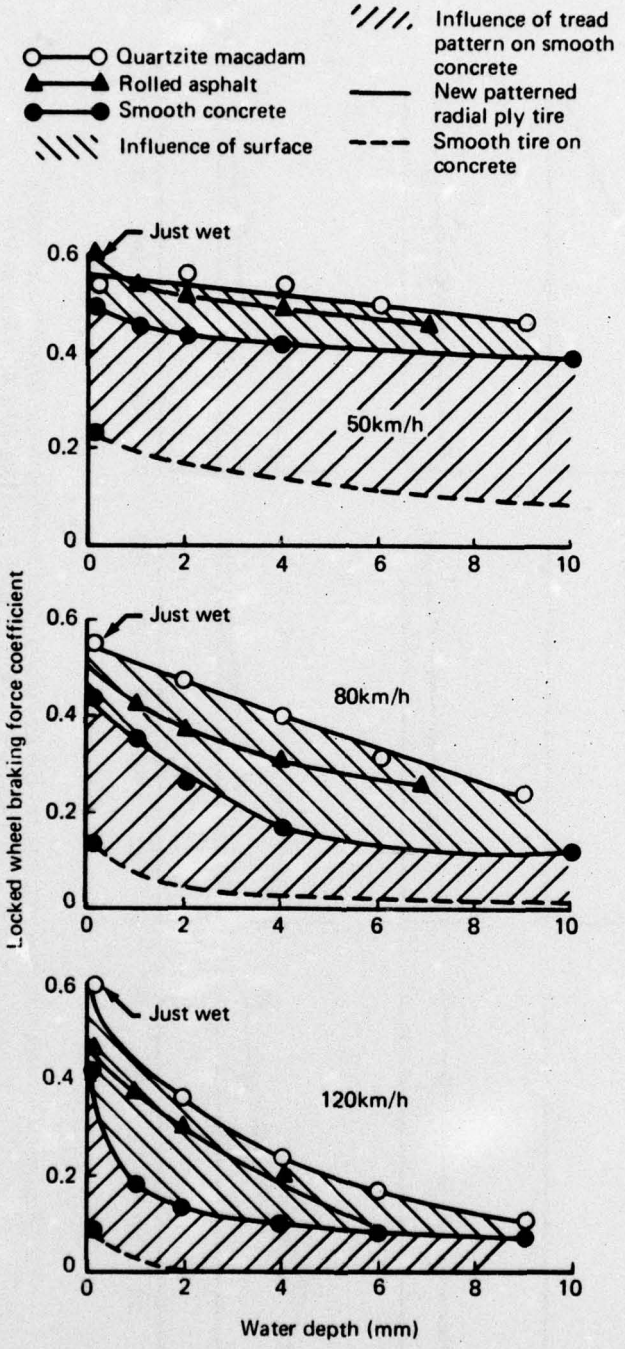

Figure E4.—Effect of Surface and Water Depth on Locked Wheel Braking Force Coefficient (Ref. 52)

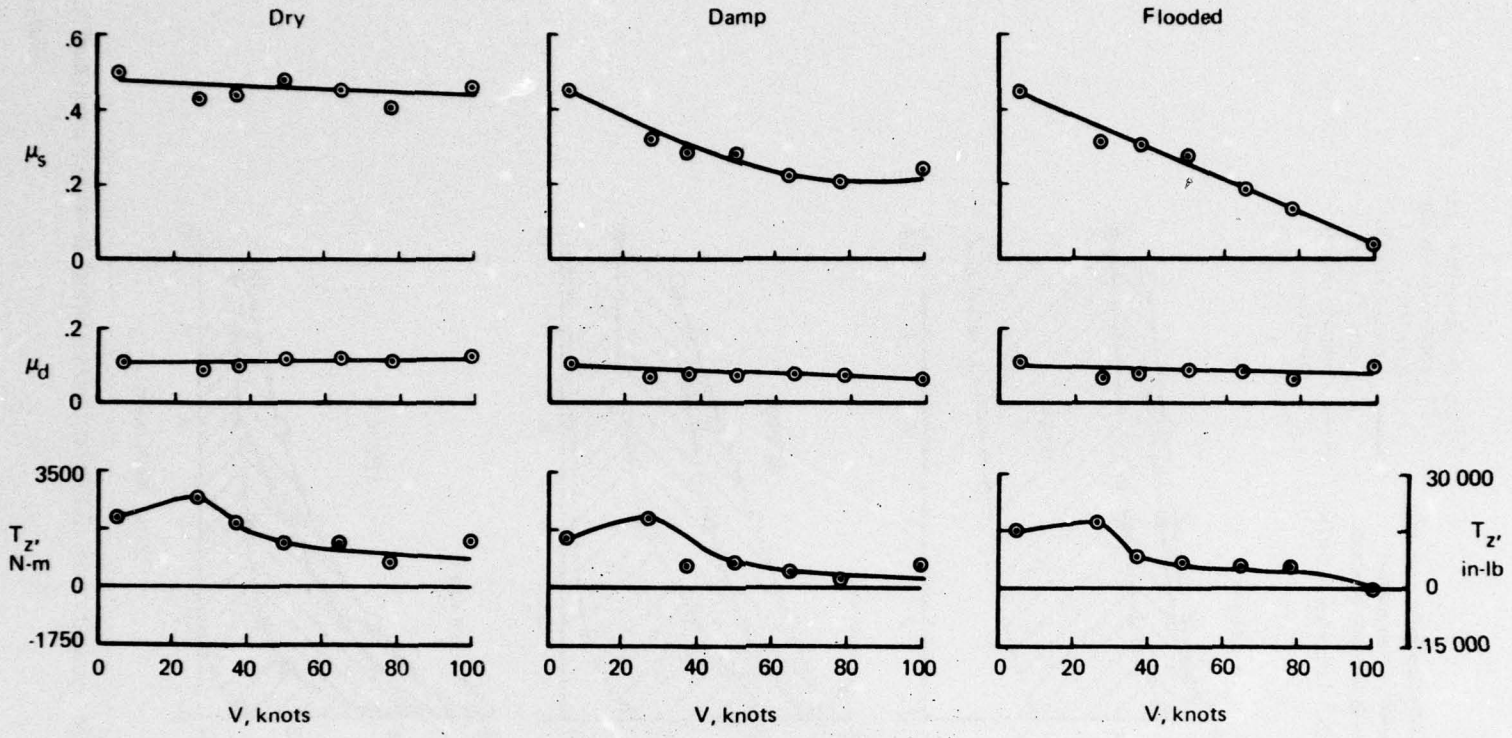

Figure E-5—Effect of ground speed on the cornering-force and drag-force friction coefficient (μ_s and μ_d respectively) and self-alining torque T_z of the 40 x 40-16 type VII aircraft tire. Brake torque, 0; yaw angle, 10°. (Ref. 53)

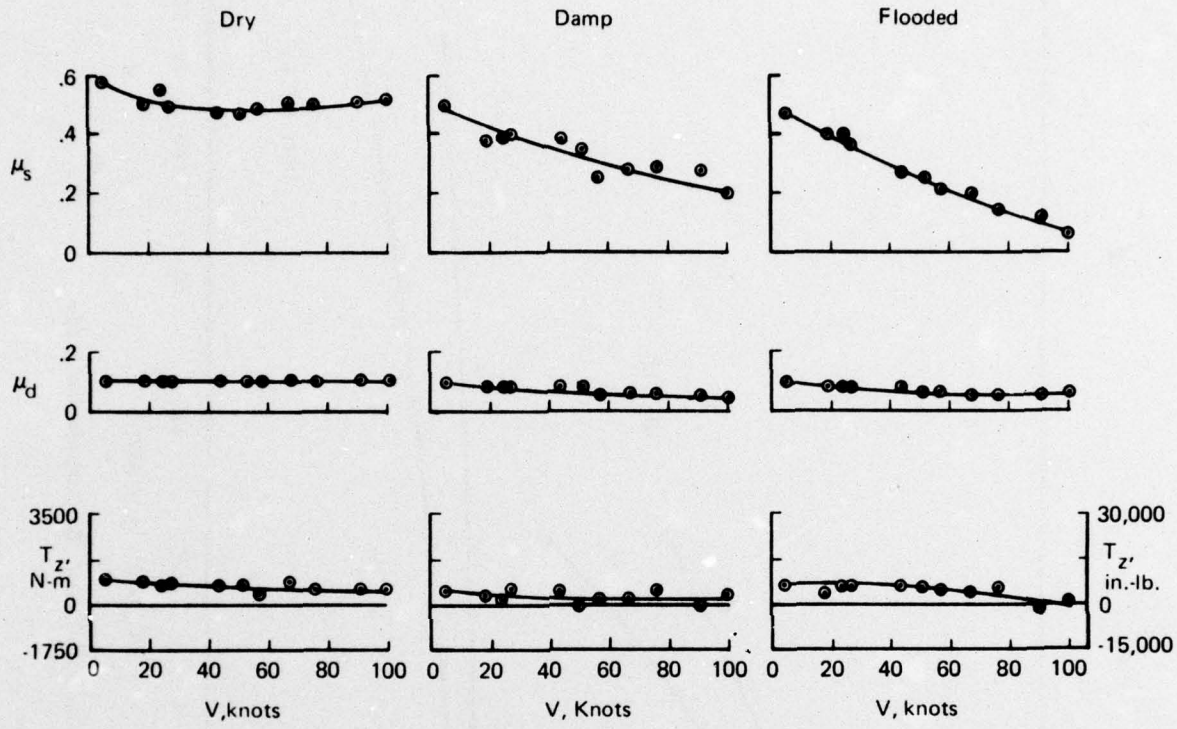

Figure E-6.—Effect of Ground Speed on μ_s, μ_d, and T_z at 10° Yaw Angle on Dry, Damp, and Flooded Surfaces. Brake Torque = 0. (Ref. 54)

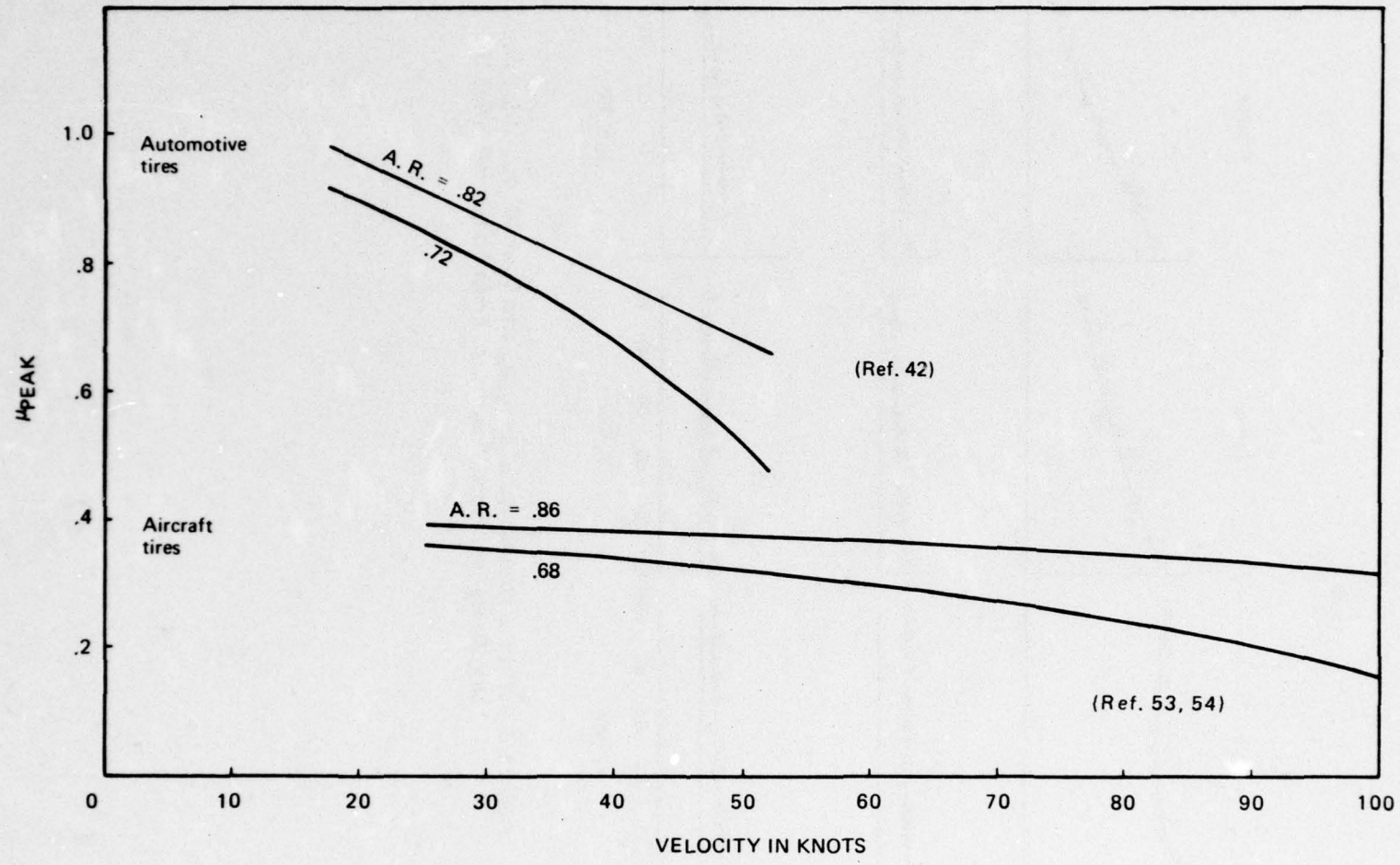

Figure E-7.—Effect of Aspect Ratio on Available Mu

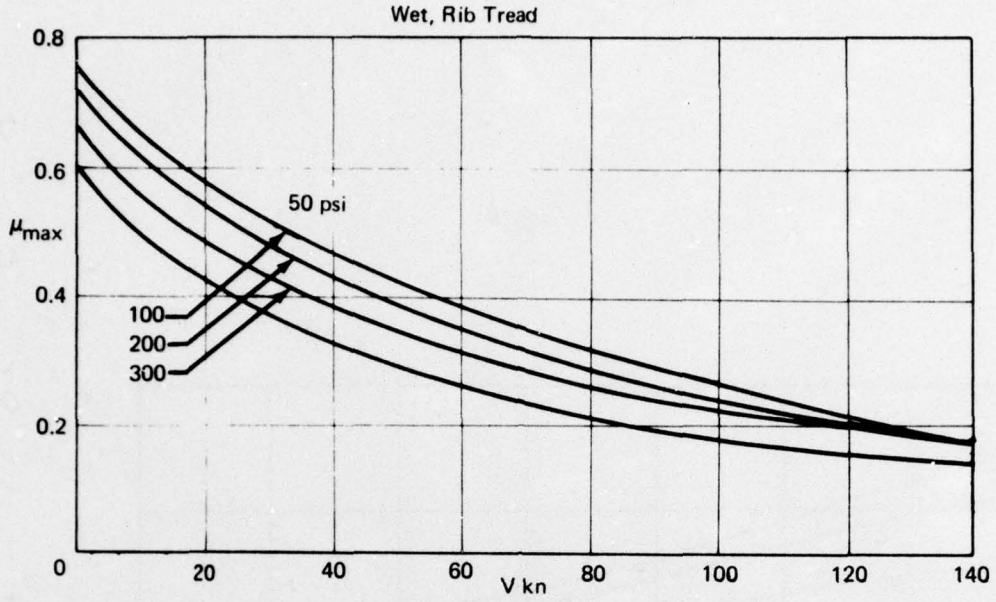

a. Surface A (Ref. 18)

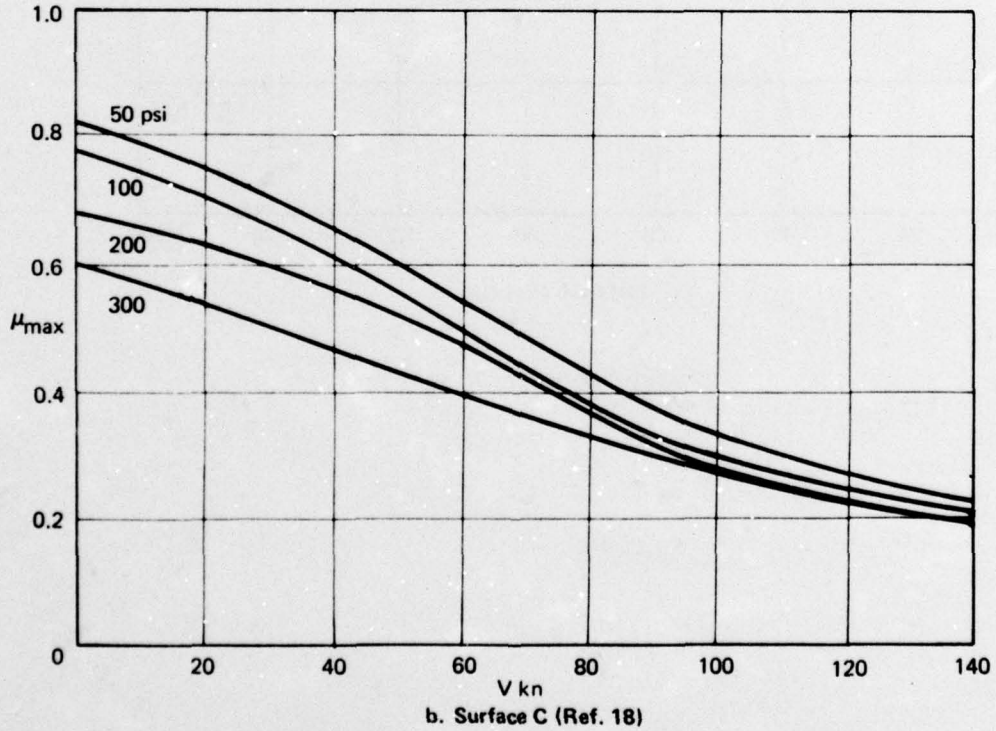

b. Surface C (Ref. 18)

Figure E-8.—Dependence of Friction on Velocity and Inflation Pressure

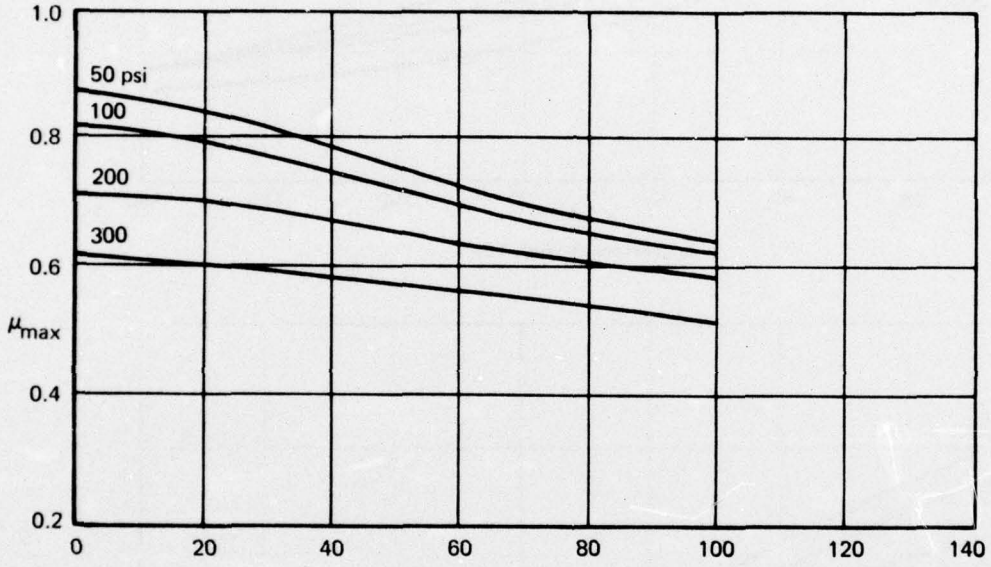

c. Surface E (Ref. 18)

Figure E-8.—(Concluded)

Table E-2.—Runway Texture Depth vs. μ Data (π_2 vs π_1)

TEXTURE DEPTH d_{tx} – in.	$\frac{d_{tx}}{D} \times 10^3$ or (π_2)	μ or (π_1) @ VELOCITY IN KNOTS				RUNWAY SURFACE*	BASIC DATA
		25	50	75	100		
.0012	.037	.165	.082	.059	.047	SC	D = 32 in.
.0013	.041	.153	.100	.071	.059	SC	h = .1 to .2 in.
.0017	.053	.110	.080	.060	.050	SC	p = 140 psi
.0059	.184	.382	.235	.129	.059	TC	z = 12000 lbs.
.0067	.209	.459	.300	.165	.071	TC	A.R. = .842
.0078	.244	.550	.395	.225	.090	TC	All Rubber (National Rubber) Tread & New
.0096	.300	.647	.412	.259	.071	SAA	
.0135	.422	.795	.600	.370	.100	SAA	
.0220	.687	.830	.685	.475	.190	LAA	

*SC = Smooth Concrete

TC = Textured Concrete

SAA = Small Aggregate Asphalt

LAA = Large Aggregate Asphalt

Table E-3.—Tire Tread Groove Depth vs μ Data (π_3 vs π_1)

AVERAGE TREAD DEPTH: d_{tr} in.	$\frac{d_{tr}}{D} \times 10^2$ or (π_3)	μ or (π_1) @ VELOCITY IN KNOTS				TREAD WORN %	BASIC DATA
		25	50	75	100		
.187	.584	.435	.340	.210	.110	20	D = 32 in.
.140	.437	.410	.390	.180	.090	60	h = .1 to .2 in.
.064	.200	.387	.290	.160	.073	75	p = 150 psi
.044	.137	.410	.240	.145	.075	80	Z = 10500 lbs.
.036	.112	.350	.222	.145	.082	85	A.R. = .842
.022	.069	.310	.200	.123	.085	90	Langley Loads
.013	.041	.325	.210	.112	.070	95	Tracks

Table E-4.—Water Depth on Runway vs μ Data (π_4 vs π_1)

WATER DEPTH mm	$\frac{h}{D}$ x D or (π_4)	μ or (π_1) @ VELOCITY IN KNOTS				SURFACE TYPE	BASIC DATA
		25	50	75	100**		
0.2	.008	.52	.437	.41	.390		New Patterned Tires A.R. = .90 Z = 7900 lbs. D = ?
1	.039	.45	.363	.18	.166		
2	.079	.44	.262	.15	.110	Smooth Concrete d_{tx} = .005 in. (A)	
4	.157	.42	.175	.12	.08		
6	.236	-	-	.10	-		
10	.394	.39	.125	.08	-		
.2	.008	.60	.50	.46	.480	Rolled Asphalt d_{tx}=.013 in. (C)	New Patterned Tires A.R. = .90 Z = 7900 lbs. D = ?
1	.039	.54	.43	.38	.230		
2	.079	.525	.363	.33	.165		
4	.157	.50	.30	.22	.120		
6	.236	-	-	.10	.100		
7	.276	.45	.26	-	-		
.2	.008	-	.538	.60	.56		
2	.079	.57	.438	.36	.21	Quartzite Macadam d_{tx}=.061 in. (E)	"
4	.157	.55	.400	.25	.155		
6	.236	.51	.312	.18	.135		
9	.354	.45	.250	.112	.111		

* Locked wheel; automotive tire test data

** Extrapolated data

Table E-5.—Tire Aspect Ratio vs μ Data (π_5 vs π_1)

REMARKS	$(\frac{D-d}{2w})$ or (π_5)	μ or (π_1) AT VELOCITY IN KNOTS				BASIC DATA
		25	50	75	100	
*	.50	.329	.263	.169	.062	D = 40 in.
*	.60	.352	.294	.214	.107	Z = 25000 lbs. p = 155 psi
**	.68	.360	.320	.255	.155	Concrete Runway @ NASA Langley
*	.80	.383	.356	.316	.254	
**	.86	.392	.375	.355	.315	
*	1.00	.409	.409	.432	.498	h = .05 in.

* Data Generated by Trend

** Raw Data

Table E-6.—Tire Inflation Pressure vs μ Data (π_6 vs π_1)

INFLATION PRESSURE p (psi)	$\frac{Z}{pD\sqrt{wD}}$ or (π_6)	μ or (π_1) AT VELOCITY IN KNOTS				SURFACE TYPE	BASIC DATA (ASSUMED)
		25	50	75	100		
50	.820	.540	.42	.335	.26		Average $\frac{Z}{D\sqrt{wD}}$ = 42 A.R. = .90 h = .14 in. d_{tr} = .3 in
100	.410	.505	.39	.305	.25	A	
200	.205	.46	.34	.270	.22		
300	.137	.445	.29	.220	.18		
50	.820	.72	.60	.45	.485		
100	.410	.675	.55	.40	.455		
200	.205	.612	.525	.39	.440	C	"
300	.137	.525	.434	.35	.360		
50	.820	.83	.755	.687	.640		
100	.410	.784	.715	.670	.622	E	"
200	.205	.685	.650	.612	.583		
300	.137	.590	.572	.544	.517		

Table E-7.—Forward Ground Speed vs μ Data (π_7 vs π_1)

V (KNOTS)	SURFACE TYPE $\frac{\rho V^2 D^2}{Z} \times 144$ or (π_7)	A				C				E				BASIC DATA
		μ OR (π_1) AT INFLATION PRESSURE IN PSI												
		50	100	200	300	50	100	200	300	50	100	200	300	
10	.028	.65	.62	.56	.50	.78	.74	.65	.57	.85	.805	.70	.61	
20	.114	.57	.54	.49	.42	.74	.70	.63	.54	.835	.79	.695	.60	
30	.256	.51	.47	.43	.37	.70	.65	.59	.50	.81	.77	.68	.59	
40	.456	.47	.43	.38	.32	.65	.61	.56	.465	.78	.745	.665	.58	
50	.712	.42	.39	.34	.29	.60	.55	.52	.43	.755	.72	.65	.575	
60	1.026	.39	.35	.31	.26	.54	.50	.47	.40	.725	.70	.63	.565	
70	1.396	.35	.32	.28	.23	.48	.43	.42	.365	.70	.675	.615	.555	
80	1.824	.32	.29	.26	.21	.42	.38	.37	.335	.68	.66	.605	.54	
90	2.308	.29	.27	.24	.19	.37	.33	.32	.30	.66	.64	.595	.53	
100	2.849	.26	.25	.22	.18	.33	.30	.28	.27	.64	.625	.585	.515	
110	3.448	.23	.23	.21	.17	.30	.28	.25	.245	-	-	-	-	
120	4.103	.21	.21	.20	.16	.28	.26	.23	.22	-	-	-	-	
130	4.815	.19	.19	.19	.15	.26	.24	.21	.20	-	-	-	-	
140	5.585	.17	.17	.18	.14	.24	.22	.20	.185	-	-	-	-	
	Basic Data: Average $\frac{D^2}{Z} = \frac{10^{-4}}{144}$; A. R. = .9, h = .14 in., d_{tr} = .3 in.													

APPENDIX F
FORMULATION OF COMPONENT EQUATIONS

1. ARRANGEMENT OF PI TERMS

The experimental data converted to nondimensional pi terms must be arranged so that all of the pi terms containing independent variables, except one, remain constant. The remaining term is then varied to establish a relationship between it and π_1, the term containing the dependent variable. This procedure is repeated for each of the independently variable pi terms in the function. Table F-1 shows the arrangement for each of the six data sets. Each page is a complete data set with four sets per page to show the data at 25, 50, 75 and 100 knots.

2. COMPONENT EQUATIONS

When the observed data had been arranged as described above, relationships between π_1, the term containing the dependent variable, and $\pi_2, \pi_3, \pi_4, \pi_5, \pi_6$, and π_7 in turn, the terms with independent variables, were obtained using statistical curve fitting programs. The relationship between π_1 and other individual π terms are called component equations.

Plots were prepared of π_1 vs π_2, π_1 vs π_3, π_1 vs π_4, π_1 vs π_5, π_1 vs π_6 and π_1 vs π_7 for all conditions using data from Table F-1. These plots are shown in Figures F-1 through F-6. This helped determine the general form of relationship that could exist between π_1 and π_2, π_1 and π_3 and so on; e.g. if the π_1 vs π_2 data plotted as a straight line on the log-log paper, the relationship should be of the form

$$y = AX^B \qquad \text{(F-1)}$$

where A is a constant and B a polynomial. Logarithms of both sides in Eq. (F-1) give:

$$\ln(y) = A + B \ln x$$

or

$$\ln(\pi_1) = \ln(A) + B \ln(\pi_2)$$

which is the equation for a straight line. Thus with π_1 and π_2 as inputs and the desired output in the form of Eq. (F-1), two computations would be necessary, namely a log transformation and a determination of the constants, the latter requiring simple regression.

Simple regression is a statistical method to help fit the 'best' line to a given set of data using the least square principle. Given that y is a linear function of an independent variable x, the most probable position of a line $y = A + Bx$ is such that the sum of squares of deviations of all points (x, y) from the line is a minimum; the deviations being measured in the direction of the y-axis.

Even though the plots shown in Figures F-1 through F-6 were not always linear; they were assumed so to keep the model (concept) simple. Better relationships such as multiple linear regression or polynomial regression etc. could be used to define these relationships when actual

test data becomes available. All component equations were thus obtained using simple regression. A flow chart depicting the formulation of component equations is illustrated in Figure F-7. The curve fitting computer programs were used from reference 55. The component equations when plotted make the raw data (Figures F-1 to F-6) look like Figure F-8 to F-13.

Table F-1.—Arrangement of Pi Terms

(π_2)	(π_1) @ (VELOCITY IN KNOTS) / $(\bar{\pi}_7)$				$(\bar{\pi}_3)$	$(\bar{\pi}_4)$	$(\bar{\pi}_5)$	$(\bar{\pi}_6)$
	25 / .3617	50 / 1.4468	75 / 3.2563	100 / 5.7872				
.037	.165	.082	.059	.047	1.25	.15	.842	.1596
.041	.153	.100	.071	.059				
.053	.110	.080	.060	.050				
.184	.382	.235	.129	.059				
.209	.459	.300	.165	.071				
.244	.550	.395	.225	.090				
.300	.647	.412	.259	.071				
.422	.795	.600	.370	.100				
.687	.830	.685	.475	.190				

Table F-1.—Arrangement of Pi Terms (Continued)

	(π_1) @ VELOCITY IN KNOTS / $(\bar{\pi}_7)$							
(π_3)	25 / .5952	50 / 1.6533	75 / 3.2405	100 / 5.3560	$(\bar{\pi}_2)$	$(\bar{\pi}_4)$	$(\bar{\pi}_5)$	$(\bar{\pi}_6)$
.594	.435	.340	.210	.110	(Variable)	.200	.842	.1304
.437	.410	.390	.180	.090				
.200	.387	.290	.160	.073				
.137	.410	.240	.145	.075				
.112	.350	.222	.145	.082				
.069	.310	.200	.123	.085				
.041	.325	.210	.112	.070				

Table F-1.—Arrangement of Pi Terms (Continued)

(π_4)	(π_1) @ Velocity in knots / $(\overline{\pi}_7)$				$(\overline{\pi}_2)$	$(\overline{\pi}_3)$	$(\overline{\pi}_5)$	$(\overline{\pi}_6)$
	25 / .9461	50 / 2.628	75 / 5.913	100 / 10.52				
.008	.52	.437	.41	.390		.75	.90	.302
.039	.45	.363	.18	.166				
.079	.44	.262	.15	.110				
.157	.42	.175	.12	.08				
.236	–	–	.10	–				
.394	.39	.125	.08	–				
.008	.60	.50	.46	.480				
.039	.54	.43	.38	.230				
.079	.525	.363	.33	.165				
.157	.50	.30	.22	.120				
.236	–	–	.10	.100				
.276	.45	.26	–	–				
.008	–	.538	.60	.56				
.079	.57	.438	.36	.21				
.157	.55	.400	.25	.155				
.236	.51	.312	.18	.135				
.354	.45	.250	.112	.111				

Table F-1.—Arrangement of Pi Terms (Continued)

(π_5)	(π_1) @ VELOCITY IN KNOTS / ($\bar{\pi}_7$)				($\bar{\pi}_2$)	($\bar{\pi}_3$)	($\bar{\pi}_4$)	($\bar{\pi}_6$)
	25 / .271	50 / 1.084	75 / 2.439	100 / 4.336				
.50	.329	.263	.169	.062	(Variable)	.37	.05	.17
.60	.352	.294	.214	.107				
.70	.360	.320	.255	.155				
.80	.383	.356	.316	.254				
.90	.392	.375	.355	.315				
1.00	.409	.409	.432	.498				

Table F-1.—Arrangement of Pi Terms (Continued)

(π_6)	(π_1) @ VELOCITY IN KNOTS / ($\overline{\pi}_7$)				($\overline{\pi}_2$)	($\overline{\pi}_3$)	($\overline{\pi}_4$)	($\overline{\pi}_5$)
	25 / .24	50 / .96	75 / 2.16	100 / 3.84				
.820	.540	.42	.335	.26	(Variable)	.75	.14	.90
.410	.505	.39	.305	.25				
.205	.46	.34	.270	.22				
.137	.445	.29	.220	.18				
.820	.72	.60	.45	.485				
.410	.675	.55	.40	.455				
.205	.612	.525	.39	.440				
.137	.525	.434	.35	.360				
.820	.83	.755	.687	.640				
.410	.784	.715	.670	.622				
.205	.685	.650	.612	.583				
.137	.590	.572	.544	.517				

Table F-1.—Arrangement of Pi Terms (Concluded)

(π_7)	(π_1) @ Pressure in PSI / $(\bar{\pi}_6)$												$(\bar{\pi}_2)$	$(\bar{\pi}_3)$	$(\bar{\pi}_4)$	$(\bar{\pi}_5)$
	50 / .84	100 / .42	200 / .21	300 / .14	50 / .84	100 / .42	200 / .21	300 / .14	50 / .84	100 / .42	200 / .21	300 / .14				
.028	.65	.62	.56	.50	.78	.74	.65	.57	.85	.805	.70	.61	Variable	.75	.14	.90
.114	.57	.54	.49	.42	.74	.70	.63	.54	.835	.79	.695	.60				
.256	.51	.47	.43	.37	.70	.65	.59	.50	.81	.77	.68	.59				
.456	.47	.43	.38	.32	.65	.61	.56	.47	.78	.745	.665	.58				
.712	.42	.39	.34	.29	.60	.55	.52	.43	.755	.72	.65	.575				
1.026	.39	.35	.31	.26	.54	.50	.47	.40	.725	.70	.63	.565				
1.396	.35	.32	.28	.23	.48	.43	.42	.365	.70	.675	.615	.555				
1.824	.32	.29	.26	.21	.42	.38	.37	.335	.68	.66	.605	.54				
2.308	.29	.27	.24	.19	.37	.33	.32	.30	.66	.64	.595	.53				
2.849	.26	.25	.22	.18	.33	.30	.28	.27	.64	.625	.585	.515				
3.448	.23	.23	.21	.17	.30	.28	.25	.245	-	-	-	-				
4.103	.21	.21	.20	.16	.28	.26	.23	.22	-	-	-	-				
4.815	.19	.19	.19	.15	.26	.24	.21	.20	-	-	-	-				
5.585	.17	.17	.18	.14	.24	.22	.20	.185	-	-	-	-				

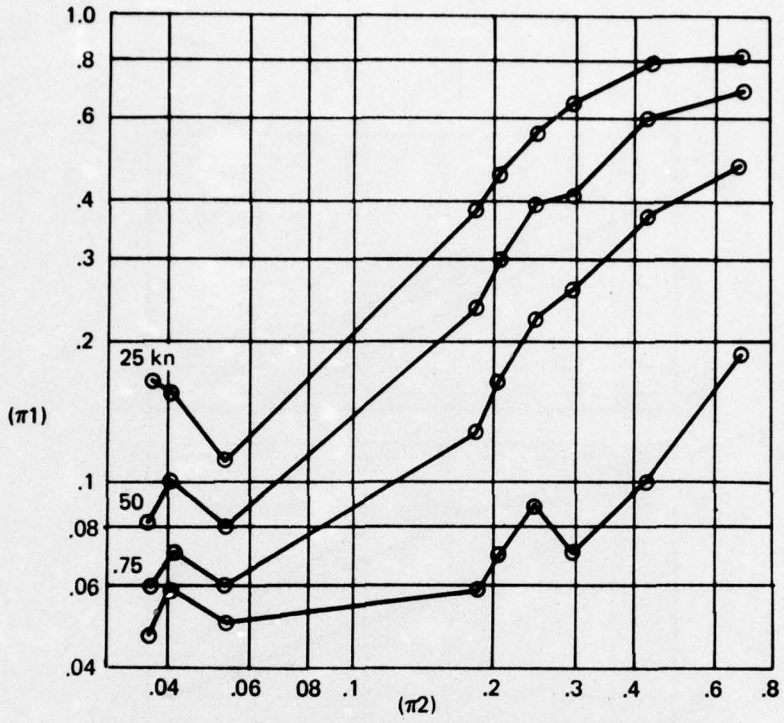

Figure F-1.—Plots of π_1 vs π_2 (Raw Data)

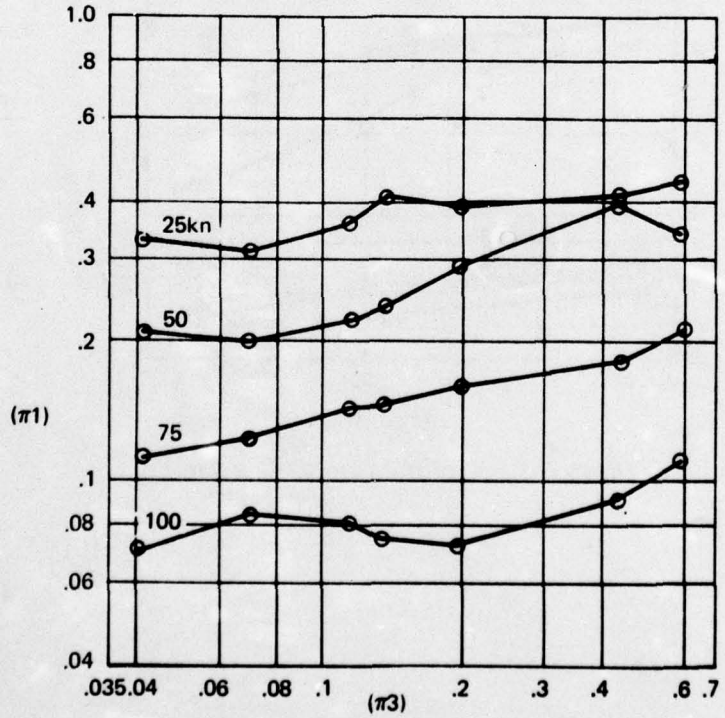

Figure F-2.—Plots of π_1 vs π_3 (Raw Data)

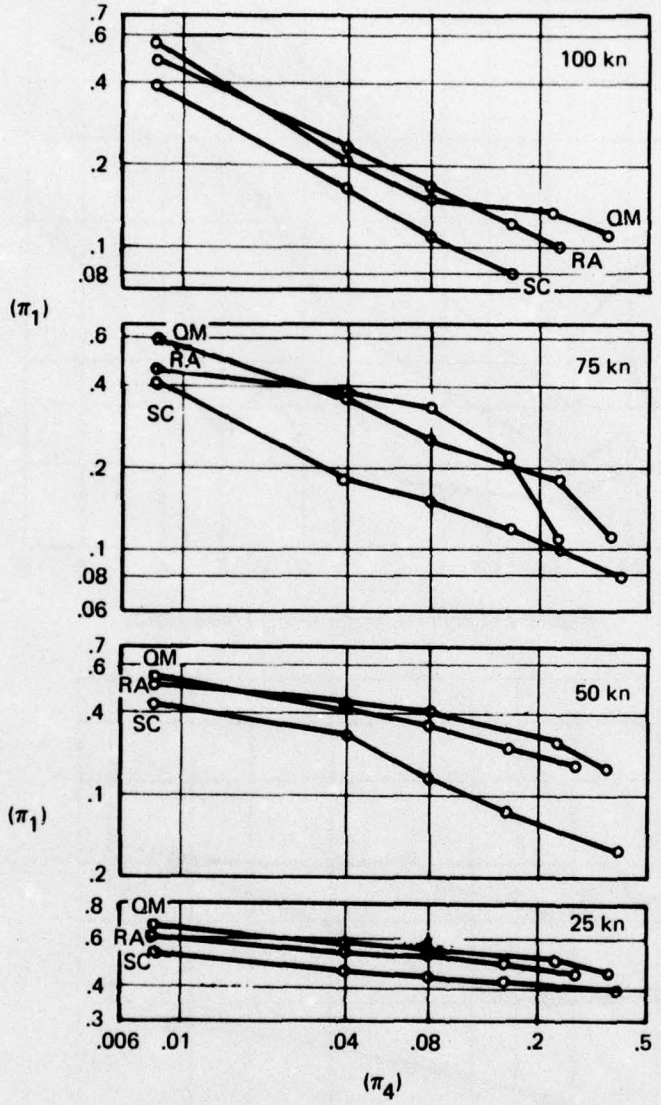

Figure F-3.—Plots of π_1 vs π_4 (Raw Data)

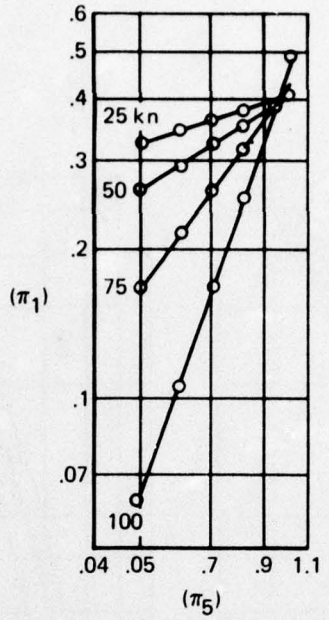

Figure F-4.—Plots of π_1 vs π_5 (Raw Data)

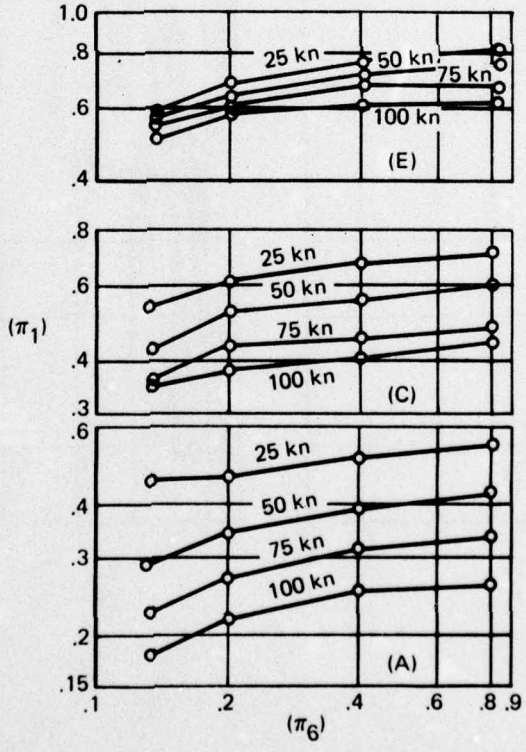

Figure F-5.—Plots of π_1 vs π_6 (Raw Data)

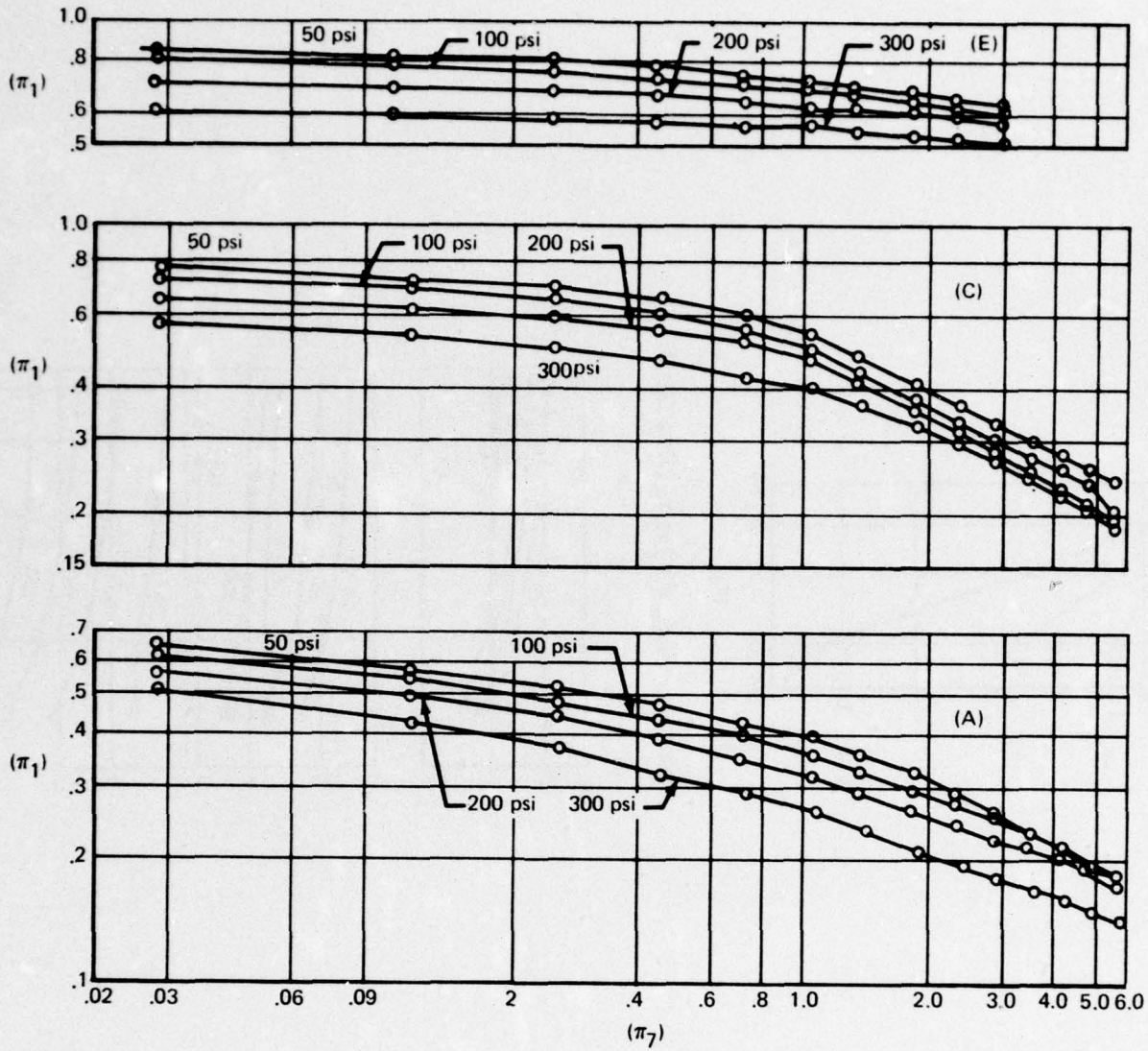

Figure F-6.—Plots of π_1 vs π_7 (Raw Data)

$X = \pi_2$ or π_3 or π_4 or π_5 or π_6 or π_7 - the independent variable

$Y = \pi_1$ - the dependent variable

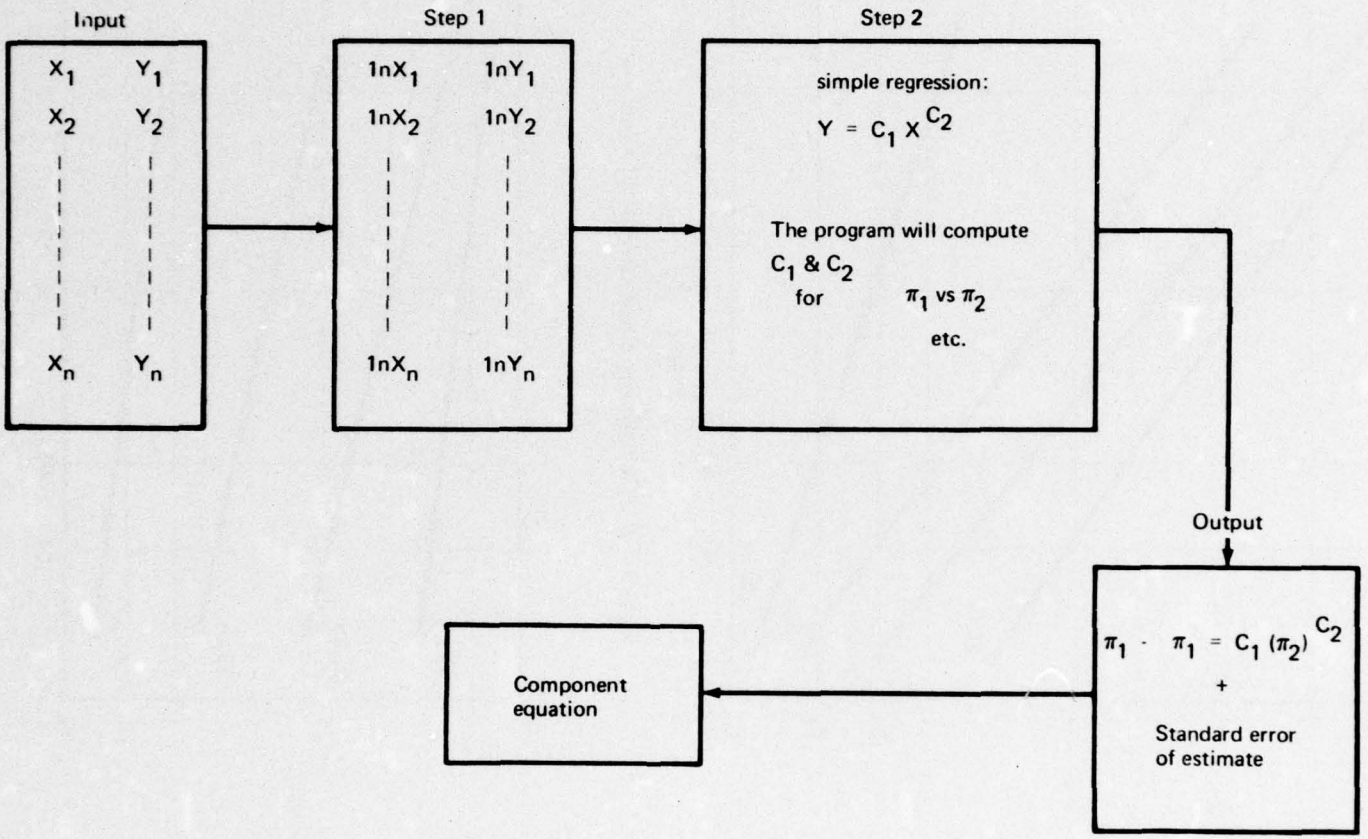

Figure F-7.—Equation Flow Chart

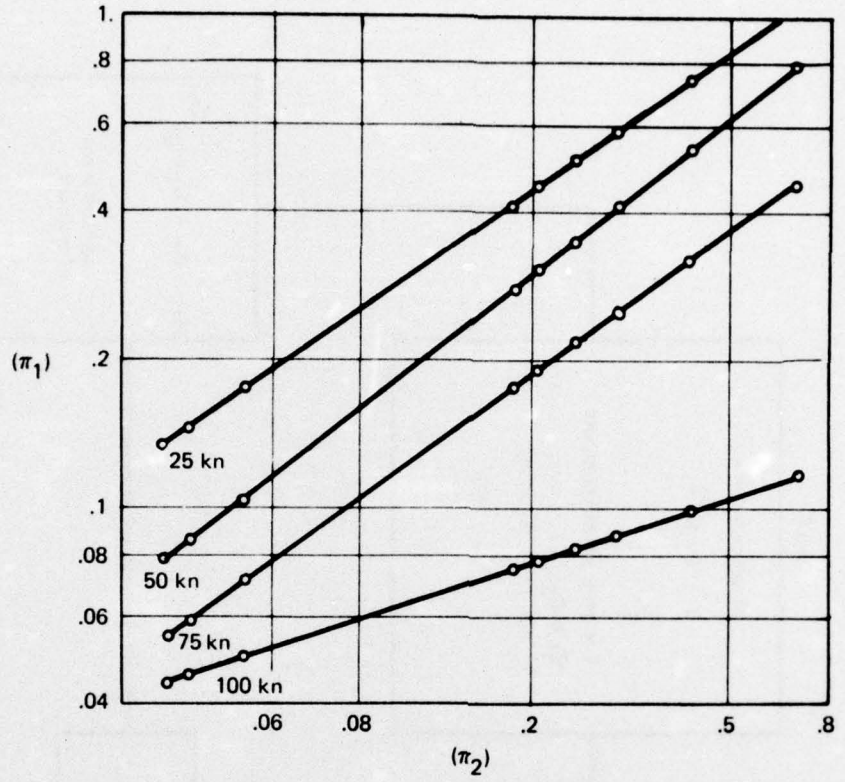

Figure F-8.—Component Equation Plot of π_1 vs π_2

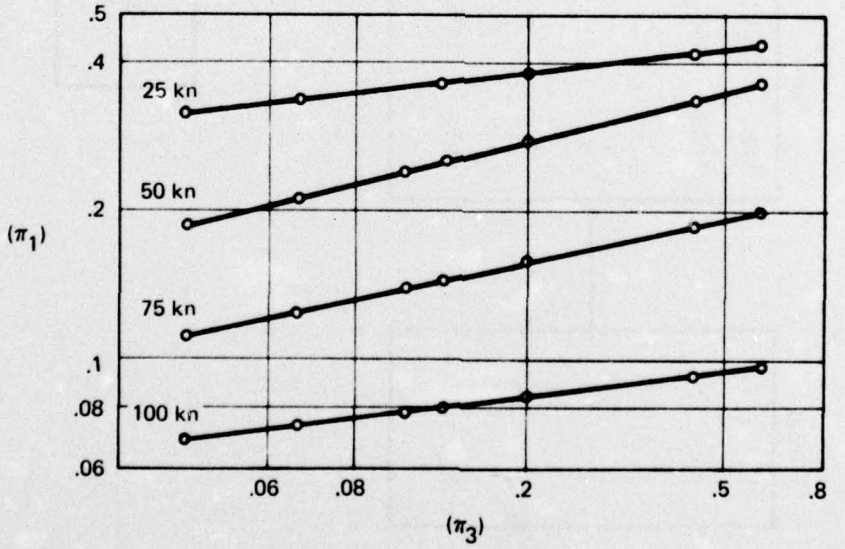

Figure F-9.—Component Equation Plot of π_1 vs π_3

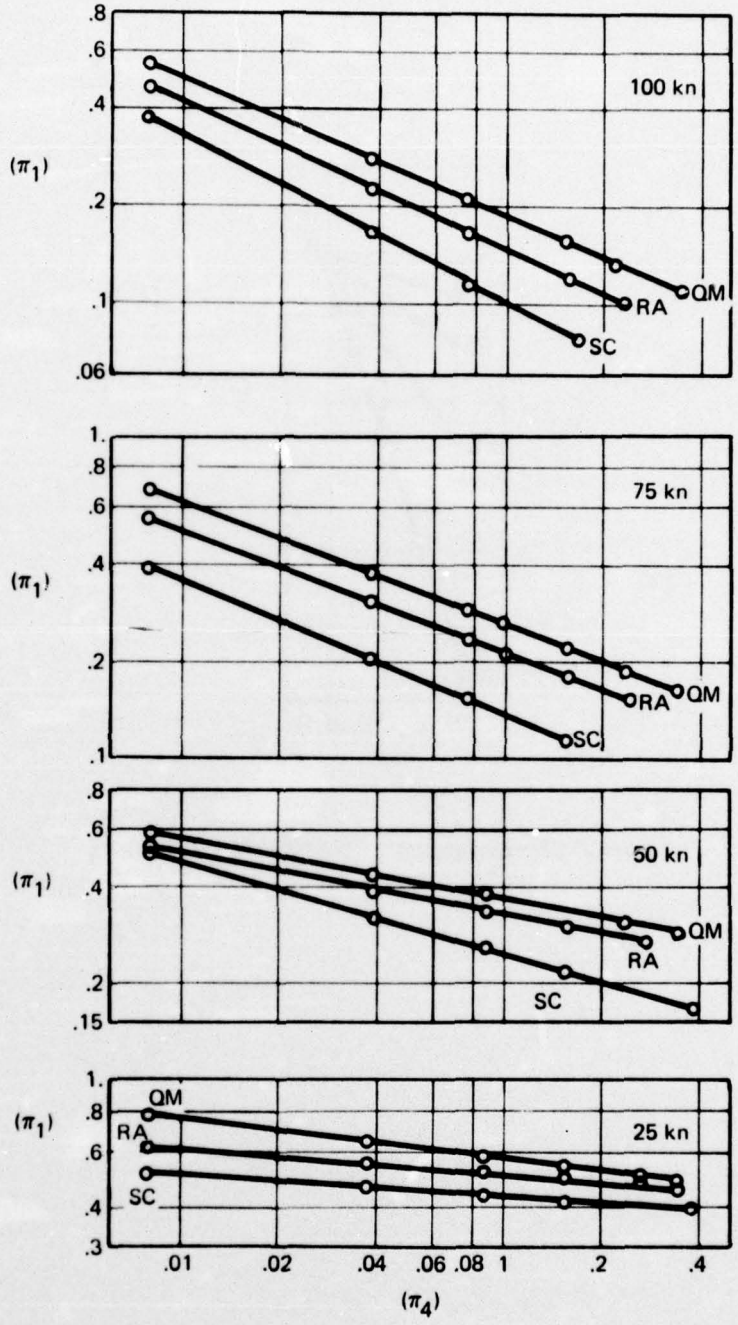

Figure F-10.—Component Equation Plot of π_1 vs π_4

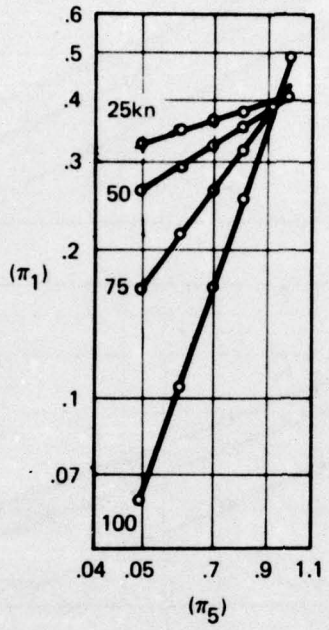

Figure F-11.—Component Equation Plot of π_1 vs π_5

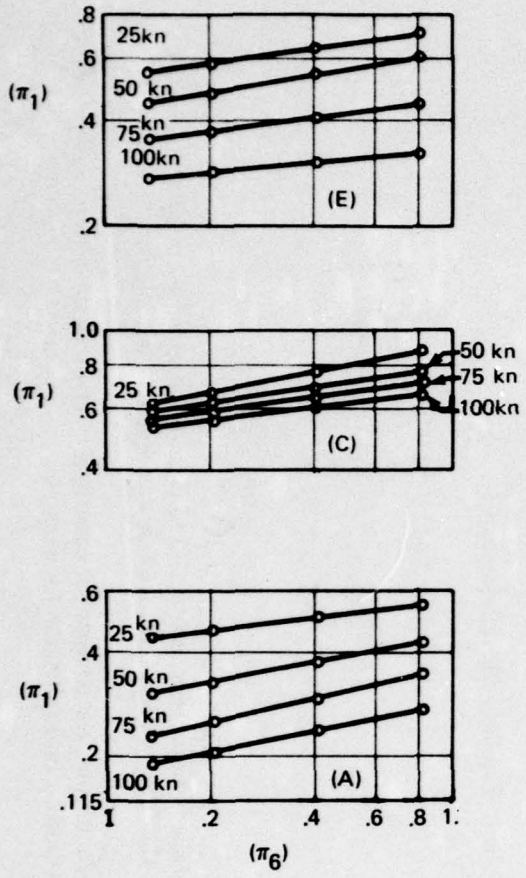

Figure F-12.—Component Equation Plot of π_1 vs π_6

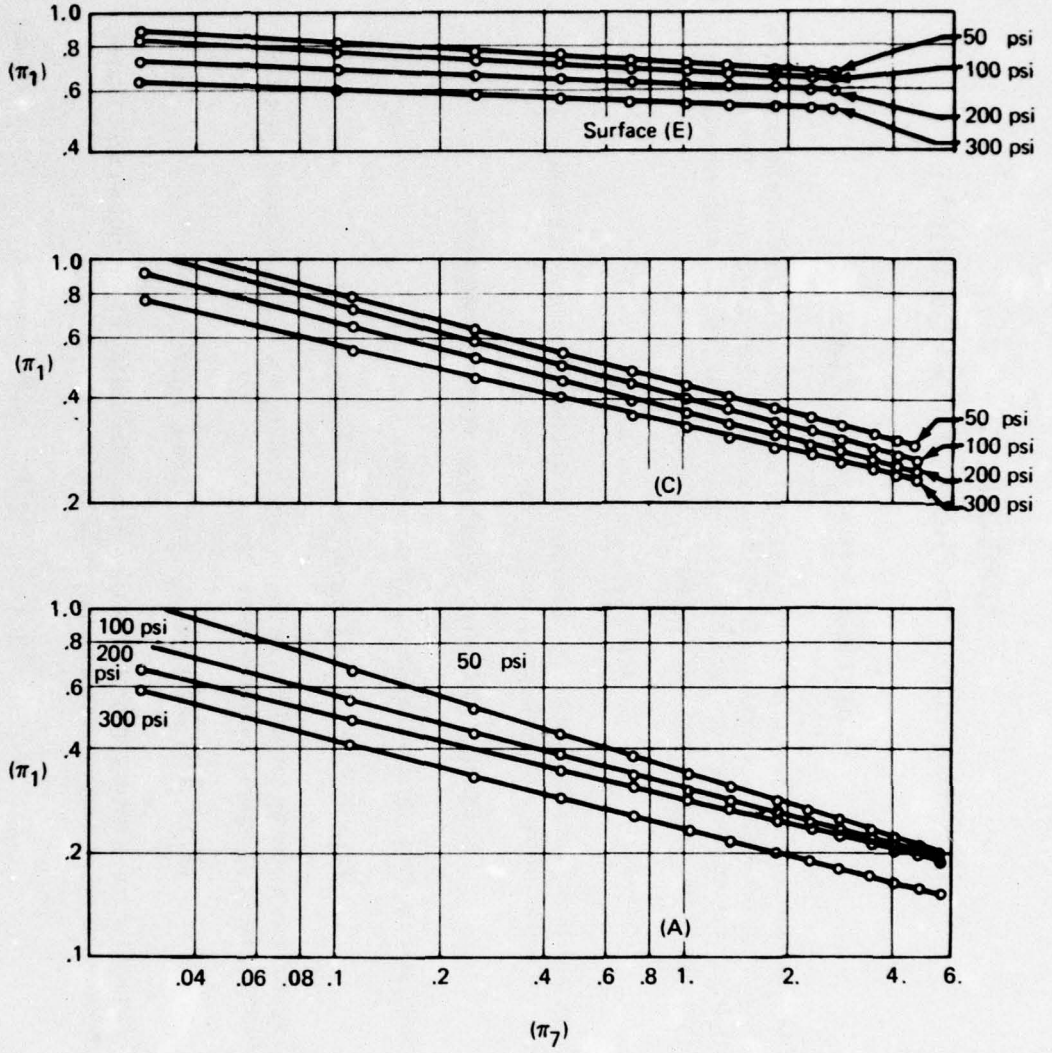

Figure F-13.—Component Equation Plot of π_1 vs π_7

APPENDIX G
FORMULATION OF PREDICTION EQUATIONS

1. DETERMINATION OF FUNCTIONS

As pointed out in section III, the component equations representing relationships between π_1 and other individual pi terms are combined to give a general relationship. This combination is not always simple, but under certain conditions it may be reasonably direct. The function on the right-hand side of the general equation:

$$\pi_1 = F\ (\pi_2, \pi_3, \pi_4 \text{ --------} \pi_k) \tag{G-1}$$

may denote any combination of the pi terms. We will now determine the conditions necessary or sufficient for certain simple combinations to exist.

2. CONDITIONS FOR FUNCTION TO BE A PRODUCT

Since seven pi terms are involved in the phenomenon:

$$(\pi_1) = F\ (\pi_2, \pi_3, \pi_4, \pi_5, \pi_6, \pi_7) = F\ (\pi_{2\rightarrow\pi_7}) \tag{G-2}$$

Experiments would be carried out varying π_2 and holding $\pi_3, \pi_4, \pi_5, \pi_6$ and π_7 constant. From a plot of π_1 against π_2, the relationship:

$$(\pi_1)\ \bar{3}, \bar{4}, \bar{5}, \bar{6}, \bar{7} = (\pi_1)\ \bar{3}\rightarrow\bar{7} = f_1\ (\pi_2, \bar{\pi}_{3\rightarrow}\bar{\pi}_7) \tag{G-3}$$

in which the bar denotes constant values, could be established. From another set of experiments, with π_2, π_4 to π_7 constant and π_3 variable:

$$(\pi_1)\ \bar{2}, \bar{4}\rightarrow\bar{7} = f_2\ (\pi_3, \bar{\pi}_{2\rightarrow}\bar{\pi}_7) \tag{G-3a}$$

may be established. Similarly the relationships:

$$(\pi_1)\ \bar{2}, \bar{3}, \bar{5}\rightarrow\bar{7} = f_3\ (\pi_4, \bar{\pi}_{2\rightarrow}\bar{\pi}7) \tag{G-3b}$$

$$(\pi_1)\ \bar{2}\rightarrow\bar{4}, \bar{6}, \bar{7} = f_4\ (\pi_5, \bar{\pi}_{2\rightarrow}\bar{\pi}_7) \tag{G-3c}$$

$$(\pi_1)\ \bar{2}\rightarrow\bar{5}, \bar{7} = f_5\ (\pi_6, \bar{\pi}_{2\rightarrow}\bar{\pi}_7) \tag{G-3d}$$

$$(\pi_1)\ \bar{2}\rightarrow\bar{6} = f_6\ (\pi_7, \bar{\pi}_{2\rightarrow}\bar{\pi}_6) \tag{G-3e}$$

could be established. Equations such as G-3 to G-3e, determined by holding all but one of the pi terms in the function constant, are called component equations.

Under certain conditions, the component equations can be combined to form the general prediction equation by multiplication for example:

$$\pi_1 = C(\pi_1)\,\bar{3}\to\bar{7}(\pi_1)\,\bar{2},\bar{4}\to\bar{7}(\pi_1)\,\bar{2},\bar{3},\bar{5}\to\bar{7}(\pi_1)\,\bar{2}\to\bar{4},\bar{6},\bar{7}(\pi_1)\,\bar{2}\to\bar{5},\bar{7}(\pi_1)\,\bar{2}\to\bar{6} \qquad \text{(G-3f)}$$

To establish those conditions, we first determine the constant C in Eq G-3f by assuming that the component equations are simply multiplied to form the general equation:

$$F(\pi_{2\to7}) = f_1(\pi_2,\bar{\pi}_{3\to7})\,f_2(\pi_3,\bar{\pi}_{2\to7})\,f_3(\pi_4,\bar{\pi}_{2\to7})\,f_4(\pi_5,\bar{\pi}_{2\to7})\,f_5(\pi_6,\bar{\pi}_{2\to7})\,f_6(\pi_7,\bar{\pi}_{2\to6}) \qquad \text{(G-4)}$$

If this is true, the first set of tests, with π_3 to π_7 constant, will give:

$$F(\pi_2,\bar{\pi}_{3\to7}) = f_1(\pi_2,\bar{\pi}_{3\to7})\,f_2(\bar{\pi}_{2\to7})\cdots f_6(\bar{\pi}_{2\to7}) \qquad \text{(G-4a)}$$

from which

$$f_1(\pi_2,\bar{\pi}_{3\to7}) = \frac{F(\pi_2,\bar{\pi}_{3\to7})}{f_2(\bar{\pi}_{2\to7})\cdots f_6(\bar{\pi}_{2\to7})} \qquad \text{(G-4b)}$$

The second set of tests, with π_2 and π_4 to π_7 constant, gives from Eq. G-4:

$$F(\pi_3,\bar{\pi}_{2\to7}) = f_1(\pi_{2\to7})\,f_2(\pi_3,\bar{\pi}_{2\to7})\,f_3(\bar{\pi}_{2\to7})\cdots f_6(\bar{\pi}_{2\to7}) \qquad \text{(G-4c)}$$

from which

$$f_2(\pi_3,\bar{\pi}_{2\to7}) = \frac{F(\pi_3,\bar{\pi}_{2\to7})}{f_1(\bar{\pi}_{2\to7})\,f_3(\bar{\pi}_{2\to7})\cdots f_6(\bar{\pi}_{2\to7})} \qquad \text{(G-4d)}$$

Similarly third, fourth, fifth and sixth sets of tests will give:

$$f_3(\pi_4,\bar{\pi}_{2\to7}) = \frac{F(\pi_4,\bar{\pi}_{2\to7})}{f_1(\bar{\pi}_{2\to7})\,f_2(\bar{\pi}_{2\to7})\,f_4(\bar{\pi}_{2\to7})\cdots f_6(\bar{\pi}_{2\to7})} \qquad \text{(G-4e)}$$

$$f_4(\pi_5,\bar{\pi}_{2\to7}) = \frac{F(\pi_5,\bar{\pi}_{2\to7})}{f_1(\bar{\pi}_{2\to7})\cdots f_3(\bar{\pi}_{2\to7})\,f_5(\bar{\pi}_{2\to7})\cdots f_6(\bar{\pi}_{2\to7})} \qquad \text{(G-4f)}$$

$$f_5(\pi_6,\bar{\pi}_{2\to7}) = \frac{F(\pi_6,\bar{\pi}_{2\to7})}{f_1(\bar{\pi}_{2\to7})\cdots f_4(\bar{\pi}_{2\to7})\,f_6(\bar{\pi}_{2\to7})} \qquad \text{(G-4g)}$$

$$f_6(\pi_7,\bar{\pi}_{2\to6}) = \frac{F(\pi_7,\bar{\pi}_{2\to6})}{f_1(\bar{\pi}_{2\to7})\cdots f_5(\bar{\pi}_{2\to7})} \qquad \text{(G-4h)}$$

Values of $f_1(\pi_2, \bar{\pi}_3 \rightarrow \bar{\pi}_7)$, $f_2(\pi_3, \bar{\pi}_2 \rightarrow \bar{\pi}_7)$ etc. From Eqs G-4b and G-4d to G-4h are substituted into Eq G-4 to give:

$$F(\pi_{2\rightarrow}\pi_7) = \frac{\left\{ \begin{array}{l} F(\pi_2, \bar{\pi}_3 \rightarrow \bar{\pi}_7)\, F(\pi_3, \bar{\pi}_2 \rightarrow \bar{\pi}_7)\, F(\pi_4, \bar{\pi}_2 \rightarrow \bar{\pi}_7) \\ F(\pi_5, \bar{\pi}_2 \rightarrow \bar{\pi}_7)\, F(\pi_6, \bar{\pi}_2 \rightarrow \bar{\pi}_7)\, F(\pi_7, \bar{\pi}_2 \rightarrow \bar{\pi}_6) \end{array} \right\}}{[f_1(\bar{\pi}_2 \rightarrow \bar{\pi}_7) \text{ ---- } f_6(\bar{\pi}_2 \rightarrow \bar{\pi}_7)]^5} \qquad \text{(G-4i)}$$

However, the denominator of Eq. G-4i is found from Eq. G-4 with all π_2, π_3, π_4, π_5, π_6 and π_7 constant:

$$F(\bar{\pi}_{2\rightarrow}\bar{\pi}_7) = f_1(\bar{\pi}_2 \rightarrow \bar{\pi}_7) \text{ ---- } f_6(\bar{\pi}_2 \rightarrow \bar{\pi}_7) \qquad \text{(G-4j)}$$

Hence:

$$F(\pi_{2\rightarrow}\pi_7) = \frac{\left\{ \begin{array}{l} F(\pi_2, \bar{\pi}_3 \rightarrow \bar{\pi}_7)\, F(\pi_3, \bar{\pi}_2 \rightarrow \bar{\pi}_7)\, F(\pi_4, \bar{\pi}_2 \rightarrow \bar{\pi}_7) \\ F(\pi_5, \bar{\pi}_2 \rightarrow \bar{\pi}_7)\, F(\pi_6, \bar{\pi}_2 \rightarrow \bar{\pi}_7)\, F(\pi_7, \bar{\pi}_2 \rightarrow \bar{\pi}_6) \end{array} \right\}}{[F(\bar{\pi}_{2\rightarrow}\bar{\pi}_7)]^5} \qquad \text{(G-4k)}$$

In addition to giving the value of C in Eq. G-3f as $1/[F(\bar{\pi}_{2\rightarrow}\bar{\pi}_7)]^5$, Eq. G-4k indicates that the six component equations must have the same form.

A test for the validity of combining the component equations as a product may now be developed by assuming that a seventh component equation is determined from a seventh set of data in which one of the pi terms is held constant at a different value than in the preceding set of data. For example, the general Eq. G-4k was determined by holding π_7 constant at a value of $\bar{\pi}_7$, but if valid, it could also have been determined from a set of data in which $\pi_7 = \bar{\bar{\pi}}_7$. Then:

$$F(\pi_{2\rightarrow}\pi_7) = \frac{\left\{ \begin{array}{l} F(\pi_2, \bar{\pi}_3 \rightarrow \bar{\bar{\pi}}_7)\, F(\pi_3, \bar{\pi}_2 \rightarrow \bar{\bar{\pi}}_7)\, F(\pi_4, \bar{\pi}_2 \rightarrow \bar{\bar{\pi}}_7) \\ F(\pi_5, \bar{\pi}_2 \rightarrow \bar{\bar{\pi}}_7)\, F(\pi_6, \bar{\pi}_2 \rightarrow \bar{\bar{\pi}}_7)\, F(\pi_7, \bar{\pi}_2 \rightarrow \bar{\bar{\pi}}_6) \end{array} \right\}}{[F(\bar{\pi}_{2\rightarrow}\bar{\bar{\pi}}_7)]^5} \qquad \text{(G-5)}$$

The right-hand side of Eq. G-4k must equal the right-hand side of Eq. G-5. Hence:

$$\frac{F(\pi_2, \bar{\pi}_3 \rightarrow \bar{\pi}_7)\, F(\pi_3, \bar{\pi}_2 \rightarrow \bar{\pi}_7)\, F(\pi_4, \bar{\pi}_2 \rightarrow \bar{\pi}_7)\, F(\pi_5, \bar{\pi}_2 \rightarrow \bar{\pi}_7)\, F(\pi_6, \bar{\pi}_2 \rightarrow \bar{\pi}_7)}{[F(\bar{\pi}_{2\rightarrow}\bar{\pi}_7)]^5} \equiv$$

$$\frac{F(\pi_2, \bar{\pi}_3 \rightarrow \bar{\bar{\pi}}_7)\, F(\pi_3, \bar{\pi}_2 \rightarrow \bar{\bar{\pi}}_7)\, F(\pi_4, \bar{\pi}_2 \rightarrow \bar{\bar{\pi}}_7)\, F(\pi_5, \bar{\pi}_2 \rightarrow \bar{\bar{\pi}}_7)\, F(\pi_6, \bar{\pi}_2 \rightarrow \bar{\bar{\pi}}_7)}{[F(\bar{\pi}_{2\rightarrow}\bar{\bar{\pi}}_7)]^5} \qquad \text{(G-6)}$$

Similarly, if π_2 had been held constant at a different value, $\bar{\bar{\pi}}_2$:

$$\frac{F(\pi_3, \bar{\pi}_{2\to}\bar{\pi}_7)\, F(\pi_4, \bar{\pi}_{2\to}\bar{\pi}_7)\, F(\pi_5, \bar{\pi}_{2\to}\bar{\pi}_7)\, F(\pi_6, \bar{\pi}_{2\to}\bar{\pi}_7)\, F(\pi_7, \bar{\pi}_{2\to}\bar{\pi}_6)}{[F(\bar{\pi}_{2\to}\bar{\pi}_7)]^5} \equiv$$

$$\frac{F(\pi_3, \bar{\bar{\pi}}_{2\to}\bar{\pi}_7)\, F(\pi_4, \bar{\bar{\pi}}_{2\to}\bar{\pi}_7)\, F(\pi_5, \bar{\bar{\pi}}_{2\to}\bar{\pi}_7)\, F(\pi_6, \bar{\bar{\pi}}_{2\to}\bar{\pi}_7)\, F(\pi_7, \bar{\bar{\pi}}_{2\to}\bar{\pi}_6)}{[F(\bar{\bar{\pi}}_{2\to}\bar{\pi}_7)]^5} \quad \text{(G-6a)}$$

Equations G-6 and G-6a constitute a test for the validity of Eq. G-4k. That is, if the supplementary sets of data satisfy either Eq. G-6 or G-6a, the general equation may be formed by multiplying the component equations together and dividing by the constant, as indicated in Eq. G-4k.

Thus, if the general equation for a system involving k pi terms was formed by multiplication of the component equations, it may be shown that the form is:

$$\pi_1 = \frac{F(\pi_2, \bar{\pi}_3, \bar{\pi}_4, \ldots . \bar{\pi}_k)\, F(\bar{\pi}_2, \pi_3, \bar{\pi}_4, \ldots . \bar{\pi}_k) \ldots . F(\bar{\pi}_2, \bar{\pi}_3, \bar{\pi}_4, \ldots . \pi_k)}{[F(\bar{\pi}_2, \bar{\pi}_3, \bar{\pi}_4, \ldots \bar{\pi}_k)]^{k-2}} \quad \text{(G-7)}$$

In this, π_2 must be the same in each component set, π_3 must be the same in each set, etc. Similarly, if the general equation for a system involving k pi terms is formed by addition of the component equations, it may be shown that the form is:

$$\pi_1 = F(\pi_2, \bar{\pi}_3, \bar{\pi}_4, \ldots . \bar{\pi}_k) + F(\bar{\pi}_2, \pi_3, \bar{\pi}_4, \ldots . \bar{\pi}_k) + F(\bar{\pi}_2, \bar{\pi}_3, \pi_4, \ldots . \bar{\pi}_k) + \ldots . F(\bar{\pi}_2, \bar{\pi}_3, \bar{\pi}_4, \ldots . \pi_k) - (k-2)\, F(\bar{\pi}_2, \bar{\pi}_3, \bar{\pi}_4, \ldots . \bar{\pi}_k) \quad \text{(G-8)}$$

In general, the possible methods of formation of general equations discussed above are adequate for the majority of engineering problems. Regardless of whether the resultant prediction equation is formed by multiplication or by addition, a constant term of the form:

$$F(\bar{\pi}_2, \bar{\pi}_3, \bar{\pi}_4, \ldots . \bar{\pi}_k)$$

is involved, and this constant can be evaluated from any one of the component equations. As a general policy, the constant should be evaluated from each of the component equations. Each should give the same value as the others. If not, error is present, and the equations should be checked. As explained earlier, section III, due to the nature of available data, both tests of validity were assumed applicable and the predictions equations were formed by the multiplication method.

The 48 component equations were listed in Table 4, section III. Table G-1 shows the possible combinations of these component equations to form 48 prediction equations. For example, the first combination consists of equations 4, 8, 12, 24, 28 and 40 and is for surface 'A' and $V\bar{\pi}_7$ = 25 knots. What follows is a sample calculation.

Table G-1.—Possible Combinations of Component Equations

Eq	Eq	Eq	Eq	Eq	Eq/Eq/Eq/Eq	$V\bar{\pi}_7$ Kn
4	8	12	24	28	40/41/42/43	25
4	8	16	24	32	44/45/46/47	
4	8	20	24	36	48/49/50/51	
5	9	13	25	29	40/41/42/43	50
5	9	17	25	33	44/45/46/47	
5	9	21	25	37	48/49/50/51	
6	10	14	26	30	40/41/42/43	75
6	10	18	26	34	44/45/46/47	
6	10	22	26	38	48/49/50/51	
7	11	15	27	31	40/41/42/43	100
7	11	19	27	35	44/45/46/47	
7	11	23	27	39	48/49/50/51	

Note: The equation numbers correspond to Table 6.

SAMPLE CALCULATION OF A PREDICTION EQUATION AND ITS CONSTANT

$(\pi_1) = 1.3757\ (\pi_2)^{.7046}$	(4)	$(\bar{\pi})$ From Table	(π_1)
$(\pi_1) = .4659\ (\pi_3)^{.1200}$	(8)	$(\bar{\pi}_3) = 1.25$	.4785
$(\pi_1) = .3650\ (\pi_4)^{-.0714}$	(12)	$(\bar{\pi}_4) = .15$	.4179
$(\pi_1) = .4098\ (\pi_5)^{.3089}$	(24)	$(\bar{\pi}_5) = .842$	.3886
$(\pi_1) = .5536\ (\pi_6)^{.1117}$	(28)	$(\bar{\pi}_6) = .1596$	.4510
$(\pi_1) = .3473\ (\pi_7)^{-.3129}$	(40)	$(\bar{\pi}_7) = .3617$	.4774

$$C = \frac{1}{.4785 \times .4129 \times .3886 \times .4510 \times .4774}$$

or

$$C = 59.77$$

$$(\pi_1) = [(59.77 \times 1.3757 \times .4659 \times .3650 \times .4098 \times .5536 \times .3473) \times (\pi_2)^{.7046} (\pi_3)^{.1200} (\pi_4)^{-.0714} (\pi_5)^{.3089} (\pi_6)^{.1117} (\pi_7)^{-.3129}]$$

or

$$(\pi_1) = 1.1017\ (\pi_2)^{.7046} (\pi_3)^{.1200} (\pi_4)^{-.0714} (\pi_5)^{.3089} (\pi_6)^{.1117} (\pi_7)^{-.3129} \quad \text{(G-9)}$$

This procedure was repeated for all possible combinations and Tables G-2 and G-3 respectively show the calculated values of 'C' and the resulting prediction equations. Equations G-9 to G-12 are different from one another only in their constant term 'C' and the exponent of the term π_7. This is true about each set of 4 prediction equations for a given surface and a velocity. Thus equations in each set generated solutions that were within ± 1% of each other as shown in Table G-4. This small deviation allowed averaging of four equations into one, resulting in only 12 prediction equations shown in Table G-5.

Table G-2.—Calculated Values of "C"

$V\bar{\pi}_7 \sim K_n$	VALUE OF CONSTANT C WITH REFERENCE TO TABLE G-1			
25	59.77	70.13	77.83	92.02
	34.18	36.80	40.13	45.97
	20.94	21.89	24.44	27.81
50	337.31	360.5	392.05	478.96
	104.47	113.6	123.15	136.12
	42.11	43.6	47.67	53.68
75	1823.71	1844.47	1982.3	2468.65
	534.96	585.14	631.8	684.19
	149.93	154.36	166.6	186.6
100	10,015.03	9747.6	10,388.0	13,115.7
	3,201.5	3515.9	3,786.1	4,040.8
	566.98	581.45	622.3	693.8

Table G-3.—List of Possible Prediction Equations.

A.	$\frac{25Kn}{(\pi_1)} = 1.1017\ (\pi_2)^{.7046}\ (\pi_3)^{.1200}\ (\pi_4)^{-.0714}\ (\pi_5)^{.3089}\ (\pi_6)^{.1117}\ (\pi_7)^{-.3129}$	(G-9)
	$(\pi_1) = 1.1796\ (\pi_2)^{.7046}\ (\pi_3)^{.1200}\ (\pi_4)^{-.0714}\ (\pi_5)^{.3089}\ (\pi_6)^{.1117}\ (\pi_7)^{-.2455}$	(G-10)
	$(\pi_1) = 1.1973\ (\pi_2)^{.7046}\ (\pi_3)^{.1200}\ (\pi_4)^{-.0714}\ (\pi_5)^{.3089}\ (\pi_6)^{.1117}\ (\pi_7)^{-.2308}$	(G-11)
	$(\pi_1) = 1.1690\ (\pi_2)^{.7046}\ (\pi_3)^{.1200}\ (\pi_4)^{-.0714}\ (\pi_5)^{.3089}\ (\pi_6)^{.1117}\ (\pi_7)^{-.2546}$	(G-12)
C.	$(\pi_1) = 1.2994\ (\pi_2)^{.7046}\ (\pi_3)^{.1200}\ (\pi_4)^{-.0742}\ (\pi_5)^{.3089}\ (\pi_6)^{.1665}\ (\pi_7)^{-.2443}$	(G-13)
	$(\pi_1) = 1.2901\ (\pi_2)^{.7046}\ (\pi_3)^{.1200}\ (\pi_4)^{-.0742}\ (\pi_5)^{.3089}\ (\pi_6)^{.1665}\ (\pi_7)^{-.2515}$	(G-14)
	$(\pi_1) = 1.2958\ (\pi_2)^{.7046}\ (\pi_3)^{.1200}\ (\pi_4)^{-.0742}\ (\pi_5)^{.3089}\ (\pi_6)^{.1665}\ (\pi_7)^{-.2469}$	(G-15)
	$(\pi_1) = 1.3304\ (\pi_2)^{.7046}\ (\pi_3)^{.1200}\ (\pi_4)^{-.0742}\ (\pi_5)^{.3089}\ (\pi_6)^{.1665}\ (\pi_7)^{-.2214}$	(G-16)
E.	$(\pi_1) = 1.3949\ (\pi_2)^{.7046}\ (\pi_3)^{.1200}\ (\pi_4)^{-.1518}\ (\pi_5)^{.3089}\ (\pi_6)^{.1855}\ (\pi_7)^{-.0640}$	(G-17)
	$(\pi_1) = 1.4045\ (\pi_2)^{.7046}\ (\pi_3)^{.1200}\ (\pi_4)^{-.1518}\ (\pi_5)^{.3089}\ (\pi_6)^{.1855}\ (\pi_7)^{-.0572}$	(G-18)
	$(\pi_1) = 1.4263\ (\pi_2)^{.7046}\ (\pi_3)^{.1200}\ (\pi_4)^{-.1518}\ (\pi_5)^{.3089}\ (\pi_6)^{.1855}\ (\pi_7)^{-.0418}$	(G-19)
	$(\pi_1) = 1.4372\ (\pi_2)^{.7046}\ (\pi_3)^{.1200}\ (\pi_4)^{-.1518}\ (\pi_5)^{.3089}\ (\pi_6)^{.1855}\ (\pi_7)^{-.0345}$	(G-20)
A.	$\frac{50Kn}{(\pi_1)} = .9653\ (\pi_2)^{.7887}\ (\pi_3)^{.2501}\ (\pi_4)^{-.3347}\ (\pi_5)^{.645}\ (\pi_6)^{.2002}\ (\pi_7)^{-.3129}$	(G-21)
	$(\pi_1) = .9415\ (\pi_2)^{.7887}\ (\pi_3)^{.2501}\ (\pi_4)^{-.3347}\ (\pi_5)^{.645}\ (\pi_6)^{.2002}\ (\pi_7)^{-.2445}$	(G-22)
	$(\pi_1) = .9365\ (\pi_2)^{.7887}\ (\pi_3)^{.2501}\ (\pi_4)^{-.3347}\ (\pi_5)^{.645}\ (\pi_6)^{.2002}\ (\pi_7)^{-.2308}$	(G-23)
	$(\pi_1) = .9448\ (\pi_2)^{.7887}\ (\pi_3)^{.2501}\ (\pi_4)^{-.3347}\ (\pi_5)^{.645}\ (\pi_6)^{.2002}\ (\pi_7)^{-.2546}$	(G-24)
C.	$(\pi_1) = 1.1578\ (\pi_2)^{.7887}\ (\pi_3)^{.2501}\ (\pi_4)^{-.1864}\ (\pi_5)^{.645}\ (\pi_6)^{.1602}\ (\pi_7)^{-.2443}$	(G-25)
	$(\pi_1) = 1.1609\ (\pi_2)^{.7887}\ (\pi_3)^{.2501}\ (\pi_4)^{-.1864}\ (\pi_5)^{.645}\ (\pi_6)^{.1602}\ (\pi_7)^{-.2515}$	(G-26)
	$(\pi_1) = 1.1593\ (\pi_2)^{.7887}\ (\pi_3)^{.2501}\ (\pi_4)^{-.1864}\ (\pi_5)^{.645}\ (\pi_6)^{.1602}\ (\pi_7)^{-.2469}$	(G-27)
	$(\pi_1) = 1.1482\ (\pi_2)^{.7887}\ (\pi_3)^{.2501}\ (\pi_4)^{-.1864}\ (\pi_5)^{.645}\ (\pi_6)^{.1602}\ (\pi_7)^{-.2214}$	(G-28)

Table G-3.—List of Possible Prediction Equations (Continued)

E.	$\frac{50Kn}{(\pi_1)} = 1.0781\ (\pi_2)^{.7887}\ (\pi_3)^{.2501}\ (\pi_4)^{-.1773}\ (\pi_5)^{.645}\ (\pi_6)^{.1482}\ (\pi_7)^{-.0640}$	(G-29)
	$(\pi_1) = 1.0756\ (\pi_2)^{.7887}\ (\pi_3)^{.2501}\ (\pi_4)^{-.1773}\ (\pi_5)^{.645}\ (\pi_6)^{.1482}\ (\pi_7)^{-.0572}$	(G-30)
	$(\pi_1) = 1.0692\ (\pi_2)^{.7887}\ (\pi_3)^{.2501}\ (\pi_4)^{-.1773}\ (\pi_5)^{.645}\ (\pi_6)^{.1482}\ (\pi_7)^{-.0418}$	(G-31)
	$(\pi_1) = 1.0667\ (\pi_2)^{.7887}\ (\pi_3)^{.2501}\ (\pi_4)^{-.1773}\ (\pi_5)^{.645}\ (\pi_6)^{.1482}\ (\pi_7)^{-.0345}$	(G-32)
A.	$\frac{75Kn}{(\pi_1)} = .7154\ (\pi_2)^{.7265}\ (\pi_3)^{.2234}\ (\pi_4)^{-.4113}\ (\pi_5)^{1.3555}(\pi_6)^{.2204}\ (\pi_7)^{-.3129}$	(G-33)
	$(\pi_1) = .6604\ (\pi_2)^{.7265}\ (\pi_3)^{.2234}\ (\pi_4)^{-.4113}\ (\pi_5)^{1.3555}(\pi_6)^{.2204}\ (\pi_7)^{-.2455}$	(G-34)
	$(\pi_1) = .6491\ (\pi_2)^{.7265}\ (\pi_3)^{.2234}\ (\pi_4)^{-.4113}\ (\pi_5)^{1.3555}(\pi_6)^{.2204}\ (\pi_7)^{-.2308}$	(G-35)
	$(\pi_1) = .6675\ (\pi_2)^{.7265}\ (\pi_3)^{.2234}\ (\pi_4)^{-.4113}\ (\pi_5)^{1.3555}(\pi_6)^{.2204}\ (\pi_7)^{-.2546}$	(G-36)
C.	$(\pi_1) = .5862\ (\pi_2)^{.7265}\ (\pi_3)^{.2234}\ (\pi_4)^{-.3820}\ (\pi_5)^{1.3555}(\pi_6)^{.1257}\ (\pi_7)^{-.2443}$	(G-37)
	$(\pi_1) = .5912\ (\pi_2)^{.7265}\ (\pi_3)^{.2234}\ (\pi_4)^{-.3820}\ (\pi_5)^{1.3555}(\pi_6)^{.1257}\ (\pi_7)^{-.2515}$	(G-38)
	$(\pi_1) = .5880\ (\pi_2)^{.7265}\ (\pi_3)^{.2234}\ (\pi_4)^{-.3820}\ (\pi_5)^{1.3555}(\pi_6)^{.1257}\ (\pi_7)^{-.2469}$	(G-39)
	$(\pi_1) = .5706\ (\pi_2)^{.7265}\ (\pi_3)^{.2234}\ (\pi_4)^{-.3820}\ (\pi_5)^{1.3555}(\pi_6)^{.1257}\ (\pi_7)^{-.2214}$	(G-40)
E.	$(\pi_1) = .4571\ (\pi_2)^{.7265}\ (\pi_3)^{.2234}\ (\pi_4)^{-.4004}\ (\pi_5)^{1.3555}(\pi_6)^{.1254}\ (\pi_7)^{-.0640}$	(G-41)
	$(\pi_1) = .4535\ (\pi_2)^{.7265}\ (\pi_3)^{.2234}\ (\pi_4)^{-.4004}\ (\pi_5)^{1.3555}(\pi_6)^{.1254}\ (\pi_7)^{-.0572}$	(G-42)
	$(\pi_1) = .4453\ (\pi_2)^{.7265}\ (\pi_3)^{.2234}\ (\pi_4)^{-.4004}\ (\pi_5)^{1.3555}(\pi_6)^{.1254}\ (\pi_7)^{-.0418}$	(G-43)
	$(\pi_1) = .4415\ (\pi_2)^{.7265}\ (\pi_3)^{.2234}\ (\pi_4)^{-.4004}\ (\pi_5)^{1.3555}(\pi_6)^{.1254}\ (\pi_7)^{-.0345}$	(G-44)
A.	$\frac{100Kn}{(\pi_1)} = .1957\ (\pi_2)^{.3361}\ (\pi_3)^{.1192}\ (\pi_4)^{-.5376}\ (\pi_5)^{3.0071}(\pi_6)^{.1942}\ (\pi_7)^{-.3129}$	(G-45)
	$(\pi_1) = .1739\ (\pi_2)^{.3361}\ (\pi_3)^{.1192}\ (\pi_4)^{-.5376}\ (\pi_5)^{3.0071}(\pi_6)^{.1942}\ (\pi_7)^{-.2455}$	(G-46)
	$(\pi_1) = .1694\ (\pi_2)^{.3361}\ (\pi_3)^{.1192}\ (\pi_4)^{-.5376}\ (\pi_5)^{3.0071}(\pi_6)^{.1942}\ (\pi_7)^{-.2308}$	(G-47)
	$(\pi_1) = .1767\ (\pi_2)^{.3361}\ (\pi_3)^{.1192}\ (\pi_4)^{-.5376}\ (\pi_5)^{3.0071}(\pi_6)^{.1942}\ (\pi_7)^{-.2546}$	(G-48)

Table G-3.—List of Possible Prediction Equations (Concluded)

C.	$\frac{100Kn}{(\pi_1)} = .1667\ (\pi_2)^{.3361}\ (\pi_3)^{.1192}\ (\pi_4)^{-.4645}\ (\pi_5)^{3.0071}\ (\pi_6)^{.0992}\ (\pi_7)^{-.2443}$	(G-49)
	$(\pi_1) = .1688\ (\pi_2)^{.3361}\ (\pi_3)^{.1192}\ (\pi_4)^{-.4645}\ (\pi_5)^{3.0071}\ (\pi_6)^{.0992}\ (\pi_7)^{-.2515}$	(G-50)
	$(\pi_1) = .1674\ (\pi_2)^{.3361}\ (\pi_3)^{.1192}\ (\pi_4)^{-.4645}\ (\pi_5)^{3.0071}\ (\pi_6)^{.0992}\ (\pi_7)^{-.2469}$	(G-51)
	$(\pi_1) = .1601\ (\pi_2)^{.3361}\ (\pi_3)^{.1192}\ (\pi_4)^{-.4645}\ (\pi_5)^{3.0071}\ (\pi_6)^{.0992}\ (\pi_7)^{-.2214}$	(G-52)
E.	$(\pi_1) = .1336\ (\pi_2)^{.3361}\ (\pi_3)^{.1192}\ (\pi_4)^{-.4254}\ (\pi_5)^{3.0071}\ (\pi_6)^{.1110}\ (\pi_7)^{-.0640}$	(G-53)
	$(\pi_1) = .1320\ (\pi_2)^{.3361}\ (\pi_3)^{.1192}\ (\pi_4)^{-.4254}\ (\pi_5)^{3.0071}\ (\pi_6)^{.1110}\ (\pi_7)^{-.0572}$	(G-54)
	$(\pi_1) = .1284\ (\pi_2)^{.3361}\ (\pi_3)^{.1192}\ (\pi_4)^{-.4254}\ (\pi_5)^{3.0071}\ (\pi_6)^{.1110}\ (\pi_7)^{-.0418}$	(G-55)
	$(\pi_1) = .1268\ (\pi_2)^{.3361}\ (\pi_3)^{.1192}\ (\pi_4)^{-.4254}\ (\pi_5)^{3.0071}\ (\pi_6)^{.1110}\ (\pi_7)\ .0345$	(G-56)

Table G-4.—Averaging of Prediction Equations with Similar Solutions

π_7	USING EQUATION	(π_1)	$(\pi_1)_{Avg.}$	% Deviation from Avg.	Average Deviation
.456	G-9	1.4085	1.4254	1.2	0.60
	-10	1.4304		0.3	
	-11	1.4352		0.7	
	-12	1.4277		0.2	
	-13	1.5742	1.5755	0.1	0.25
	-14	1.5718		0.2	
	-15	1.5730		0.2	
	-16	1.5830		0.5	
	-17	1.4668	1.4716	0.3	0.25
	-18	1.4690		0.2	
	-19	1.4739		0.2	
	-20	1.4767		0.3	
1.026	-21	.9576	0.9407	1.8	0.87
	-22	.9356		0.5	
	-23	.9310		1.0	
	-24	.9386		0.2	
	-25	.1506	1.1494	0.1	0.32
	-26	1.1534		0.3	
	-27	1.1520		0.2	
	-28	1.1417		0.7	
	-29	1.0763	1.071	0.5	0.40
	-30	1.0740		0.3	
	-31	1.0680		0.3	
	-32	1.0657		0.5	

Table G-4.—Averaging of Prediction Equations with Similar Solutions (Concluded)

π_7	USING EQUATION	(π_1)	$(\pi_1)_{Avg.}$	% Deviation from Avg.	Average Deviation
2.308	G-33	.5507		1.8	
	-34	.5378	.5408	0.5	0.87
	-35	.5352		1.0	
	-36	.5395		0.2	
	-37	.4779		.10	
	-38	.4790	.4773	.40	0.35
	-39	.4783		.20	
	-40	.4741		.70	
	-41	.4333		.5	
	-42	.4323	.4311	.3	0.4
	-43	.4300		.3	
	-44	.4289		.5	
3.448	-45	.1329		2.8	
	-46	.1283	.1293	.8	1.4
	-47	.1273		1.6	
	-48	.1289		.3	
	-49	.1231		.2	
	-50	.1236		.5	
	-51	.1233	.1229	.3	.48
	-52	.1217		.9	
	-53	.1234		.8	
	-54	.1230		.5	
	-55	.1219	.1224	.4	.62
	-56	.1215		.8	

Table G-5.—Reduced List of Prediction Equations

SURFACE TYPE	V_{π_7}	AVERAGE OF FOUR PREDICTION EQUATIONS
A	25	$(\pi_1) = 1.1619\ (\pi_2)^{.7046}\ (\pi_3)^{.1200}\ (\pi_4)^{-.0714} (\pi_5)^{.3089}\ (\pi_6)^{.1117}\ (\pi_7)^{-.2609}$
C		$(\pi_1) = 1.3039\ (\pi_2)^{.7046}\ (\pi_3)^{.1200}\ (\pi_4)^{-.0742} (\pi_5)^{.3089}\ (\pi_6)^{.1665}\ (\pi_7)^{-.2410}$
E		$(\pi_1) = 1.4157\ (\pi_2)^{.7046}\ (\pi_3)^{.1200}\ (\pi_4)^{-.1518} (\pi_5)^{.3089}\ (\pi_6)^{.1855}\ (\pi_7)^{-.0494}$
A	50	$(\pi_1) = .9470\ (\pi_2)^{.7887}\ (\pi_3)^{.2501}\ (\pi_4)^{-.3347} (\pi_5)^{.6450}\ (\pi_6)^{.2002}\ (\pi_7)^{-.2609}$
C		$(\pi_1) = 1.1566\ (\pi_2)^{.7887}\ (\pi_3)^{.2501}\ (\pi_4)^{-.1864} (\pi_5)^{.6450}\ (\pi_6)^{.1602}\ (\pi_7)^{-.2410}$
E		$(\pi_1) = 1.0724\ (\pi_2)^{.7887}\ (\pi_3)^{.2501}\ (\pi_4)^{-.1773} (\pi_5)^{.6450}\ (\pi_6)^{.1482}\ (\pi_7)^{-.0494}$
A	75	$(\pi_1) = .6731\ (\pi_2)^{.7265}\ (\pi_3)^{.2234}\ (\pi_4)^{-.4113} (\pi_5)^{1.3555} (\pi_6)^{.2204}\ (\pi_7)^{-.2609}$
C		$(\pi_1) = .5840\ (\pi_2)^{.7265}\ (\pi_3)^{.2234}\ (\pi_4)^{-.3820} (\pi_5)^{1.3555} (\pi_6)^{.1257}\ (\pi_7)^{-.2410}$
E		$(\pi_1) = .4494\ (\pi_2)^{.7265}\ (\pi_3)^{.2234}\ (\pi_4)^{-.4004} (\pi_5)^{1.3555} (\pi_6)^{.1254}\ (\pi_7)^{-.0494}$
A	100	$(\pi_1) = .1789\ (\pi_2)^{.3361}\ (\pi_3)^{.1192}\ (\pi_4)^{-.5376} (\pi_5)^{3.0071} (\pi_6)^{.1942}\ (\pi_7)^{-.2609}$
C		$(\pi_1) = .1657\ (\pi_2)^{.3361}\ (\pi_3)^{.1192}\ (\pi_4)^{.4645} (\pi_5)^{3.0071} (\pi_6)^{.0992}\ (\pi_7)^{-.2410}$
E		$(\pi_1) = .1302\ (\pi_2)^{.3361}\ (\pi_3)^{.1192}\ (\pi_4)^{-.4254} (\pi_5)^{3.0071} (\pi_6)^{.1110}\ (\pi_7)^{-.0494}$

APPENDIX H
DESCRIPTION OF TIRE TEST FACILITIES

NASA LANGLEY TEST TRACK

FACILITY

The Langley landing loads track is shown schematically in Fig. H-1. The main test carriage of this facility is 60 feet long and runs on steel rails located 30 feet apart on each side of the 2,200 - foot runway. The carriage is accelerated to test speed by a hydraulic water-jet catapult system which expels a 7-inch diameter jet of water under the influence of air at pressures up to 3,200 pounds per square inch. Fig. H-2 shows the catapult system in operation. A bucket on the back of the carriage deflects the jet of water down and through approximately 180° to develop a thrust of approximately 350,000 pounds. The catapult accelerates the 100,000 pound carriage to a top speed of over 100 knots in about three seconds, in a distance of 300 to 400 feet.

After being catapulted to the desired speed, the test carriage coasts for about 1,200 feet during which time the drop frame and test fixture are released and braking cycles are initiated on five test surfaces. At the end of the test run, the carriage engages five arresting gear cables, which are attached to a system of 20 hydraulic arresting engines. These bring the carriage to a stop in the remaining 600 feet of track between the cable engegement point and the storage shed at the end of the track.

APPARATUS

Test Fixture

The test tire is mounted in the special test fixture shown schematically in Fig. H-3. This fixture contains the tire, wheel, and brake assembly mounted on a special axle. The axle is mounted in a five component system of strain gage dynamometer beams. Drag, vertical and side loads are each measured individually at the axle. Vertical load is obtained by measuring load from the two vertical load beams, and the sum of the two drag-beam measurements gives the drag load. The side load beam needs to be monitored only if runs are made at some yaw angle. Axle loads are corrected for inertia forces by vertical and drag accelerometer readings to give instantaneous tire-ground reaction values throughout the entire brake cycle. Brake torque can be measured by a system of strain gage links mounted about the axle.

Because of the limited space available in the test fixture, part of the instrumentation is mounted on an auxiliary axle, driven at axle speed by a toothed timing belt. Values of wheel angular velocity, acceleration, and displacement are measured here. Wheel vertical displacement and brake pressure are also recorded during each test run. These data are recorded by an 18-channel oscillograph recorder located on the carriage.

TEST RUNWAY

In order to determine the braking effectiveness of a given tire over a wide spectrum of runway surfaces ranging from very smooth to very rough, a special test runway has been constructed on

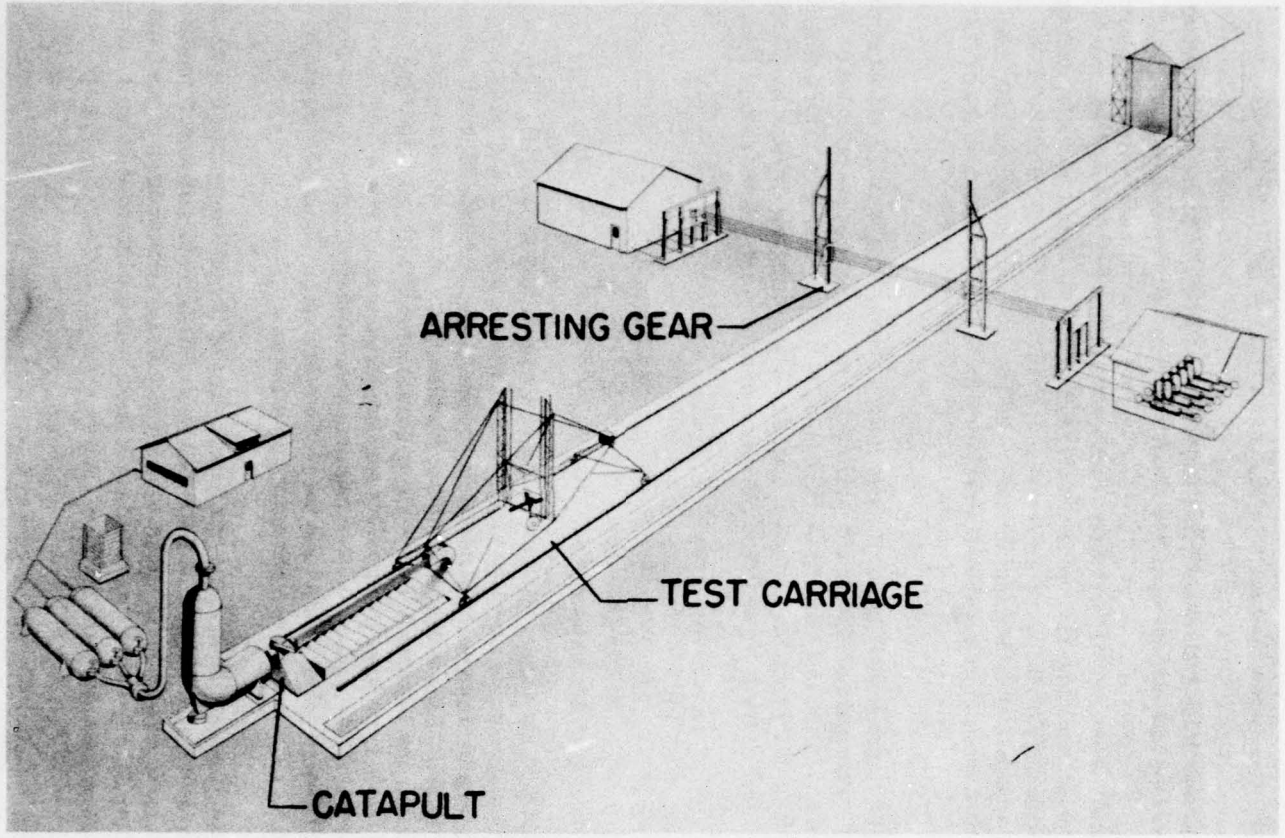

Figure H-1.—Schematic of Landing Loads Track.

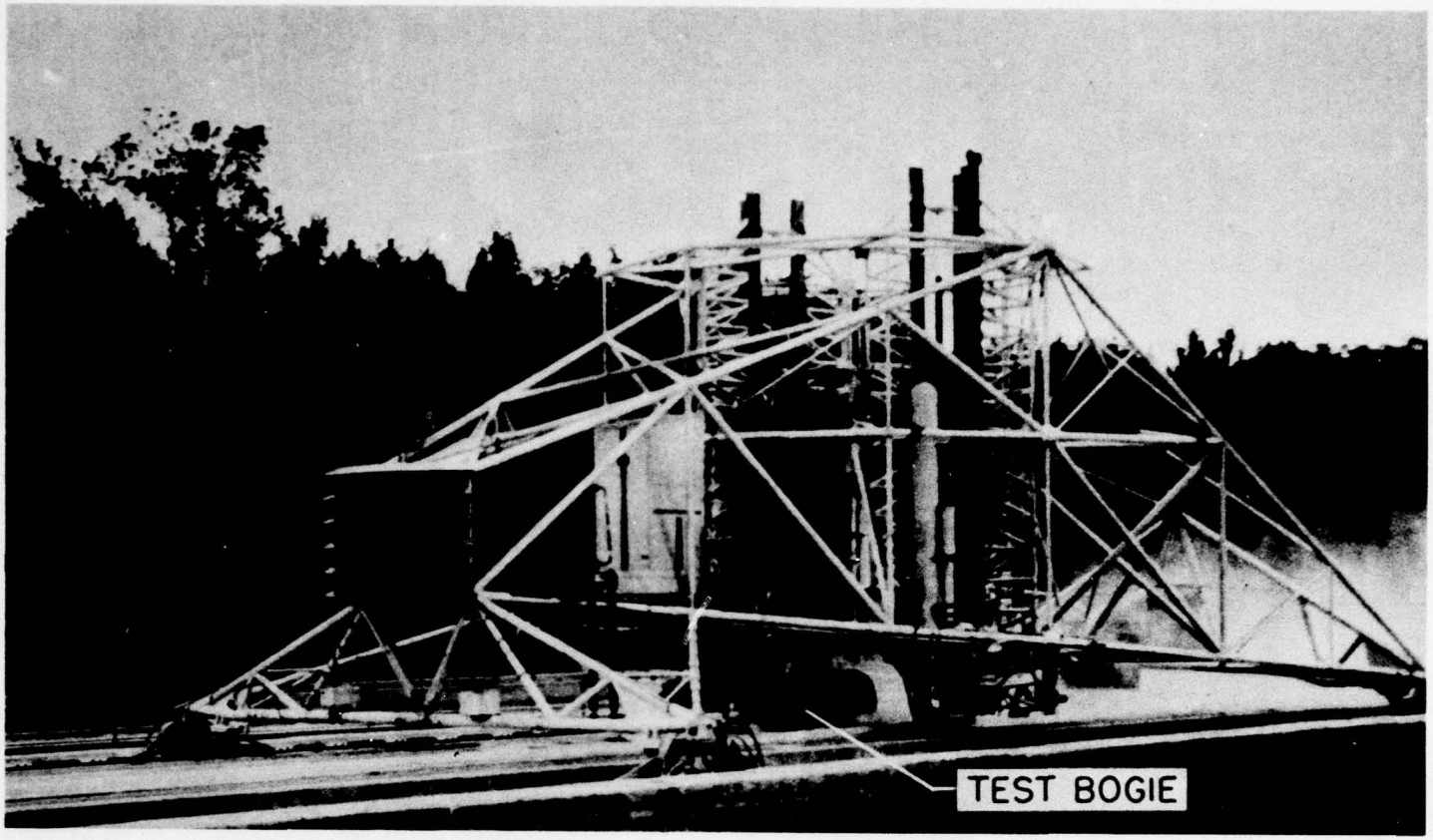

Figure H-2.—Test Carriage of Landing Loads Track.

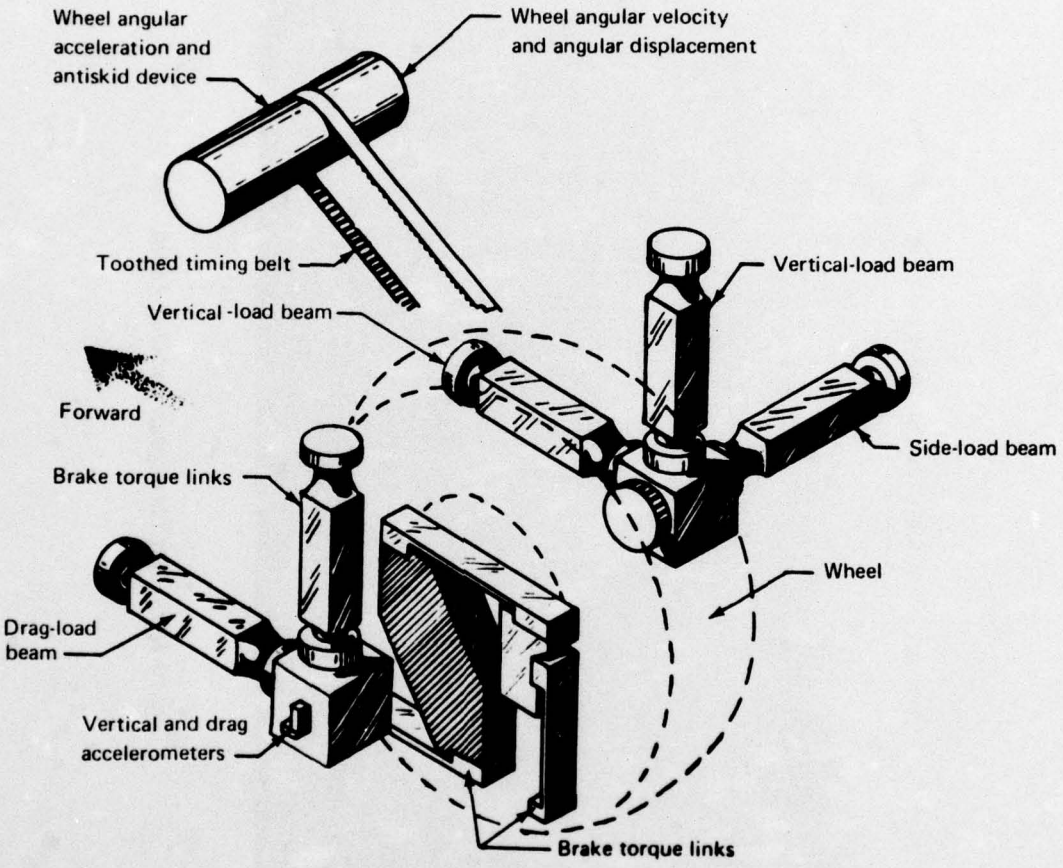

Figure H-3.—Schematic of Single Wheel Test Fixture

top of the existing concrete surface. The test runway, which is shown schematically in Fig. H-4, is divided into five braking surfaces: smooth concrete, textured concrete, small aggregate asphalt, large aggregate asphalt, and ice. Wheel drop and spin-up occurs on the 100-foot ramp, and the tire is braked from a free roll to a locked wheel, and then allowed to return to the free roll condition on each of the five test surfaces as the carriage proceeds down the track. Pre-loaded side wheels on the carriage prevent any lateral movement of the test fixture so the test tire follows the same path down the center of the runway.

The next two braking surfaces are asphalt; the first of which is termed small aggregate asphalt. This surface has an aggregate or stone size within accepted practices for runways today. The second asphalt surface is termed large aggregate asphalt and has an aggregate or stone size outside accepted runway practices. Stone size does not exceed 1/2 inch in any dimension.

It is difficult to give a meaningful word description of runway surfaces, and photographs show little of the actual runway surface texture.

The fifth braking surface is 200 feet of ice runway. This surface is maintained by a refrigeration system located at the side of the track, which pumps brine into pipes located two inches below the ice surface. The brine inlet temperature varies from 12 to 16 degrees Fahrenheit with a two-degree drop through the ice section. The ice surface temperature, which measured before and after each test run with a thermocouple probe, varies from 31 to 34 degrees. Doors covering the entire 200 feet of ice surface are opened just before each test run to minimize the amount of surface change. About every two weeks, the ice surface is allowed to melt completely and then refrozen to maintain a smooth, clean surface.

BRAKING SYSTEM

Braking cycles are initiated on each of the five surfaces by cams placed at desired locations along the test track. A timer controls the length of time the brake pressure is applied, with a backup timer in the circuit to limit skid lengths in case the primary system fails. The brake timer setting is changed for each test speed to obtain approximately constant locked-wheel skid lengths e.g. 5 to 10 feet.

NAVAL AIR TEST FACILITY, LAKEHURST, N. J.

FACILITY

The FAA's National Aviation Facilities Experimental Center (NAFEC) Atlantic City, N. J., was assigned a program requiring creation of a full scale dynamic test facility capable of testing modern jet transport aircraft tires on various runway surfaces. A study revealed that the test tracks at the Naval Air Test Facility at Lakehurst Naval Air Station, only 60 miles from NAFEC, had the ideal capabilities for such a program. An Inter-Agency Agreement was prepared between the FAA and Lakehurst Naval Air Station providing almost exclusive use of their track No. 1 for this program.

The program required speeds up to 150 knots and tire loads up to 40,000 pounds. A 4,000-pound-test dynamometer was designed, built, and installed.

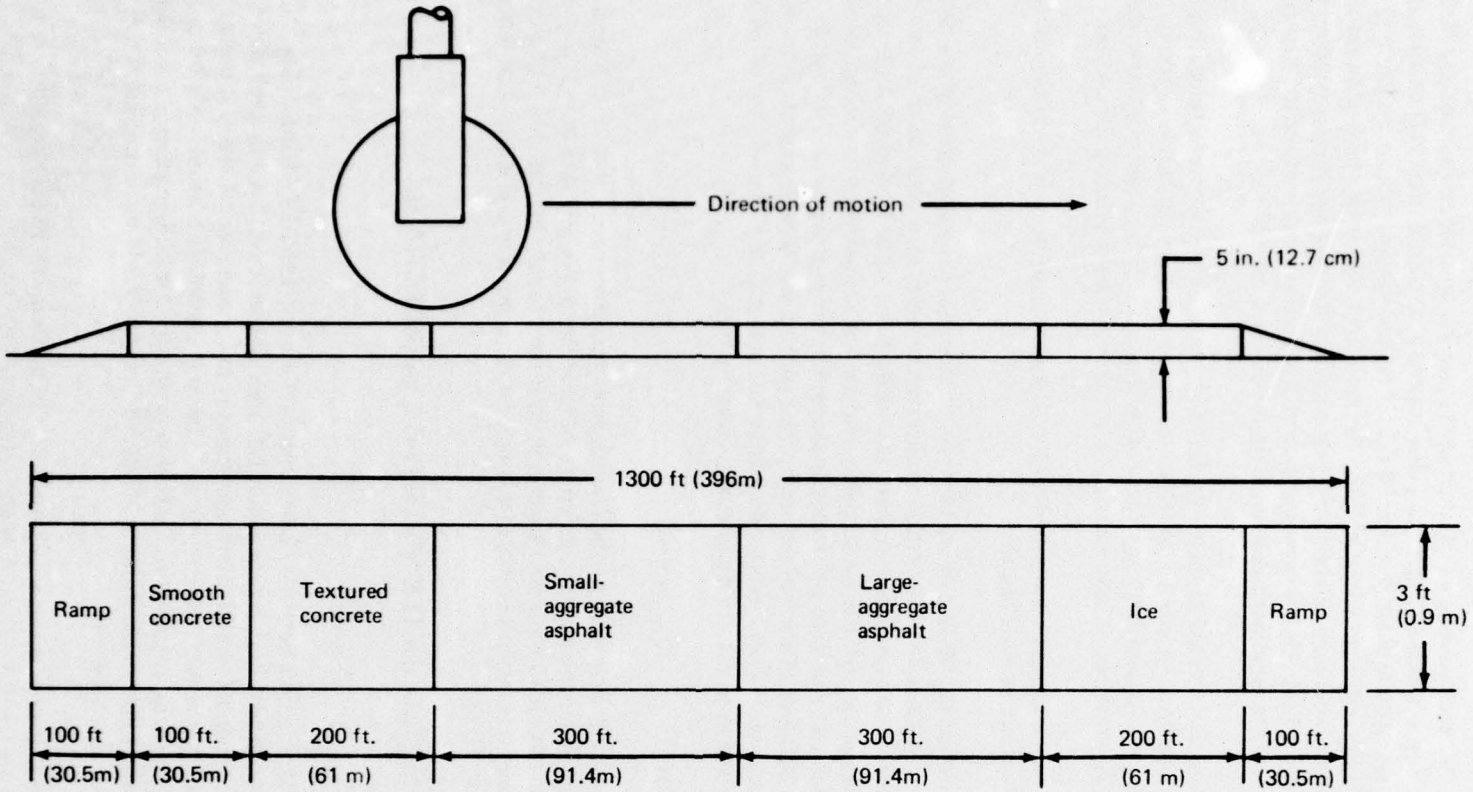

Figure H-4.—Schematic of Test Section

The test dyamometer is essentially a fixture containing a 3-axis-load cell and brake system. Two strain links measure the drag loads, two strain links measure vertical loads, and one strain link measures side loads. Brake torque is measured by a system of parallel strain links. Test wheel speeds (spin-up and spin down) as well as test vehicle (dead load) speeds are measured by means of magnetic pick-ups. An 18-channel telemetric system is mounted on the dead load to transmit the following data:

Drag load
Vertical load
Brake torque
Brake pressure
Dead load acceleration
Dynamometer vertical acceleration
Test wheel speed
Dead load speed
Load cylinder pressure
Sink rate speed and inclination of test dynamometer

The test dynamometer has been designed to simulate aircraft sink rates. The present system utilizes 1-1/2 inch hydraulic cylinders to produce sink rates up to 5 feet per second. The tire loading system utilizes 4-inch cylinders capable of producing test loads of 40,000 pounds at 1,800 psi hydraulic pressure as well as corresponding lighter test loads.

The test track No. 1 at Lakehurst Naval Air Station is over 1 mile long (See Figure H-5.) A four engine jet car is used to accelerate the dead load containing the test dynamometer to the programmed test speed within ± 1/2 knot of that specified. This jet car weighs 22,000 pounds and is powered by four J-48 jet engines which produce a total thrust of approximately 26,000 pounds. Three hundred feet from the end of the track the jet car is braked to a stop and the 60,000 pound dead load continues over the runway test section. This runway test section is 200 feet long and consists of an excavation wherein 20, 10-foot x 30-inch runway test slabs are installed. These test slabs are diked for wet runway and hydroplaning tests. Knife switches are placed along the track to activate the various test operations such as cameras, touch down, load and brake application, etc. It is estimated that as many as 10 to 15 tests can be made a day for data gathering purposes. At the terminal end of the test track, at Station No. 5860, the primary arresting gear is installed to halt the free rolling dead load. This is a MARK-21 arresting gear utilized for SATS (Marine Corps-Short Airfield for Tactical Support) installations. This arresting gear has a capacity of absorbing 60 million foot-pounds of kinetic energy and will have a run-out of 640 feet. At Station No. 6130 a MARK 5 MOREST backup arresting gear is installed. This gear has a 25 to 26 million foot-pound capacity and a 200-foot run-out. The primary arresting gear picks up the tail hook of the dead load while the back-up gear engages the front of the dead load. Along side the test track, a 200-foot long test slab manufacturing bed was created to facilitate test slab fabrication, surfacing, grooving and friction testing. The test slabs are stored in the adjacent field ready for test installation.

The gathered test data is telemetered to the Data Gathering Center adjacent to the test track where it is recorded on tape. A quick read-out arrangement is provided so that the important parameters can be studied for completeness and to provide information for the next "shot". The data is then taken to the Data Processing Center at Lakehurst where it is processed by the computer into the desired format.

DATA ACQUISITION

The primary instrumentation feature at NATF is the series of data acquisition sites located adjacent to each major test site. At each of these sites is the capability of recording by ground wire and telemetry over 60 different parameters, onto magnetic tape, for quick-look readout and for subsequent data analysis. At some sites, this capability exceeds 100 channels, and data is converted immediately into digital format for real-time monitoring of test events. The telemetry utilizes 16-channel RF systems that relay data from switch positions, strain gages, and attitude sensors installed on deadloads and barricade test frames as the need dictates.

The NATF has the capability to maintain and calibrate all the electronic test equipment used, and to maintain its accuracy to within 1 tenth of 1 percent, thus insuring correct information from the test data systems.

Pressure, vacuum, acceleration, tension, and compression transducers are also calibrated in-house. Hydraulic pressures of a fraction of a pound per square inch up to 100,000 pounds per square inch are available to calibrate pressure gauges and electronic transducers. All in all, more than 1,000 pieces of test equipment are calibrated and maintained in the electronics and physical standards section.

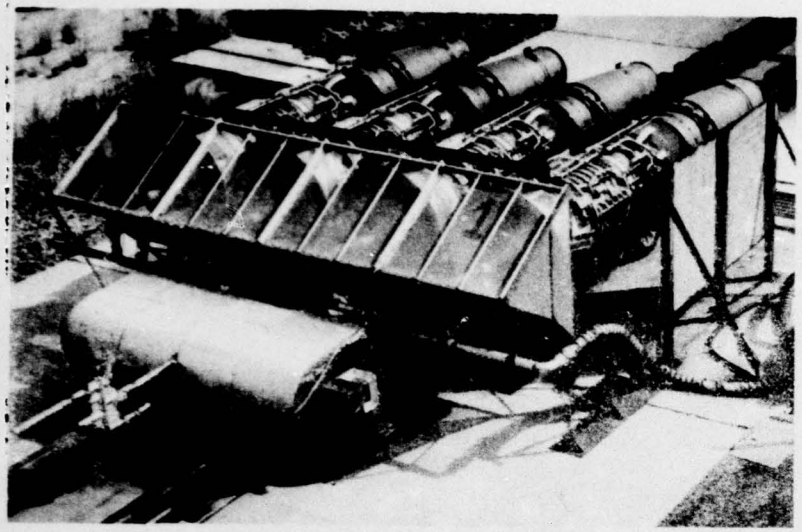

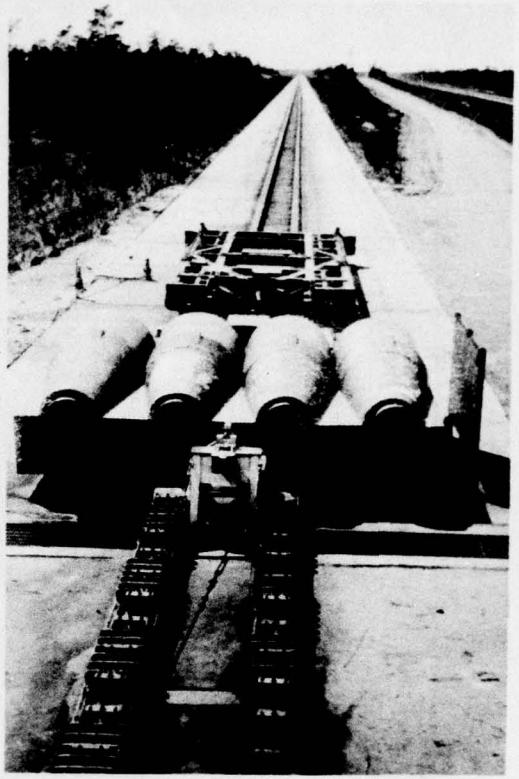

Jet-Car Characteristics

Engine(four)	J79-13	J48-P-8
Number of wheels	4	4
Tire size (inches)	30 x 7.7	30 x 7.7
Thrust (pounds)	38,000	24,000
Fueled weight (pounds)	22,000	18,000
Length	21 Ft 4 In.	21 Ft. 4 In.
Width	17 Ft. 7 in.	17 Ft. 7 In.
Maximum speed (knots)	300	260
Maximum design deceleration (G)	4	8

Figure H-5.—NATF, Lakehurst Track 1.

Table H-1.—Test-Track Characteristics (NATF)

Cleared Area Length (Feet)	7,500
Reinforced Concrete Strip	
Length (Feet)	6,200
Track Width (Feet)	28
Slab Thickness (Inches)	12
Design Strength of Wheel Load (Pounds)	54,000
Guide Rails	
Length (Feet)	5,851
Cross Section (Inches WF 49)	10
Spacing, Centerlines (Inches)	52-1/2
Brake Rails (Movable) Length (Feet)	795
Runout Area	
Length (Feet)	900
Width (Feet)	100
Surface	

APPENDIX I
DESCRIPTION OF GROUND VEHICLES

1. U. S. DBV

The diagonally braked vehicle (DBV) is an automotive type vehicle equipped with a high-performance engine for fast acceleration, power steering, power brakes, and a fifth wheel to provide speed and stopping distance information. The braking system is modified to permit one pair of diagonally opposite wheels to be braked while the other diagonal pair remain unbraked, Figure I-1. The braking system has an electrically-operated solenoid shut-off valve installed in the brake system of each wheel. The proper valves are actuated by the test personnel to change from the normal four-wheel braking mode for highway use to the diagonal braking mode for conducting tests. This diagonal braking technique enables the DBV to perform locked-wheel skids at high speed on slippery surfaces and maintain directional control while being braked to a complete stop. The braked wheels of the test vehicle are equipped with ASTM tires, Specification E-249, size 7.50 x 14, smooth tread configuration, inflated to 24 psi pressure. The unbraked wheels are equipped with production tires having good tread design to insure directional control, and are inflated to 32 psi. The vehicle weighs approximately 5,200 pounds in the test configuration with a driver and 1/2 fuel load. The use of bald or smooth tread tires on the braking wheels of the DBV eliminates effects caused by tread wear and tread design. Power steering and power brakes assist in maintaining better directional control and in providing necessary brake pressure to lock the two diagonal test wheels.

Stopping distance of the test vehicle is measured by electronic digital readout meters which are actuated by the brake application switch. The meters record the stopping distance in feet from brake application to vehicle stop. Digital displays of fifth wheel speed in one mile per hour increments provide the DBV operator with an accurate indication of vehicle speed. An electronic hold circuit in the speed meter system locks the speed on the meter upon brake application. The speed is recorded after the vehicle comes to a complete stop. The speed and distance meters are located on the instrument panel. Figure I-2 shows the fifth wheel attached to the test vehicle.

During a test run, the vehicle is accelerated to a speed of 60 mph whereupon the driver shifts the transmission to the neutral position. The diagonal braked wheels are locked at the desired test section where the vehicle is braked to a stop. In evaluating pavement surface friction, DBV tests are conducted for both dry and wet surface conditions and a wet/dry stopping distance ratio is computed which reflects the pavement's slipperiness for the wet surface condition tested.

The pavement wetting is achieved by using a water truck with spray bar to ensure a water depth of 0.01 inch or greater as measured by the NASA water depth gauge, Figure I-3, or equivalent.

Figure I-4 provides the method for use in determining the average wet/dry stopping distance ratio for the complete runway, or any portion thereof.

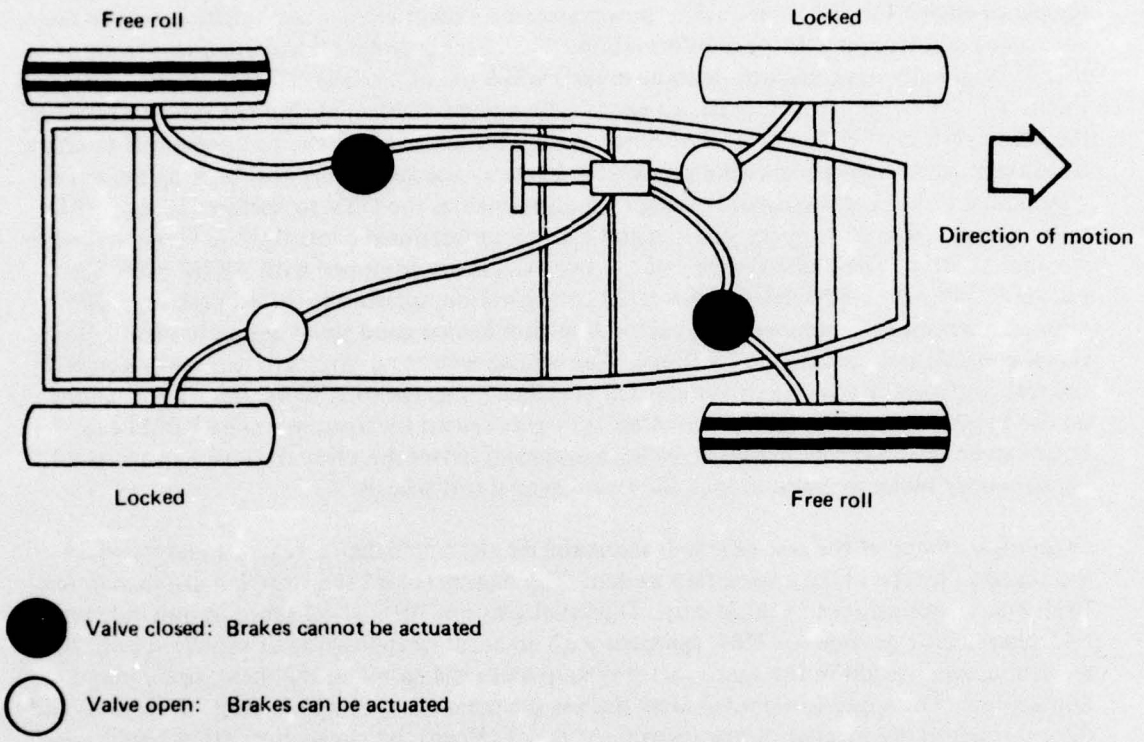

Figure I-1.—Diagram of Diagonal Braking System

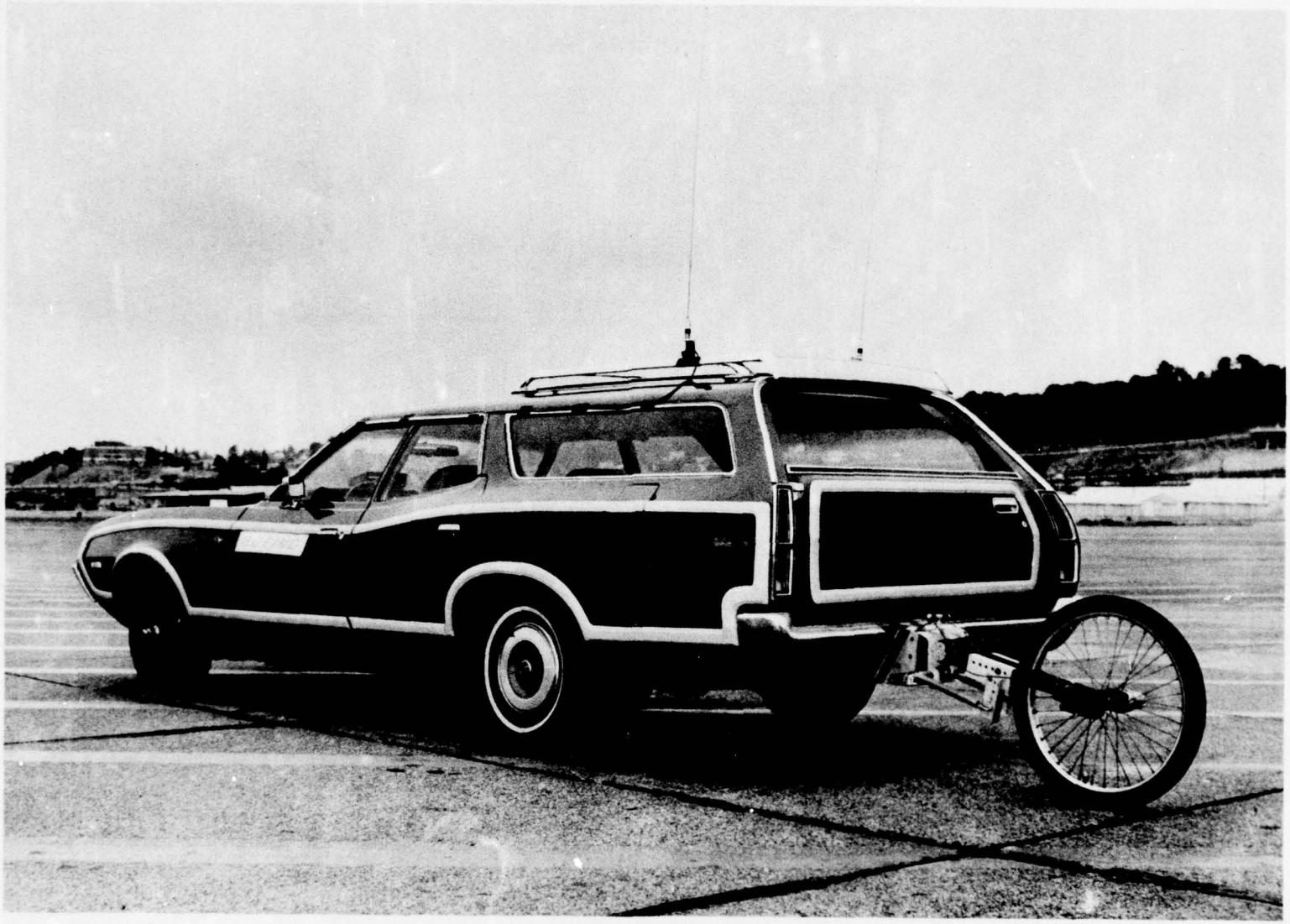

Figure I-2.—Fifth Wheel Attachment for DBV

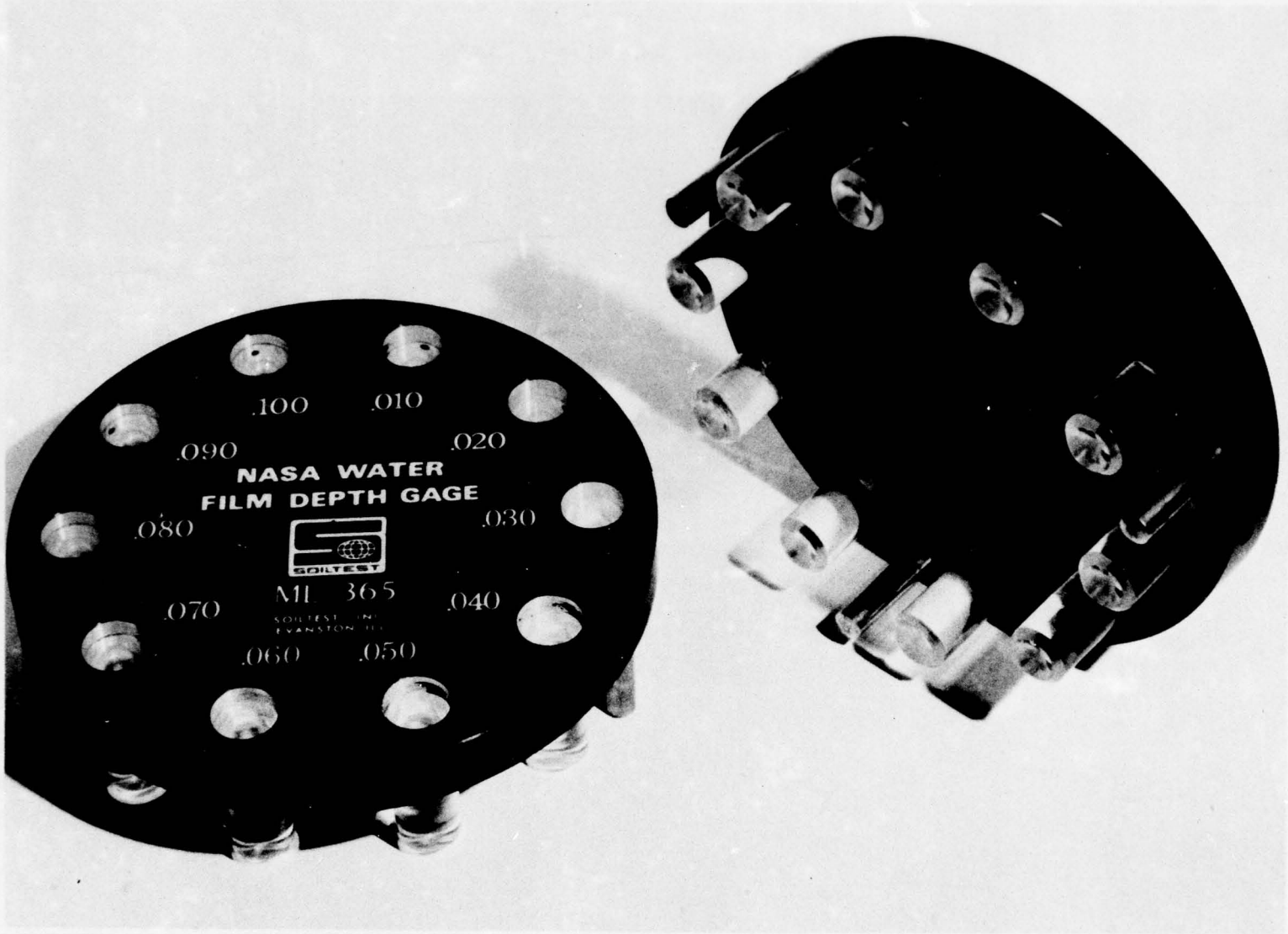

Figure I-3.—NASA Water Depth Gage

NASA DIAGONAL-BRAKED CAR RUNWAY SLIPPERINESS MEASUREMENTS	
Runway Location	Stopping Distance Ratio Wet/Dry
Touchdown Zone A, Rubber contaminated	$\bar{X}_A$
Braking Zone B, Clean	$\bar{X}_B$
Roll-out Zone C, Rubber contaminated	$\bar{X}_C$

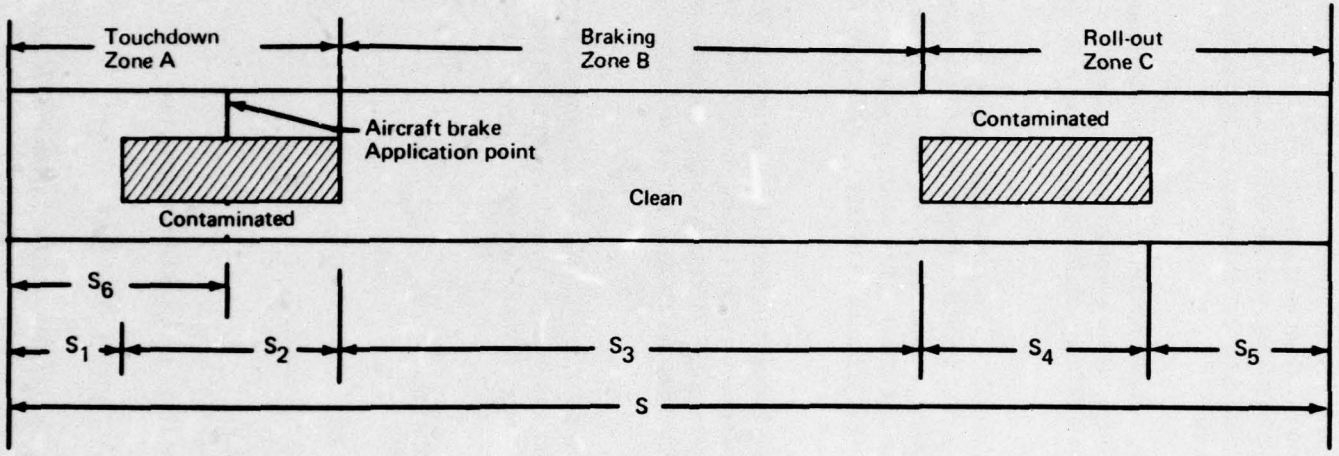

Average wet/dry stopping distance ratio
During landing roll = X

$$X = \frac{(S_1 + S_2 - S_6)\,\bar{X}_A + (S_3 + S_5)\,\bar{X}_B + S_4\,\bar{X}_C}{S - S_6}$$

Figure I-4.—Method for Calculating the Average Diagonal-Braked Car Wet/Dry Stopping Distance Ratio, X, for a Given Landing Condition

2. U. S. – ASTM SKID TESTER (STANDARD-METHOD)

Implementation of the Highway Safety Act of 1966 has resulted in considerable activity in all of the states to institute highway skid resistance inventory and control programs. Various full-scale and portable skid testers have been employed, operating in a variety of skidding or slipping modes. The test method used primarily in this country is the American Society for Testing and Materials (ASTM) test for Skid Resistance of Paved Surfaces Using a Full-scale Tire (E 274-70), which describes the apparatus and procedures for measuring skid resistance in locked wheel mode.

The method utilizes a measurement representing the steady state friction force on a locked test wheel as it is dragged over a wetted pavement surface under constant load and at a constant speed while its major plane is parallel to its direction of motion and perpendicular to the pavement.

The test apparatus consists of an automotive vehicle with one or more test wheels incorporated into it or forming part of a suitable trailer towed by a vehicle. The apparatus contains a transducer, instrumentation, a water supply and proper dispensing system, and actuation controls for the brake of the test wheel. The test wheel is to be equipped with the pavement test standard tire (7.50 x 14) as specified in ASTM Specification E 249, for Standard Tire for Pavement Tests.

The test apparatus is brought to the desired test speed. Water is delivered ahead of the test tire and the braking system is actuated to lock the test tire. The resulting friction force acting between the test tire and the pavement surface (or some other quantity that is directly related to this force) and the speed of the test vehicle are recorded with the aid of suitable instrumentation.

The skid resistance of the paved surface is determined from the resulting force or torque record and reported as skid number, SN, whic is determined from the force required to slide the locked test tire at a stated speed, divided by the effective wheel load and multiplied by 100.

ASTM Suggested Marking on Tire

7.50 - 14
4 Ply
Pavement Test Standard
1085 Lb. Load
24 psi Inflation
ASTM Designation: E249
Skid Test Tire - Not for General Highway Use
Rim - 14 x 5J
Manufacturer's Name or Trademark

Figure I-5 shows typical chart recordings from ASTM type trailers.

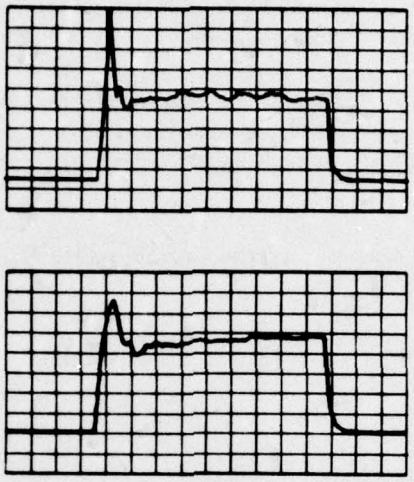

(K) Chart recording showing double wheal "lock-up"

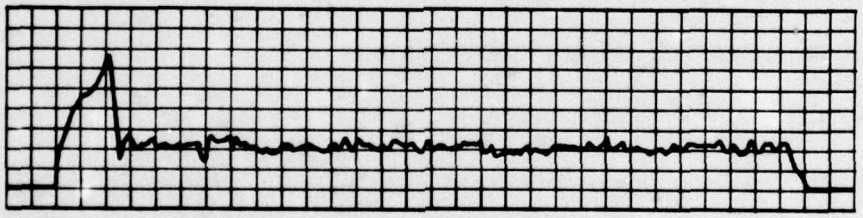

Typical chart recording of test data, single wheel "lock-up."

Figure I-5.—Typical Output ~ ASTM Type Trailer

3. FRENCH – STRADOGRAPHE (SEE FIGURE I-6)

All the measuring devices are located in one vehicle (Citroen station wagon). They consist of two wheels on either side of the longitudinal axis of the vehicle. These wheels can be braked or towed in at an angle varying from 0 to 15° in relation to the vehicle's direction of movement or may even be completely locked.

The problems of suspension and loading of the measuring wheels are resolved by a regulated oleopneumatic suspension system reacting against the chassis of the vehicle to which the wheels are fixed. The vertical load applied to each measuring wheel can be set at 220-880 lbs (100-400 kg.).

The Stradographe is equipped with an electronic chain, which records nine parameters simultaneously:

1 – Right transverse effort
2 – Left transverse effort
3 – Right longitudinal effort
4 – Left longitudinal effort
5 – Speed of rotation of right wheel
6 – Speed of rotation of left wheel
7 – Speed of vehicle
8 – Right vertical load
9 – Left vertical load

The equipment includes a sprinkler.

All the operations can be programmed in advance and are conducted automatically from a control panel in front of the operator.

LONGITUDINAL FRICTION COEFFICIENT (LFC)

Ratio of reaction effort F_L to the actual load.

This coefficient can be determined with the wheels completely locked or with a given skid rate (0 to 15%).

COEFFICIENT OF TRANSVERSE FRICTION (TFC)

When the vehicle has reached a constant given speed, the wheels are inclined at a certain angle in relation to the longitudinal axis of the Stradographe when the recording is activated.

The TFC is the ratio between the normal effort F_T at the measuring wheel and the weight P of the wheel.

COEFFICIENT OF OBLIQUE FRICTION

The wheels are inclined as above and braked.

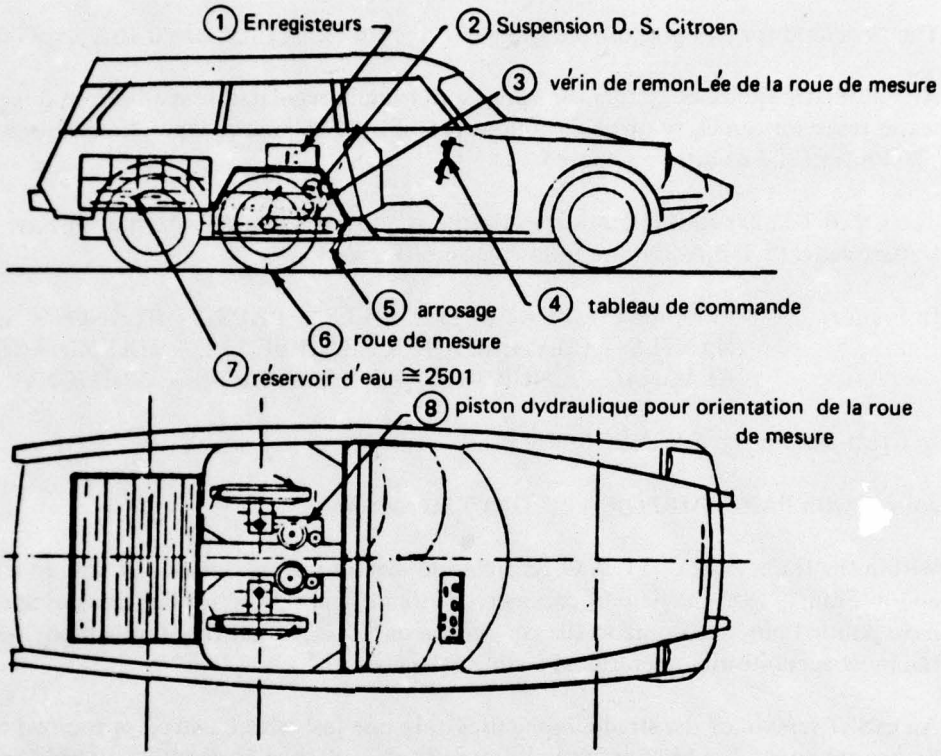

(1) Automatic data recording apparatus
(2) Citroen car suspension
(3) Screw jack for upward motion of the measuring wheel
(4) Command console (control panel)
(5) Sprinkler
(6) Measuring wheel
(7) Water reservoir (250 litres)
(8) Hydraulic piston for aligning the measuring wheel

Figure I-6.—Stradographe

The coefficient of oblique friction is the ratio between the pull of the wheel and the load on the wheel.

TIRES

The tires used for this purpose are generally smooth radial tires, size 6.10 x 15.75 (155 x 400).

An automatic sprinkler system can spray water under regulated pressure from 0 to 30 psi. A water reservior can carry up to 65 gallons (250 litres) on board. Operational speeds of up to 170 km/hr (92 kn) can be achieved.

The C.E.B.T.P. has carried out tests with the stradograph jointly with the Air-Base Technical Departments (S.T.B.A.) on the following aerodromes:

In France : ROISSY - BEAUVAIS - LILLE - BREST - RENNES - LANDIVISIAU - NANTES - CHATEAUROUX - MARSEILLE - MARIGNANE - TOULOUSE - BLAGNAC - COURCHEVEL - LYON-BRON - BRETIGNY.

In Great-Britain : FARNBOROUGH.

Jointly with PARIS AIRPORT : ORLY Aerodrome.

Within the framework of I.C.A.O., correlation measurements carried out both in Great-Britain and in France, with the help of commercial aircraft and skid resistance measuring equipments have pointed out, according to the conclusion of S.T.B.A. that the stradographe was one of the most accurate and operational testing vehicles.

An earlier version of the stradographe uses only one test wheel instead of the two and disc brakes are used. The braking force is transmitted back by a horizontal ball bearing slide bar. The vehicle maximum operational speed is somewhat lower.

4. FRENCH LPC–TRAILER

DESCRIPTION

The equipment consists of a single wheel trailer and a traction vehicle.

The trailer has the following components:

- an automobile wheel equipped with a tire 6.5 x 15 (165 x 380) linked to a traction vehicle by an articulated frame on a universal joint and placed under load by two oleopneumatic devices bearing an upper weighted frame.
- a servo-brake enabling the wheel to be immobilized by the action of two brake shoes and controlling a brake for the universal joint, designed to ensure that the trailer does not yaw.
- a draw bar with a potentiometric dynamometer (0 - 750 daN) measuring the torque transmitted by the countershaft fixed to the axle.

- a magnetic sensor group to indicate the wheel rotation speed.

An autonomous sprinkler is situated at the rear of the traction vehicle, and the control panel and the recorder is in front.

MEASUREMENTS

The LPC-trailer enables the longitudinal friction coefficient (LFC) of pavements to be measured, with the wheels locked at speeds between 22 and 75 kn (40 and 140 km/h).

At each test, the measuring chain enables three parameters to be recorded:

- the dynamometric signal giving the LFC,
- the impulses of the magnetic sensor showing the wheel speed and thus enabling the locking of the wheel to be checked;
- the wheel locking impulses.

All the measuring operations can be performed automatically.

TIRES

In most cases smooth tires are used.

5. BRITISH – MILES TRAILER

CONFIGURATION

The Miles Trailer was developed by the Ministry of Transport, Road Research Laboratory, of Great Britain to measure the coefficient of friction of a wetted hard surface for use in complying with Civil Aviation Authority (CAA) (formerly British Air Registration Board) regulations. The trailer was commercially manufactured by F. G. Miles Engineering, Ltd., England. The test equipment (Fig. I-7) consists of a small, light, single-wheel trailer, towed at the required speeds by a high performance sedan automobile. The single wheel of the trailer (Fig. I-8) is mounted on a pendulum pivot and is restrained from aft relative motion by an instrumented load cell. The output of the load cell is proportional to the tire-ground horizontal forces (drag load). The braking force coefficient (μ_B) is obtained by dividing the drag load by the normal load on the tire (313 pounds under static conditions). The wheel of the trailer is instrumented to provide velocity information. The test tire, size 16 x 4, is manufactured by Firestone of England and conformed to the specifications outlined by the Road Research Laboratory. Fig. I-9 shows construction details.

INSTRUMENTATION

The trailer instrumentation consists of signal conditioning equipment to convert the load cell output to a braking coefficient value and a frequency converter to convert trailer wheel revolution pulses to ground speed. Fig. I-10 shows a portion of the signal conditioning

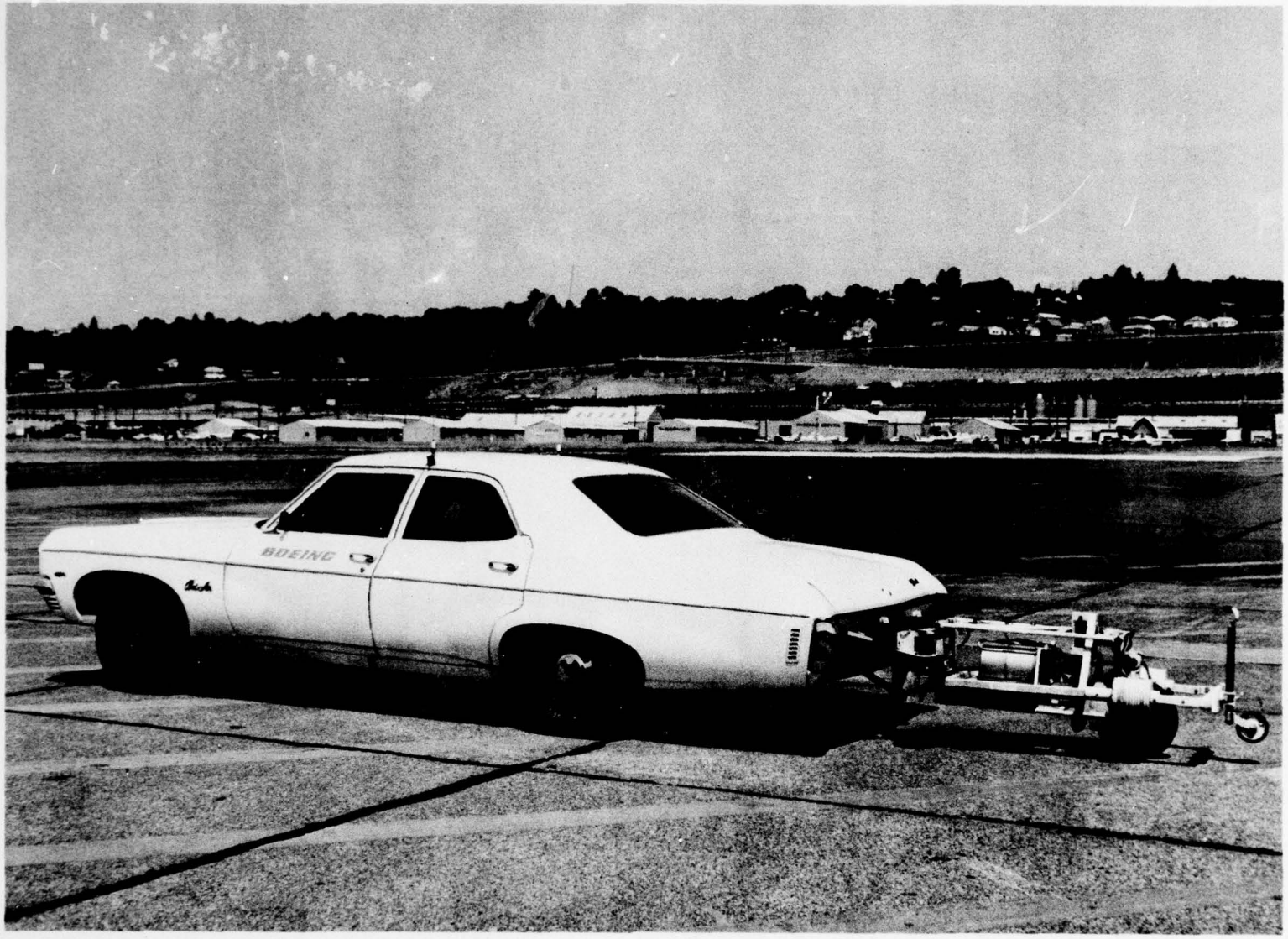

Figure I-7.—Miles Trailer and Tow Vehicle

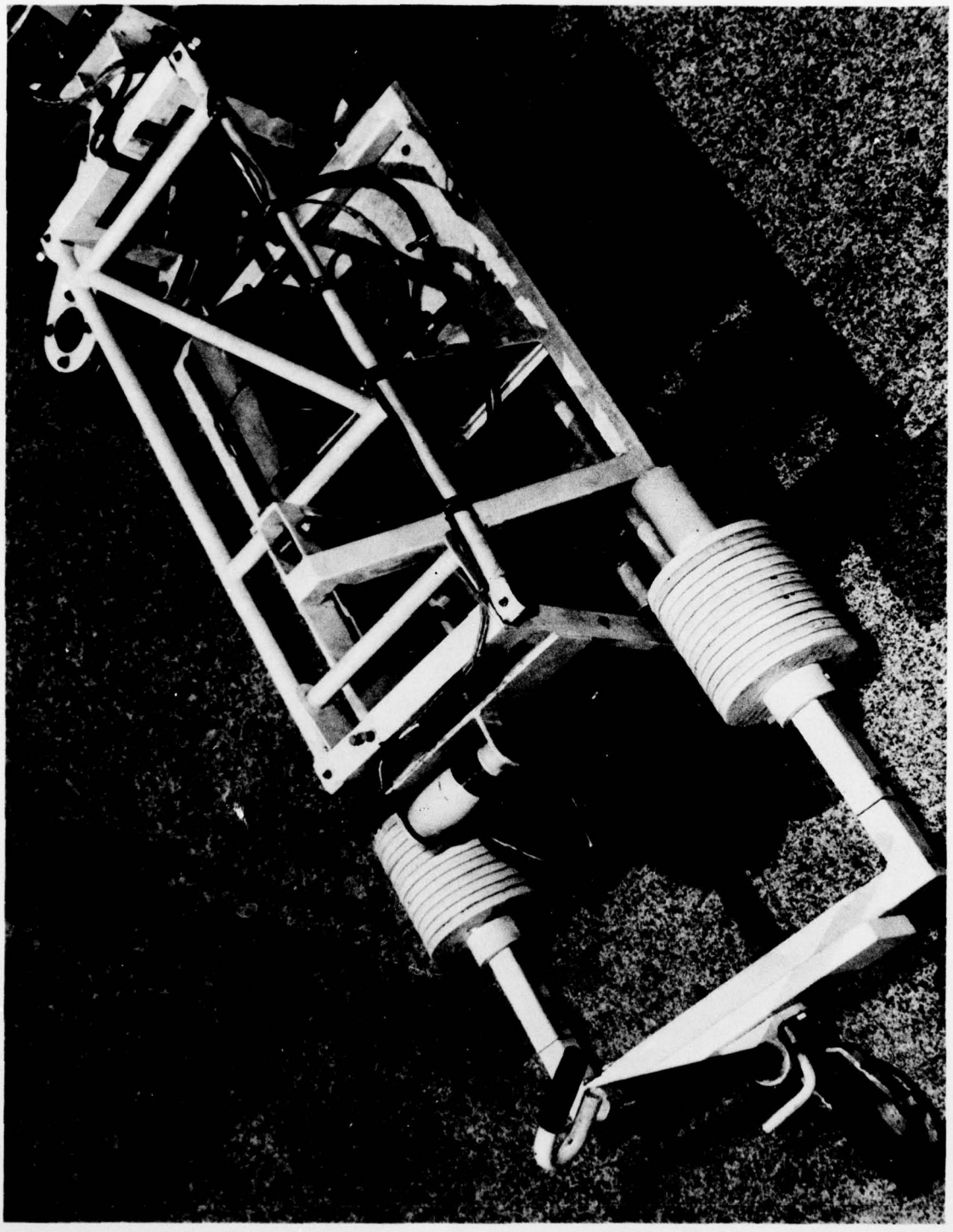

Figure I-8.—Miles Trailer

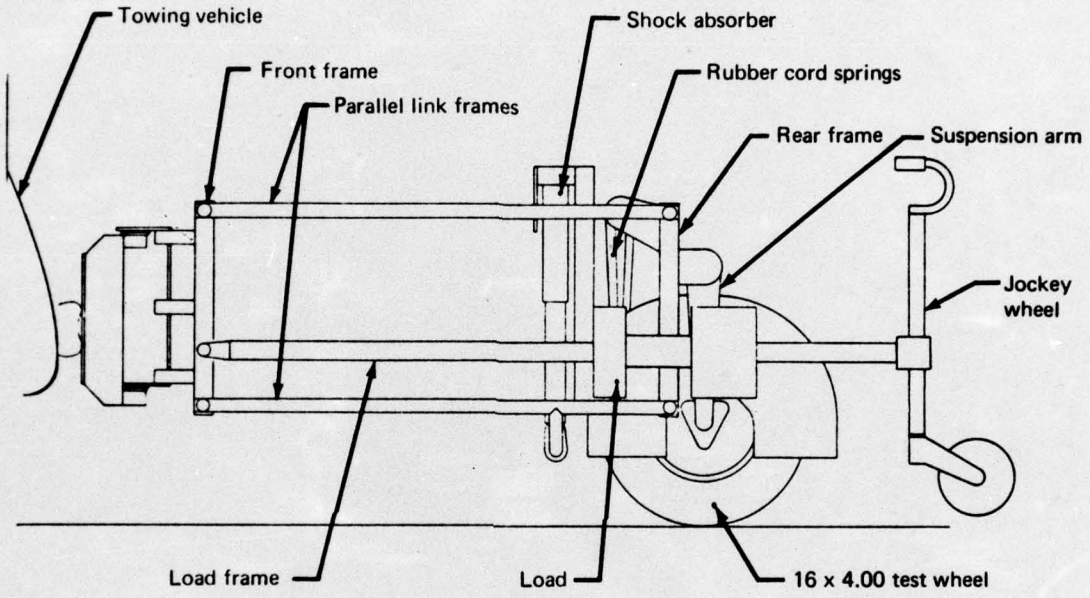

Figure I-9.—Miles Trailer Constructional Details

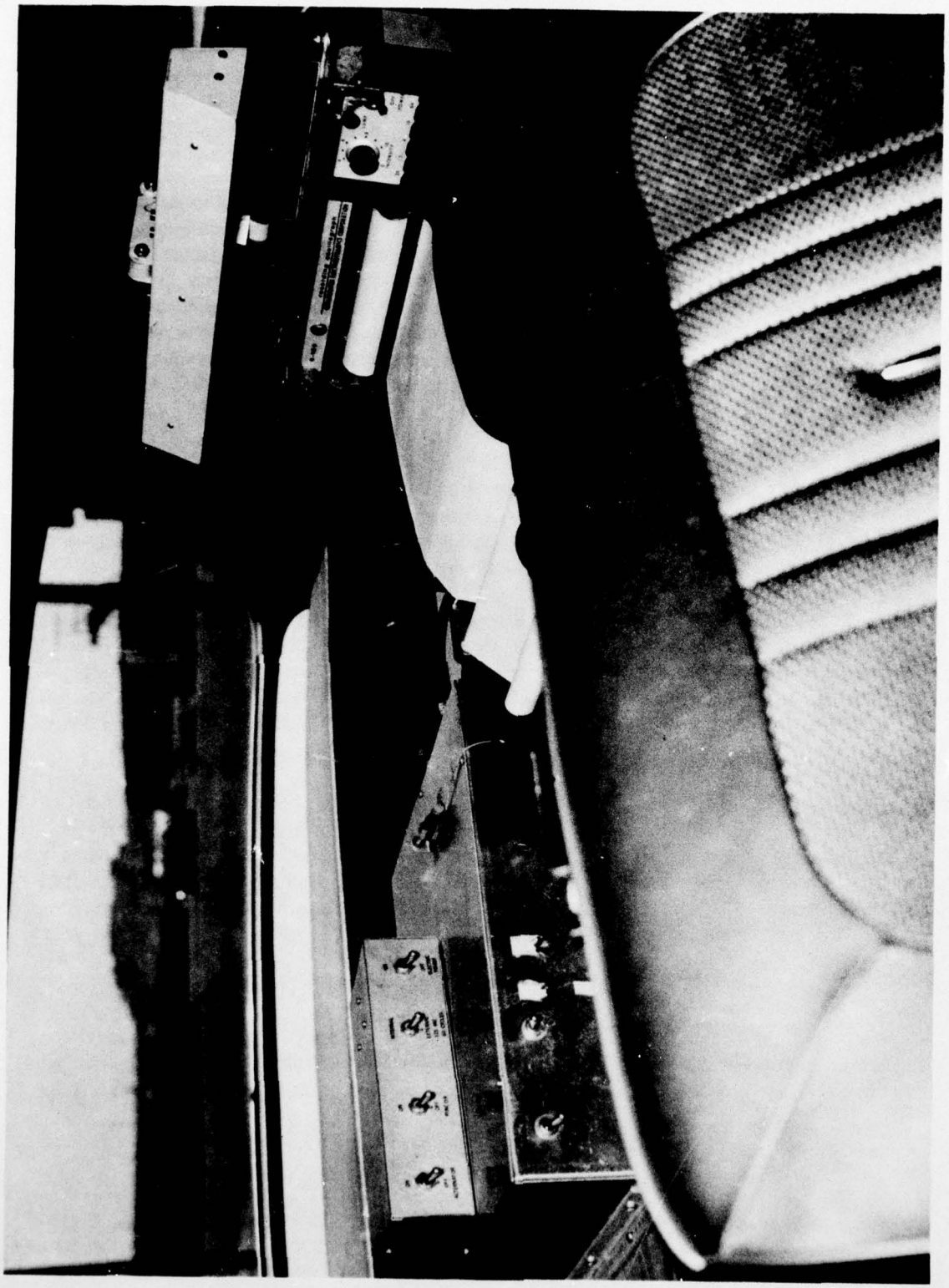

Figure I-10.—Tow Vehicle Instrumentation

equipment and the Consolidated Electrodynamics Corporation recording oscillograph used to obtain a permanent record of each test condition. A typical condition record is presented in Figure I-11.

6. BRITISH – MU-METER

The British Ministry of Technology has developed the friction meter shown in figure I-12 and I-13, generally called the Mu-Meter. It consists of three wheels, two of which are mounted at the ends of independently moveable arms, pivoted at the towing point and adjusted to a tow-out angle of 7½°. When towed, the resulting side loads imposed on the arms are sensed by a pressure capsule mounted between them and the pressure variations transmitted to a pen recorder, the side load being a measure of the surface friction. The third wheel drives the recorder chart. The recording apparatus includes an integrator which enables the average friction value to be calculated over any distance. An event pen operated by the driver can be used to mark the record at any selected point.

The total weight of the equipment is about 530 lb. of which about 250 lb. is removeable ballast. The tires are 16 inches in diameter and 4 inches wide operating at a pressure of 10 psi and are closely controlled in manufacture to maintain consistency of results. The length, width, and height are 60, 32, and 34 inches, respectively, and the chart is arranged to move at 450 feet per inch and each chart roll has a total capacity of approximately 40 miles.

So that the equipment can be operated by a single person who may have to remain in the towing vehicle whilst on an active runway, a remote recorder has been developed which is actuated by the friction recording mechanism in the friction meter itself. In fact, a set of three remote recorders can be used so that each may be switched on to record and hold the average friction values for each third of a runway; no time is then spent on the actual runway in writing down numbers.

To enable a towing speed to be used which is both within the capability of a normal road vehicle and which will still discern the presence of aquaplaning, a tire pressure of 10 psi was chosen. When towed at 40 mph, this pressure gives a speed equivalent to 1.2 times the theoretical aquaplaning speed. To make sure that tread wear would have no effect on the results, a smooth tire is used. The third (rear) wheel uses a patterned tire with an inflation pressure of 30 psi. A sample output is shown in figure I-14.

MECHANICAL LOAD ANALYSIS OF EQUIPMENT

When a horizontal force is applied to the towing point of the Mu-Meter causing it to move in a forward direction over a surface to be sampled the toed-out wheels tend to move apart. This tendency is resisted by the load sensing capsule positioned between the arms of the "V" frame.

The load sensing capsule feeds the load data to the recorder by hydraulic pressure in a flexible pipe.

The force to be resisted by the capsule originates at the main wheel tire where it contacts the surface, and is the load on that point multiplied by the side force coefficient. The component of this force is fed back in the form of a couple via the pivoted leg of the "V" frame.

Typical Traces

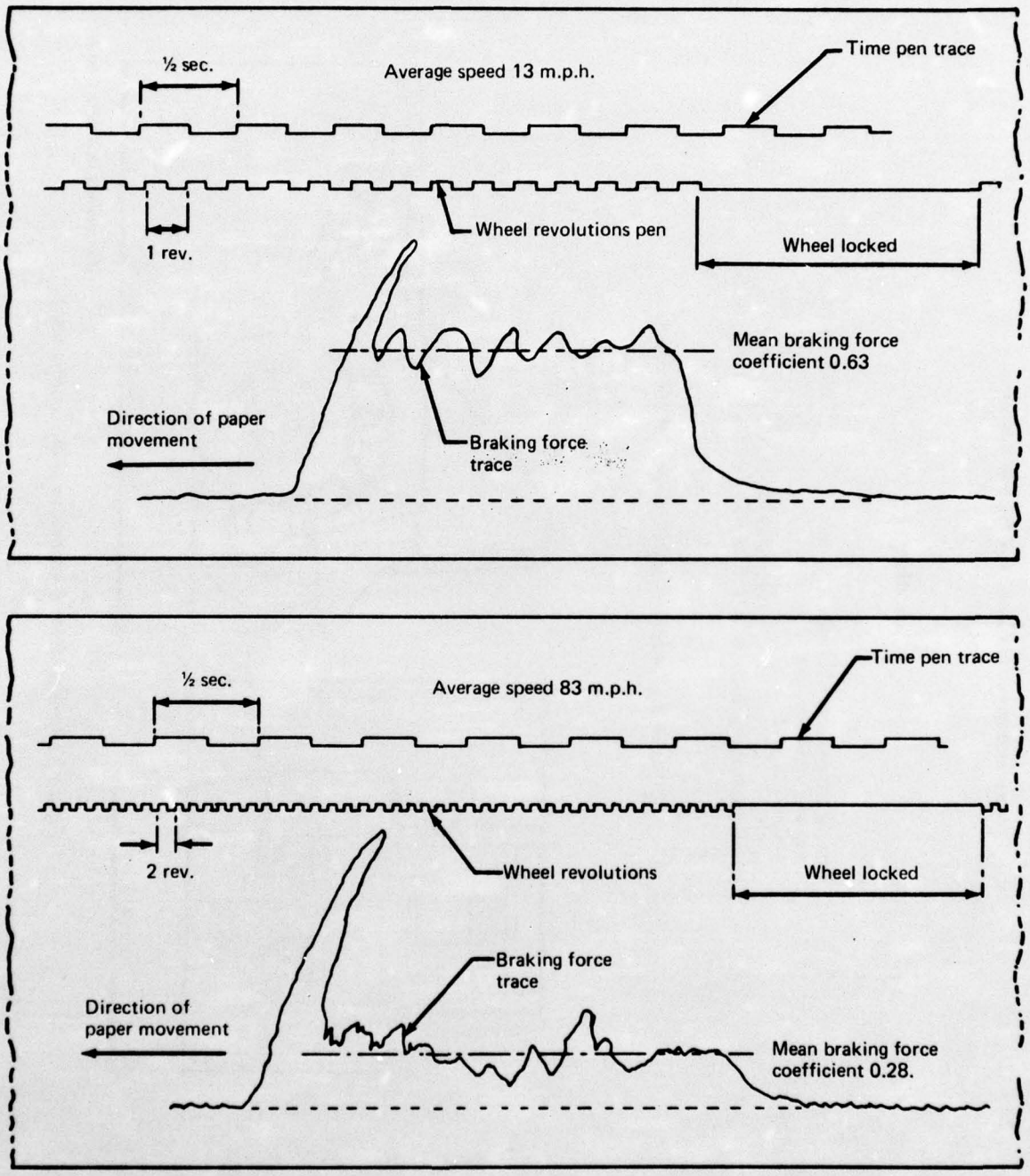

Figure I-11.—Typical Traces

Airport Runway and Motorway Friction Recorder

Specification

Total weight (including ballast)	528 lb. (240 kg)
Range of μ values measured	From zero to unity
Chart drum capacity	40 ft. (12192 mm)
Chart scale	1 in. (25.4 mm) = 150 yds. (137.1 m)

Average Runway of 3000 yds. (2743 m) = 20 in. (508 mm) chart scales

Effective at all speeds up to well in excess of 100 m.p.h.

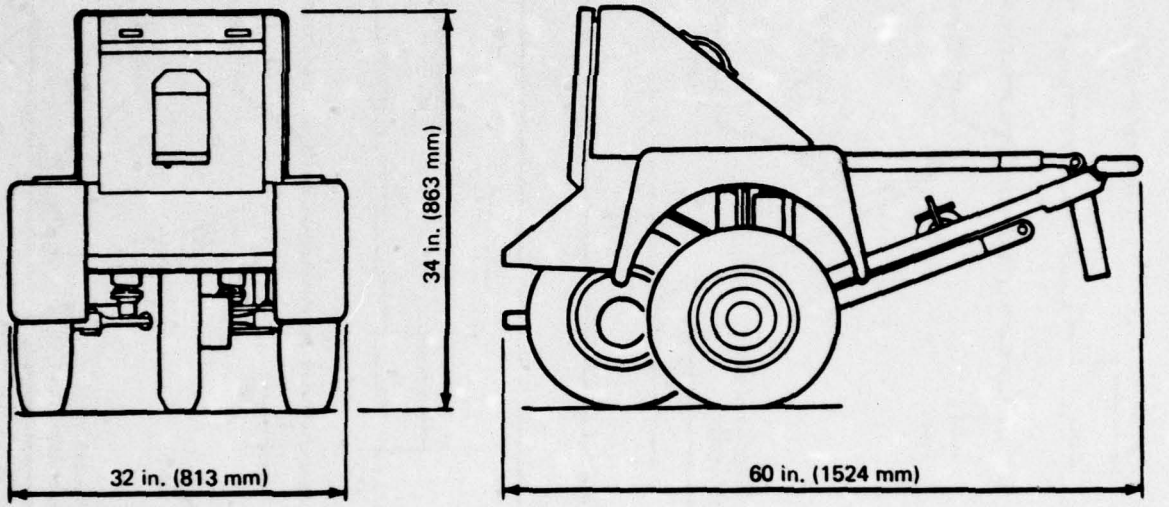

Dimensions in inches (mm)

Figure I-12.—Mu-Meter Dimensions and Specifications

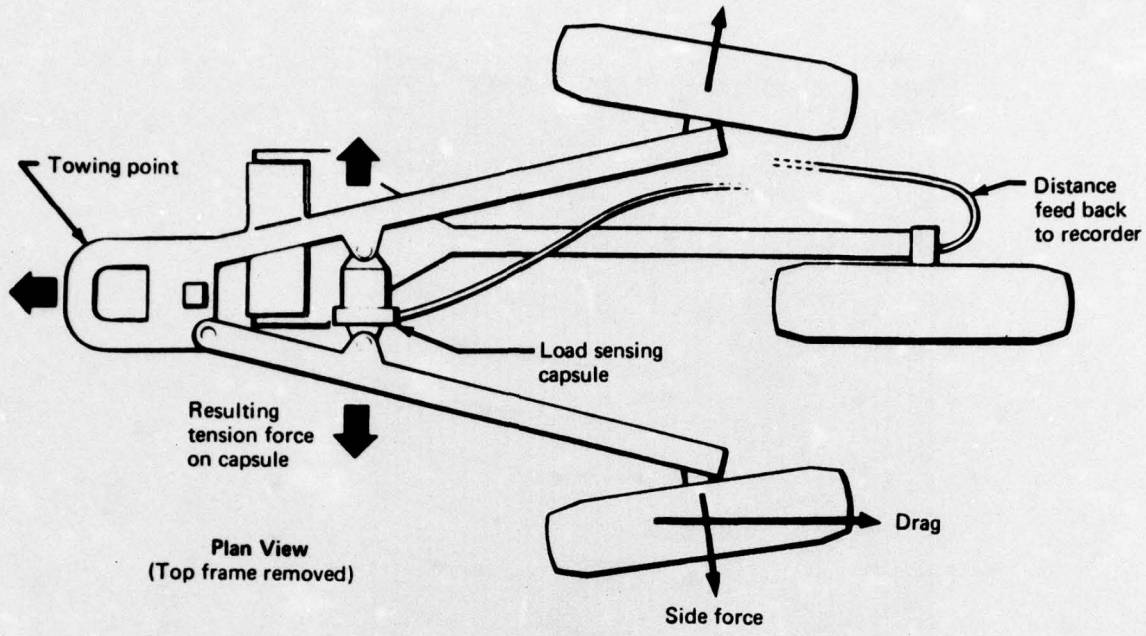

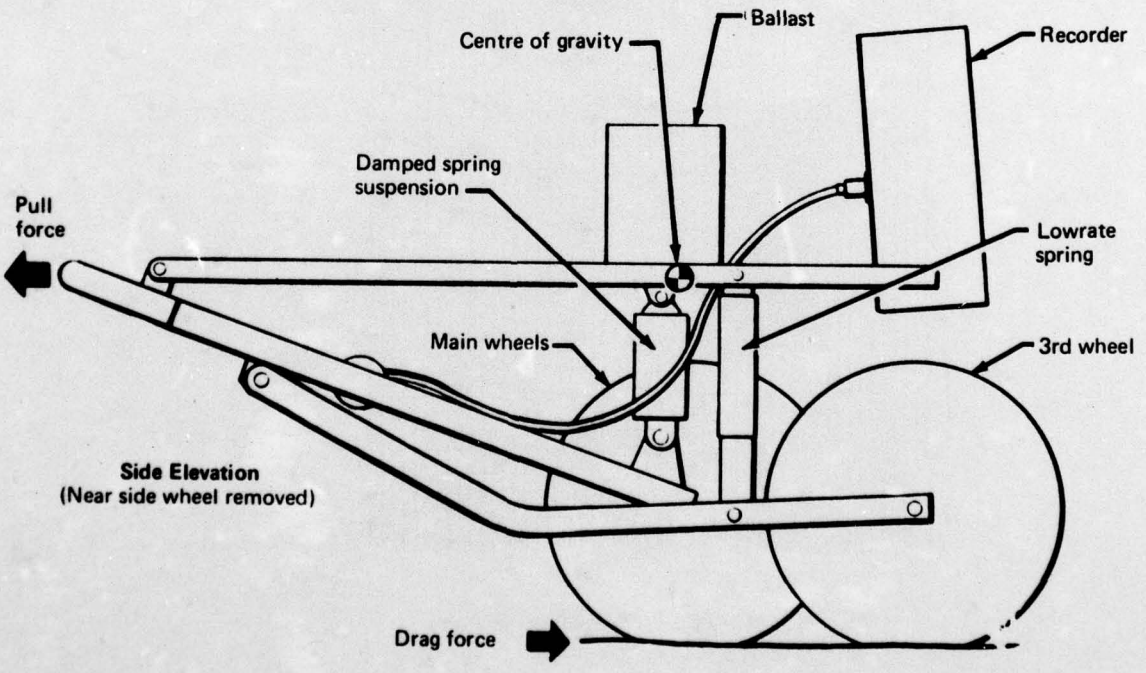

Figure I-13.—Diagrammatic Layout of 'Mu-Meter.'

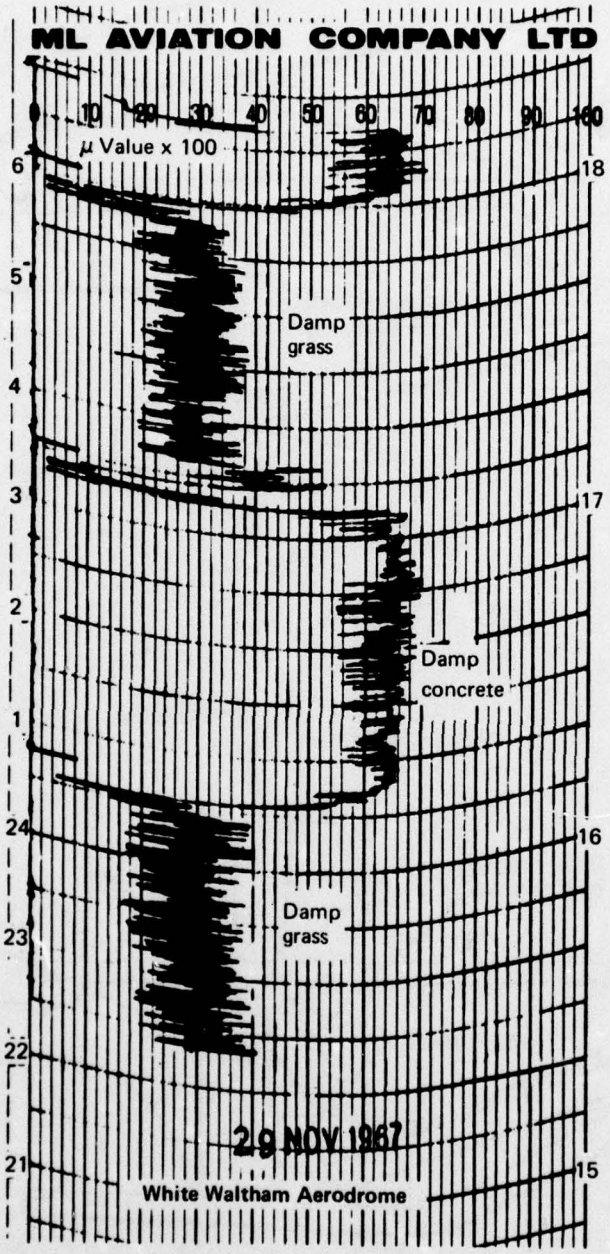

Figure I-14.—Typical Mu-Meter Traces

This force is modified by the combined effect of the drag on the wheel, and the pull force being at a height above the ground, forming a couple tending to relieve the actual weight on the wheels.

Again, the goemetry relative to the Center of Gravity is arranged to render the force on the capsule substantially constant for any given side force coefficient irrespective of towing point height within the range 17 in. to 22 in.

The third wheel does not influence the loads applied to the load sensing unit as it is connected to the ballasted frame by a very low rate spring; thus the modification to the effective ballast weight is substantially constant.

The net result of complete load analysis is that the device reads consistently and accurately values of surface friction between its rubber tires and the surfaces being sampled.

The Mu-Meter is qualitatively used in the United Kingdom as follows (Ref. 68):

MU-METER TABLE OF BRAKING ACTION

Code	Estimated braking action*	Measured or calculated coefficient of friction
5	Good	0.40 and above
3	Medium	0.35 - 0.30
1	Poor	0.25 and below

*Good- Indicates that aircraft can expect to land comfortably within the scheduled "wet" distance without undue directional control problems.

Medium- Aircraft are likely to use all the "wet" scheduled distance including the safety factor part of the distance, and may run even further. Directional control might be impaired.

Poor- Aircraft can expect to run for at least the full "very wet" or aquaplaning distance where this too is scheduled. Directional control will also be poor.

7. SWEDISH – SKIDDOMETER BV-11

This is a small friction test trailer, primarily designed for continuous measuring of the braking action on runway surfaces.

The trailer frame is carried by three wheels, size 4.00-8 mounted side by side but individually suspended by means of swing arms and loaded by 1 kN (Kilo Newton) each. Total weight of the trailer is about 340 kgs. See figures I-15 and I-16.

The three wheels are connected by means of roller chains in the swing arms and the gearing is chosen so that the wheel in the middle - the test wheel - is forced to a brake slip of 17 percent when the trailer is towed forwards. It is assumed that within a reasonable degree of accuracy,

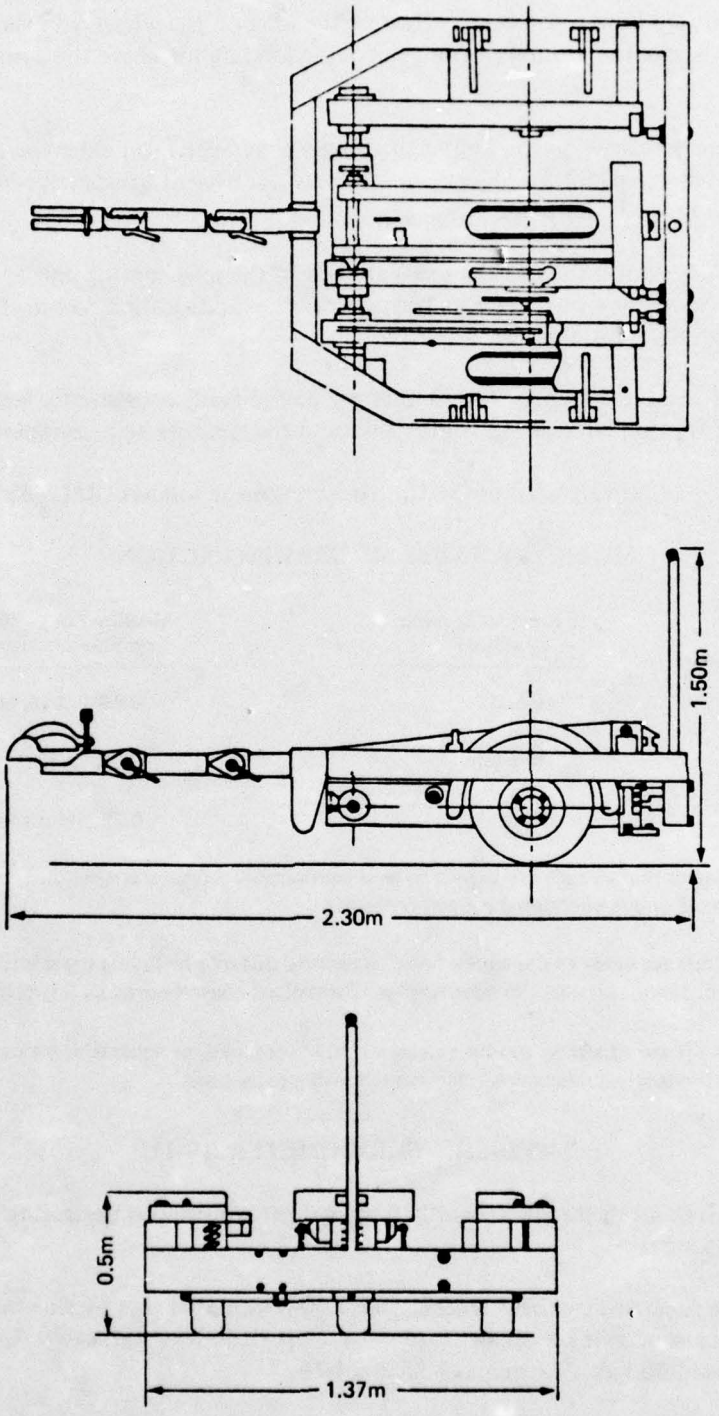

Figure I-15.—BV - II - 2 Skiddometer

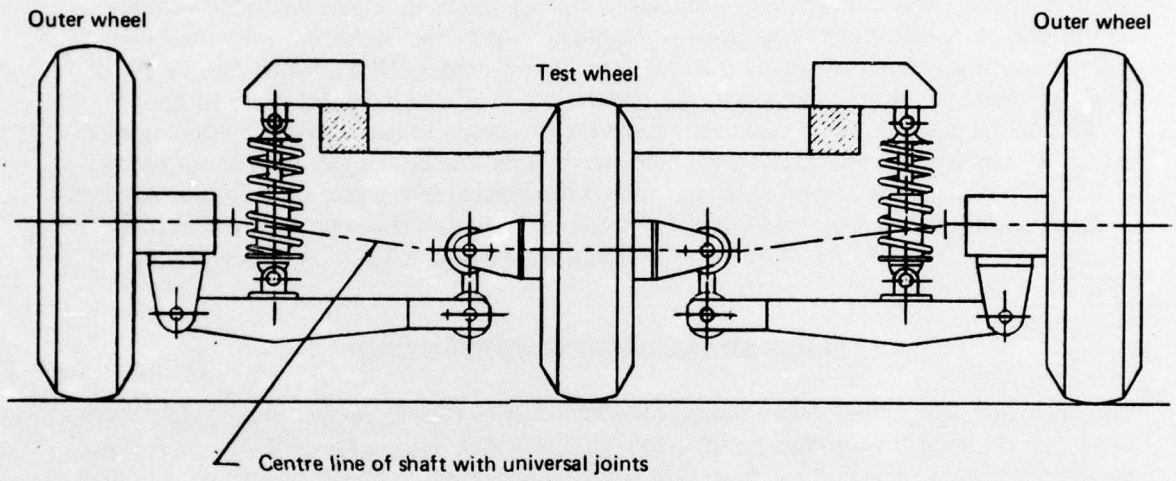

Figure I-16.—Suspension of the Trailer

a tire of common design, braked to a slip of about 15 percent on a surface, makes use of the maximum friction force possible for the tire on the surface in question. The outer tires are inflated to 25 psi and the measuring wheel pressure is 17 psi.

The brake slip on the test wheel is thus governed by the two outer wheels, which thereby obtain a relatively small drive spin. This method - that is to feed back the brake force from the test wheel to the outer wheels - means that the force necessary to tow the trailer when making tests is only about 15 percent of the friction force. The operating speed of the Skiddometer is a constant 40 mph.

The test wheel center is designed as a measuring hub by means of which the friction torque on the wheel is transformed to an electrical signal in an inductive transducer. The signal is - without slip rings - fed through a cable to a paper strip recorder (12 V), which may be placed on the desired spot in the towing vehicle. The friction number can be directly read on the record and the damping properties of the recorder are chosen to facilitate calculation of mean values. Paper feed is proportional to distance traveled by means of a tacho-generator on one of the outer swing arms governing the paper feed mechanism of the recorder. Recording range of the friction coefficient is from 0 to 1.0. A value as low as 0.05 can be clearly read (deflection of 5mm). The accuracy of the measuring system is within ± 1.5%. A sample output is shown in Figure I-17.

8. JAMES BRAKE DECELEROMETER (JBD)

This is a small, light (3 lb.) device used for the reporting of runway surface conditions. It consists of an air damped pendulum coupled to a pointer which indicates deceleration in feet per second per second. The pointer remains in position until released by the manual reset button. The instrument is graduated in increments from 0 to 32 feet per second per second, the top number being equivalent to the theoretical maximum deceleration capability of the carrier vehicle on a dry surface. These numbers are referred to as the James Brake Index (JBI). See Figure I-18.

The J.B.D. can be used in any mechanically sound car or light truck fitted with non-studded tires. The J.B.D. is placed on the floor of the vehicle and leveled. It has a low center of gravity and ordinarily will remain in position when the brakes are applied. The vehicle is driven at a speed of 30 ± 5 m.p.h. and the brakes applied firmly until all four wheels are locked. The reading is taken and the meter reset.

Measurements are made at 1,000 foot intervals at a distance of 30 feet on each side of the runway center line over the entire runway length. The runway is divided into three sections and the J.B.I. recorded for each section is averaged to the nearest whole number. Readings are taken at a frequency appropriate to site conditions.

The J.B.D. has seen extensive use by the USAF for a number of years. USAF Technical Order 33-1-23, dated December 15, 1965 sets forth the requirements for use of the J.B.D. in the Runway Condition Reading (RCR) system of identifying runway surface characteristics to the pilot. An extensive evaluation of the J.B.D. was conducted by the FAA in 1968 in two parts: (1) tests of the J.B.D. and a CV-880 commercial jet transport; and (2) development of calibrated jet transport landing distance ratios as a function of J.B.D. indices. Results of this program

AD-A039 968 BOEING COMMERCIAL AIRPLANE CO SEATTLE WASH F/G 1/2
TIRE RUNWAY INTERFACE FRICTION PREDICTION SUBSYSTEM.(U)
MAR 77 M K WAHI, H H STRAUB F33657-74-C-0129
UNCLASSIFIED ASD-TR-77-7 NL

3 OF 3
AD
A039968

END
DATE
FILMED
6-77

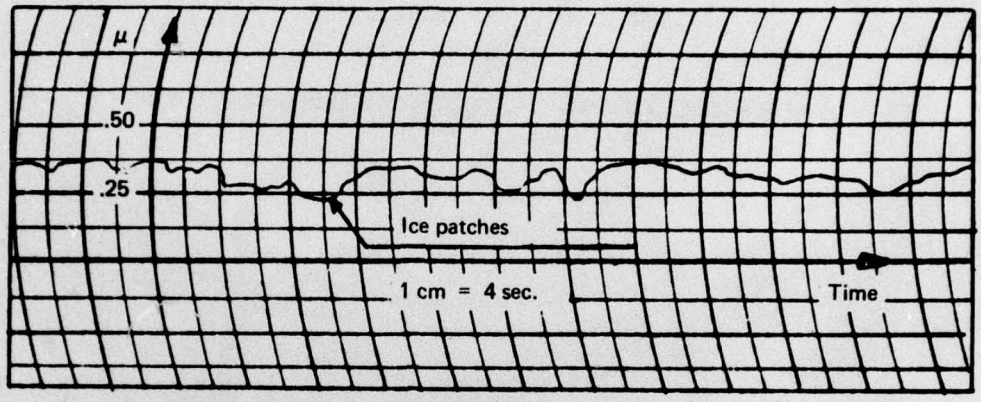

Test conditions: wet snow on ice, temp. 0° C
test speed = 20 mph, i.e. here
1 cm = 120 ft.

Figure I-17.—Example of Braking Action Record from Tests with Trailer

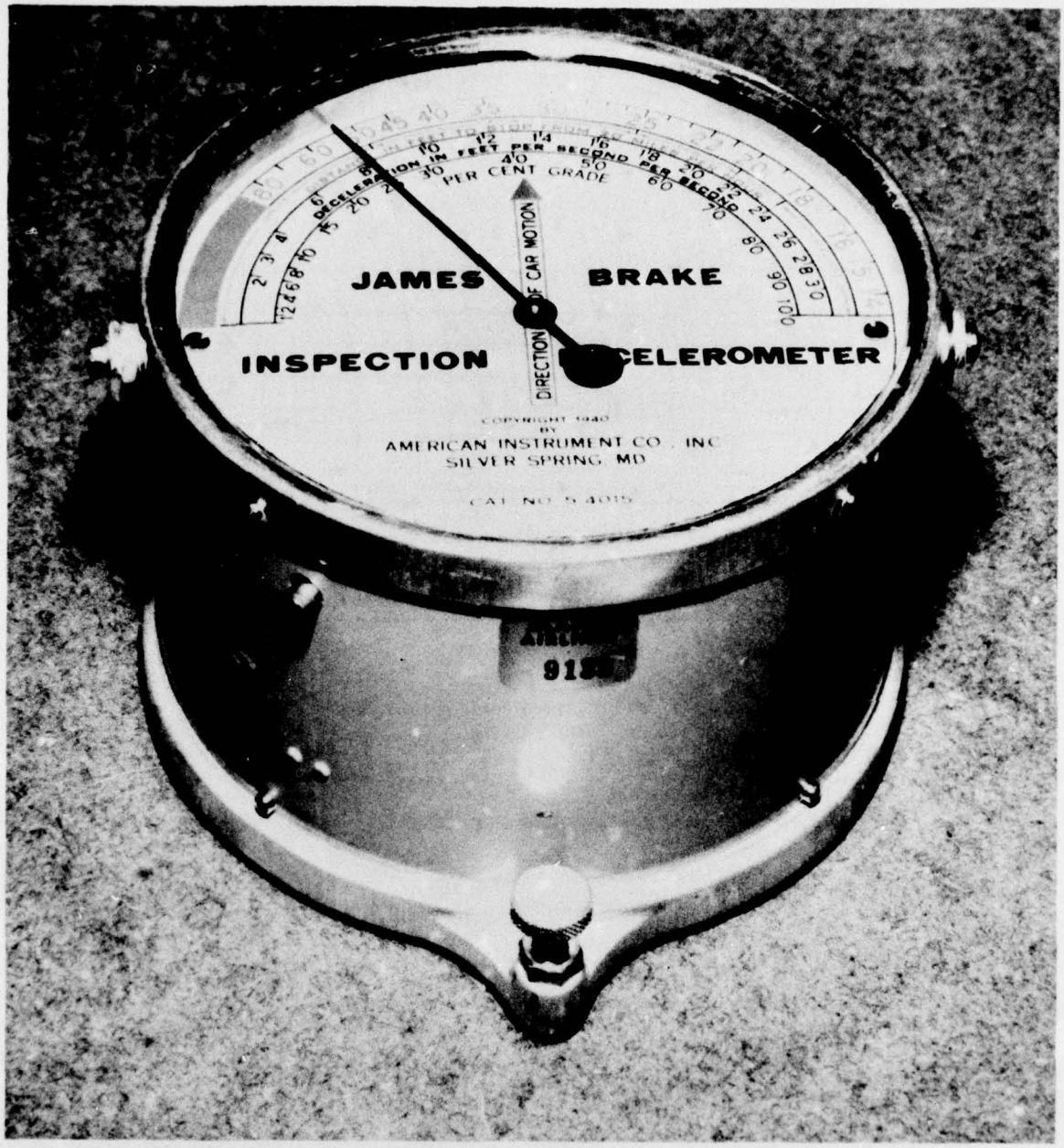

Figure I-18.—James Brake Dececerometer

showed that the J.B.D. would not produce accurate data for wet runways. Since the FAA evaluation it has been shown by the Canadian Department of Transport and Alaska Airlines that the J.B.D. can be used on hard-packed snow or dry ice covered runways. Reference (68) spells out the manner in which the J.B.D. can be used in Canada, and limits its use to ice and snow-covered runway surfaces. Qualitative use of the data, as recommended in reference (69) are:

Estimated braking action	James brake index (JBI)
Excellent	25 - 32
Good	22 - 24
Fair	18 - 21
Poor	10 - 17
Nil to very poor	0 - 9

Alaska Airlines has used the J.B.D. to establish Runway Condition Reading (RCR) values as a function of stopping distance for the Boeing 727 on ice or hard-packed snow-covered runways. These data were established by flight test and correlation with J.B.D. data obtained at the same time.

J.B.I. readings are converted to coefficient of friction Mu, by:

$$Mu = \frac{JBI}{32.2}$$

It is readily apparent that choice of vehicle, proper suspension system, careful choice of location for installation of the J.B.D. and manner of sampling the runway all influence the data obtained. Some error is introduced into the reading of the J.B.D. due to pitch down of the front of the vehicle as brakes are applied. The driver's skill is another important contributor since the operation technique is the key to success in use of the J.B.D.

9. BRITISH – TAPLEY-METER

This is a pendulum type decelerometer. It was originally designed to measure the efficiency of motor vehicle brakes and consists - as indicated above - of a freely-suspended pendulum in a housing. By a special mechanism the movements of the pendulum produce proportional movements on a movable scale. There is also a scale holding mechanism arranged so that the reading of the scale stays set after a test has been carried out.

When carried on a vehicle moving at any uniform speed or stationary, the pendulum takes up a vertical position. If the vehicle's speed is then reduced, as by the application of the brakes, the pendulum will swing forward to an angle away from vertical and it may be proved that the tangent of this angle is a measure of the force exerted to decelerate the vehicle.

The pendulum is immersed in a liquid which damps out irregular movements and overswing and the damping properties are chosen so that full indication is not registered until the braking has been effective for 0.8-1.0 seconds.

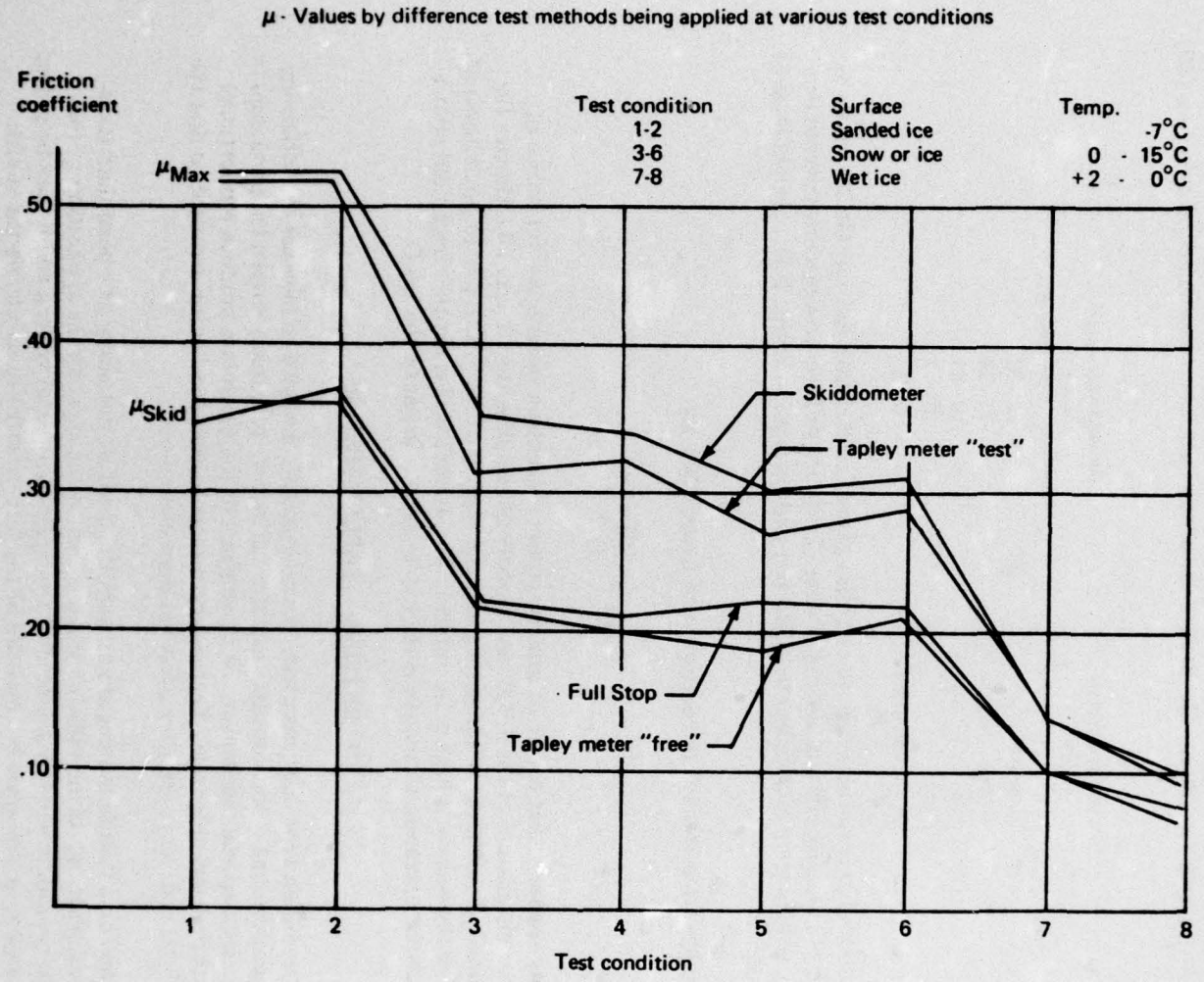

Figure I-19.—Tapley Meter Test Data

When used for determining braking action on runway surfaces the instrument must be carried in a vehicle with small tendency of the body to tilt down forward when braking as this tendency otherwise would cause a high decelerometer reading. The tests on runway surfaces are generally carried out as stop tests from 25 mph. The brakes are fully applied for about 1 second and then released.

Qualitative use of the data, as used in reference 68 are:

Code	Estimated braking action*	Measured or calculated coefficient of friction
5	Good	0.4 and above
4	Medium/good	0.39 - 0.36
3	Medium	0.35 - 0.30
2	Medium/poor	0.29 - 0.26
1	Poor	0.25 and below

*Good- Indicates that aircraft can expect to land comfortably within the scheduled "wet" distance without undue directional control problems.

Medium- Aircraft are likely to use all the "wet" scheduled distance including the safety factor part of the distance, and may run even further. Directional control might be impaired.

Poor- Aircraft can expect to run for at least the full "very wet" or aquaplaning distance where this too is scheduled. Directional control will also be poor.

REFERENCES

1. Wahi, M. K. et al: Combat Traction II, Phase II, Technical Report Number ASD-TR-74-41, Volumes I and II, October 1974.

2. Segal, L.; Ludema, K. C. and Dugoff, H. J.: ASTM Mater. Res. Std., June 1968.

3. Kern, W. F.: Rubber Chem. Technol., 40 (1967) 984.

4. DeVinney, W. E.: SAE Paper 670461, Chicago, May 1967.

5. Goetz, W. and Rice, G. M.: 1st Intern Skid Prevention Conf., Charlottesville, U.S.A., pt 2 (1958) p. 237.

6. Moyer, R. A.: 1st Intern Skid Prevention Conf. Charlottsville, U.S.A., pt. 2 (1958) p.411.

7. Holmes, T.; Lees, G. and Williams, A. R.: "A combined approach to the optimization of Tire and Pavement Interaction." In proceedings of the American Chemist Society, Spring meeting, Miami Beach, April 1971.

8. Clark, S. K., Editor: Mechanics of Pneumatic Tires, National Bureau of Standards Monograph 122, 1971.

9. Rose, J. G., Hutchinson, J. W. and Gallaway, B. M.; "Summary and Analysis of the Attributes of Methods of Surface Texture Measurement," Skid Resistance of Highway Pavements, ASTM STP 530, American Society for Testing and Materials, 1973, pp. 60-77.

10. Schulze, K. H. and Beckman, L., in Skid Resistance, ASTM STP 326, American Society for Testing and Materials, 1962, pp. 42-49.

11. Sabey, B. E., Journal, British Granite and Whinstone Federation, Vol. 5, No. 2, Autumn 1965, pp. 1-12.

12. Horne, W. B., and Joyner, U. T., "Traction of Pneumatic Tires on Wet Runways," Report SP-83, National Aeronautics and Space Administration, May 1965, pp. 9-17.

13. Gillespie, T. D., "Pavement Surface Characteristics and Their Correlation with Skid Resistance," Report No. 12, Pennsylvania Department of Highways - Pennsylvania State University Joint Road Friction Program, 1965.

14. Moore, D. F., "Prediction of Skid Resistance Gradient and Drainage Characteristics for Pavements," Highway Research Record 131, 1966, pp. 181-203.

15. Shilling, B., "R.A.E. Aircraft Tests on Grooved, Open Graded and Asphalt Runways in Great Britain," NASA SP-5073, National Aeronautics and Space Administration, 1968, p. 67.

REFERENCES (Continued)

16. Williams, J. R., "Aquaplaning - The British Ministry of Technology Programme," Special Publication 5073, National Aeronautics and Space Administration, Nov. 1968, pp. 81-99.

17. Anon.: Frictional and Retarding Forces on Aircraft Tires, Part 1: Introduction, ESDU Item No. 71025; London, October 1971 with Amendment A, August 1972.

18. Ibid, Part 2, Estimation of Braking Force, ESDU Item No. 71026.

19. Horne, W. B.: Results from studies of highways grooving and texturing at NASA Wallops Station. In pavement grooving and traction studies, the proceedings of a conference held at Langley Research Center, Hampton, Virginia, U.S.A. Paper 26, NASA SP-5073, November 1968.

20. Yager, T. J.: Comparative Braking Performance of Various Aircraft on Grooved and Ungrooved Pavements at the Landing Research Runway, NASA Wallops Station. Ibid, Paper 3, November 1968.

21. Leland, T. J. W.; Yager, T. J.; and Joyner, U. T.: Effect of Pavement Texture on Wet-Runway Braking Performance. NASA Tech. Note D-4323, January 1968.

22. Horne, W. B.; Yager, T. J.: and Taylor, G. R.: Review of Causes and Alleviation of Low Tire Traction on Wet Runways. NASA Tech. Note D-4406, April 1968.

23. Yager, T. J. et al: A Comparison of Aircraft and Ground Vehicle Stopping Performance on Dry, Wet, Flooded, Slush-Snow and Ice Covered Runways. Final Report on Project - Combat Traction, a Joint USAF-NASA Program. NASA Tech. Note D-6098, November 1970.

24. Tests with a Heavy Load Skidding Test Vehicle Incorporating a Mark 1 Maxaret Anti-Locking Brake System to Determine Braking Force Coefficients Between an Aircraft Tire and Various Wet Surfaces. Trials at the Road Research Track at Crawthorne and at Wisley Aerodrome, White Waltham Aerodrome and London (Heathrow) Airport. Ministry of Aviation S & T Memor. 10/64, January 1965.

25. Lander, F.T.W.; and Williams, T.: The Skidding Resistance of Wet Runway Surfaces with Reference to Surface Texture and Tire Conditions. Road Research Laboratory Lab. Rep. 184, 1968.

26. Yang, Nai C.: Design of Functional Pavements, McGraw Hill, 1972.

27. Murphy, Glenn C., Similitude in Engineering, The Ronald Press Co., New York, 1950

28. Ludema, K. C. and Gujrati, B. D.: An Analysis of the Literature on Tire-Road Skid Resistance. ASTM Special Technical Publication 541, 1973.

REFERENCES (Continued)

29. Aircraft Tire Manual, B. F. Goodrich Aerospace and Defense Products, Fifth Edition, 1972.

30. Aircraft Tire Manual, Goodyear Tire and Rubber Company.

31. Hytrol Skid Control Systems Brochure, Hydro-Aire Division, Crane, 1975.

32. Goodyear Brake Control Systems Booklet.

33. Jane's All the World's Aircraft, 1973-74.

34. 1974 Tire and Rim Association, Inc. Book, Section 9.

35. Profiles of Scheduled Air Carrier Airport Operations, "Top 100 U.S. Airports" DOT (FAA) Pub. August 1973.

36. Aeronautical Information Publication (AIP), DOT (FAA) Air Traffic Service Flight Services Division, "Aerodromes, AGA #2," Fifth Edition, April 1974.

37. Airman's Information Manual, AIP-AGA #3, Airport Directory, Part 2, 1974-75.

38. DOD Flight Information Publication, IFR – Supplements: United States, Alaska, Pacific and South Asia, Europe, North Africa and Middle East, 1975.

39. DOD Flight Information Publication (Terminal), Instrument Approach Procedures: United States, Alaska, Pacific and South Asia, Europe, North Africa and Middle East, 1975.

40. Greech, D. E. and Donald, H. G.: Aircraft Ground Flotation Analysis Procedures – Paved Airfields. Technical Report ASD-TR-70-43, January 1971.

41. Allbert, B. J.: Tires and Hydroplaning In: Proceedings of the Automotive Engineering Congress, Detroit. S.A.E. paper 680140, January 1968.

42. Harned, J. L.: Johnson, L. E.: and Scharpf, G.: Measurement of Tire Brake Force Characteristics as Related to Wheel Slip (Antilock) Control System Design. SAE Paper No. 690214, 1969.

43. Allbert, B. J., and Walker, J. C.: Tire to Wet Road Friction at High Speeds, In Proc. Inst. Mech. Engrs., Vol. 180, Part 2A, No. 4, pp. 105-158, 1965-66.

REFERENCES (Continued)

44. Sabey, B. E.: The Road Surface in Relation to Friction and Wear of Tires In: Proceedings of the Conference of Friction and Wear in Tires held at ERDE, Waltham Abbey, October 1968. Paper 2. Ministry of Technology D. Mat. Rep. 157, Junes 1969.

45. Maycock, G.: Experiments on Tire Tread Patterns. Road Research Laboratory Lab. Rep. 122, 1967.

46. Sugg, R. W.: Joint NASA-British Ministry of Technology Skid Correlation Study - Results from British Vehicles. In Pavement Grooving and Traction Studies, the Proceedings of a Conference held at Langley Research Center, Hampton, Virginia, U. S. A. Paper 24, NASA SP-5073, Nov. 1968.

47. Moore, D. F.: An Elastohydrodynamic Theory of Tire Skidding. Paper presented at 12th FISITA Congress, Barcelona, Spain, May, 1968.

48. Sabey, B. E., et al: Factors Affecting the Friction of Tires on Wet Roads. SAE paper 700376, 1970.

49. Staughton, G. C.: The Effect of Tread Pattern Depth on Skidding Resistance, Road Research Laboratory Lab. Rep. 323, 1970.

50. Leland, T.J.W. and Taylor, G. R.: An Investigation of the Influence of Aircraft Tire - Tread Wear on Wet-Runway Braking. NASA TN D-2770, 1965.

51. Baker, W. E. and Wilfred J. W.: Similarity Methods in Engineering Dynamic Theory and and Practice of Scale Modeling, Sparton Books, 1973.

52. Williams, T.: Skidding Resistance of Runway Surfaces. Aircraft Engineering, September 1971, pages 6-9.

53. Dreher, Robert C. and Tanner, John A.: Experimental Investigation of the Cornering Characteristics of a C40X14-21 Cantiliver Aircraft Tire. NASA TN D-7203, 1973.

54. Tanner, John A. and Dreher, Robert C.: Cornering Characteristics of a 40X14-16 Type VII Aircraft Tire and a Comparison with Characteristics of a C40X14-21 Cantiliver Aircraft Tire. NASA TN D-7351, 1973.

55. MAINSTREAM - CTS (STAT-PK) Statistical Package Reference Manual Boeing Computer Services (BCS), 1974.

56. Anon., "Programme for correlating Equipment in Measuring Runway Braking Action" Final Report, ICAO, Feb. 22, 1974.

57. Merritt, L. R., "Concorde Landing Requirement Evaluation Tests" Report No. FAA-FS-160-74-2, August 1974.

REFERENCES (Concluded)

58. Anon, "Scandinavian Procedures of Determining and Reporting the Braking Qualities of Icy or Snow Covered Runways" SAS Rep. GP/136, August 19, 1960.

59. Anon, "Measurement of Runway Friction Characteristics on Wet, Icy or Snow Covered Runways." Report No. FAA-FS-160-65-68-1, April 1, 1971.

60. Anon, "Stradographe, Apparatus for Measuring Slipperiness" Brochure in French, CEBTP, Paris.

61. Annual Book of ASTM Standards, American Society for Testing and Materials, Part 11.

62. Foxworth, T. G. and Marthinsen, H. F. (ALPA): "Another Look at Landing and Stopping Criteria" AIAA Paper No. 74-956, presented at AIAA 6th Aircraft Design, Flight Test and Operations Meeting, Los Angeles, California, August 12-14, 1974.

63. Ferrarese, J. A. (FAA) "Influence of Runway Traction on Operation of Jet Transport Aircraft," Ibid, Paper No. 74-958.

64. Horne, W. B. and Joyner, U. T.: "Pneumatic Tire Hydroplaning," SAE Paper No. 650145 (Inter-Auto Engr. Conf., Detroit, Michigan 1965).

65. Stocker, A. J. et al: "Variables Associated with Automobile Tire Hydroplaning" Texas Transportation Institute Research Rep. # 147-2, College Station, Texas, September 1972.

66. Meyer, W. E., Hegmon, R. R. and Gillespie, T. D.: "Locked Wheel Pavement Skid Tester Correlation and Calibration Techniques," Report TTSC 7118, Pennslyvania State University, Dec. 1971.

67. Smith, H. A., "Pavement Skid Resistance - A Summary of NCHRP Research," Better Roads, April 1972, pp 21-25.

68. "Measurement and Notification of Runway Braking Action in Ice, Snow, and Slush," NOTAM No. 849/1969, United Kingdom Board of Trade, Civil Aviation Department, Aeronautical Information Service, Tolcarne Drive, Pinner, Middlesex, December 1969.

69. Information Circular, "Use of James Brake Decelerometer," Canadian Department of Transport, Air Service Civil Aviation Branch, 0/6/70, 23 February.